2014-07-02

Synthesis of Conductive Nanofillers/Nanofibers and Electrical Properties of their Conductive Polymer Composites

Sarvi, Ali

UNIVERSITY OF CALGARY

Synthesis of Conductive Nanofillers/Nanofibers and Electrical Properties of their Conductive Polymer Composites

by

Ali Sarvi

A THESIS

SUBMITTED TO THE FACULTY OF GRADUATE STUDIES

IN PARTIAL FULFILMENT OF THE REQUIREMENTS FOR THE

DEGREE OF FOR THE DEGREE OF DOCTOR OF PHILOSOPHY

GRADUATE PROGRAM IN CHEMICAL AND PETROLEUM ENGINEERING

CALGARY, ALBERTA

JUNE, 2014

To My Parents, Brother and Sister

Acknowledgment

I would like to express the deepest appreciation to my supervisor, Dr. Uttandaraman Sundararaj, who was inspiring for me in many aspects, which are not limited to research and scholarship. His kind consideration, support and affability besides of his guidance in repute to research provided a medium full of spirit of adventure in regard to research and innovation.

I take this opportunity to place my sincere thanks to all the members of Polymer Processing Group, particularly, Dr. Mohammad Arjmand and Dr. Genaro Gelves for their help and encouragement. I would also like to thank the supervisory committee members for their insight and helpful comments, namely: Dr. Nader Mahinpey and Dr. Maen Husein. In addition, I am grateful to my friends Dr. Mehdi Mahmoodi, Mr. Majid Mehrpouya and Mr. Majid TabkhPaz who assisted me with my graduate life in Calgary.

I would like to thank "Zandmer Graduate International Educational Experience Award" for offering me the opportunity to advance my research work by collaborating with our colleagues at the University of Sao Carlos, Sao Carlos, Brazil. I would also like to thank Dr. Rosario Bretas and Dr. Aline Silva in University of Sao Carlos for their hospitality and assistance.

The financial support from the Natural Science and Engineering Research Council (NSERC) is highly appreciated. Thanks to Dr. Michael Schoel, Dr. Tobias Furstenhaupt and Dr. Wei Dong who helped me with microscopy imaging.

The last but not the least, I send my deepest gratitude to my parents and siblings who have been my very first teachers and for their wholehearted support.

Abstract

Thanks to their corrosion resistance, light weight, low cost, and ease of processing, electrically conducting polymer composites (CPCs) have received significant attention for the replacement of metals and inorganic materials for sensors, actuators, supercapacitors, and electromagnetic interference (EMI) shields.

In this PhD thesis, high aspect ratio conductive nanofillers namely copper nanowires (CuNWs) and multiwall carbon nanotubes (MWCNTs) were coated with polyaniline (PANi) using solution mixing and in-situ polymerization method, respectively. Transmission electron microscopy (TEM) showed a smooth polyaniline nano-coating between 5-18 nm in thickness on the nanofillers' surface. The coating thickness and; consequently, electrical conductivity was controlled and tuned by polyaniline/aniline concentration in solution. Composites with tunable conductivity may be used as chemisensors, electronic pressure sensors and switches.

Coated nanofillers demonstrated better dispersion in polystyrene (PS) and provided lower electrical percolation threshold. Dispersion of nanofillers in PS was investigated using rheological measurements and confirmed with electron micrographs and nano-scale images of CPCs. Polyaniline (PANi), when used as a coating layer, was able to attenuate electromagnetic (EM) waves via absorption and store electrical charges though pseudocapacitance mechanism. The dielectric measurements of MWCNT-PANi/PS composites showed one order of magnitude increase in real electrical permittivity compared to that of MWCNT/PS composites making them suitable for charge storage purposes.

Incorporation of PANi also brought a new insight into conductive network formation mechanism in electrospun mats where the orientation of conductive high aspect ratio nanofillers is a major

problem. Conductive nanofibers of poly(vinylidene fluoride) (PVDF) filled with coated multiwall carbon nanotubes (MWCNTs) were fabricated using electrospinning. These highly oriented PVDF nanofibers exhibited high beta (β) crystal content and enhanced piezoelectricity. Moreover, multilayer electrospun nanofibers, in which MWCNTs were located at the shell layer, were fabricated for further decrease in electrical percolation threshold.

In addition to the PANi coated nanofillers, immiscible polymer blends (poly(methyl methacrylate) (PMMA) and styrene-acrylonitrile copolymer (SAN) blends) were employed to deliver lower percolation threshold via double percolation phenomenon. Conductivity measurements revealed a significant decrease in electrical percolation threshold (0.4 wt%) for PMMA70/SAN30 blends compared with MWCNT-filled SAN and PMMA (ca 0.8 wt%).

Table of Contents

List of Tables

List of Figures

List of Symbols and Abbreviations

Abbreviations

AC	Alternating current
AFM	Atomic force microscopy
Al	Aluminum
AN	Acrylonitrile
APAM	Alberta Polymer Asymmetric Mixer
APS	Ammonium persulfate
ASTM	American society for testing and material
BLT	Barrier layer thinning
CB	Carbon black
CNT	Carbon nanotube
CPC	Conductive polymer composites
Cr	Chromium
Cu	Copper
CuNW	Copper nanowire
CVD	Chemical vapor deposition
DC	Direct current
DMF	N,N-Dimethylformamide
DMS	Dynamic mechanical spectroscopy
DNA	Deoxyribonucleic acid
DSC	Differential scanning calorimetry

EAP	Electroactive polymer
EB	Emeraldine base
EMI	Electromagnetic interference
ES	Emeraldine salt
ESD	Electrostatic discharge
FCC	Fluid catalytic cracking
Fe	Iron
FTIR	Fourier transform infra-red
hr	Hour
ICP	Intrinsically conductive polymer
LCST	Lower critical solution temperature
LFD	Low-frequency dispersion
MeOH	Methanol
min	Minute
MSMP	Miscible solvents mixing and the precipitation
MWCNT	Multiwall carbon nanotube
Ni	Nickel
NG	Nucleation and growth
PAC	Poly(acetylene)
PANi	Polyaniline
PAO	Porous aluminum oxide
PE	polyethylene
PC	Polycarbonate

PMMA	Poly(methyl methacrylate)
PNA	Programmable network analyzer
PP	Polypropylene
PPG	Polymer Processing Group
PPV	Poly(p-phenylene vinylene)
PPy	Polypyrol
PS	Polystyrene
PVDF	Poly(vinylidene fluoride)
SAN	Poly(styrene-acrylonitrile)
SAOS	Small amplitude oscillatory shear
SD	Spinodal decomposition
SE	Shielding effectiveness
SEM	Scanning electron microscopy
SWCNT	Single-walled carbon nanotube
TEM	Transmission electron microscopy
TGA	Thermogravimetric analysis
UCST	Upper critical solution temperature
UV-vis	Ultraviolet (UV) and visible (vis)
VDC	Voltage direct current
VNA	Vector network analyzer
WAXD	Wide angle x-ray diffraction
XRD	X-Ray diffraction
XPS	X-ray photoelectron spectroscopy

1D	One dimensional
3D	Three dimensional

Symbols

A	Ampere
aq	Aqueous
Ch	Chiral vector
C_0	Constant for electrical impedance
d	Electrical permittivity: Thickness; XRD: d-spacing
d33	Piezoelectric strain constant
dB	Decibel (unit of shielding effectiveness)
dyne	unit of force
E	Electric field
E_{in}	Incident electric field
E_{out}	Transmitted electric field
eV	Electron volt
F	Farad (unit of charge storage capacitance)
f	Electromagnetic wave frequency
H	Magnetic field
H_{in}	Incident magnetic field
H_{out}	Transmitted magnetic field
Hz	Hertz

I	Electric current
g	Gram (unit of weight)
G'	Storage modulus
G''	Loss modulus
G^*	Complex modulus
L	Liter
m	Meter
M	Mole
$M.I$	Melt index
M_w	Molecular weight
n	Critical relaxation exponent
nm	Nanometer
P	Power density
P_{in}	Incident power
P_{out}	Transmitted power
Pa	Pascal (unit of pressure)
R	Surface area; Gel stiffness
rpm	Revolutions per minute
S	Siemens (unit of electrical conductivity)
t	Critical exponent of percolation threshold; time
$tan\delta$	Electrical: Dissipation Factor; Rheological: damping factor
T_g	Glass transition temperature
T_m	Melting point

V	Voltage
V_C	Percolation threshold
vol	Volume
W	Watt (Unit of power)
wt.	Weight
W_f	Weight fraction of nanofillers
X_C	Degree of crystallinity
Z'	Real impedance
Z''	Imaginary impedance
ΔH_m	heat of fusion for the sample
ΔH_c	heat of cold crystallization
ΔH_f	heat of fusion for a 100% crystalline sample

Greek Letters

α	Alpha crystal phase
β	Beta crystal phase
γ	Interfacial energy
γ^d	Dispersion component of surface energy
ε'	Dielectric (real) permittivity
ε	Dielectric loss (Imaginary permittivity)
ε_0	Dielectric permittivity of free space
ε_r	Relative dielectric permittivity

ρ_0	Volume resistivity of conductive filler
σ	Electrical conductivity
Ω	Ohm (unit of resistance)
ω	Angular frequency
ω_a	Wetting coefficient
π	Pi orbital
θ	Chiral angle
φ^*	Percolation concentration
η^*	Complex viscosity
λ	Wave length
χ	Thermodynamic interaction parameter of polymers

Chapter 1

Introduction to Conductive Polymer Composites (CPCs)

Here, general background information regarding conductive polymer composites (CPCs) is given, synthesis of conductive nanofiller and nanofiller modification/coating for different applications. The objective of this PhD thesis work is to modify conductive nanofillers to achieve enhanced electrical properties at reduced nanofiller loading. Metal nanofillers ushered a new era in CPCs. In section 1.2, synthesis of metal nanofillers, is introduced. In section 1.3, carbon nanofillers are presented. Fabrication of polymer nanocomposites is presented in section 1.4. Fundamentals of electrical conductivity, electromagnetic interference shielding (EMI), electrical permittivity and piezoelectricity in polymer composites are discussed in section 1.5. The effects of different types of nanofiller and nanofiller coating on electrical percolation thresholds and electrical properties are shown in section 1.6. In this PhD thesis, different mixing procedures were investigated to decrease the electrical percolation threshold and simultaneously improve the desired electrical properties. To achieve this, conductive nanofillers were coated with intrinsically conductive polymers (ICPs). It has been suggested that coated nanofillers exhibit outstanding electrical properties compared to conventional polymer composites and have enhanced electrical properties compared to uncoated nanofillers. Further reduction in electrical percolation was achieved by selective localization of nanofillers in an immiscible polymer blend, and these details are presented in the Chapter 8.

1.1 Polymer Composites

Polymers are lightweight, inexpensive synthetic materials which, due to their excellent mechanical properties, have found a wide variety of applications in the last five decades. However, compared to metals, they still demonstrate poor thermal, mechanical and electrical properties. Thus, different types of fillers are mixed with polymers to ameliorate these properties. To achieve the desired mechanical properties, large filler loading (~30 vol%) was needed, which shows a negative effect on the processibility and toughness of polymer composites [1]. To overcome this issue, a new generation of fillers which hold their dimension in nano-scale was developed. Nano-scale fillers provide a larger surface area at lower concentrations compared to traditional micron-scale fillers. Larger surface area provides more interfacial interactions. Hence, better mechanical properties were obtained at significantly low nanofiller loadings (~5 vol%) [2]. Nanofillers are gaining a more share of the market in composite production, especially polymer composites. Polymer composites, due to their lightweight, lower cost, excellent mechanical properties and functionality, are outstanding candidates to replace metals in many applications. Reinforced plastics and polymer composites are used in automotive and aerospace industries and recently they have been employed in constructions. However, polymers are electrically and thermally insulative, which limits their application in the aerospace, automotive and electronics industries. Therefore, scientists are motivated to make polymer materials conductive. To synthesize electrically conducting polymer, it is necessary to locate numerous π-bonds in the main polymer chain, and make it capable of π-resonance in the entire polymer chain. Most of the industrial polymers such as polypropylene (PP) and polyethylene (PE) contain only single bonds and do not have any free electrons to conduct electricity. Polystyrene (PS), which has many applications in industry, also is not conductive. There are a limited number of polymers which

are intrinsically conductive, such as polyaniline (PANi), polypyrol (PPy), poly(acetylene) (PAC) and poly(p-phenylene vinylene) (PPV). The main chains of these polymers contain double bonds (like PAC), aromatic cycles (like PANi and PPy), or a combination of both (like PPV). Conductivity of intrinsically conductive polymers (ICPs) varies according to their oxidation states and can be enhanced via chemical doping with strong acids (like PANi, which shows a range of conductivity from 10^{-9} to 10^{1} S/cm (Siemens/cm)) [3]. The difficulties involved with synthesizing and processing of ICPs, as well as their poor mechanical properties, make it difficult to expand their use to application in the electronics area.

The invention of conductive nanofillers opens up new opportunities for conventional polymers to replace metals in electronic applications. Introducing nanofillers into a polymer matrix increases their conductivity to levels even higher than those of ICPs. Many different types of conductive nanofillers have been investigated in the last decades, such as carbon black, carbon nanotube, and graphite, and recently graphene and metal nanowires [5-13]. Figure 1-1 shows examples for mechanical and electrical applications of carbon nanotubes (CNTs). In the present project, we employed and manipulated carbon nanotubes and copper nanowires as conductive nanofillers to fabricate conductive nanocomposites for different types of applications.

Since the development and introduction of new techniques, such as electron microscopy (SEM and TEM), and more recently, atomic force microscopy (AFM), the knowledge of the morphology, structure, and properties of nanostructures has steadily progressed. New materials, with at least one dimension in the nanoscale (i.e. less than hundreds of nanometers) were developed and characterized. The need for different types of nanofillers challenged researchers to develop different methods for nanomaterial fabrication. The synthesis and characterization of

nanowires and nanotubes have been reported over the last three decades. Xia et al. provided an extensive review of the synthesis, characterization, and applications of 1D-nanostructures [5].

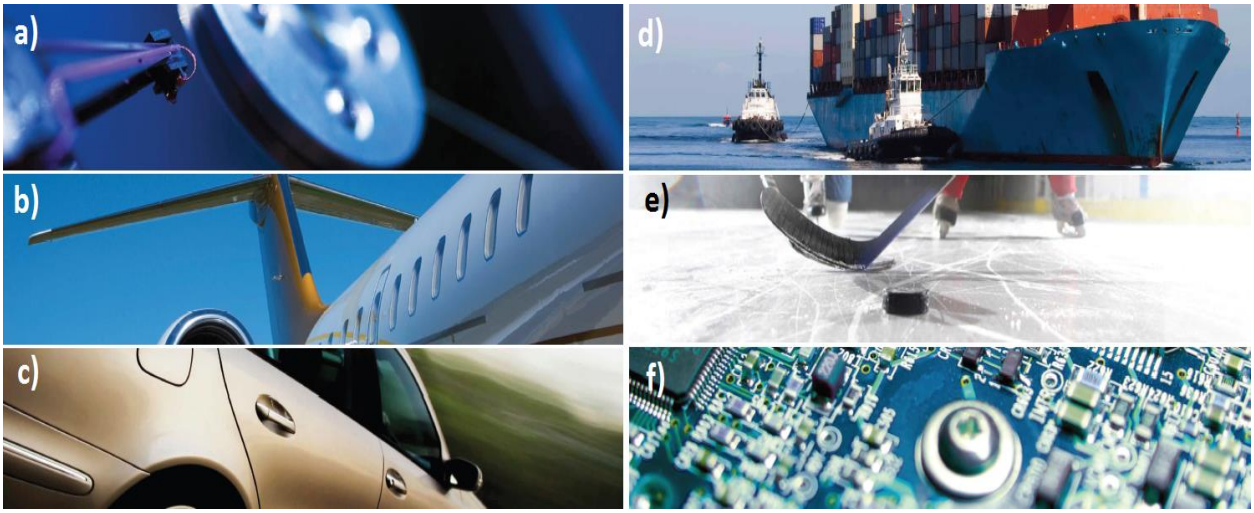

Figure 1.1 Some applications of carbon nanotubes in a) hard disk drives (HDD) trays b) aeronautic c) automotive d) marine coating e) sport gears and f) electronics [4]

1.2 Metal Nanowires

Metal nanowires are new class of 1D, high aspect ratio conductive nanofillers which can be synthesized using different methods of nanofiller synthesis such as hard template method or soft template. Hard template method which has been used in this PhD project resulted in high aspect ratio nanowires (l/d ~ 50-70) with diameter of 25 nm. Figure 1.2 shows the scheme of metal nanowire synthesis using hard template method. The detail of hard template method for synthesis of nanowires is presented in following chapter. These nanowires can be copper, nickel and silver nanowires which show high electrical conductivity and good electrical properties such as

excellent electromagnetic wave shielding and electrical permittivity. In this PhD project, copper nanowire were synthesized and employed for making conductive polymer composites.

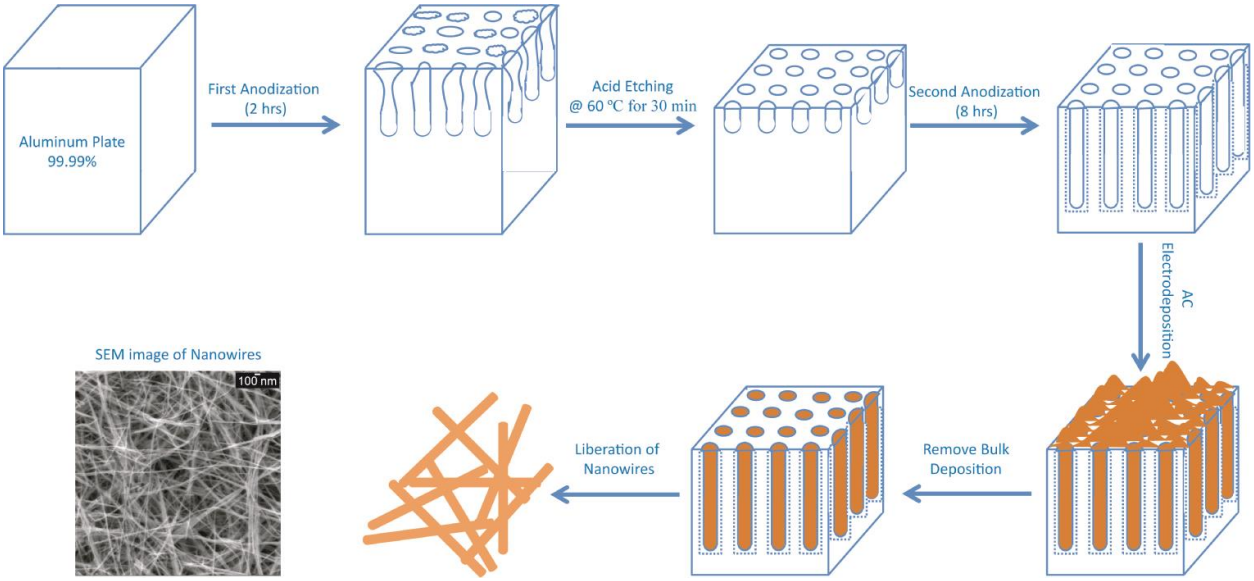

Figure 1.2 Synthesis of copper nanowires

1.3 Carbon nanofillers

There are different types of carbon nanofillers, identified based on their shape and structure. Some nanofiller are spherical-shaped in the scale of hundreds of nanometers such as carbon black. Some are platelet-shaped, like graphene, and some are rod-shaped, like carbon nanotubes and carbon nanofibers. Graphene is a 2-dimensional, crystaline allotrope of carbon. In graphene, carbon atoms are densely packed and bonded with each other via sp^2-hybridized orbitals and form a hexagonal pattern (like chicken wire). Carbon nanotubes are rod-shaped filler with a diameter of 1-10 nm and length of several microns. Carbon nanotubes, according to the number

of uniaxial carbon cylinders they have, are classified as single-wall carbon nanotubes (SWCNTs) and multiwall carbon nanotubes (MWCNTs).

1.3.1 Carbon black

Carbon black (CB) is a carbon nanofiller produced by the incomplete combustion of heavy petroleum products such as fluid catalytic cracking (FCC) tar, coal tar, ethylene cracking tar, and a small amount from vegetable oil [8]. CB is widely used as a reinforcing filler to improve dimensional stability, as a conductive filler to produce CPCs, as an ultraviolet light stabilizer, as an antioxidant to extend the lifetime of rubber against thermal degradation, and as a pigment or colorant [9]. CB is an amorphous form of carbon with a structure similar to disordered graphite.

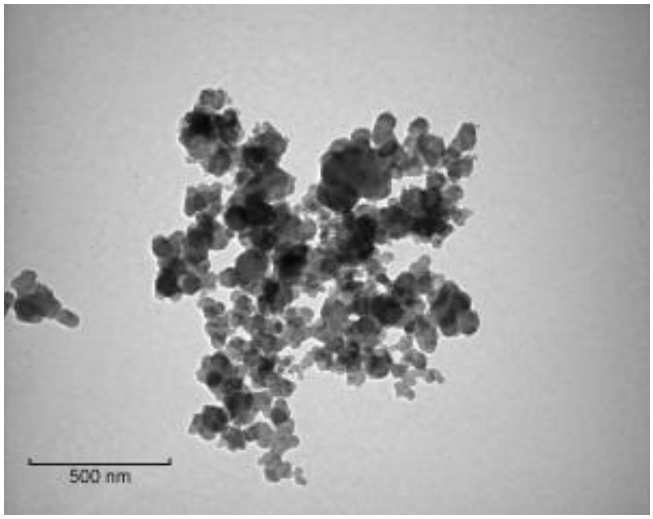

Figure 1.3 TEM image of high-structure carbon black [14]

There are five types of CB manufactured in industry, with furnace black being the most common for electrical conductivity applications. Specifications for furnace black CB are: electrical resistivity of 10^2 S/cm; surface area of 25-1500 m^2/g; and particle diameter of 10-100 nm [9]. CBs, based on their aggregate size and number of particles in the aggregate, are categorized as high-structure and low-structure. High-structure CBs tend to aggregate and form a chain (see Figure 1.3). Therefore, high structure of the primary aggregate is important in achieving high electrical conductivity [9]. Low-structure CBs do not have the high-structure tendency of aggregating, and they have long distances in between which makes it difficult to form an interconnected network. An interconnected network is crucial to achieving a conductive composite.

1.3.2 Carbon Nanotubes

Carbon nanotubes (CNTs) are allotropes of carbon with a cylindrical nanostructure. Nanotubes have been constructed with a high aspect ratio up to 10,000 [10]. CNTs were first discovered in 1991 by Ijima [11]. Nanotubes are members of the fullerene structural family, with a long and hollow structure like a tube. A carbon nanotube is a hexagonal network of carbon atoms rolled up into a seamless, hollow cylinder, with each end capped with half of a fullerene molecule [12, 15, 16].

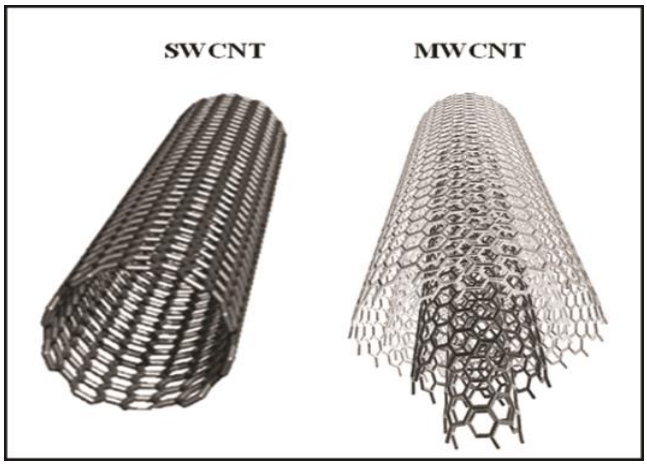

Figure 1.4 Scheme of multiwall carbon nanotube (MWCNT) and single-wall carbon nanotube (SWCNT)[1] [17]

There are two types of nanotubes: single-wall carbon nanotubes (SWCNTs) and multiwall carbon nanotubes (MWCNTs) (see Figure 1.4). The chirality and diameter of a nanotube determines its electrical and mechanical properties. The atomic structure of the CNT is described by two terms: tube chirality, which is defined by the chiral vector, C_h; and, the chiral angle, θ which is shown in Figure 1.5 [18]. According to these two parameters CNTs can be metallic, like copper (armchair structure) or a semiconductor, such as silicon (zig-zag structure).

The tube chirality is defined by the chiral vector, which is explained by the following equation:

$$\overrightarrow{C_h} = n\overrightarrow{a_1} + m\overrightarrow{a_2}$$

where the integers (n, m) are the number of steps along the unit vector $\overrightarrow{a_1}$ and $\overrightarrow{a_2}$ of the hexagonal lattice. The chiral angle determines the amount of twist in CNT [18]. Using this (n, m) naming systems, three types of orientation of carbon atoms around the nanotube circumference are itemized.

[1]

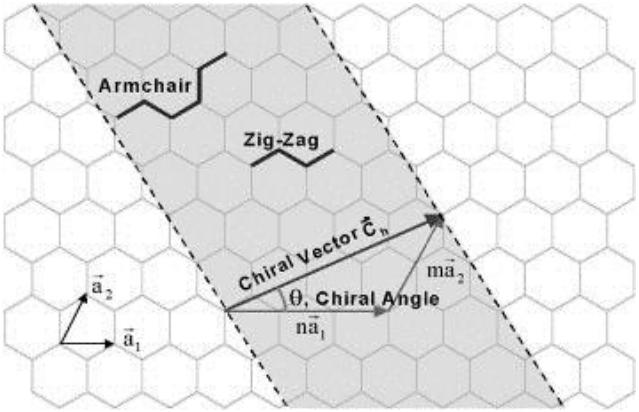

Figure 1.5 Schematic diagram showing how a hexagonal sheet of graphite is rolled to form a carbon nanotube [18].

Electrical and mechanical properties of CNTs are presented in Table 1.1. Since carbon-carbon bonds are strong covalent bonds, CNTs which hold a perfect arrangement of carbon-carbon SP^2 bonds along the axis of the nanotubes result in a strong material with outstanding tensile strength [12,18,19].

Table 1.1 Mechanical and electrical properties of CNTs compared with stainless steel and Kevlar

Material	*Young's modulus (TPa)*	*Tensile strength (GPa)*	*Electrical Conductivity (S/cm)*
SWNT	~1 [19]	13–53[19]	1×10^3 - 1×10^4 [20]
MWNT	0.2[21]–0.8[22]–0.95[21]	11[21]–63[21]–150[22]	5×10^2 - 1×10^4 [20]
Stainless steel	0.186[23]–0.214[24]	0.38[23]–1.55[24]	----------
Kevlar–29&149	0.06–0.18[25]	3.6–3.8[25]	----------

There are many different techniques used to synthesize CNTs: arc discharge, laser ablation, plasma torch, chemical vapor deposition (CVD) and other methods such as fluidized bed reactors [26-28]. The commercial method of CNT synthesis, however, is the CVD technique. There are several different CVD processes which thermally decompose hydrocarbon gases and use metal catalysts to grow nanotubes [26-28]. Using CVD, well-aligned SWCNTs and MWCNTs can be produced. Other nanotube structures, like bamboo structures, can also be produced [29, 30], although, this is not a low-cost method for mass production.

CNT/polymer composites have received attention in the last decade for their electrical and mechanical properties. Many structural applications have been proposed, ranging from everyday items like clothes and sports gear to combat jackets and space elevators [31]. Pioneering work from the *NanoTech* Institute has shown that single- and multiwalled nanotubes can produce materials stronger than any existing materials in nature [32,33].

Nanotubes also reveal a high electrical and thermal conductivity due to free electrons at carbon-carbon π-bonds. These π-bonds have resonance in the entirety of CNT which result in a high conductivity. Highly conductive polymer composites with low CNT loading and enhanced electrical properties have been reported, which makes these materials superior in comparison to carbon black.

1.3.3 Graphene

Graphene is another allotrope of carbon which is a two-dimensional sheet of sp^2-hybridized carbon. Graphene is a sheet of packed hexagonal carbon atoms with the thickness of one atom. Graphene, like CNTs, is formed from organized and dense carbon-carbon bonds, resulting in

high tensile strength and Young's modulus. Graphene sheets can be stacked to form 3D graphite, rolled to form 1D nanotubes, and wrapped to form 0D fullerenes (see Figure 1.6) [34]. Long-range π-conjugation in graphene, like nanotubes, yields extraordinary thermal, mechanical, and electrical properties. Due to these outstanding properties, graphene has been the focus of many theoretical studies and, more recently, has become an exciting area for experimentalists [35, 36].

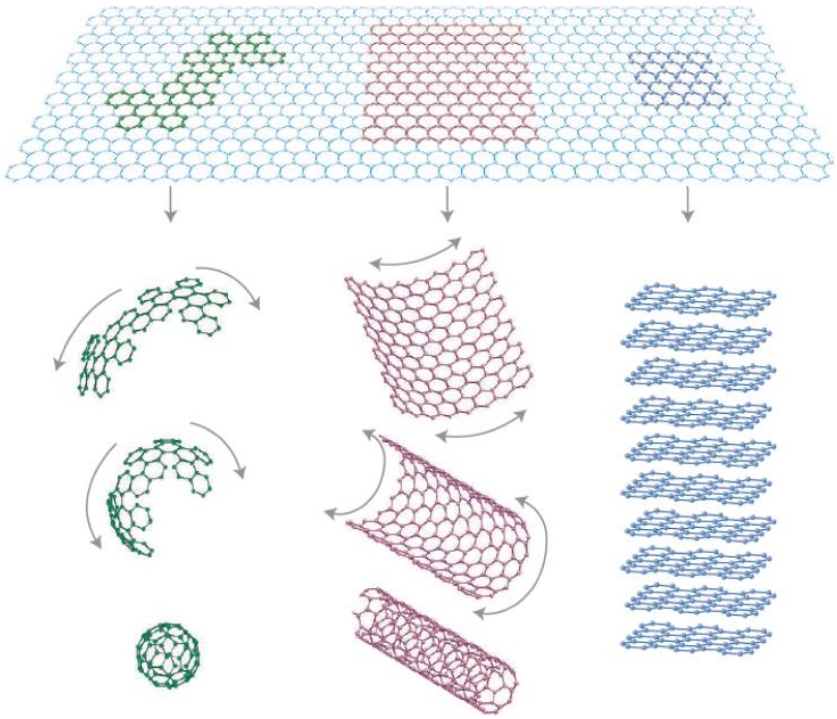

Figure 1.6 Graphene, mother of all graphitic forms [35]

Large numbers of graphene layers usually stack on top of each other. It has been found that the electronic structure rapidly grows with the number of layers, approaching the 3D limit of graphite at 10 layers [35, 37]. Moreover, only graphene and its bilayer have simple electronic spectra. They are both zero-gap semiconductors. For graphene with three or more layers, the spectra become more and more complicated, with the appearance of several charge carriers [38,

39]. The conduction and valence bands also start to notably overlap [37, 38]. Thicker structures of graphene should be considered as thin films of graphite.

Therefore, it is important to fully exfoliate graphene stacks in order to obtain excellent graphene electrical properties. One method for obtaining graphene is exfoliation of graphite to a single layer, which presents many difficulties due to possible inter-layer bonding [40, 41]. There have also been some attempts to grow graphene using typical CNT synthesis methods such as chemical vapor deposition of hydrocarbons on metal substrates [42, 43].

1.4 Introducing Conductive Nanofillers into Polymer

Electrical properties, structure and geometry of conductive nanofillers play an important role in the electrical and mechanical properties of polymer composite products. Additionally, the morphology and structure of nanofillers in a polymer matrix are found to be crucial in product properties. Controlling nanofiller morphology became of interest for researchers in adjusting the final properties of CPCs [44-46]. There are different methods for incorporation of nanofillers into a polymer matrix, such as melt mixing, solution mixing and in-situ polymerization of monomer in the presence of nanofillers. The goal is to improve dispersion of nanofillers in a polymer matrix in order to achieve better properties at lower filler loading, which decreases the cost and weight of a product and improves its processibility. Regarding the batch quantity, filler type and quality of nanofiller dispersion, different mixing methods can be used for melt mixing. Lab-scale melt mixing equipment typically refers to internal batch mixers and low capacity extruders (Figure 1.7). Twin-screw extruders result in better filler dispersion compared with internal mixers for platelet and fibrous nanofillers [47]. In the case of melt mixing, the dispersion

mechanism of nanoparticles in polymer melt has been previously studied [48, 49]. Kasaliwal et al. [50] mentioned that two mechanisms, so-called rupture and erosion, can be used to explain the dispersion of nanoparticles. They discussed a critical shear stress, above which the particles undergo dispersion by rupture, and under which the particles undergo dispersion by erosion. At low mixing speeds, dispersion was found to be governed by both mechanisms, whereas at higher shear rates, the rupture mechanism was dominant. They proposed a model for dispersion of nanofillers into polymers which consisted of filler incorporation, wetting and infiltration by polymer melt, and dispersion, distribution and flocculation of fillers in the polymer melt.

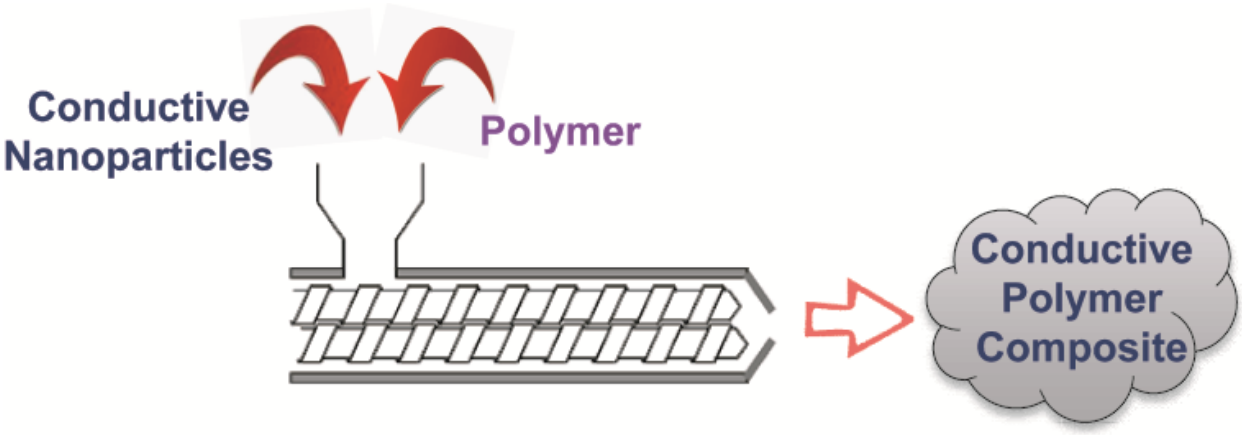

Figure 1.7 Melt mixing using twin screw extruder

The internal batch mixer is the most popular lab scale melt mixing technique to synthesize composites in small quantities. It comprises two blades which usually rotate counter-clockwise, and which have placed in a closed chamber. For melt mixing, polymer granules can be dry-mixed with a nanofiller first and then melt-mixed in the batch mixer. There is also the possibility of pre-melting the polymer in the mixer for a certain time, then adding the nanofillers. The high viscosity of the polymer, combined with the high speed of the extruder's rotation, causes a high shear field. This high shear breaks down nanofiller aggregates.

Solution mixing, results in a better nanofiller dispersion than melt mixing. However, there are difficulties with solution mixing solvent elimination, time, high cost and environmental concerns. Solution mixing is usually accompanied with ultrasonication of nanofillers in solvent. Bath type and horn type ultrasonciators (see Figure 1.8) helps to create a better dispersion of nanofillers by breaking down the nanofiller aggregates. In the case of platelet nanofillers, it helps with intercalation and exfoliation.

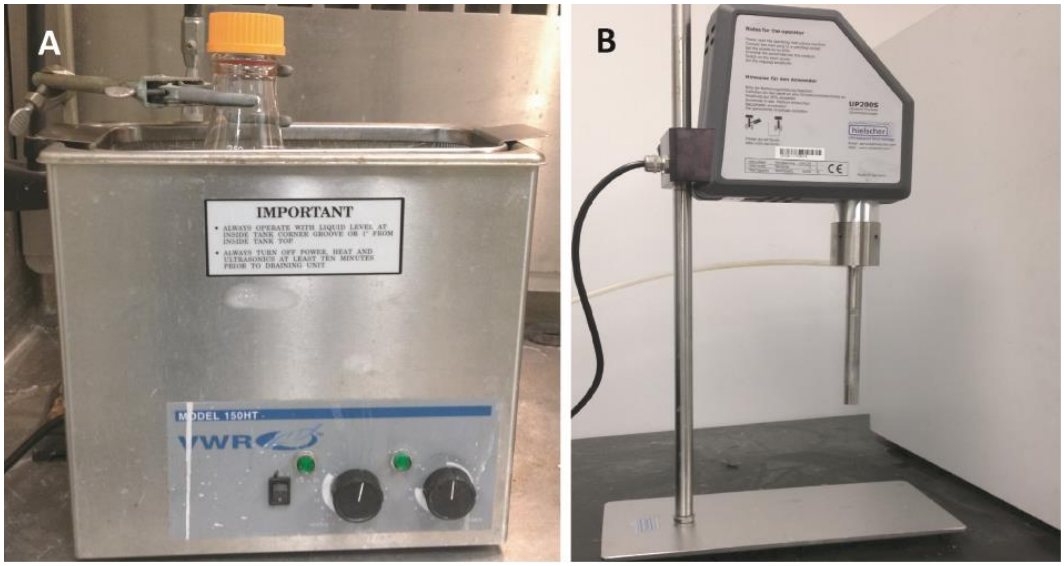

Figure 1.8 a) bath type and b) horn type sonicator

Solution mixing consists of dissolving polymer in a solvent and dispersing nanofillers, in the same solvent, in two different beakers. The two solutions are combined and mechanically stirred to establish a good distribution and dispersion. Figure 1.9 shows a schematic of the solution mixing method which has been used in this project.

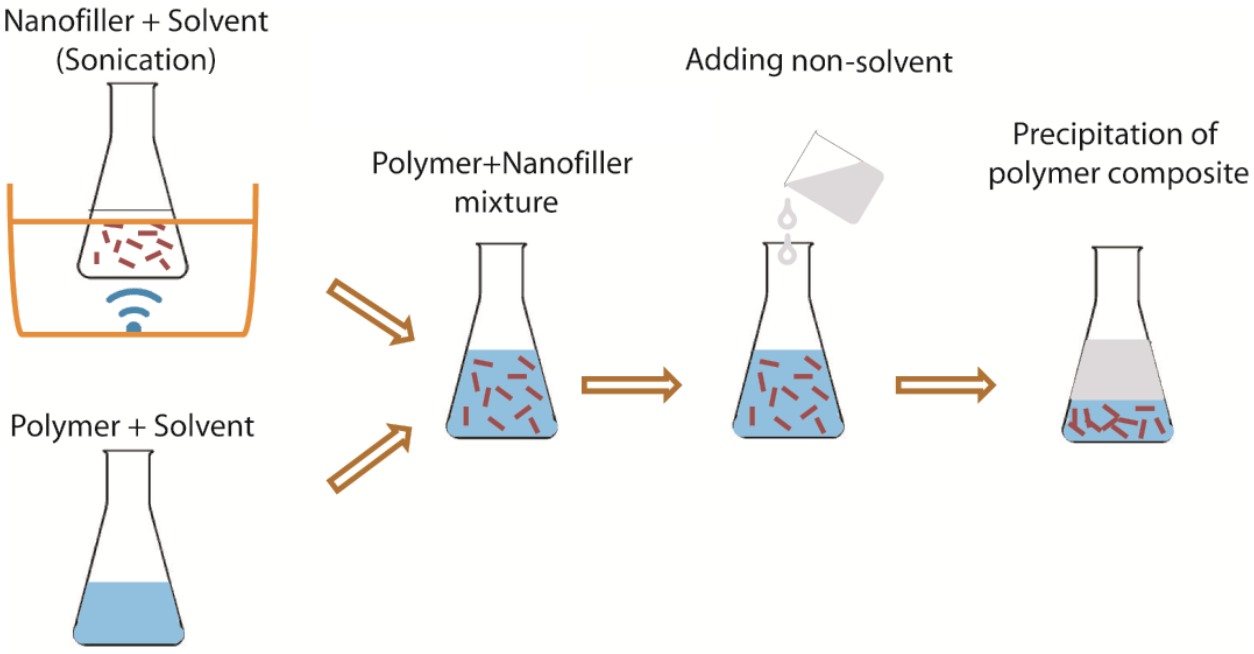

Figure 1.9 Solution mixing method for synthesis of CPCs

The substrate for nanofiller dispersion can be a polymer co-solvent. Gelves et al. [46] reported mixing polystyrene (PS) with copper nanowire using miscible solvent mixing and precipitation (MSMP) method. They dissolved PS in dimethylformamide (DMF) in one beaker; while in another, they dispersed copper nanowire in methanol (MeOH), which is a non-solvent for PS. Combining these two mixtures resulted in precipitation of micron-sized PS particles covered by CuNWs. Compression-molding of these covered PS particles resulted in composites with a conductive network of CuNWs in the form of honey-comb structure and led to unique and very high electrical properties.

1.5 Electrical Properties

1.5.1 Electrical Conductivity

Electrical conductivity is a measure of a material's ability to conduct an electric current, using the unit of Siemens per meter (S/m). The electrical conductivity for a polymer composite filled with conductive nanofillers is a function of nanofiller conductivity and nanofiller loading. Critical nanofiller loading must be incorporated into the polymer to make it conductive. At this critical filler loading point, long-range connectivity between the conductive nanofillers through the entire polymer matrix becomes evident. This critical loading is called the electrical percolation threshold, where electrical conductivity suddenly increases by several orders of magnitude (see Figure 1.10). Many theoretical and experimental investigations were performed to evaluate the electrical percolation threshold and to find a model which can simply predict the percolation threshold in polymer composites [51, 52]. Weber et al. proposed the following equation to estimate the percolation threshold in conductive polymer composite. The equation is valid at concentrations above the percolation threshold:

$$\rho = \rho_0 (v - v_c)^{-t} \qquad 1.1$$

where ρ is the electrical resistivity of the composite, ρ_0 is a scaling factor, v is the volume fraction of the filler, v_c is the percolation threshold of the volume fraction and t is a critical exponent. The scaling factor is used to validate the percolation theory.

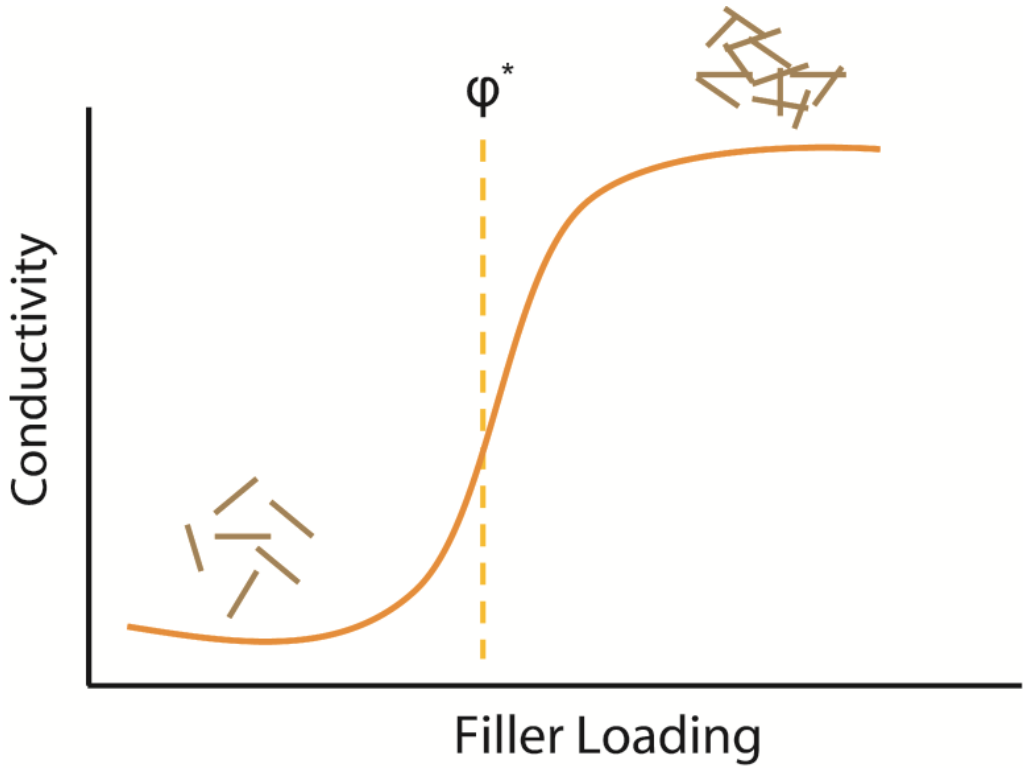

Figure 1.10 Electrical conductivity as a function of filler loading

Percolation threshold is a function of conductivity, geometry and the aspect ratio of nanofiller. High aspect ratio nanofillers, such as carbon nanotubes (0.61 vol%) [53] and metal nanowires (0.67 vol%) [46], revealed a much lower electrical percolation threshold than carbon black (3.3 vol%) [54-57]. High aspect ratio 1-D nanofillers form a network at a lower filler loading, decreasing the percolation threshold. Percolation threshold is a mathematical term related to percolation theory, which is the formation of long-range connectivity in random systems. From an electrical point of view, however, random distribution increases the percolation threshold. Selective positioning of nanofillers can significantly decrease the percolation threshold. As it was mentioned in section 1.4, Gelves et al. [46] reported a relatively low percolation threshold for PS/CuNW system by placing NWs on the surface of submicron PS particles. A greater decrease in the percolation threshold was observed in Goldel et al. [45], in

conductivity results for the immiscible blend of polycarbonate (PC) with poly(styrene-acrylonitrile) (SAN) filled with CNTs. The electrical percolation threshold is decreased by localizing CNTs in the percolated PC phase, and taking advantage of the double percolation phenomenon (percolation of CNTs in percolated phase of SAN in PC matrix).

The dispersion of nanofillers in a polymer matrix is the subject of many investigations undertaken to improve the desired properties in polymer composites. For a better dispersion, an established method is the coating/functionalization of nanofillers. This method has been used to improve the affinity of nanofillers, decrease interfacial tension between nanofillers and polymer, and improve the dispersion of nanofillers in polymer.

Due to the significant effect of conductive nanofillers' dispersion on percolation threshold and electrical properties, coating/functionalization of the conductive nanofiller was recommended as an effective method to reduce the percolation threshold. Additionally, the coating layer may integrate new charge transfer mechanisms to the polymer composite, which improves electrical properties. Gelves et al. [7] functionalized CuNWs with $C_8H_{17}SH$ short branches grafted on the surface of CuNWs. They found that the functionalized CuNWs have a better affinity with the polymer, resulting in a better dispersion and lower percolation threshold. However, the electrical conductivity of the product decreased due to covering CuNWs with an insulative layer. Therefore, it is necessary to coat/functionalize conductive nanofillers with a conductive material which does not electrically insulate the nanofillers. Coating/functionalization of nanofillers, based on the type of bonding between a coating layer and nanofillers, can be categorized as a covalent or non-covalent coating/functionalization [58-61].

Adding any covalent bonded coating/functional group to the CNTs inevitably changes the CNTs electronic structure [62]. Controlling the coating/functionalization is essential for fine-

tuning the electrical properties of the CPCs. Conductivity of CPCs has a wide range and determine their application (see Figure 1.11). In the current study, we investigated both non-covalent (Chapter 3) and covalent interactions (Chapter 4). The non-covalent interactions manifested as various types of forces acting between the nanofillers and molecule or ion constituting the nanofillers' nature.

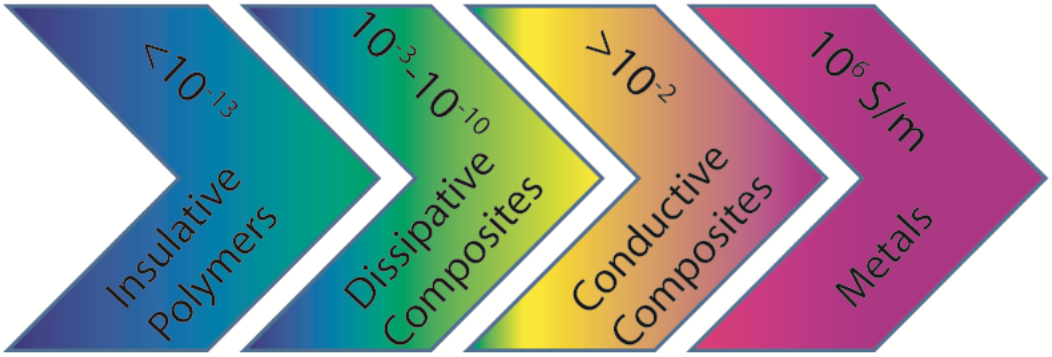

Figure 1.11 Classification of materials according to their surface conductivity

1.5.2 Electromagnetic Interference Shielding Effectiveness (EMI SE)

Electronic devices both radiate, and are affected by, electromagnetic (EM) waves. Electromagnetic interference (EMI) is disturbance that affects the functionality of electronic devices. This disturbance, which may be due to either electromagnetic induction or radiation from an external device, can interrupt or obstruct the effective performance of the circuit. The frequency of these waves can be any frequency above 10^4 Hz.

Electromagnetic interference (EMI) shielding denotes the reflection and/or absorption of electromagnetic radiation by a material which resists the penetration of the EM waves through the shield [63]. The ability of shielding material to attenuate EM waves is called shielding effectiveness (SE). The two main EMI shielding mechanisms of CPCs are absorption and

reflection of EM waves. A third mechanism of shielding, considered significant for concentrated or thick samples, is commonly known as multiple-reflections, which represents internal reflections within the conductive composite [64-67]. Figure 1.12 is schematic showing the three different mechanisms of shielding in a CPC shield. The EMI SE is expressed in dB, as defined by the following equation (ASTM D 4935-99):

$$SE = 10\log(\frac{P_{in}}{P_{out}}) = 20\log(\frac{E_{in}}{E_{out}}) = 20\log(\frac{H_{in}}{H_{out}}) \quad 1.2$$

where P_{in} is the incident energy field, P_{out} is the transmitted energy field, and E and H are the root mean squares of the electric and magnetic field strengths of the electromagnetic wave, respectively.

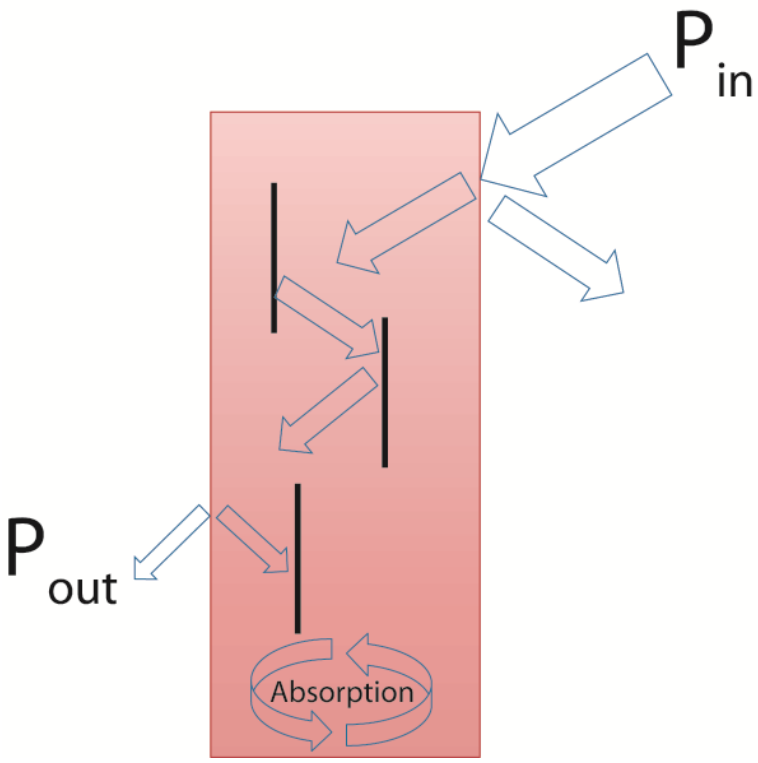

Figure 1.12 Schematic sketch shows how a shielding material attenuates electromagnetic waves

Metals have excellent capability in attenuating EM waves. Due to their weight, cost, and difficult processing, a huge demand for light-weight and low-cost materials to replace metals and inorganic materials exists. CPCs exhibit excellent EMI SE and are good candidates for EM shields [7, 46, 55, 68]. Carbon nanofillers use both mechanisms of reflection and absorption to attenuate the incident wave, while metallic nanofillers mainly use reflection [69]. Intrinsically conductive polymers (ICPs) also demonstrate EMI SE to a good extent [70]. In this study, ICPs used as the coating layer for nanofillers demonstrated a synergistic effect on EMI SE, as well as electrical conductivity (Chapter 4).

1.5.3 Electrical Permittivity

CPCs, due to their special structure, are suitable for charge storage and supercapacitor applications. These superior lightweight materials can be used in electronic circuit boards as an embedded capacitor. Some of these nanocomposites showed high charge capacitance similar to ceramic materials and inorganic composites [71, 72]. The electrical permittivity of a material under given conditions, such as applied voltage, reflects the ability of material to store electrical energy [73]. Supercapacitors store electrical energy through double-layer charging, faradaic processes, or a combination of both [72]. The amount of energy stored is usually small and can be delivered instantaneously, making supercapacitor devices able to provide a pulsed high power rather than a high amount of energy [72].

The relative electrical permittivity denoted as $\varepsilon_r(\omega)$ is the ratio of absolute electrical permittivity of a material, $\varepsilon(\omega)$, to the electrical permittivity of vacuum, ε_0. It is defined as [73]:

$$\varepsilon_r(\omega) = \frac{\varepsilon(\omega)}{\varepsilon_0} \quad 1.3$$

Electrical permittivity is a complex number which is frequency dependent. Relative permittivity is dimensionless and in its complex form is defined as:

$$\varepsilon_r(\omega) = \varepsilon'_r(\omega) + \varepsilon''_r(\omega) \quad 1.4$$

Real permittivity, $\varepsilon'_r(\omega)$, is related to the charge storage ability of a material and imaginary permittivity, $\varepsilon''_r(\omega)$, is related to the dissipation/leakage of the electrical energy within the material.

Due to their high conductivity, large specific area and cycle stability, MWCNTs exhibit a large and stable double-layer capacitance, which is one of the charge storage mechanisms. MWCNTs can be used for the electrical charge storage function in supercapacitors or any other kind of charge storage. Supercapacitors can also store energy through pseudocapacitance. Pseudocapacitance is a faradic process, while double-layer charging is non-faradic. ICPs utilize a large pseudocapacitance. Thus, a combination of MWCNTs and ICPs results in a high capacitance CPC which uses both faradic and non-faradic processes [74-79].

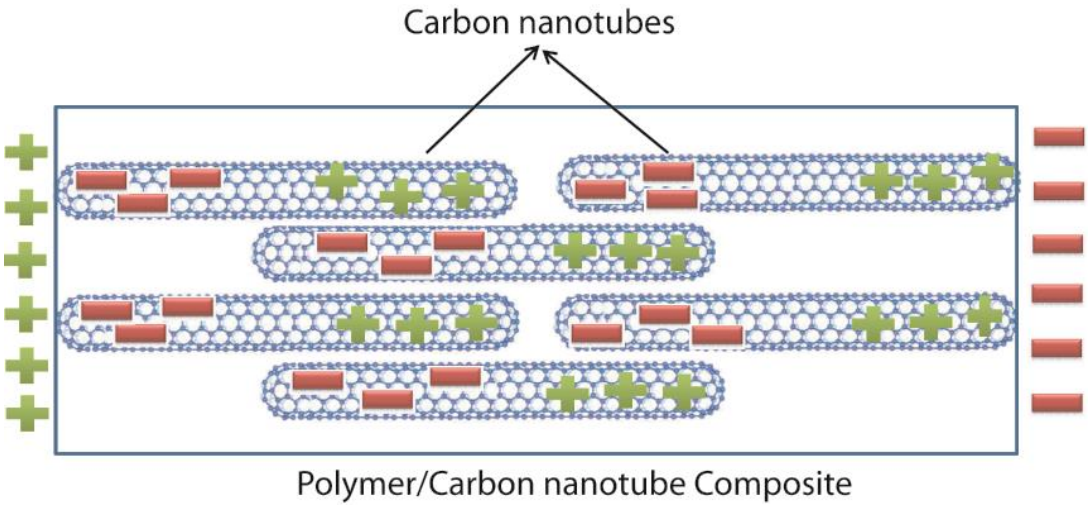

Figure 1.13 Schematic of charge storage mechanism in CPCs

Interfacial polarization in conductive nanocomposites happens when localized charge carriers overcome certain potential barriers and jump to another localized site. An increase in conductive filler loading enhances the polarization and enhanced electrical permittivity of CPCs. In addition to this is the formation of microcapacitors, which are composed of two nanofiller particles with insulating polymer in between. More microcapacitors created results in a higher real permittivity. Figure 1.13 illustrates the mechanism of the charge storage in the microcapacitors formed, due to nanofiller dispersion in a CPC.

Dielectric (permittivity) spectroscopy of materials over a wide range of frequency shows different behaviors. Varied dielectric mechanisms occur depending on the way that materials respond to the applied electric field. Figure 1.14 shows the different mechanisms involved in a material from the atomic and electronic stage, at very high frequencies, to ionic and dipolar reactions at low frequencies. The drop in real permittivity after 10^8 Hz is attributed to the polarization relaxation mechanism.

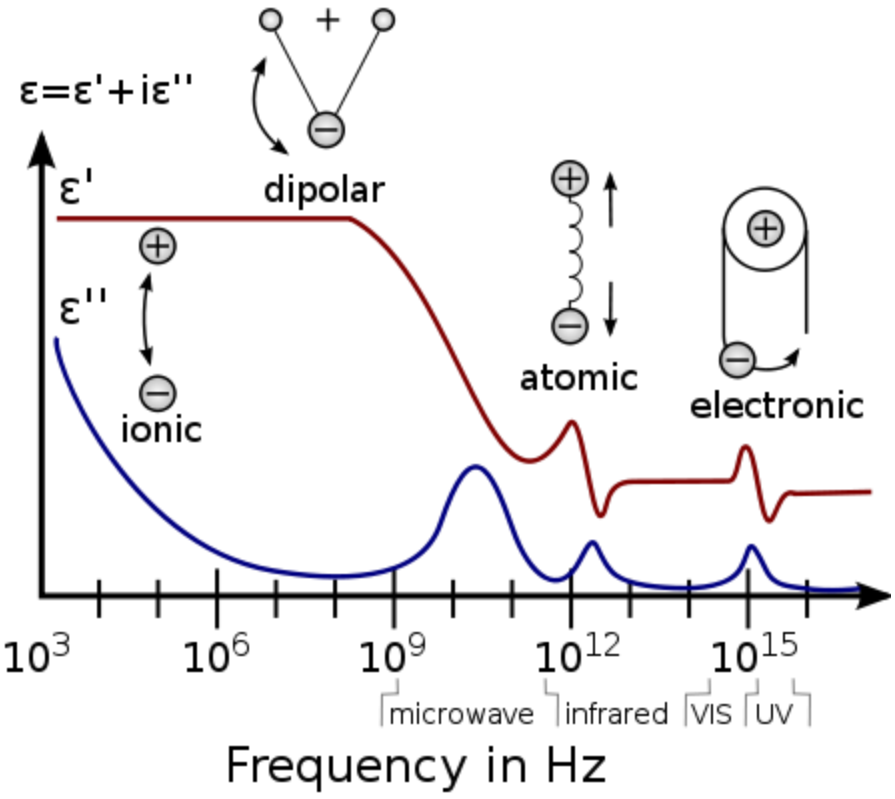

Figure 1.14 Dielectric permittivity spectrum over a wide range of frequencies [81].

1.5.4 Piezoelectric effect

Piezoelectricity indicates how much electric charge is generated in a piezoelectric material in response to an applied mechanical force (see Figure 1.15) [82]. The investigation of quartz crystal behavior by brothers, Pierre Curie and Jacques Curie, in 1880, revealed its pyroelectricity [83]. Quartz and Rochelle salt exhibited the most piezoelectricity, with the ability to generate potential differences of thousands of volts. More investigations were performed on piezoelectric materials in later years. The first practical application for these materials was sonar, developed during World War I [84]. Currently, piezoelectric materials have a wide range of industrial and

manufacturing applications, from the automotive industry to medical instruments. Sensors, high voltage sources, actuators and photovoltaic cells are the most common applications.

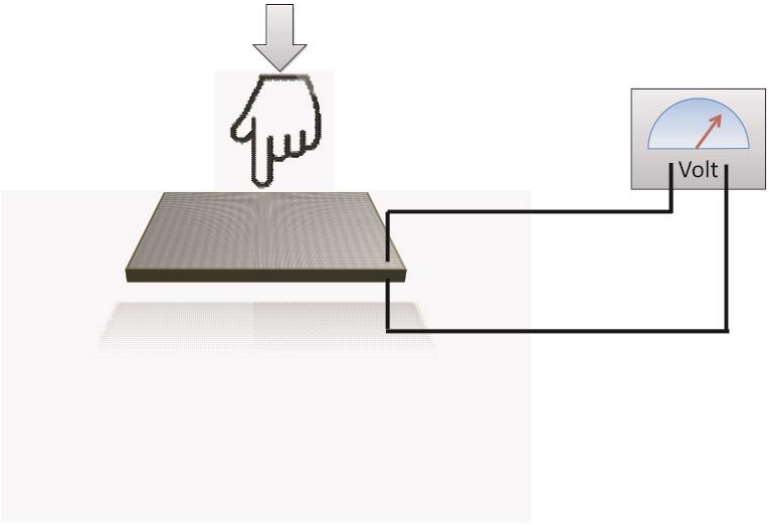

Figure 1.15 Piezoelectric fabric transforms mechanical force into electrical pulse

The physical properties of piezoelectric and pyroelectric electroactive polymers (EAPs) differ from those of conventional ceramic materials, indicating immense potential for these materials in electronic devices. EAPs revealed good flexibility and processability which is ideal for many applications requiring large and thin films and fabrics. Poly(viylidene fluoride) (PVDF), as an EAP, exhibits piezoelectricity several times greater than quartz. Long chain molecules of PVDF consist of polar segments which can attract or repel each other under an applied electric field. PVDF crystals exist in several forms of alpha, beta, and gamma phases, depending on the chain conformations as trans (T) or gauche (G) linkages. A combination of trans and gauche linkages, like alpha crystal (TGTG), leads to an overall nonpolar crystal, while a beta crystal with all gauche (GGGG) or trans (TTTT) results in a polar crystal which demonstrates piezoelectricity (see Figure 1.16). The minimum beta phase content for PVDF should be 19% to be piezoelectric.

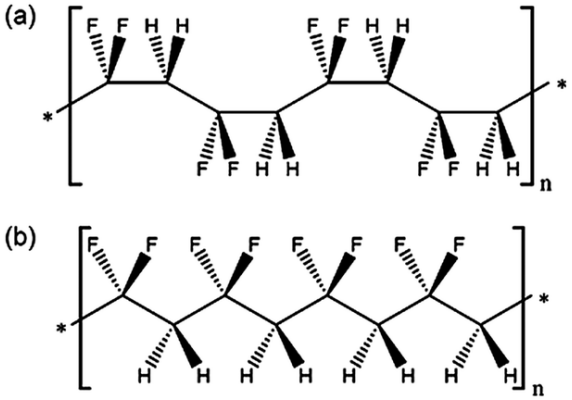

Figure 1.16 Different conformational structures of PVDF a) alpha (α) and b) beta (β) crystals [85]

Crystallography of PVDF, therefore, is a direct way to study its piezoelectric behavior. For this purpose, X-Ray diffraction (XRD), differential scanning calorimetry (DSC) and Fourier transform infra-red (FTIR) techniques were employed to study the crystalline structure and therefore, piezoelectricity of PVDF under different processing and compounding conditions [47, 86-88]. In this project, we studied the effect of processing conditions and nanofiller-polymer interaction on the formation of beta phase crystals in PVDF, as discussed in Chapters 6 and 7.

1.6 Intrinsically Conducting Polymers (ICPs) as coating layer

As mentioned earlier in section 1.5.1, one way to decrease the electrical percolation threshold in CPCs is to increase the nanofiller dispersion through coating/functionalization of nanofillers. ICPs are appropriate choices for coating of nanofillers due to their good affinity with the host polymer and the synergistic effect on electrical properties. ICPs contain free radicals, due to either packed SP^2-hybridized bonding (polypyrol and polyaniline) or conjugated π-orbitals in the entirety of the polymer chain (polyacetylene). Due to their molecular structure, ICPs are able to

conduct electrical charges and belong to the semiconductor category. These semiconducting materials are capable of EM wave attenuating via absorption and also demonstrate excellent charge storage capacity through the pseudocapacitance mechanism [89].

Coating and functionalizing of conductive nanofillers, with an insulating material, may enhance dispersion but, at the same time, dramatically decrease the electrical conductivity of nanofillers. Using ICPs helps to keep the conductivity of the nanofiller high, as well as increase the dispersion. Table 1.2 shows conductivities of some commercial ICPs. In this project, polyaniline (PANi) was used as an outstanding candidate for coating CuNWs and MWCNTs. The coating procedure and characterization of core-shell nanofillers are discussed in Chapter 3 (non-covalent coating of CuNWs) and Chapter 4 (covalent coating of MWCNTs).

Table 1.2 Electrical conductivity of some well-known ICPs

Polymer	*Chain assembly*	*Dopant*	*Conductivity (S/cm)*	*Ref.*
Polyaniline (emeraldine salt)	Aromatic cycles	HCl (pH~1-3)	10	[3]
Polyaniline (emeraldine base)	Aromatic cycles	HCl (pH~4-7)	10^{-9}	[3]
Poly(pyrrole)	Aromatic cycles	0.1 mole/dm^3 of $Fe_2(SO_4)_3$	40.7	[90]
Poly(acetylene)	Double bonds	10% of AsF_5	~200	[91]
Poly(p-phenylene vinylene)	Aromatic cycles and double bonds	AsF_5 at draw ratio of 10	50	[92]

PANi was discovered over 150 years ago [93], but since the early 1980s, it began to gain popularity as a conducting polymer with high electrical conductivity. Among ICPs and organic semiconductors, PANi has attracted attention due to its processing properties, electrical

conductivity, corrosion resistance and stability. The conductivity of PANi is tunable over a wide range of conductivity (10^{-9}-10^{1} S/cm). Chiang and MacDiarmid, in 1986 [94] demonstrated that the conductive states of PANi can be enhanced via protonic doping of the emeradine form of PANi. The three most common existing forms of PANi are leucoemeraldine (white/clear & colorless), emeraldine (green for the emeraldine salt, blue for the emeraldine base) and (per)nigraniline (blue/violet). Figure 1.17 shows the different oxidation states of PANi via doping with halogen acids. The conductivity of PANi for different oxidation states varies from 10^{-9} S/cm to 10^{1} S/cm [95].

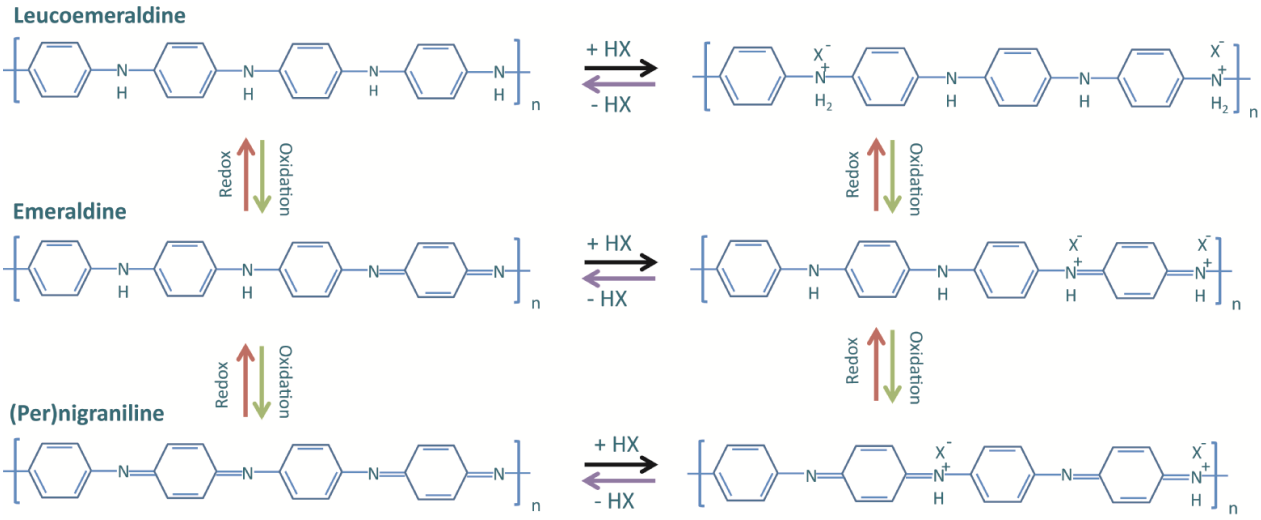

Figure 1.17 Different oxidation states of polyaniline

McDiarimid et al. [95] used a hydrochloric acid (HCl) solution as dopant and found that after 50% doping (pH~0, 1M HCI) PANi reached to its highest electrical conductivity. PANi can be synthesized via a solution polymerization of aniline in the presence of a doping agent. Though the synthetic method of polyaniline is simple, the mechanism of polymerization is complex [97]. The emeraldine base form of polyaniline contains equal numbers of reduced and oxidized repeat units and it can be doped to the metallic conducting regime (emeraldine salt) using a doping

agent such as HCl [94]. For synthesizing emeraldine salt, in this project, 1 M HCl solution was used both as a medium for polymerization and dopant. Aniline is soluble in HCl and different concentrations of solution can be prepared. PANi polymerization in HCl solution is preceded by the radicalization mechanism. To initiate the reaction, aniline by itself was not active enough; with the aid of an initiator, the reaction began. Before using aniline, however, it must be distilled to get rid of reaction inhibitors. Ammonium persulfate (APS), a strong oxidizing agent with the formula $(NH_4)_2S_2O_8$, is soluble in HCl. Both aniline and APS were dissolved in 1 M HCl in two different beakers. To initiate the reaction, the APS solution was transferred into a buret and added drop-wise (1 drop every 3 seconds) to the aniline solution. Figure 1.18 shows a schematic of the in-situ polymerization of aniline in the presence of MWCNT.

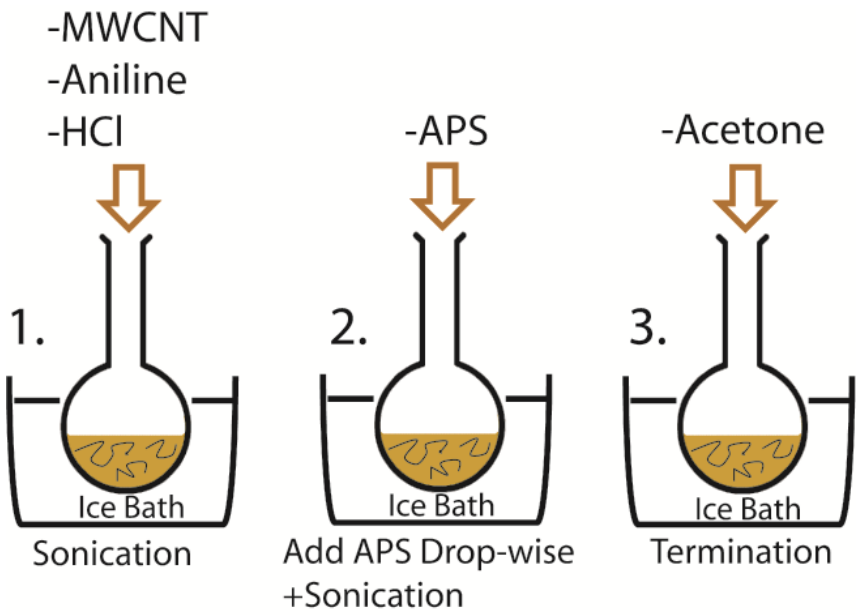

Figure 1.18 Schematic of in-situ polymerization of PANi in presence of MWCNTs

After four hours of polymerization, the reaction terminated, with acetone as a radical killer. The product was filtered and rinsed with water to remove the solvent and unreacted species, then kept overnight in the vacuum oven at 70 ºC to dry.

Due to the poor mechanical properties of PANi, usually PANi is blended with other polymers. PANi is barely soluble in organic solvents and does not mix well with other polymers via melt blending. Solution mixing and melt mixing methods, therefore, are not suitable for incorporating PANi with other polymers. An alternative method to produce PANi/polymer blends is using in-situ polymerization of aniline in the presence of the host polymer [97]. We used the in-situ polymerization method to coat MWCNTs with PANi [44]. MWCNTs prior to coating were treated in 1M HCl solution under sonication, at an elevated temperature (70 ºC). This treatment caused some defects on the MWCNTs for the PANi chains to attach themselves. Further details of the MWCNT/PANi synthesis and characterization of core-shell nanofiller are discussed in Chapter 4.

1.7 Immiscible Polymer Blends

Mixing two or more polymers should result in properties somewhere between properties of individual polymers. Polymer blends, based on their phase number and phase behavior, are classified as miscible and immiscible polymer blends. Immiscible polymer blends demonstrate interesting phase behavior with an increase in temperatures. There is critical temperature which, below and above that temperature, the miscibility of the polymer blend abruptly changes [98]. Significant changes can be observed in the linear viscoelastic properties when polymer blends are heated above the critical temperature [99]. The measured critical temperature varies with the materials used, blend composition and processing [98, 99]. Immiscible polymer blends, based on

the position of the miscibility window with respect to the critical temperature, are divided in two groups of lower critical solution temperature (LCST) and upper critical solution temperature (UCST). In LCST blends, components of a mixture are miscible for all compositions at temperatures below the critical temperature. In the UCST blends, components of a mixture are miscible for all compositions at temperatures above the critical temperature. The miscibility temperature changes with blend compositions. Figure 1.19 shows a plot of a typical polymer binary solution phase behavior, including both an LCST and a UCST.

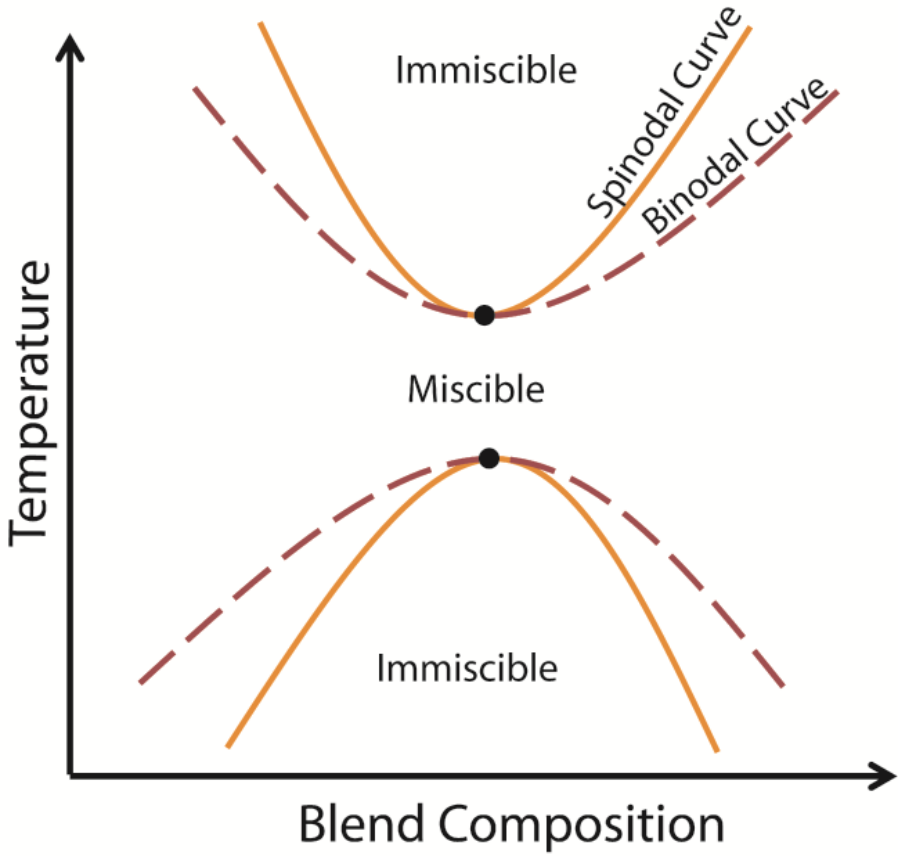

Figure 1.19 Phase diagram in LCST and UCST blends

A key physical factor which differentiates the LCST from other mixture behaviors is that the LCST phase separation is driven by an unfavorable entropy of mixing [100]. The unfavorable

entropy of mixing, responsible for phase separation behavior, has two physical bases. The first is interactions between the two components, such as strong polar interactions or hydrogen bonds, which prevent random mixing. The second is compressibility effects, especially in polymer-solvent systems [100].

Immiscible blends provide new ways to decrease the electrical percolation threshold through the double percolation phenomenon. Sumita et al. [101] first depicted this phenomenon by mixing carbon black with an immiscible blend to form a conductive filler network within a co-continuous polymer phase: the double percolation phenomenon. Conductive nanofillers are selectively dispersed in a percolated blend phase (first percolation) and form a conductive network (second percolation), which results in significantly reduced filler loading.

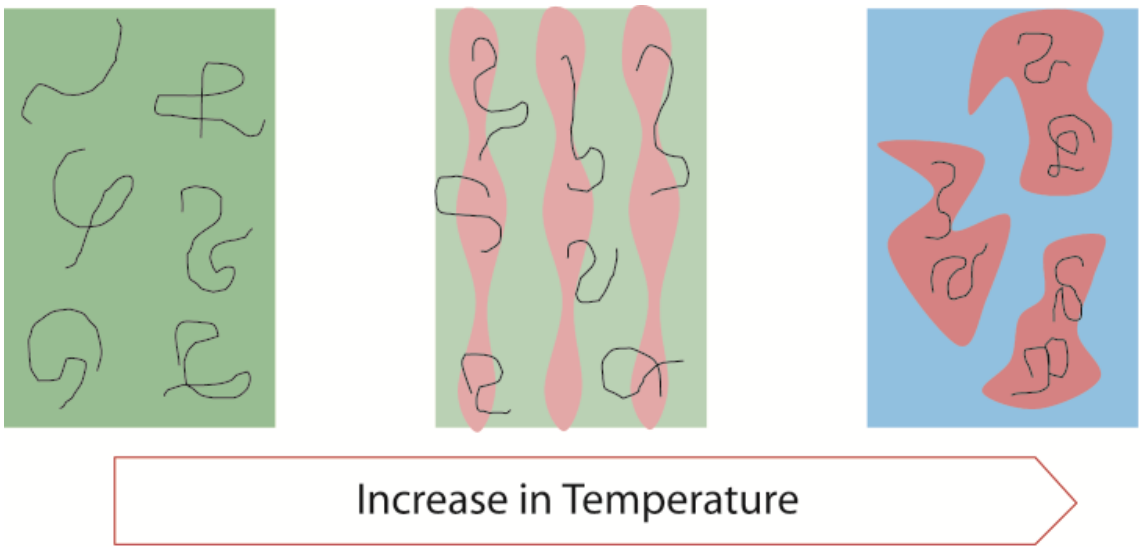

Figure 1.20 Phase separation behavior in immiscible blend containing nanofillers with preferential selectivity

In this project, the immiscible blend of poly(methyl methacrylate) (PMMA) with styrene co-acrylonitrile (SAN) is investigated (Chapter 8). MWCNT, used as conductive nanofiller and

selectively localized in the SAN phase, resulted in a significant decrease in electrical percolation (see Figure 1.20). Nanofiller localization can be controlled via nanofiller surface modification to make them more compatible with a particular phase [102].

1.8 Electrospinning

Electrospinning is a technique to fabricate micro- or nano-scale fibers. Electrospinning uses an extreme electric field to draw very fine fibres from a polymeric solution or a polymer melt. Electrospinning possesses characteristics of both electrospraying and dry spinning.

In this technique, a capillary (where the polymeric solution/melt is placed) is connected to a high power supply. It accumulated electrostatic charges and, when the electrical field was applied, the tip of the droplet outside the capillary was elongated. During the path between the capillary and the collector, the solvent evaporated. Nanofibers were produced by viscoelastic jet instabilities and deposited on the grounded collector [103-105]. Figure 1.21 shows the electrospinning apparatus, consisting of: a syringe where the solution is placed; an injection pump to adjust for a constant flow rate of the solution; an electrically conductive nozzle, connected to the syringe using proper plastic tubing (nozzle can be a needle or a coaxial nozzle); a high voltage power supply which provides a DC current and electric potential up to 30 KV; and a collector. The collector can be a high speed rotating drum, flat screen or a collector with parallel electrode. In this project, we employed a high speed drum collector (rotating speed up to 3000 rpm).

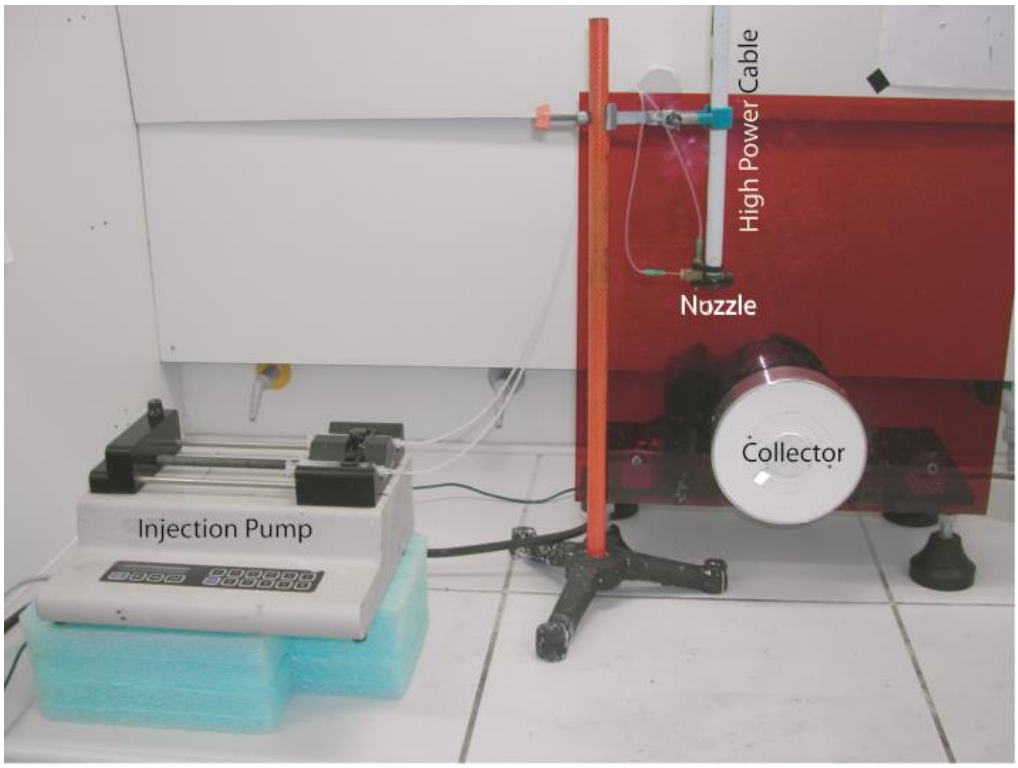

Figure 1.21 Electrospinning setup for synthesis of nanofibers

An adequately high voltage increased the accumulated charge in the body of the droplet and electrostatic repulsion overcame the surface tension of the solution. Thus, the droplet began to stretch and, at a critical point, a fluid stream erupted from the surface. The droplet, at the point of eruption, is known as the Taylor cone (see Figure 1.22) [104]. The fluid stream whips in the air as a result of electrostatic repulsion initiated at small bends in the fiber [106], dries and deposits on the ground collector. This bending instability leads to the elongation and thinning of fibers and, at the end, uniform fibers with nanometer-scale diameters are formed.[106]

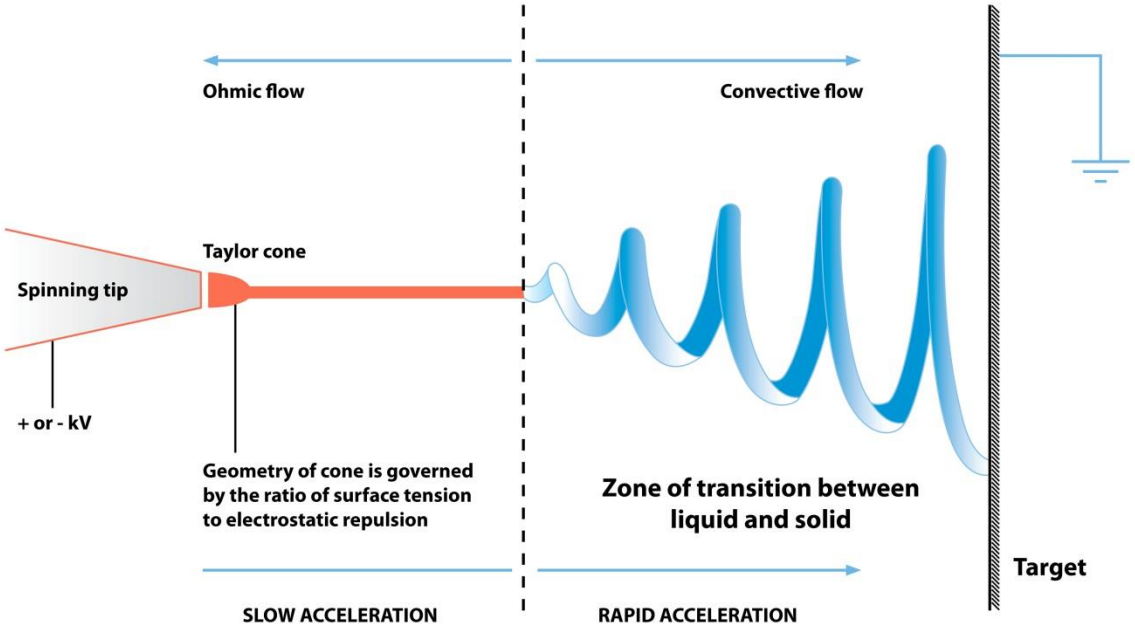

Figure 1.22 Diagram demonstrating fibre formation by electrospinning [107]

The solvent should be volatile enough that the fibers dry in the air before settling on the collector. Other processing conditions and material characteristics must be considered to get a continuous and smooth nanofiber, such as the solubility of polymer in the solvent, molecular weight and polydispersity index of the polymer, processing temperature, work distance (the distance between needle and collector), motion and the size of collector, electric potential, flow rate of the solution and polymer concentration in the solution. A low molecular weight polymer or too dilute a solution results in stream break-up due to low molecular entanglement. The polymer, therefore, must be long enough and have good solubility to achieve a stable Taylor cone and continuous fluid stream. Other parameters, such as electric potential, draw ratio and solution concentration could influence the fiber diameter. Figure 1.23 shows uniform smooth and nanofibers of PVDF.

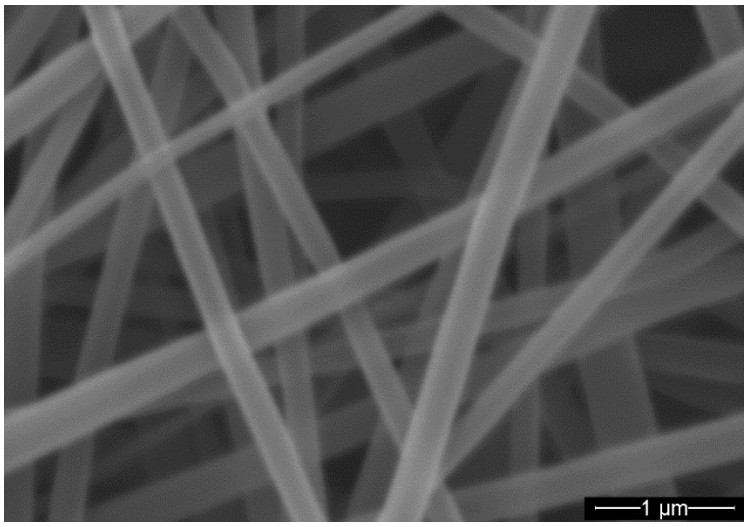

Figure 1.23 SEM image of electrospun nanofibers of poly (vinylidene fluoride)

Some polymers, due to low solubility in common solvents, cannot be electrospun. PANi, as a conducting polymer, exhibited very low solubility in common solvents. Thus, nanofibers of PANi were produced through blending with electrospinnable polymers [108, 109]. In Chapters 6 and 7 of this PhD thesis, conductive nanofibers of PVDF were fabricated. Chapter 6 discussed the effect of PANi coating on MWCNTs in electrospun nanofibers, which produced a novel conductive mat. Chapter 7 addressed the synthesis of the novel multilayer nanofibers of PVDF/PANi filled with MWCNTs, using a custom-built coaxial nozzle.

1.9 Project Motivation and Objectives

The objective of this PhD project was to synthesis conductive core-shell nanoparticles to decrease the electrical percolation threshold in CPCs. A coating layer was used to improve the dispersion of nanofillers in a polymer matrix by providing a lower interfacial energy between nanofiller and polymer matrix. The coating layer was chosen from ICPs which are conductive to

synthesis conductive core-shell nanofiller. In addition to improving dispersion, the coating layer added other properties to CPCs, which led to an enhancement in the electromagnetic interference shielding effectiveness (EMI SE) and dielectric properties of CPCs. Establishing a Lower electrical percolation threshold, as a primary objective of this PhD project, resulted in samples with better processability, lower cost and lighter weight.

Immiscible polymer blends, with co-continuous morphology, as discussed in the last chapter of this thesis, were employed as an effective way to significantly decrease the electrical percolation threshold. The selective localization of MWCNTs in the percolated phase of a co-continuous polymer blend resulted in a double-percolation phenomenon and could significantly decrease the percolation threshold of CPCs.

Core-shell nanofibers were also incorporated to PVDF nanofibers using the electrospinning technique. The miscibility/immiscibility of PVDF and PANi lead to a unique network structure in the PVDF nanofibers mat. PANi coatings were used to decrease the percolation threshold in PVDF nanofibers mat. To summarize this section, the objectives of this PhD project were:

- ✓ Synthesis of conductive CuNW-PANi core-shell nanowires for better dispersion and lower electrical percolation threshold of CuNWs in PS matrix
- ✓ Synthesis of conductive MWCNT-PANi crore-shell nanofibers for better dispersion and lower electrical percolation threshold of CuNWs in PS matrix
- ✓ Enhancement of EMI SE and dielectric in CPCs by using PANi-coated MWCNTs.
- ✓ Lower electrical percolation threshold through use of an immiscible blend (i.e. PMMA/SAN)
- ✓ Incorporation of conductive coated nanofillers into electrospun PVDF for synthesis of conductive nanofibers mat

1.9 References

[1] Premalal H, Ismail H, Baharin A. Comparison of the mechanical properties of rice husk powder filled polypropylene composites with talc filled polypropylene composites. Polymer Testing. 2002;21(7):833-9.

[2] Svoboda P, Zeng C, Wang H, Lee L, Tomasko D. Morphology and mechanical properties of polypropylene/organoclay nanocomposites. Journal of Applied Polymer Science. 2002;85(7):1562-70.

[3] MacDiarmid A. "Synthetic metals": A novel role for organic polymers (Nobel lecture). Angewandte Chemie-International Edition. 2001;40(14):2581-90.

[4] Available from: http://www.nanocyl.com/en/Products-Solutions/Sectors/Sectors

[5] Xia Y, Yang P, Sun Y, Wu Y, Mayers B, Gates B, et al. One-dimensional nanostructures: Synthesis, characterization, and applications. Advanced Materials. 2003;15(5):353-89.

[6] Gelves G, Murakami Z, Krantz M, Haber J. Multigram synthesis of copper nanowires using ac electrodeposition into porous aluminium oxide templates. Journal of Materials Chemistry. 2006;16(30):3075-83.

[7] Gelves G, Lin B, Sundararaj U, Haber J. Electrical and rheological percolation of polymer nanocomposites prepared with functionalized copper nanowires. Nanotechnology. 2008;19(21).

[8] Donnet JB, Voet A. Carbon black, physics, chemistry, and elastomer reinforcement. New York: Dekker; 1976.

[9] Huang J. Carbon black filled conducting polymers and polymer blends. Advances in Polymer Technology. 2002;21(4):299-313.

[10] Wang X, Li Q, Xie J, Jin Z, Wang J, Li Y, et al. Fabrication of Ultralong and Electrically Uniform Single-Walled Carbon Nanotubes on Clean Substrates. Nano Letters. 2009;9(9):3137-41.

[11] Iijima S. Helical Microtubules of Graphitic Carbon. Nature. 1991;354(6348):56-8.

[12] Saito R, Dresselhaus G, Dresselhaus MS. Physical Properties of Carbon Nanotubes. London: Imperial College Press; 1999.

[13] Sarvi A, Gelves G, Sundararaj U. Facile one step-synthesis and Characterisation of High Aspect Ratio Core-shell Copper-Polyaniline Nanowires. Canadian Journal of Chemical Engineering. 2014; DOI: 10.1002/cjce.21973.

[14] Available from: http://www.mvainc.com/capabilities/transmission-electron-microscopy/

[15] Dresselhaus M, Dresselhaus G, Eklund P, Saito R. Carbon nanotubes. Physics World. 1998;11(1):33-8.

[16] Dresselhaus M, Lin Y, Rabin O, Jorio A, Souza A, Pimenta M, et al. Nanowires and nanotubes. Materials Science & Engineering C-Biomimetic and Supramolecular Systems. 2003;23(1-2):129-40.

[17] Yellampalli S. Carbon Nanotubes - Polymer Nanocomposites. InTech; 2011.

[18] Thostenson E, Ren Z, Chou T. Advances in the science and technology of carbon nanotubes and their composites: a review. Composites Science and Technology. 2001;61(13):1899-912.

[19] Meo M, Rossi M. Prediction of Young's modulus of single wall carbon nanotubes by molecular-mechanics based finite element modelling. Composites Science and Technology. 2006;66(11-12):1597-605.

[20] Breuer O, Sundararaj U. Big returns from small fibers: A review of polymer/carbon nanotube composites. Polymer Composites. 2004;25(6):630-45.

[21] Yu M, Lourie O, Dyer M, Moloni K, Kelly T, Ruoff R. Strength and breaking mechanism of multiwalled carbon nanotubes under tensile load. Science. 2000;287(5453):637-40.

[22] Demczyk B, Wang Y, Cumings J, Hetman M, Han W, Zettl A, et al. Direct mechanical measurement of the tensile strength and elastic modulus of multiwalled carbon nanotubes. Materials Science and Engineering a-Structural Materials Properties Microstructure and Processing. 2002;334(1-2):173-8.

[23] Available form: https://www.assda.asn.au/technical-info/properties-of-stainless-steels

[24] Available from: http://www.goodfellow.com/E/Stainless-Steel-17-7PH.html

[25] Wagner HD. EPST. John Wiley & Sons; 2002.

[26] Ajayan P, Ebbesen T. Nanometre-size tubes of carbon. Reports on Progress in Physics. 1997;60(10):1025-62.

[27] Lau K, Hui D. The revolutionary creation of new advanced materials - carbon nanotube composites. Composites Part B-Engineering. 2002;33(4):263-77.

[28] Sinnott S, Andrews R. Carbon nanotubes: Synthesis, properties, and applications. Critical Reviews in Solid State and Materials Sciences. 2001;26(3):145-249.

[29] Chizari K, Deneuve A, Ersen O, Florea I, Liu Y, Edouard D, et al. Nitrogen-Doped Carbon Nanotubes as a Highly Active Metal-Free Catalyst for Selective Oxidation. Chemsuschem. 2012;5(1):102-8.

[30] Chizari K, Sundararaj U. The Effects of Catalyst on the Morphology and Physicochemical Properties of Nitrogen-doped Carbon Nanotubes. Materials Letters. 2014;116:289-92.

[31] Edwards BC, Ragan P. Leaving the Planet by Space Elevator. Seattle, USA: Lulu; 2006.

[32] Zhang M, Fang S, Zakhidov A, Lee S, Aliev A, Williams C, et al. Strong, transparent, multifunctional, carbon nanotube sheets. Science. 2005;309(5738):1215-9.

[33] Dalton A, Collins S, Munoz E, Razal J, Ebron V, Ferraris J, et al. Super-tough carbon-nanotube fibres - These extraordinary composite fibres can be woven into electronic textiles. Nature. 2003;423(6941):703-.

[34] Allen M, Tung V, Kaner R. Honeycomb Carbon: A Review of Graphene. Chemical Reviews. 2010;110(1):132-45.

[35] Geim A, Novoselov K. The rise of graphene. Nature Materials. 2007;6(3):183-91.

[36] Polschikov S, Nedorezova P, Klyamkina A, Kovalchuk A, Aladyshev A, Shchegolikhin A, et al. Composite materials of graphene nanoplatelets and polypropylene, prepared by in situ polymerization. Journal of Applied Polymer Science. 2013;127(2):904-11.

[37] Partoens B, Peeters F. From graphene to graphite: Electronic structure around the K point. Physical Review B. 2006;74(7).

[38] Novoselov K, Geim A, Morozov S, Jiang D, Zhang Y, Dubonos S, et al. Electric field effect in atomically thin carbon films. Science. 2004;306(5696):666-9.

[39] Morozov S, Novoselov K, Schedin F, Jiang D, Firsov A, Geim A. Two-dimensional electron and hole gases at the surface of graphite. Physical Review B. 2005;72(20).

[40] Dresselhaus M, Dresselhaus G. Intercalation compounds of graphite. Advances in Physics. 2002;51(1):1-186.

[41] Shioyama H. Cleavage of graphite to graphene. Journal of Materials Science Letters. 2001;20(6):499-500.

[42] Land T, Michely T, Behm R, Hemminger J, Comsa G. STM Investigation of Single Layer Graphite Structures Produced on Pt(111) by Hydrocarbon Decomposition. Surface Science. 1992;264(3):261-70.

[43] Nagashima A, Nuka K, Itoh H, Ichinokawa T, Oshima C, Otani S. Electronic States of Monolayer Graphite Formed on TiC(111) Surface. Surface Science. 1993;291(1-2):93-8.

[44] Sarvi A, Sundararaj U. Electrical permittivity and electrical conductivity of multiwall carbon nanotube-polyaniline (MWCNT-PANi) core-shell nanofibers and MWCNT-PANi/polystyrene composites. Macromolecular Materials & Engineering. 2014; DOI: 10.1002/mame.201300406

[45] Goldel A, Kasaliwal G, Potschke P. Selective Localization and Migration of Multiwalled Carbon Nanotubes in Blends of Polycarbonate and Poly(styrene-acrylonitrile). Macromolecular Rapid Communications. 2009;30(6):423-9.

[46] Gelves G, Al-Saleh M, Sundararaj U. Highly electrically conductive and high performance EMI shielding nanowire/polymer nanocomposites by miscible mixing and precipitation. Journal of Materials Chemistry. 2011;21(3):829-36.

[47] Sadeghi F, Sarvi A, Sundararaj U. PVDF/ Carbonnanotubes /Nanoclay Composites for Piezoelectric Aapplications, International Polymer Processing. 2014;29(1):81-87.

[48] Scurati A, Feke D, Manas-Zloczower I. Analysis of the kinetics of agglomerate erosion in simple shear flows. Chemical Engineering Science. 2005;60(23):6564-73.

[49] Ke K, Wang Y, Liu X, Cao J, Luo Y, Yang W, et al. A comparison of melt and solution mixing on the dispersion of carbon nanotubes in a poly(vinylidene fluoride) matrix. Composites Part B-Engineering. 2012;43(3):1425-32.

[50] Kasaliwal G, Pegel S, Goldel A, Potschke P, Heinrich G. Analysis of agglomerate dispersion mechanisms of multiwalled carbon nanotubes during melt mixing in polycarbonate. Polymer. 2010;51(12):2708-20.

[51] Lux F. Models Proposed to Explain the Electrical-Conductivity of Mixtures Made of Conductive and Insulating Materials. Journal of Materials Science. 1993;28(2):285-301.

[52] Weber M, Kamal M. Estimation of the volume resistivity of electrically conductive composites. Polymer Composites. 1997;18(6):711-25.

[53] Bauhofer W, Kovacs J. A review and analysis of electrical percolation in carbon nanotube polymer composites. Composites Science and Technology. 2009;69(10):1486-98.

[54] Al-Saleh M, Sundararaj U. A review of vapor grown carbon nanofiber/polymer conductive composites. Carbon. 2009;47(1):2-22.

[55] Li J, Xu J, Zhang M, Rong M. Carbon black/polystyrene composites as candidates for gas sensing materials. Carbon. 2003;41(12):2353-60.

[56] Al-Saleh M, Sundararaj U. Mechanical Properties of Carbon Black-Filled Polypropylene/Polystyrene Blends Containing Styrene-Butadiene-Styrene Copolymer. Polymer Engineering and Science. 2009;49(4):693-702.

[57] Al-Saleh M, Sundararaj U. Nanostructured carbon black filled polypropylene/polystyrene blends containing styrene-butadiene-styrene copolymer: Influence of morphology on electrical resistivity. European Polymer Journal. 2008;44(7):1931-9.

[58] Fei B, Qian B, Yang Z, Wang R, Liu W, Mak C, et al. Coating carbon nanotubes by spontaneous oxidative polymerization of dopamine. Carbon. 2008;46(13):1795-7.

[59] Dyke C, Tour J. Covalent functionalization of single-walled carbon nanotubes for materials applications. Journal of Physical Chemistry a. 2004;108(51):11151-9.

[60] Wong S, Joselevich E, Woolley A, Cheung C, Lieber C. Covalently functionalized nanotubes as nanometre-sized probes in chemistry and biology. Nature. 1998;394(6688):52-5.

[61] Gomez F, Chen R, Wang D, Waymouth R, Dai H. Ring opening metathesis polymerization on non-covalently functionalized single-walled carbon nanotubes. Chemical Communications. 2003(2):190-1.

[62] Britz D, Khlobystov A. Noncovalent interactions of molecules with single walled carbon nanotubes. Chemical Society Reviews. 2006;35(7):637-59.

[63] Chung D. Electromagnetic interference shielding effectiveness of carbon materials. Carbon. 2001;39(2):279-85.

[64] Arjmand M, Mahmoodi M, Gelves G, Park S, Sundararaj U. Electrical and electromagnetic interference shielding properties of flow-induced oriented carbon nanotubes in polycarbonate. Carbon. 2011;49(11):3430-40.

[65] Kaiser KL. Electromagnetic Shielding. Boca Raton, FL: CRC Press; 2006: 1-52.

[66] Schulz R, Plantz V, Brush D. Shielding Theory and Practice. IEEE Transactions on Electromagnetic Compatibility. 1988;30(3):187-201.

[67] Sadchikov V, Prudnikova Z. Amorphous materials in electromagnetic shields. Steel in Translation. 1997;27(4):71-5.

[68] Zhang C, Ni Q, Fu S, Kurashiki K. Electromagnetic interference shielding effect of nanocomposites with carbon nanotube and shape memory polymer. Composites Science and Technology. 2007;67(14):2973-80.

[69] Posdorfer J, Wessling B. Oxidation of copper in the presence of the organic metal polyaniline. Synthetic Metals. 2001;119(1-3):363-4.

[70] Makela T, Pienimaa S, Taka T, Jussila S, Isotalo H. Thin polyaniline films in EMI shielding. Synthetic Metals. 1997;85(1-3):1335-6.

[71] Gupta V, Miura N. Polyaniline/single-wall carbon nanotube (PANI/SWCNT) composites for high performance supercapacitors. Electrochimica Acta. 2006;52(4):1721-6.

[72] Peng C, Zhang S, Jewell D, Chen G. Carbon nanotube and conducting polymer composites for supercapacitors. Progress in Natural Science-Materials International. 2008;18(7):777-88.

[73] Chen L, Varadan VK. Microwave electronics: Measurement and Materials Characterization. John Wiley and Sons; 2004.

[74] Huang J, Virji S, Weiller B, Kaner R. Polyaniline nanofibers: Facile synthesis, chemical sensors and nanocomposites. Abstracts of Papers of the American Chemical Society. 2004;228:U445-U.

[75] Liao Y, Zhang C, Zhang Y, Strong V, Tang J, Li X, et al. Carbon Nanotube/Polyaniline Composite Nanofibers: Facile Synthesis and Chemosensors. Nano Letters. 2011;11(3):954-9.

[76] Pinto N, Acosta A, Sinha G, Aliev F. Dielectric permittivity study on weakly doped conducting polymers based on polyaniline and its derivatives. Synthetic Metals. 2000;113(1-2):77-81.

[77] Ramamurthy P, Malshe A, Harrell W, Gregory R, McGuire K, Rao A. Polyaniline/single-walled carbon nanotube composite electronic devices. Solid-State Electronics. 2004;48(10-11):2019-24.

[78] Yakuphanoglu F, Yahia I, Barim G, Senkal B. Double-walled carbon nanotube/polymer nanocomposites: Electrical properties under dc and ac fields. Synthetic Metals. 2010;160(15-16):1718-26.

[79] Lin H, Li L, Ren J, Cai Z, Qiu L, Yang Z, et al. Conducting polymer composite film incorporated with aligned carbon nanotubes for transparent, flexible and efficient supercapacitor. Scientific Reports. 2013;3.

[80] Hippel ARV, Dielectrics and Waves. Boston: Artech House; 1995.

[81] Available from: http://en.wikipedia.org/wiki/File:Dielectric_responses.svg

[82] Skoog DA, Holler FJ, Crouch SR. Principles of Instrumental Analysis. 6th ed. Cengage Learning; 2007

[83] Curie J, Curie P. Development, via Compression, of Electric Polarization in Hemihedral Crystals with Inclined Faces, Bulletin de la Société minérologique de France, 1880;3:90-3.

[84] Available from: http://en.wikipedia.org/wiki/Piezoelectricity

[85] Li L, Zhang M, Rong M, Ruan W. Studies on the transformation process of PVDF from α to β phase by stretching. RSC Adv. 2014;4:3938-43

[86] Nuriel S, Liu L, Barber A, Wagner H. Direct measurement of multiwall nanotube surface tension. Chemical Physics Letters. 2005;404(4-6):263-6.

[87] Sadeghi F, Ajji A, Carreau P. Microporous membranes obtained from polypropylene blends with superior permeability properties. Journal of Polymer Science Part B-Polymer Physics. 2008;46(2):148-57.

[88] Kim Y, White J. Melt-intercalation nanocomposites with fluorinated polymers and a correlation for nanocomposite formation. Journal of Applied Polymer Science. 2004;92(2):1061-71.

[89] Mottaghitalab V, Xi B, Spinks G, Wallace G. Polyaniline fibres containing single walled carbon nanotubes: Enhanced performance artificial muscles. Synthetic Metals. 2006;156(11-13):796-803.

[90] Kudoh Y. Properties of polypyrrole prepared by chemical polymerization using aqueous solution containing Fe-2(SO4)(3) and anionic surfactant. Synthetic Metals. 1996;79(1):17-22.

[91] Heeger A. Semiconducting and metallic polymers: The fourth generation of polymeric materials. Journal of Physical Chemistry B. 2001;105(36):8475-91.

[92] Gagnon D, Capistran J, Karasz F, Lenz R. Conductivity anisotropy in oriented Poly(p-phenylene vinylene). Polymer Bulletin. 1984;12(4):293-8.

[93] Letheby, H. "XXIX.-On the production of a blue substance by the electrolysis of sulphate of aniline". Journal of the Chemical Society. 1862; 15: 161.

[94] Chiang J, MacDiarmid A. Polyaniline - Protonic Acid Doping of the Emeraldine form to the Metallic Regime. Synthetic Metals. 1986;13(1-3):193-205.

[95] MacDiarmid A, Chiang J, Richter A, Epstein A. Polyaniline - A New Concept in Conducting Polymers. Synthetic Metals. 1987;18(1-3):285-90.

[96] Ćirić-Marjanović G. Polyaniline Nanostructures, in Nanostructured Conductive Polymers. A. Eftekhari ed. Chichester, UK: John Wiley & Sons, Ltd; 2010.

[97] Ghasemi H, Sundararaj U. Electrical properties of in situ polymerized polystyrene/polyaniline composites: The effect of feeding ratio. Synthetic Metals. 2012;162(13-14):1177-83.

[98] Charlet G, Delmas G. Thermodynamic Properties of Polyolefin Solutions at High-Temperature .1. Lower Critical Solubility Temperatures of Polyethylene, Polypropylene and Ethylene-Propylene Co-Polymers in Hydrocarbon solvents. Polymer. 1981;22(9):1181-9.

[99] Keestra B, Goossens J, Anderson P. Structure development of PMMA/SAN blends in shear flow. Chemical Engineering Science. 2011;66(21):4960-71.

[100] Sanchez IC, Stone MT. Statistical Thermodynamics of Polymer Solutions and Blends. DR Paul and CB Bucknall ed. John Wiley & Sons, Inc; 2000.

[101] Sumita M, Sakata K, Asai S, Miyasaka K, Nakagawa H. Dispersion of Fillers and the Electrical-Conductivity of Polymer Blends Filled with Carbon-Black. Polymer Bulletin. 1991;25(2):265-71.

[102] Wu D, Zhang Y, Zhang M, Yu W. Selective Localization of Multiwalled Carbon Nanotubes in Poly(epsilon-caprolactone)/Polylactide Blend. Biomacromolecules. 2009;10(2):417-24.

[103] Sarvi A, Chimello V, Silva AB, Bretas RES, Sundararaj U. Coaxial Electrospun Nanofibers of Poly(vinylidene fluoride)/Polyaniline Filled With Multi-Walled Carbon Nanotubes. Polymer Composites. 2014;35(6):1198-1203.

[104] Ramakrishna S, Fujihara K, Teo W-E, Lim T-C, Ma Z. An Introduction to Electrospinning and Nanofibers, London: World Scientific; 2005.

[105] Choi S, Jo S, Lee W, Kim Y. An electrospun poly(vinylidene fluoride) nanofibrous membrane and its battery applications. Advanced Materials. 2003;15(23):2027-32.

[106] Li D, Xia Y. Electrospinning of nanofibers: Reinventing the wheel? Advanced Materials. 2004;16(14):1151-70.

[107] Available from: http://en.wikipedia.org/wiki/File:Electrospinning_Diagram.jpg

[108] Norris I, Shaker M, Ko F, MacDiarmid A. Electrostatic fabrication of ultrafine conducting fibers: polyaniline/polyethylene oxide blends. Synthetic Metals. 2000;114(2):109-14.

[109] Pinto N, Johnson A, MacDiarmid A, Mueller C, Theofylaktos N, Robinson D, et al. Electrospun polyaniline/polyethylene oxide nanofiber field-effect transistor. Applied Physics Letters. 2003;83(20):4244-6.

Chapter 2

Materials, Processing and Characterization

The main objective of this desertion dissertation was to decrease the electrical percolation threshold in CPCs by improving the dispersion and selective localization of MWCNTs in polymer or polymer blends. This has been achieved through material selection, nanofiller coating, employing different processing methods. Characterization and properties' measurements were carried out on samples to relate nanofillers' properties and nanofiller/polymer morphology to the final properties of CPCs. This chapter complements the experimental sections of the proceeding chapters. Sample preparation methods as well as measurement and characterization techniques were discussed and presented in following sections.

2.1 Materials

Copper nanowires (CuNWs): This section presents an overview of the synthesis of 1D metal nanostructures, with an emphasis on copper nanowires (CuNWs).

Copper nanowires were synthesized using a hard template method. Porous aluminum oxide (PAO) templates were prepared by anodization of 10 × 25 cm Al templates (99.99%, Alpha Aesar) in a dilute solution of sulfuric acid (0.3 M). As shown in Figure 2.1, the preparation of a

PAO template has three steps [1]. All the aluminum plates were cleaned in 1M NaOH solution to eliminate aluminum oxide on their surface. Then the plates were immersed in an anodization tank, which was filled with 30 L of 0.3 M H2SO4 aq. The electrodes (aluminum plates) were first anodized at 25.0 V (producing a current of 1.5 A) for two hours. It is crucial to keep the solution temperature between 0-4 ºC. Temperatures above 4 ºC cause a change in the current and a change in the anodization conditions. The tanks were cooled down with the aid of three chillers, two of which circulated a mixture of water and ethylene glycol through the U-shaped heat exchanger pipes installed on the tank's walls. The third chiller circulated the acidic solution inside the tank. A marine-style propeller stirred the solution to homogenize the temperature in the entire anodization tank.

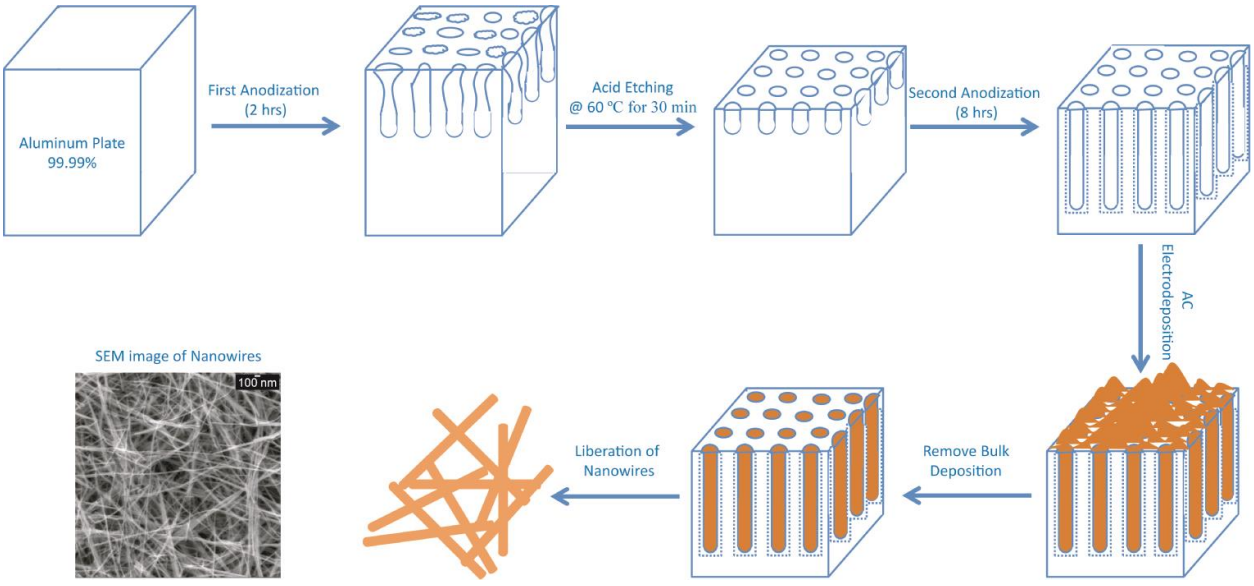

Figure 2.1 Synthesis of copper nanowires

Ten aluminum electrodes were connected parallel to the positive terminal of the Lambda LK351FM DC-power supply (0-36 VDC at 25 A); ten counter-electrodes were connected parallel to the negative terminal (see Figure 2.2). Figure 2.2 is the anodization process for making PAO which is the top section in Figure 1.2. Materials used for the counter-electrodes were either 304 stainless steel gauze (150 mesh, 0.066 mm dia., Fe:Cr:Ni; 70:19:11 wt. %) or 316 stainless steel plates (1 mm thickness, Fe:Cr:Ni:Mo; 69:18:10:3 wt. %). At the end of the first step, disordered pores were created on the surface, while at the bottom they were all organized and uniform (see Figure 2.1). To remove the disordered layer at the top of pores, Al electrodes were kept for 30 min in a 60°C mixture of 0.20 M H_2CrO_4 and 0.60 M H_3PO_4 (etching step). At the end of the etching step, the surface of the Al electrodes was covered with well-organized, uniform, but shallow, pores. The plates were rinsed with distilled water and immersed again in the anodization tank for the second anodization step. The second anodization step was conducted for eight hours under the same conditions as the first anodization to obtain deep uniform pores with a 25 nm diameter and 36 μm depth (Figure 2.1). At the end of 8 hours of anodization, a barrier layer of copper oxide (an electrically insulating layer) was formed at the bottom of the pores. The next step was to reduce the thickness of the barrier layer via the barrier layer thinning (BLT) method. The barrier layer thickness was reduced by decreasing the voltage from 25 V to 15 V, by 2 V increments every two minutes and then 1 V increments every one minute, until 9 V was reached. The potential was held at 9 V for five minutes, and then the power supply was turned off. The aluminum templates were rinsed with distilled water and dried with compressed air. At the end of this step, the porous aluminum oxide was ready for copper electrodeposition.

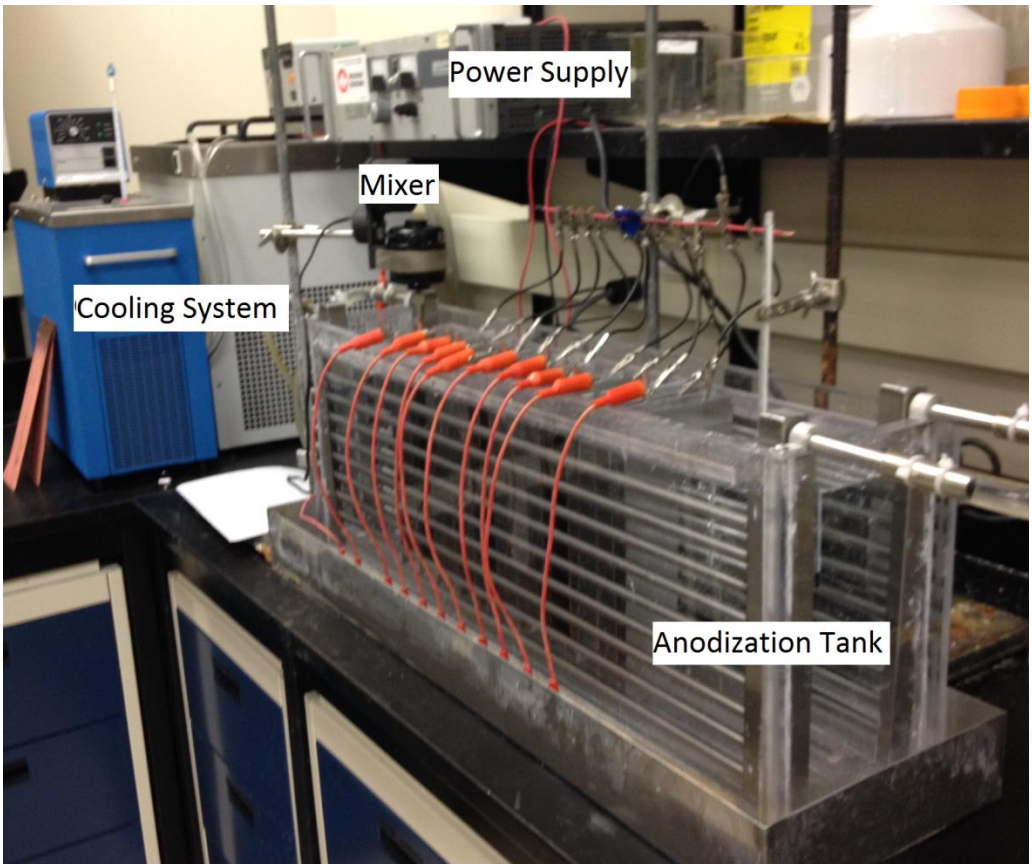

Figure 2.2 Anodization setup for synthesis of the PAO template

The edges of the aluminum plates were filled with nail polish, to avoid the irregular pores filling with copper. The copper ions were electrodeposited on the porous aluminum oxide (PAO) template pores using 200 Hz, 10 V_{rms} between the copper plates and the PAO electrodes in a copper electrolyte solution [1, 2]. A four-liter beaker, filled with a mixture of 0.50 M $CuSO_4$ and 0.285 M H_3BO_3 (aq), was used as a medium for the electrodeposition of copper. Two copper electrodes (99.999%, Alfa Aesar) were immersed in the solution and an aluminum plate was placed between them with a 2 cm distance from the counter-electrodes. The deposition signal was generated using a Kepco power supply (BOP 50-20MG DC Bipolar Power) with an output

of 0-50 V and 0-20 A. After 10 minutes of electrodeposition, the aluminum plates filled completely with copper and they became a shiny dark brown colour. The nail polish was removed using acetone after the electrodeposition was completed.

Bulk copper deposits over the surface of the plates were removed by dipping the electrode in 60 °C, 0.6 M H_3PO_4 for one minute, followed by wiping the surface with cleaning paper. Then the alumina plates were rinsed with distilled water and transferred to a 1 M NaOH solution at room temperature to liberate CuNWs. After five minutes, CuNWs were harvested through solution filtration. The nanowires were rinsed with a mixture of methanol and NaOH to remove aluminum residuals. The CuNWs were washed with methanol and filtered. These nanowires were ready to introduce into a polymer matrix directly or be modified in advance to gain desirable properties [3]. CuNWs produced using this method are 25 nm in diameter and their aspect ratio is 50-70. The aspect ratio may decrease during the mixing process by nanowires' breakage.

Multiwall Carbon Nanotube (MWCNT): The MWCNTs (NanocylTM NC7000) were obtained from Nanocyl S.A. (Sambreville, Belgium). According to the manufacturer, the MWCNTs were produced by the catalytic carbon vapor deposition (CCVD) process. Specifications of NC7000 are: average diameter: 9.5 nm, average length: 1.5 μm, surface area: 250-300 m2/g, specific gravity: 1.3-2.0 g/cm3, and electrical conductivity: 104-105 S/cm.

Polystyrene (PS): PS was used because of the excellent electrical and mechanical properties of its composites with conductive nanofillers. PS, supplied from Dow Chemical, was Americas Styrenics Styron 666D with M.I=7.5, Mw=200,000 g/mol and T_g=100˚C.

Poly(vinylidene Fluoride) (PVDF): PVDF is a fluoropolymer plastic known for its piezoelectric/pyroelectric properties. It has many applications in electronics industry, due to its low electrical conductivity, resistance to heat, and piezoelectric properties. The PVDF Kynar® Arkema Inc. with the density of 1.78 g/cm3 and melt flow rate of 1.1g/10 min (at 230 ºC/5.0 kgf) was used.

Polyaniline (PANi): Polyaniline is an intrinsically conductive polymer with many applications in electrical industries. The PANi, which has been used in Chapters 6 and 7 for making PVDF/PANi blends, were supplied from Sigma Aldrich. Emeraldine salt PANi with an average molecular weight of Mw=65000 g/mo was used

Aniline: Monomer of Aniline was employed for in-situ polymerization in the presence of MWCNTs. The method of polymerization was radicalization, with ammonium persulfate used as an initiator. The Aniline, purchased from Sigma Aldrich, was ACS reagent grade with 99.5% purity.

2.2 Sample preparation, processing and molding

2.2.1 CuNW-PANi core-shell

Based on the expectation of a good surface interaction between the imine group in PANi and copper atoms [4], we applied solution mixing to make core-shell nanoparticles. PANi, in this study, was undoped PANi supplied from Sigma Aldrich (Mw=65,000). Doped PANi with $(NH_4)_2S_2O_8$ was an oxidant and HCl/DBSA was dopant, synthesised by Dr. M. T. Cortes group's lab at Universidad de Los Andes in Colombia. After testing of several solvents, N,N-Dimethylformamide (DMF) was selected as the medium for mixing. PANi dissolves in DMF in low concentrations. CuNWs were dispersed in DMF and sonicated for 30 min. Then PANi-DMF solution was added to the CuNWs in different concentrations (PANi concentrations in DMF were 0.0061g/L, 0.018g/L, 0.0122g/L, 0.030g/L, 0.055g/L and 0.1g/L) to make core-shell nanostructures. This solution was again sonicated for 20 minutes to homogenize the coating and disperse the bundles of nanowires. Without sonication, the process resulted in inconsistent coating. Finally, samples were rinsed with extra solvent to dissolve unbounded PANis to the surface of nanowires. This core-shell nanowires was transferred to the DMF solvent for solution mixing with PS.

2.2.2 MWCNT-PANi core-shell

PANi polymer and MWCNT surfaces do not have a strong affinity for each other. Therefore, core-shell nanofibers cannot be created by solution mixing. Rather, in situ polymerization of aniline monomers, in the presence of MWCNTs, was been carried out to create core-shell

nanofibers. Aniline, prepared by Sigma Aldrich Corporation, was distilled before being used to remove the additives and inhibitors.

The MWCNTs were treated in concentrated hydrochloride acid (HCl) in a beaker under low power sonication for ten hours at 70°C. Four mmol of aniline were dissolved in 1 mole HCl. Different amounts of MWCNTs were then added to the solution, and the mixture was sonicated to disperse the MWCNTs. In another beaker, one mmol of ammonium persulfate (APS) was dissolved in 1 mole HCl. This APS solution was used as an initiator and was added drop-wise (one drop every three seconds) into the aniline/MWCNT mixture. Adding initiators through this drop ratio increases the average molecular weight of synthesized PANi which consequently enhances electrical conductivity.

The polymerization setup was kept in an ice bath under low-power sonication during the reaction. After four hours of polymerization, acetone was added to the mixture to terminate the reaction. The core-shell nanofibers were filtered, rinsed with water, and dried in a vacuum oven. Four different compositions of aniline with MWCNT were prepared: 5, 10, 15 and 20 wt% of PANi. Thermogravimetric analysis (TGA) results were in agreement with the initial composition of core-shell nanofibers.

2.2.3 CPC preparation

As explained in Chapters 4 and 5, polymer composite samples were prepared using solution mixing. The methodology is described in section 1.4. Nanofillers were dispersed in a DMF medium in a beaker. Sonication was applied for one hour to disperse nanofillers. In another beaker, PS was dissolved in DMF. The contents of the two beakers were combined, mixed and

stirred for 20 minutes. While the final mixture was under sonication, methanol, as a non-solvent for PS, was added to precipitate the polymer composites at the bottom of beaker. The polymer composite particles were collected by filtration and rinsed with extra methanol. Samples were dried in a vacuum oven for 24 hours at elevated temperatures (80 ˚C for MWCNTs and 40 ˚C for CuNWs).

In Chapter 5, MWCNT/PS composites were prepared via the melt mixing method using Alberta Polymer Asymmetric Mixer "APAM". PS granules were dry-mixed with MWCNTs, then melt-mixed in the APAM at 250 ˚C for 15 min. The rotor speed was set at 80 rpm. All solution and melt-mixed samples were preheated and compressed at 200 ˚C at 40 MPa for 20 minutes.

Immiscible polymer blend samples, filled with MWCNTs, as explained in Chapter 8, also were prepared using the melt mixing method. SAN and MWCNTs were first mixed at 260°C for an additional 10 minutes. PMMA were added and mixed for an additional10 minutes. The PMMA/SAN/MWCNT blends were molded using a hot press at 6,000 psi at different molding temperatures and then quenched to freeze the blend structure.

2.2.4 Electrospinning

The PVDF (Kynar 1000HD) was supplied by Arkema. A mixture of N,N-dimethylformamide (DMF, 99.5%, Merck) and acetone (Merck, 99.7%) was used as a solvent. The volume ratio of DMF to acetone was 3:1. Acetone was used to decrease the vapor temperature in solution. The concentration of PVDF in the solution was kept at 12 wt% [5, 6], and different amounts of MWCNT and MWCNT-PANi core-shell nanofillers were added. The solutions were sonicated for 1 hour for a good dispersion. The nanofibers were electrospun with a voltage of 20 kV and a

work distance (i.e. distance between the syringe and the collector) of 5 cm. The nanofibers were collected on a high speed rotor rotating at 2,000 rpm. The injection speed of the solutions was adjusted by 0.03 ml/min based on the solution viscosity.

To produce the blend's nanofibers, PANi was dissolved in DMF and the solution was filtered to remove non-dissolved PANi. The concentration of PANi in the solution, based on thermal gravimetric analysis (TGA) of nanofibers, was found to be ~ 8 wt%. Different amounts of MWCNTs were added to the PVDF solution; both the PVDF/PANi mixture and the solution were sonicated for 1 hour.

For coaxial electrospinning, a custom-built spinneret was employed. Two different solutions at the same flow rate (0.03 ml/min to 0.6 ml/min based on the solution viscosity) were injected into the spinneret. The voltage, work distance and solution concentration was the same as those for the simple electrospinning method.

2.3 Electrical Property Measurement

2.3.1 Electrical Conductivity

In this PhD thesis, the resistivity measurements were performed using two different setups. For a volume resistivity of more than 10^{+4} ohm·cm, a Keithley 6517A electrometer connected to a Keithley 8009 test fixture was used. For the samples with a volume resistivity of less than 10^{+4} ohm·cm, the measurements were conducted according to the ASTM 257-75 standards, using a Loresta GP resistivity meter (MCP-T610 model, Mitsubishi Chemical Co., Japan) connected with a four-pin probe. Figure 2.3 shows a schematic of electrode construction and 4-terminal

configuration for the four-point probe. In the four-terminal method, a known current is passed through the two outer probes and output voltage (V) is measured across the inner probes using a voltmeter. In Figure 2.3, r_1, r_2 and R_x represent the contact resistance, resistance of cable and resistance of sample, respectively.

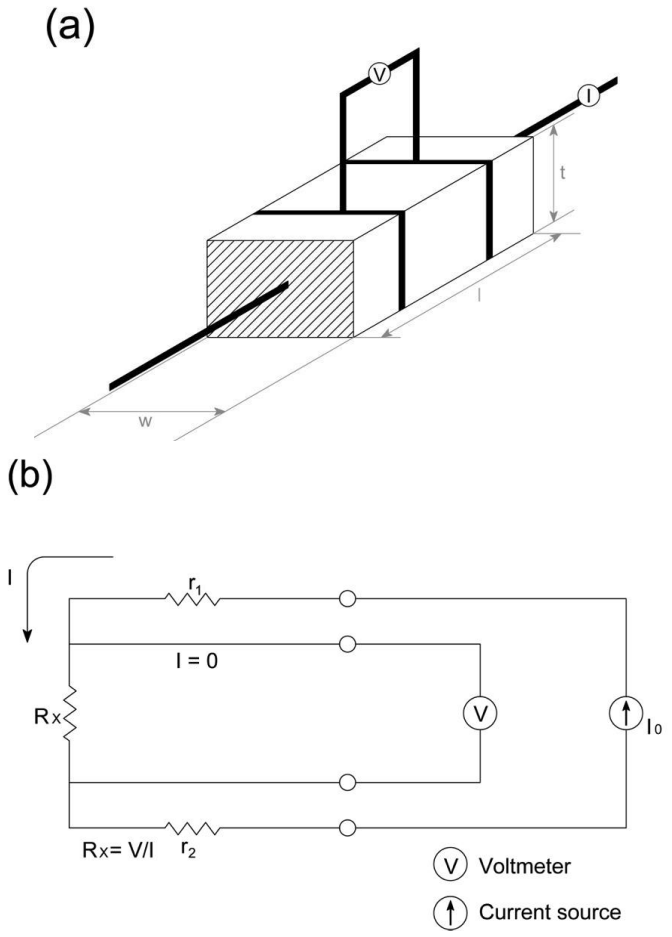

Figure 2-3 a) Electrode construction, b) equivalent circuit for 4-point probe technique [7, 8].

The applied voltage for all the resistivity measurements was 10 V. The volume resistivity can be calculated as follows:

$$\rho_v = \frac{RA}{t} \qquad 2.1$$

ρ_v: volume resistivity

R: measured resistance in ohms ($\frac{Voltage}{Current}$)

A: area of the sample

t: average thickness of the sample

In this study, we employed three different resistivity measurement machines to cover the range of volume resistivity from insulating materials to conducting materials (see Figure 2.4). Volume resistivity measurements were performed according to ASTM 257-75 standards, employing a Loresta GP resistivity meter (MCP-T610 model, Mitsubishi Chemical Co., Japan) for samples with a volume resistivity less than 10^4 Ω.cm. A four-pin probe was used so that the effect of contact resistance did not distort the measurement. To measure the volume resistivity of materials with resistivities higher than 10^4 Ω.cm, we used two different machines. A Hiresta UP resistivity meter and UR type probe were used at 100 V; and a Keithley 6517A electrometer connected to a Keithley 8009 test fixture (Keithley Instruments, USA) was used at an applied voltage of 10V.

Figure 2.4 a) Loresta GP, b) Hiresta UP and c) Keithley resistivity meter

2.3.2 Electrical Permittivity

Dielectric spectroscopy was performed using a standard electrochemical interface (1287 Potentiostat + 1260 FRA, Solartron Analytical). The samples were coated with silver paste to reduce the contact resistance. They were placed between the two keepers of the sample holder, , locked and then sandwiched between the sample holders. The signal was applied to the sample through circular electrodes located in the middle of the sample holder (diameter of 1 mm). Real and imaginary resistances of samples were measured in the frequency range of 0.1-106 Hz. Real and imaginary permittivities were calculated using the complex resistance and frequency results. The real electrical permittivity,$\varepsilon_r^{'}(\omega)$, and imaginary electrical permittivity, $\varepsilon_r^{''}(\omega)$, were calculated from impedance spectra using the following equations [8]:

$$\varepsilon_r^{'}(\omega) = \frac{1}{\omega C_0}\frac{-Z^{''}}{Z^{'2}+Z^{''2}} \quad 2.2$$

$$\varepsilon_r^{''}(\omega) = \frac{1}{\omega C_0}\frac{Z^{'}}{Z^{'2}+Z^{''2}} \quad 2.3$$

where $Z^{'}$ and $Z^{''}$are real and imaginary parts of complex resistivity, ω angular is frequency which is equal to $\omega = 2\pi f$ (f is frequency in Hertz). C_0 is constant and defined by the following equation:

$$C_0 = \varepsilon_0 \frac{S}{d} \quad 2.4$$

where S and d are the area and thickness of the sample and vacuum electrical permittivity is $\varepsilon_0 = 8.85 \times 10^{-12}\ \mathrm{F/m}$.

2.3.3 Electromagnetic Interference Shielding

The EMI shielding properties' measurements in the X-band (8.2 – 12.4 GHz) frequency range were carried out in a WR-90 rectangular waveguide, using an Agilent programmable network analyzer (PNA) (Model E8364B). Figure 2.5 shows a schematic diagram of network analyzer used to measure the EMI shielding properties. A network analyzer consists of a signal source, a receiver and a display. The source dispatches a signal at a single frequency to the material under test (MUT). The receiver is adjusted to that frequency to detect the reflected and transmitted waves from the material.

Scatter parameters, also called S-parameters, are used to calculate shielding parameters in a two-port EMI shielding setup. The S-parameters describe the performance of a two-port EMI shielding setup completely [10, 11]. The S-parameters are defined as:

| S11 |: Reflected voltage magnitude divided by the incident voltage magnitude in port 1

| S12 |: Transmitted voltage magnitude from port 2 to port 1 divided by incident voltage magnitude in port 2

| S21 |: Transmitted voltage magnitude from port 1 to port 2 divided by incident voltage magnitude in port 1

| S22 |: Reflected voltage magnitude divided by the incident voltage magnitude in port 2

The reflectance and transmittance are defined as follow:

$$R = \left|\frac{P_R}{P_I}\right| = |S_{11}|^2 = |S_{22}|^2 \quad 2.5$$

$$T = \left|\frac{P_T}{P_I}\right| = |S_{12}|^2 = |S_{21}|^2 \quad 2.6$$

where R and T are reflectance and transmittance, respectively, and P_I, P_R and P_T are incident, reflected and transmitted powers, respectively. Therefore, shielding by reflection (SE_R), absorption (SE_A) and overall shielding (SE_{Ov}) are:

$$SE_R = 10 \times log_{10}\left(\frac{1}{1-R}\right) = 10 \times log_{10}\left(\frac{1}{1-|S_{11}|^2}\right) \quad 2.7$$

$$SE_A = 10 \times log_{10}\left(\frac{1-R}{T}\right) = 10 \times log_{10}\left(\frac{1-|S_{11}|^2}{|S_{12}|^2}\right) \quad 2.8$$

$$SE_{Ov} = SE_R + SE_A \quad 2.9$$

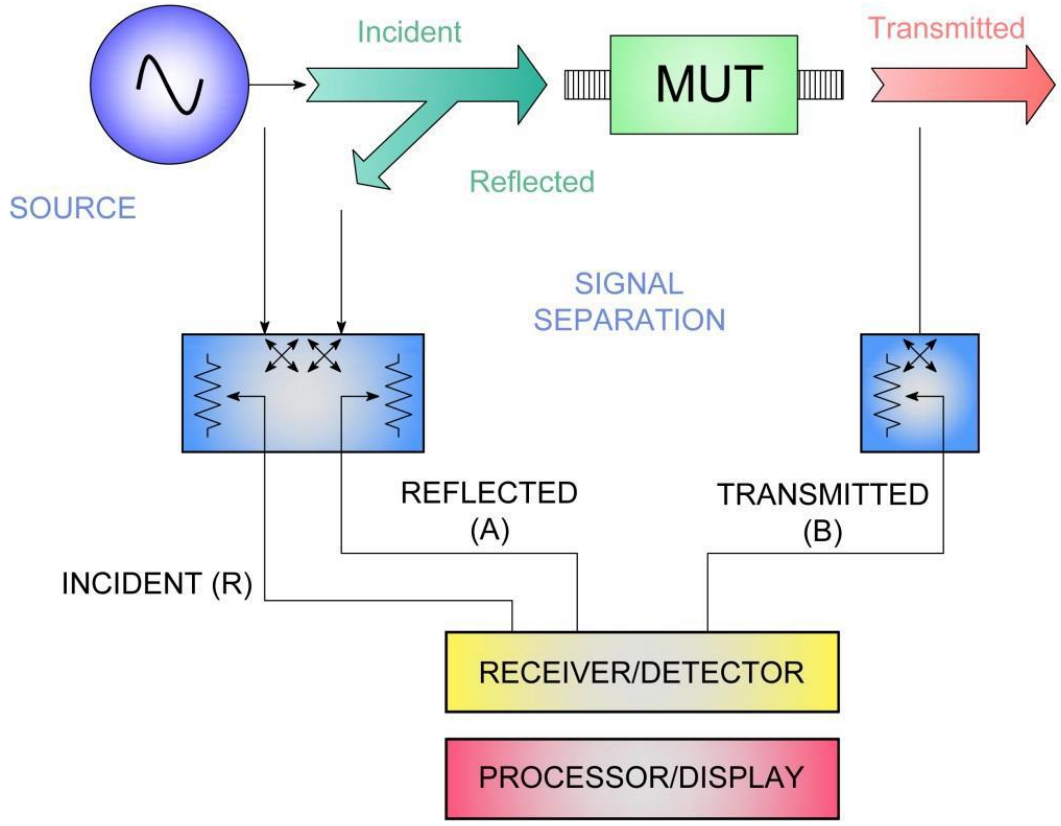

Figure 2.5 Schematic of network analyzer diagram [8, 10, and 11]

The EMI shielding measurements were carried out in the X-band (8.2–12.4 GHz), using an Agilent vector network analyzer (model 8719 ES). The sample under test was sandwiched between two X-band waveguide sections which were connected to separate ports of the vector network analyzer (VNA), and a signal was sent to the sample. The reflected and transmitted signals were measured by the VNA. The setup for the EMI SE measurement is shown in Figure 2.6.

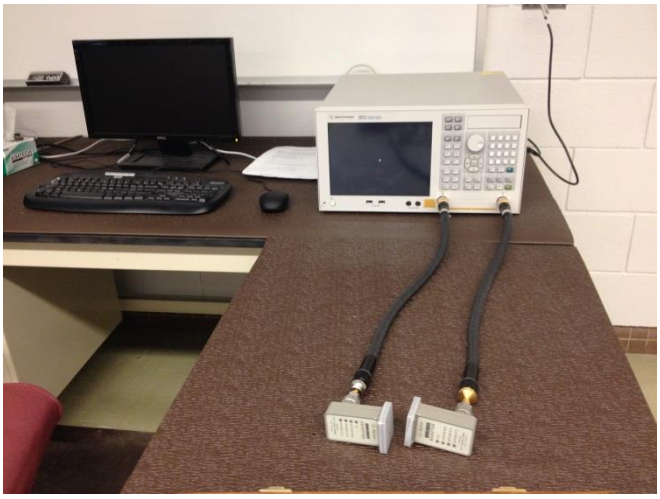

Figure 2.6 Electromagnetic interference shielding effectiveness (EMI SE) setup

2.4 Rheological Measurements

Rheological measurements were performed using a strain/stress controlled rheometer, MCR-302 Anton Paar. Disk-like samples, with a 25 mm diameter and 1 mm thickness, were placed between the cone and plate of the rheometric fixture, with a 25 mm diameter and angle of 1˚. Applied strain was set to be constant at 0.1%. Frequency sweeps from 0.1 to 300 Hz were performed to measure the loss and storage modulus. The measurement temperature was set at 250 ºC.

Loss moduli (G'') and storage moduli (G') where measured and complex moduli (G^*) where calculated using following equation:

$$G^* = \sqrt{(G')^2 + (G'')^2} \quad 2.10$$

Critical gel parameters, such as gel stiffness (S) and relaxation exponent (n), were calculated by fitting the following power-law relaxation on storage moduli in the terminal zone:

$$G'(\omega) = St^{-n} \quad 2.11$$

2.5 References

[1] Gelves G, Murakami Z, Krantz M, Haber J. Multigram synthesis of copper nanowires using ac electrodeposition into porous aluminium oxide templates. Journal of Materials Chemistry. 2006;16(30):3075-83.

[2] Gelves G, Lin B, Sundararaj U, Haber J. Electrical and rheological percolation of polymer nanocomposites prepared with functionalized copper nanowires. Nanotechnology. 2008;19(21) 215712.

[3] Sarvi A, Gelves G, Sundararaj U. Facile one step-synthesis and Characterisation of High Aspect Ratio Core-shell Copper-Polyaniline Nanowires. Canadian Journal of Chemical Engineering. 2014; DOI: 10.1002/cjce.21973.

[4] Gospodinova N, Mokreva P, Tsanov T, Terlemezyan L. A new rout to polyaniline composites. Polymer 1997;38(3):743-746.

[5] Sarvi A, Chimello V, Silva A B, Bretas R E S, Sundararaj U. Coaxial Electrospun Nanofibers of Poly(vinylidene fluoride)/Polyaniline Filled With Multi-Walled Carbon Nanotubes. Polymer Composites. 2014;35(6):1198-1203,

[6] Gasparini T M, Bretas R E S, Silva A B, Jr R G. Processing and characterization of oriented electrospun poly(vinylidene fluoride) mats. J. Polymer Science B: Polymer Physics. 2012;50:1304–1311.

[7] Instruction manual for low resistivity meter (Lorest-GP). Mitsubishi Chemical Co.; 2004.

[8] Arjmand M. Calgary, AB, Canada, University of Calgary, PhD Thesis, 2014.

[9] Hippel ARV, Dielectrics and Waves. Boston: Artech House; 1995.

[10] Basics of measuring the dielectric properties of materials. Application note; Agilent Technolgies, 2006, 1-31.

[11] Agilent network analyzer basics. Agilent Technologies, 2004, 1-94.

Chapter 3

Facile one step-synthesis and characterization of high aspect ratio core-shell copper-polyaniline nanowires[♣]

3.1 Presentation of the Article

This article presents a simple method of coating copper nanowires with polyaniline. Polyaniline helps CuNWs to disperse better in a polymer matrix which can reduce the electrical percolation threshold. Establishing a decrease in the electrical percolation threshold was an objective for this PhD project.

The first part of this article shows a simple solution mixing method for coating CuNWs with PANi. The smooth coating was achieved by sonication during mixing. Morphological and elemental characterizations were performed in the following parts of this work to study the conductivity of PANi after coating and the possible bindings between the coating layer and core metal. XPS results showed a spontaneous chemisorption process which led to a stable and uniform coating XPS results showed that the PANi's conductivity decreased due to the oxidation of PANi after a reaction with copper atoms. However, the rate of oxidation of coated CuNWs was also significantly lowered, as compared to uncoated CuNWs. In this work, the major work has been done by Ali Sarvi and Dr. Sundararaj has supervised this work. Dr. Gelves helped with result and discussion part and XPS measurments.

♣ Sarvi A, Gelves GA, Sundararaj U "Novel high aspect ratio core-shell copper-polyaniline nanowires", *CJChE*, 2013, doi:10.1002/cjce.21973.

Facile one step-synthesis and characterization of high aspect ratio core-shell copper-polyaniline nanowires

Ali Sarvi, Genaro A. Gelves, Uttandaraman Sundararaj*

Department of Chemical and Petroleum Engineering

University of Calgary, 2500 University Dr,

Calgary, Alberta, Canada T2N 1N4

3.2 Abstract

Metal nanowire/polyaniline core-shell nanoparticles have significant potential for the development of materials for electrostatical dissipation, electromagnetic interference shields, chemical and biological sensors, charge and hydrogen storage. In this study, the synthesis of novel core-shell nanostructures of polyaniline-coated copper nanowires (PANi/CuNWs) is presented. CuNWs of 25 nm in diameter and several microns in length were synthesized using hard template method and were subsequently coated with doped or undoped polyanilines to obtain high aspect ratio core-shell nanoparticles. SEM, TEM, XPS and electrical conductivity measurements were used to characterize these novel nanomaterials. TEM characterization showed a smooth polyaniline nanocoating of about 6 nm in thickness over the CuNW surface. The thickness of the coating can be controlled by changing PANi concentration in solution. XPS results indicate that spontaneous adsorption of polyaniline results from the strong surficial

interaction between copper atoms at the nanowire surface and imine groups in the polyaniline backbone.

3.3 Introduction

Polymer composites are novel materials that exhibit improved and outstanding properties versus conventional microcomposites. There is increased interest in these materials as a viable alternative to replace metals in many applications because of enhanced mechanical properties and processability, high conductivity and light-weight. Therefore, the syntheses of nanoparticles and polymer composites are being intensively studied. Different kinds of nanoparticles can be used in terms of obtaining new properties. Some of the nanoparticles that have been investigated extensively in the last decades are nanoclays, carbon nanotubes (CNTs), and more recently, graphene, and metal nanowires [1-10]. Our group has been working in the synthesis and modification of metal nanowires, and the fabrication of novel metal nanowire/polymer composites. In this work, we present the synthesis of copper nanowires coated with a thin layer of a conductive polymer by using spontaneous adsorption of PANi on the copper surface.

Recently, conductive composites with useful electrical properties at low nanofiller concentrations have been demonstrated. Among all conductive nanofillers, CNTs have been extensively investigated [7-11]. Introducing these high aspect ratio conductive nanoparticles into polymers results in the decrease of rheological and electrical percolation thresholds to very low amount of nanofillers in comparison to micron-sized spherical (carbon black), fibers, or platelet shape particles (graphite) [1, 2, 4, 6]. However, dispersion of the nanoparticles is of paramount importance in order to reach a low electrical percolation at low nanofiller concentration. Because

of high van der Waals interactions between nanoparticles, good dispersion is hard to attain without surface functionalization. In addition, a variety of processing methods and conditions have been used to get lower percolation thresholds. Another way to fabricate conductive polymer nanocomposite is by using intrinsically conductive polymers (ICPs) [8-10, 12]. One of the benefits from ICPs in conductive polymer composites is that these materials can increase EMI shielding performance of the composites by increasing the asorption mechanism [13-17]. However, ICPs do not melt before they decompose, they are hardly processable, and they are hard to disperse in other more processable polymers. These factors lead to electrical percolation of ICP composites at higher concentrations than those attained for high-aspect ratio nanofillers like carbon nanotubes and metal nanowires.

Previous literature using CuNWs as conductive nanoparticles in polymer composites has demonstrated excellent electrical properties in terms of EMI shielding [1-5]. These high aspect ratio nanoparticles form electrically conductive networks in concentrations lower than one volume percent [1-5]. Higher electrical conductivity in nanowire composites make CuNWs a good alternative for CNTs. Our group recently reported highly electrically conductive CuNW/PS composites prepared by a novel method named miscible solvent mixing and precipitation (MSMP) [1]. The conductivity for composites with concentrations of about 2 vol. % was reported to reach extremely high values of up to 10^4 S/m, which is higher than conductivity for CNT composites reported in the literature. Also, thin films of 200 micron thickness of these composites with only 1.8 vol. % of copper nanowires exhibited EMI SE of more than 40 dB, which is of interest for commercial purposes and never attained to date using carbon nanotubes.

The two main EMI shielding mechanisms of conductive nanocomposite are absorption and reflection of EM waves. A third mechanism of shielding that is considered significant for concentrated or thick samples is commonly known as multiple-reflections and represents internal reflections within the conductive composite [18-21]. Copper nanowires have the ability to reflect electromagnetic waves, but aggregation of nanowires after their synthesis and oxidation of copper can lead to an increase in percolation threshold and a dramatic decrease in the conductivity of the composites [22]. In this study, CuNWs were coated with an intrinsically conductive polymer (ICP). ICP-coated copper nanowires are expected to exhibit increased dispersion in polymers, decreased nanowire oxidation as the ICP can act as a protective layer, decreased electrical percolation threshold of the composites and most importantly, increased EMI shielding of the composites by increasing the amount of absorption of electromagnetic radiation. Among all the ICPs, polyaniline (PANi) is an outstanding candidate for application as electrode materials in batteries, supercapacitors, electrochemical sensors, and hydrogen storage materials, due to its good environmental stability and controllable electrical conductivity over a wide range through protonation and charge-transfer doping [14, 15]. These core-shell materials have potential for applications in chemical vapor sensors, biosensors, and static dissipative materials. Higher conductivity of these nanoparticles in comparison to pure PANi may offer a good opportunity to be used as conductive inks. The high electrical permittivity of PANi also make it a promising material to replace inorganic materials in supercapacitors and embedded capacitors in electronic circuit boards [23].

Coating of copper with PANi has been investigated in macroscale and in micron scale in the literature. Chen et al. [24] coated fine copper powders with PANi using in-situ polymerization method and using different kind of surfactants. They found that better core-shell

structure composite can only be generated if copper is pretreated by oxidation. Vera et al. [25] demonstrated that PANi polymer coating can protect copper against corrosion. PANi is well known to be an air-stable but unprocessable conducting polymer. Several research groups have attempted to increase the processability of PANi by various methods such as mixing with another processable polymer, and in-situ polymerization in presence of other polymer micro-particles or polymer latex [17, 26- 29]. All these methods to improve processability of PANi lead to a composite with lower conductivity than pure polymer and high electrical percolation thresholds, typically higher than 10 vol.%. High aspect ratio core-shell CuNW-PANi nanowires are a very good alternative that can yield conductive composites with low electrical percolation thresholds.

In this study, we demonstrate that core-shell CuNW-PANi nanowires can be synthesized using a simple and reproducible approach by spontaneous chemisorption of PANi on copper surface. The layer thickness of PANi on the surface of nanowires of 25 nm in diameter was controlled from 5 to 20 nanometers by using different concentrations of PANi in solution.

3.4 Experimental Section

3.4.1 Synthesis of copper nanowires.

Copper nanowires were synthesized using hard template method. Porous aluminum oxide (PAO) templates were prepared by anodization of Al templates (99.99%) in dilute solution of sulfuric acid. The copper nanowires were electrodeposited on PAOs using 200Hz, 10 V_{rms} sine wave between copper plates and PAO electrodes in a copper electrolyte solution and this method is described elsewhere [6]. Then alumina plates were transferred to NaOH solution (1M) to liberate

CuNWs. After rinsing with methanol and filtration, these nanowires are ready to introduce into a polymer matrix directly or to be modified first before addition to polymer.

3.4.2 Synthesis of core-shell CuNW-PANi nanostructures

Based on the expectation of a good surface interaction between imine group in PANi and copper atoms [27], we applied solution mixing to make core-shell nanoparticles. PANi in this study was undoped PANi supplied from Sigma Aldrich (Mw=65,000) and doped PANi with (NH4)2S2O8 as an oxidant and HCl/DBSA as a dopant, synthesised by Dr. M. T. Cortes group's lab at Universidad de Los Andes in Colombia. After testing of several solvents, N,N-Dimethylformamide (DMF) was selected as the medium for mixing. PANi dissolves in DMF in low concentrations. CuNWs were dispersed in DMF and sonicated for 30 min. Then PANi-DMF solution was added to the CuNWs in different concentrations (PANi concentrations in DMF were 0.0061g/L, 0.018g/L, 0.0122g/L, 0.030g/L, 0.055g/L and 0.1g/L) to make core-shell nanostructures. This solution was again sonicated for 20 min to homogenize the coating and disperse the bundles of nanowires. Without sonication, the process resulted in inconsistent coating. Finally, samples were rinsed with extra solvent to dissolve unbounded PANi's to the surface of nanowires.

3.4.3 Morphological and Elemental Characterization

For all characterizations, the samples were vigorously rinsed several times with DMF to remove excess PANi which did not absorb to the surface of nanowires before testing. Scanning and transmission electron microscopy (SEM and TEM) were used to investigate the morphology of

the nanostructures. Samples were prepared by placing drops of a suspension of core-shell nanoparticles in DMF on Al stubs for SEM and on carbon grids for TEM imaging. A high resolution Philips XL30 was used at 20 kV to obtain SEM images. TEM images were obtained at 60 kV using a Hitachi H-7650.

X-ray photoelectron spectroscopy (XPS) was carried out in PHI VersaProbe 5000-XPS. The spectra were taken using monochromatic Al source, 1486.6 eV, at 49.3 W and beam diameter of 200.0 μm. The samples were pressed on double sided tape and underwent double neutralization. For each sample, a high sensitivity mode spectrum was taken with a wide binding energy range of 0-1,350 eV (survey) to determine the surface elemental composition of the samples. After determination of which elements are present in the sample, a narrower binding energy window, pass energy of 23.50 eV, was used to get high energy resolution spectra of the elements present in the sample to determine its chemical environment.

3.5 Results and Discussions

Characterization of core-shell nanostructures by transmission electron microscopy (TEM) and scanning electron microscopy (SEM) provided accurate information about the thickness of coating and size distribution of nanowire bundles. Figure 3.1 shows SEM images of CuNW/PANi nanostructures prepared with different concentrations of PANi in solution. The images show increased agglomeration and coating of CuNWs with increase in concentration of PANi. We found that the excess of PANi (that was not adsorbed on the CuNW surface) could be removed easily by rinsing with DMF. The PANi that is absorbed on the CuNW surface resulted in a smooth coating over the range of concentrations of PANi studied. We found that using 0.030

g/L concentration of PANi in DMF resulted in core-shell nanostructures with less agglomeration and less excess of PANi, giving smoother ICP coating on the nanowire surface.

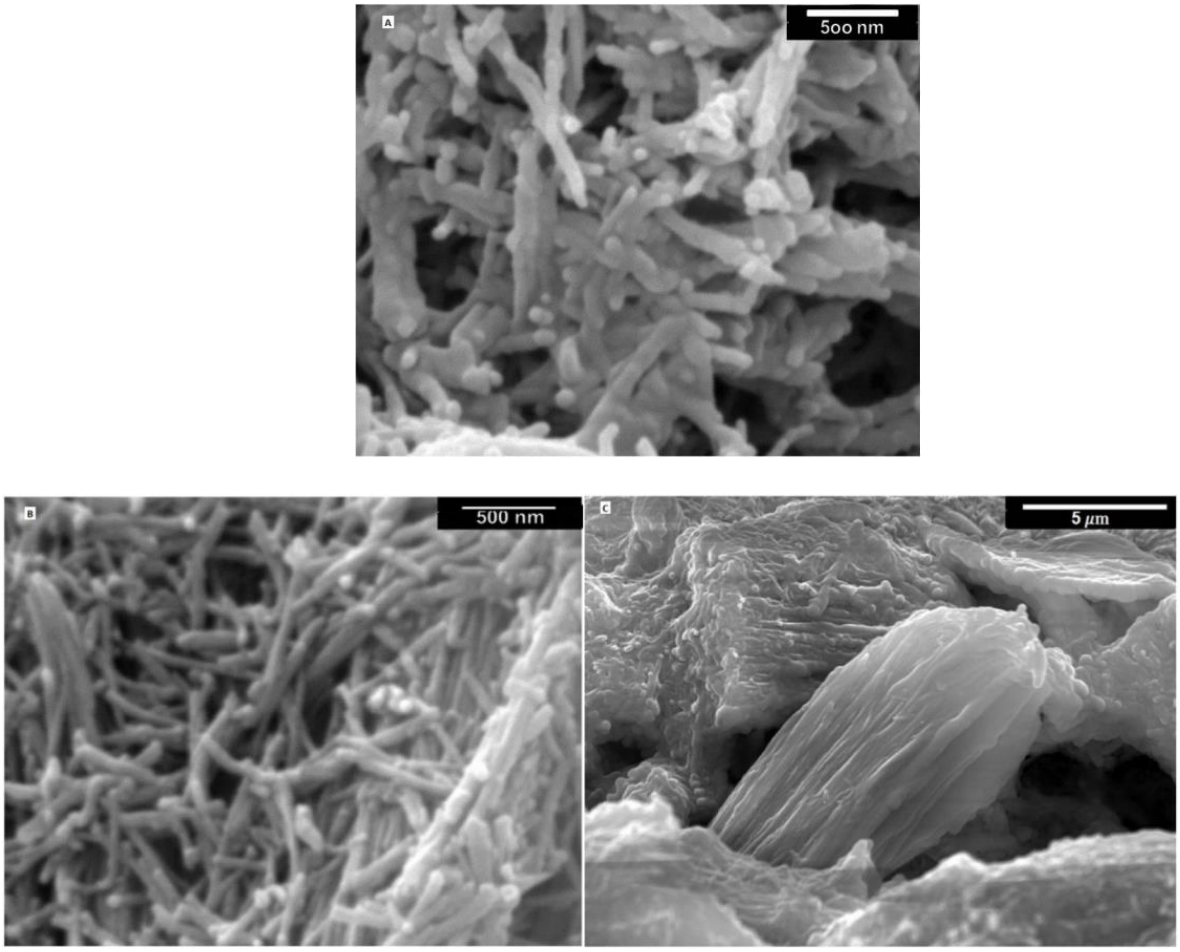

Figure 3.1 SEM images of CuNW-PANi core-shell nanoparticles A) 0.030g/L concentration of PANi B) 0.055g/L concentration of PANi C) 0.1g/L concentration of PANi

TEM images in Figure 3.2 show that there is a uniform coating over the surface of nanowires. TEM observations also indicate that the coating thickness changes with the concentration of PANi in solution and measurements of the thickness were carried out with image analysis. The coating thickness obtained from TEM characterization of core-shell

nanoparticles as a function of PANi concentration is presented in Figure 3.3. The coating thickness for 0.030g/L concentration of PANi is about 17 nm. As the amount of PANi increases, the excess of PANi could be removed by rinsing with solvent. Using less PANi than 0.030g/L resulted in thinner coating thickness. The coating on the nanowire surface indicated that there is an interaction between surficial copper atoms and PANi macromolecules. Theoretical calculation of expected coating thickness based on sample composition and their densities is in good agreement with experimental data. Using weight of components and their densities, shell volume and thickness were calculated.

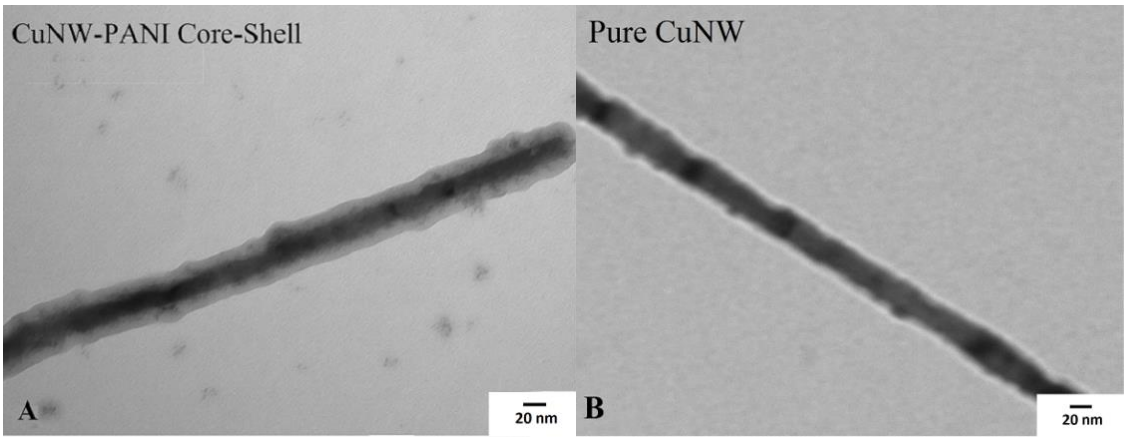

Figure 3.2 TEM images of CuNW-PANi core-shell nanostructures (A) and pristine CuNWs (B). The core-shell nanoparticles were synthesized using 0.030 g/L PANi concentration in DMF.

Assuming DMF is a theta solvent for PANi, PANi macromolecules in dilute solutions will be coils with radius of gyration of about 30 nm. If there is no strong interaction between copper atoms and PANi, polymer molecules will lay on the surface of CuNWs in low energy state (free chain coil). In this state, the thickness of coating in low concentrations will approach the radius of gyration. Interestingly, TEM images for low PANi concentration in the solution

indicated that the thickness of coating is much smaller than the radius of gyration of PANi macromolecules. Thus, if the surface of CuNW strongly absorbs PANi chains, they will orient parallel to the surface, leading to lower coating thickness as illustrated in Figure 3.4. In concentrated solutions, a higher density of macromolecules near the nanowire surface does not allow each macromolecule to completely interact with the Cu surface. Therefore, several polymer chains can simultaneously interact with the nanowire surface and each macromolecule will have sections on the nanowire surface with the rest of the chain extending from the surface in random coil shape leading to thicker coating.

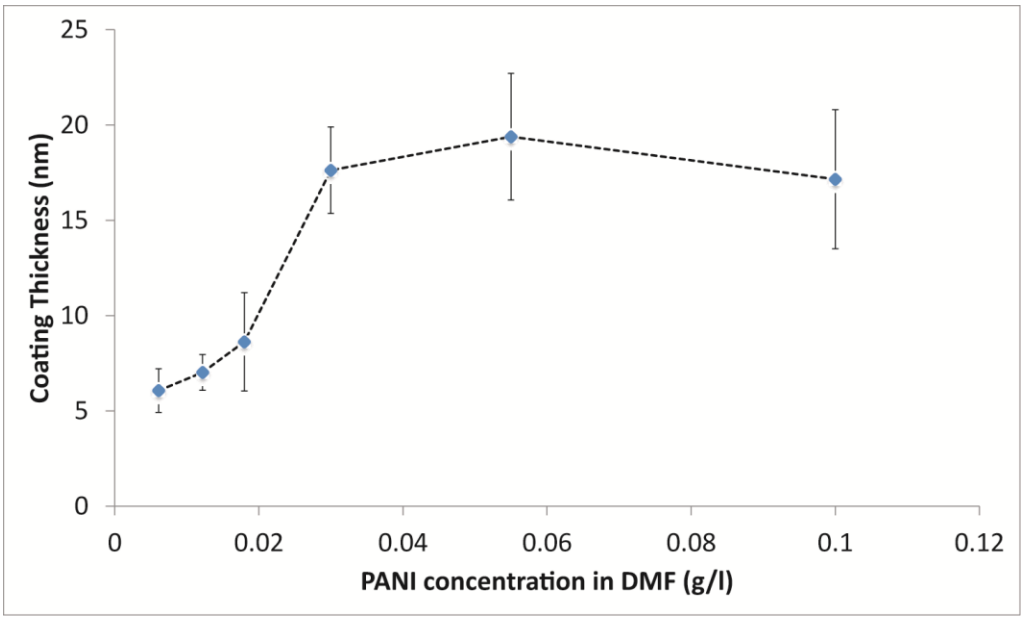

Figure 3.3 Coating thickness of CuNW/PANi core-shell nanoparticles as a function of PANi concentration in solution.

To study the surface interaction between CuNW and PANi layer, XPS characterization was carried out. The XPS results are presented in Figure 3.5 and the respective binding energies of interest in this study are provided in Table 3.1. The XPS Cu $2p_{3/2}$ spectra show a main peak for CuNW/PANi, CuNW/DMF and CuNW/MeOH respectively at BEs 932.5, 932.7 and 932.05

eV. Lim et al [30] reported that this peak at the initial stages of Cu deposition over the PANi film is 932.8 eV, which by increasing Cu coverage reaches 932.6 eV. Based on XPS results, it can be proposed that the imine sites of PANi interact preferentially with copper atoms. The Cu LMM spectra for CuNWs shows the most intense peak at 569.5 eV, which corresponds to a thin Cu_2O layer obtained after nanowire synthesis [6]. The shapes of the high resolution CuLMM spectra remained the same for the core-shell nanowires, which suggest that further oxidation of the nanowires did not occur during the synthesis of the core-shell nanoparticles in DMF. As expected, the CuLMM spectra showed a shift to higher BE associated to the adsorption of PANi on the nanowire surface.

Table 3.1 Binding energies obtained from XPS analysis in this work for various copper and nitrogen containing species

Chemical component	Cu $2p_{3/2}$ (eV)	N 1S (eV)	
		-NH-	-N=
CuNW/PANI	932.4	398.3	399.0
CuNW/DMF	932.7	398.9	398.1
CuNW/Me(OH)	932.0	-	-
PANI	-	400.2	399.1

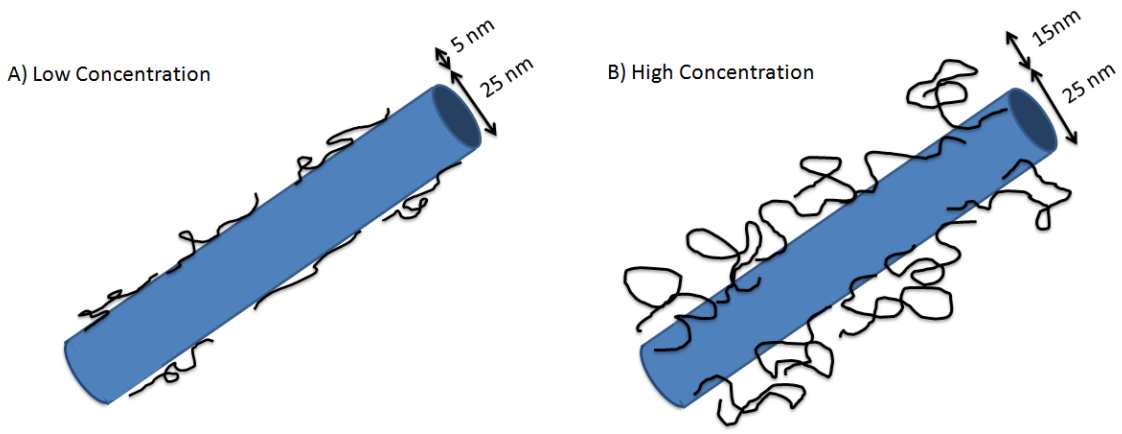

Figure 3.4 Scheme of polyaniline coating on CuNWs at (A) low and (B) high concentration of PANi in solution.

Figure 3.5 shows the XPS survey for the samples. As this graph indicates, there is some evidence of CuO and Cu_2O formation. Oxygen and Carbon peaks are related to copper oxide layer and PANi, respectively. As the plot shows the intensity of peaks are much smaller for the core-shell sample compared with uncoated copper nanowires. Therefore, the XPS results show that the PANi layer cannot stop oxidation but it can reduce the rate of growth in oxide layer. Posdorfer and Wessling [22] immersed copper foils in water dispersion of polyaniline. They measured the change in the thickness of oxidizing layer with time using electrochemical reduction experiments. They found that the PANi treated Cu surface shows an exponential decrease in Cu_2O layer.

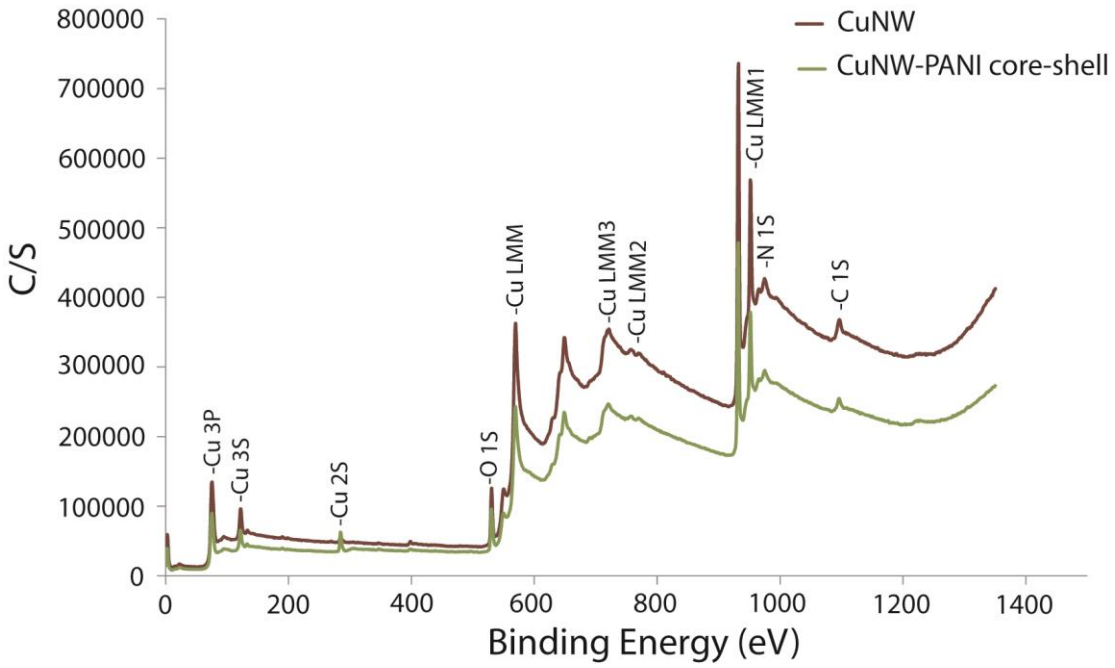

Figure 3.5 XPS survey for CuNW/PANi core-shell nanoparticles and CuNW suspension in DMF

The high resolution N1S spectrum for CuNW/PANi shows a shift to higher BE (from BE 398.4 to 399.6 eV) compared with pure CuNW without exposure to PANi in the solvent, which indicates there is a surface interaction between quinonoid imine group (=N- structure) in PANi and copper atoms. This interaction increases the amount of benzoid amine (-NH- structure) and decreases the oxidation state of the polymer backbone. Therefore, doped PANi loses some of its conductivity in presence of copper atoms. Lim et al [29] showed that Cu atoms predominantly affect the imine sites along the conjugated backbone of the polymer. They also observed that the intrinsic oxidation state of PANi film decreases with Cu coverage, approximately proportional to Cu coverage. The Auger spectrum in Figure 3.6b shows a shift to higher BEs for CuNW/PANi and CuNW/DMF in comparison to CuNW/MeOH. Both DMF and PANi have nitrogen atoms in their structure, which have two free electrons that can interact with the electrons in the d-orbitals

of copper atoms. Thus, these samples shift to higher BEs. These shifts indicate that there is a predominant interaction between nitrogen sites of the conjugated backbone and surficial copper atoms in the nanowires. Based on XPS results of these core-shell nanostructures, a decrease in oxidation state of doped PANi in presence of copper was observed. Shift in the peaks for sample of CuNW/PANi in N1S spectra indicate that there is charge transfer between Cu atoms and =N- sites which decreases the level of oxidation of PANi [30-32]. Also we can infer that Cu atoms interact strongly with imine sites of the polymer resulting in a strongly bound shell.

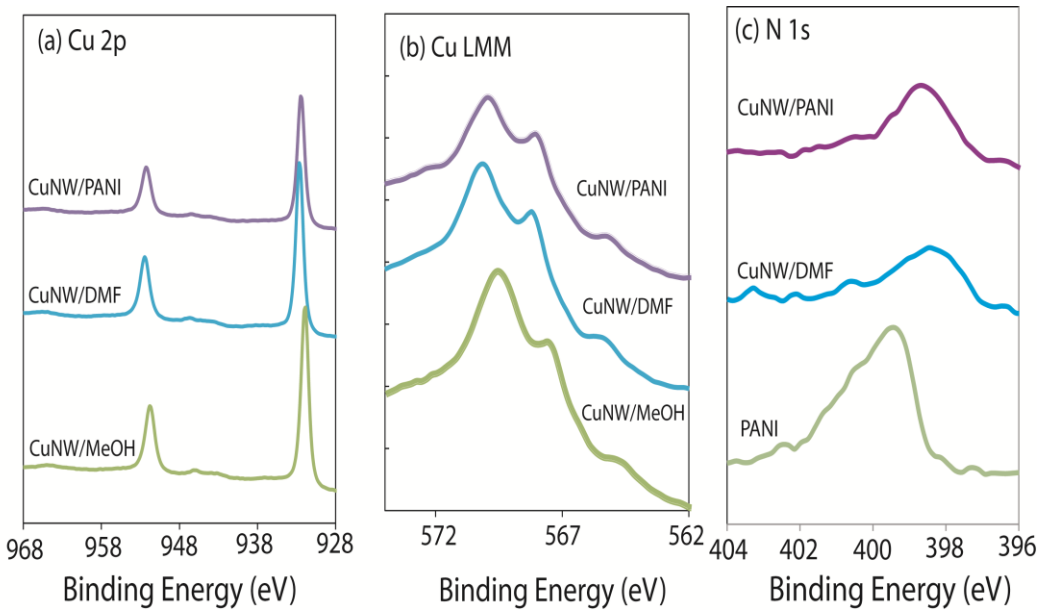

Figure 3.6 (a) Cu 2p3/2 XPS, (b) Cu LMM Auger, and (c) N 1S XPS spectra of CuNW/PANi core-shell nanoparticles, pure PANi, and CuNW obtained after evaporation of suspensions in DMF and Me(OH)

Table 3.2 Coating thickness and conductivity of CuNW/PANi core-shell nanoparticles

PANI* concentration in DMF (g/L)	Coating Thickness (nm)	Conductivity (S/cm)
0	0	9.09E-02
0.006	6.07	1.67E-06
0.012	7.026	5.98E-06
0.018	8.63	6.80E-06
0.030	17.63	3.15E-07

* Conductivity of doped PANI is 0.383 S/cm

Electrical conductivity measurements of core-shell nanoparticles at room temperature were carried out. Table 3.2 shows the electrical conductivity of core-shell nanostructures with different coating thicknesses of PANi (conductivity of PANi is 0.383 S/cm). The results in Table 3.2 show that the increase in PANi concentration in the solution leads to an increase in the coating thickness but a decrease in the electrical conductivity. These core-shell nanostructures show a lower conductivity than pure doped PANi and this result agrees with XPS observations that indicate a decrease in oxidation state of PANi backbone in presence of Cu atoms, which leads to decrease in conductivity of nanostructures. The electrical conductivity of the nanostructures can be improved by changing the oxidation state of shell layer with an acid-base treatment [31]. Also the fully reduced leucoemeraldine coating can be obtained by treating the emeraldine base film with phenylhydrazine, according to the method of Green and Woodhead [33]. These subjects are currently under investigation.

3.6 Conclusions

High aspect ratio CuNW-PANi core-shell nanostructures were successfully synthesized by a simple and reproducible technique. A stable and uniform PANi coating over the surface of 25 nm diameter CuNW has been demonstrated with PANi thickness ranging between 6 to 18 nm controlled using different concentration of PANi. Thin coating layer of PANi did not have a significant effect on the aspect ratio of original nanowires. XPS characterization of core-shell nanoparticles indicated a spontaneous chemisorption of the coating of polyaniline on the nanowires resulting from the interaction between the imine groups in PANi and the surficial copper atoms. The results also indicate that the level of oxidation of PANi layer decreases after coating of copper nanowires, which led to a decrease in electrical conductivity of core-shell nanowires.

3.7 References

[1] Gelves, G.A.; Al-Saleh, M.; Sundararaj, U. *Journal of Materials Chemistry* **2011,** 21,829.

[2] Gelves, G.A.; Sundararaj, U.; Haber, J. *Macromolecular Rapid Communications* **2005,** 26, 1677.

[3] Lin, B.; Gelves, G.A.; Haber, J.; Sundararaj, U. *Industrial & Engineering ChemistryResearch* **2007,** 46, 2481.

[4] Gelves, G.A.; Lin, B.; Sundararaj, U.; Haber, J. *Advanced Functional Materials* **2006,** 16, 2423.

[5] Gelves, G.A.; Lin, B.; Sundararaj, U.; Haber, J. *Nanotechnology* **2008,** 19, 12.

[6] Gelves, G.A.; Murakami, Z.; Krantz, M.; Haber, J. *Journal of Materials Chemistry* **2006,** 16, 3075.

[7] Li, X.; Wang, G.; Li, X.; Lu, D. *Applied Surface Science* **2004,** 229, 395.

[8] Zhou, Y.; Qin, Z.; Li, L.; Zhang, Y.; Wei, Y.; Wang, L.; Zhu, M. *Electrochimica Acta* **2010,** 55, 3904.

[9] Dong, B.; He, B.; Xu, C.; Li, H. *Medecine Et Maladies Infectieuses* **2007,** 37, 7.

[10] Wu, T.; Lin, Y. *Polymer* **2006,** 47, 3576.

[11] Li, L.; Qin, Z.; Liang, X.; Fan, Q.; Lu, Y.; Wu, W.; Zhu, M. *Journal of Physical Chemistry C* **2009,** 113, 5502.

[12] Pud, A.; Ogurtsov, N.; Korzhenko, A.; Shapoval, G. *Progress in Polymer Science* **2003,** 28, 1701.

[13] Koul, S.; Chandra, R.; Dhawan, S. *Polymer* **2000,** 41, 9305.

[14] Cottevieille, D.; Le Mehaute, A.; Challioui, C.; Mirebeau, P.; Demay, J. *Synthetic Metals* **1999,** 101, 703.

[15] Cottevieille, D.; Le Mehaute, A.; Challioui, C. *Journal De Chimie Physique Et De Physico-Chimie Biologique* **1998,** 95, 1502.

[16] Makela, T.; Sten, J.; Hujanen, A.; Isotalo, H. *Synthetic Metals* **1999,** 101, 707.

[17] Huang, J.; Virji, S.; Weiller, B.; Kaner, R. *Abstracts of Papers of the American Chemical Society* **2004,** 228, 445.

[18] Arjmand, M.; Mahmoodi, M.; Gelves, G.A.; Park, S.; Sundararaj, U. *Carbon* **2011,** 49, 3430.

[19] Kaiser KL. *CRC Press*: **2006**. p 1.

[20] Schulz RB, Plantz VC, Brush DR. *IEEE Trans* **1998**, 30, 187.

[21] Sadchikov VV, Prudnikova ZG. *Stal'*. **1997**, 66.

[22] Posdorfer, J.; Wessling, B. *Synthetic Metals* **2001**, 119, 363.

[23] Boyea JM, Camacho RE, Turano SP, Ready WJ. *NLB* **2007**. 585.

[24] Chen, J.; Guo, Y.; Jiang, B.; Zhang, S. Journal of Dispersion Science *and Technology* **2008,** 29, 97.

[25] Vera, R.; Schrebler, R.; Cury, P.; Del Rio, R.; Romero, H. *Journal of Applied Electrochemistry* **2007,** 37, 519.

[26] Ruckenstein, E.; YANG, S. *Synthetic Metals* **1993,** 53, 283.

[27] Gospodinova, N.; Mokreva, P.; Tsanov, T.; Terlemezyan, L. *Polymer* **1997,** 38, 743.

[28] Beadle, P.; Armes, S.; Gottesfeld, S.; Mombourquette, C.; Houlton, R.; Andrews, W.; Agnew, S. *Macromolecules* **1992,** 25, 2526.

[29] Davis, S.; Ryan, T.; Wilde, C.; Beyer, G. *Synthetic Metals* **1995,** 69, 209.

[30] Lim, S.; Tan, K.; Kang, E. *Langmuir* **1998,** 14, 5305.

[31] Kang, E.; Neoh, K.; Tan, K. *Surface and Interface Analysis* **1993,** 20, 833.

[32] Kang, E.; Neoh, K.; Tan, K. *Surface and Interface Analysis* **1992,** 19, 33.

[33] Green, A.; Woodhead, A. *Journal of the Chemical Society* **1912,** 101, 1117.

Chapter 4

Electrical permittivity and electrical conductivity of multiwall carbon nanotube-polyaniline (MWCNT-PANi) core-shell nanofibers and MWCNT-PANi/polystyrene composites[♣]

4.1 Presentation of the Article

This chapter presents the results of MWCNT coating with PANi and the electrical properties of their composites. Similar to the process discussed in Chapter 3, PANi coating were used for a better dispersion of nanofillers and for decreasing the electrical percolation threshold. The first section of this article presents the coating process of MWCNTs via in-situ polymerization of aniline.

The following sections in this article present the electrical properties of MWCNT-PANi/PS composites. The electrical percolation threshold of coated MWCNTs showed a significant decrease as compared to uncoated MWCNTs. Establishing a decrease in the electrical percolation threshold was a primary objective of this PhD project. The PANi coating layer also enhanced the dielectric of polymer composites.

In this work, the major work has been done by Ali Sarvi and Dr. Sundararaj has supervised this work and helped with result and discussion section.

♣ Sarvi A, Sundararaj U "Electrical permittivity and electrical conductivity of multiwall carbon nanotube-polyaniline (MWCNT-PANi) core-shell nanofibers and MWCNT-PANi/polystyrene composites" *Macromolecular Materials & Engineering*, 2014, doi: 10.1002/mame.201300406.

Electrical permittivity and electrical conductivity of multiwall carbon nanotube-polyaniline (MWCNT-PANi) core-shell nanofibers and MWCNT-PANi/polystyrene composites

Ali Sarvi and Uttandaraman Sundararaj*

Department of Chemical & Petroleum Engineering, University of Calgary, 2500 University Dr, NW, Calgary, AB, T2N 1N4, Canada

4.2 Abstract

In situ polymerization of aniline monomers in the presence of multiwall carbon nanotubes (MWCNTs) led to core-shell nanostructures for use in conductive polymer composites. We tuned the conductivity of core-shell nanofibers by coating thickness. These high aspect ratio MWCNT-polyaniline core-shell nanofibers were dispersed in polystyrene (PS) using solution mixing. These composites exhibited electrical percolation at a much lower concentration than MWCNT/PS composites. Polyaniline (PANi), when used as a coating layer, was able to attenuate electromagnetic (EM) waves via absorption. The dielectric measurements of MWCNT-PANi/PS composites showed one order of magnitude increase in real electrical permittivity compared to that of MWCNT/PS composites makes them suitable for charge storage purposes.

4.3 Introduction

Electrically conducting polymer composites, due to their corrosion resistance, light weight, low cost and ease of processing, have received significant attention for the replacement of metals and inorganic materials for sensors, actuators, supercapacitors and electromagnetic interference (EMI) shields [1-5]. High electrical capacitance makes these composites suitable for use as embedded capacitors and supercapacitors [6-11]. Composites with tunable conductivity maybe used as chemisensors and different types of electronic pressure sensors and switches [11-14].

Multiwall carbon nanotubes (MWCNTs) are high aspect ratio nanofillers that demonstrate high conductivity, excellent mechanical properties and corrosion resistance. Different kinds of conductive nanofillers, such as MWCNTs, metal nanowires and graphene, can be used to make conductive composites. Among conductive nanofillers, MWCNTs have been most extensively investigated, since they provide high electrical conductivity in polymer composites at low filler loading and thus, are very relevant to industry [2, 15].

Due to their high conductivity, large specific area and cycle stability, MWCNTs exhibit a large and stable double-layer capacitance, which is one of the charge storage mechanisms. MWCNTs can be used for the electrical charge storage function in supercapacitors or any other kind of charge storage. Supercapacitors store electrical energy through double-layer charging, pseudocapacitance or a combination of both. Pseudocapacitance is a faradic process, while double-layer charging is non-faradic. Intrinsically conducting polymers (ICPs) utilize a large pseudocapacitance. Thus, a combination of MWCNTs and ICPs results in a high capacitance product that utilizes both faradic and non-faradic processes [13, 14, 17-20].

Van der Waals forces lead to agglomerates of MWCNT in a polymer matrix. Due to significant van der Waals interactions between nanotubes, there is much agglomeration and good dispersion is hard to attain without surface functionalization and/or coating [21-23]; and, an optimum dispersion of fillers is of paramount importance in reaching a low electrical percolation threshold. A coating of conducting polymer on the surface of MWCNTs can help with the dispersion of MWCNTs in a polymer matrix because it results in a significant decrease in interfacial energy between MWCNTs and polymer matrix.

Carbon nanotubes coated with conducting polymers have been proposed for widely differing applications, including an amperometric biosensor for DNA [24], a chemisensor for nitrogen oxide [25], a contact in plastic electronics [26], and in electrorheology [27]. PANi nanofibrils have been suggested as candidates for field-emitting applications [28]. PANi-coated CNT might prove to be an even more promising material. Improvement of the mechanical properties of composites has been reported as a goal for implementation of PANi coating [29-32].

Among all conducting polymers, polyaniline (PANi) is the most suitable candidate for a coating layer of on the surface of MWCNTs. PANi has good stability and tunable conductivity over a broad range, i.e. 10^{-10} to 10 S/cm. PANi also has the ability to shield devices from EMI via absorption of electromagnetic waves [6, 33]. Moreover, PANi exhibits large pseudocapacitance. Thus, these core-shell nanofibers showed higher EMI shielding effective (SE) and higher electrical permittivity than those of MWCNTs alone [34, 35].

In this study, multiwall carbon nanotubes (MWCNTs) were coated with PANi, using *in situ* polymerization to make MWCNT-PANi core-shell nanofibers. Using core-shell nanofibers in

polymer composites, we expect higher electrical permittivity and a lower electrical percolation threshold than using pure MWCNT.

4.4 Experimental Section

4.4.1 Synthesis of MWCNT-PANi core-shell nanofibers

PANi polymer and CNT surfaces do not have strong affinity for each other. Therefore, core-shell nanofibers cannot be created by solution mixing. Rather, *in situ* polymerization of aniline monomers in the presence of MWCNTs has been carried out to create core-shell nanofibers. Aniline (prepared by Sigma Aldrich Corporation) was distilled before being used.

The MWCNTs were obtained from Nanocyl™; product no. NC7000, with average diameter of 9.5 nm, average length of 1.5 μm and specific surface area of 250-300 m^2/g. Figure 4.1 shows the TEM of MWCNTs and PANi-coated MWCNTs. MWCNTs were treated in concentrated hydrochloride acid (HCl) in a beaker under low power sonication for ten hours at 70°C. Four mmol of aniline were dissolved in 1 mole HCl. Different amounts of MWCNTs were then added to the solution, and the mixture was sonicated to disperse the MWCNTs. In another beaker, one mmol of ammonium persulfate (APS) was dissolved in 1 mole HCl. This APS solution was used as an initiator and was added dropwise into the aniline/MWCNT mixture.

The polymerization setup was kept in an ice bath under low-power sonication during the reaction. After four hours of polymerization, acetone was added to the mixture to terminate the reaction. The core-shell nanofibers were filtered, rinsed with water, and dried in a vacuum oven. Four different compositions of aniline with MWCNT were prepared: 5, 10, 15 and 20 wt% of

PANi [2, 35]. Thermogravimetric analysis (TGA) results were in good agreement with the initial composition of core-shell nanofibers.

4.4.2 Synthesis of composites of MWCNT-PANi/polystyrene

After making the MWCNT-PANi core-shell nanofibers, the next step was the dispersion of the core-shell nanofibers in polystyrene (PS). PS was used because of the excellent electrical and mechanical properties of its composites with conductive nanofillers. Core-shell nanofibers were dispersed in dimethylformamide (DMF) which was used as the medium for the mixing with PS. Sonication was applied for an hour to ensure a good dispersion. PS (Americas Styrenics Styron 666D, Dow Chemical, $M.I$=7.5, M_w=200,000 g mole^{-1} and T_g=100˚C) was also dissolved in DMF in a separate beaker. The nanofibers/DMF mixture was added to the PS solution, and the final mixture was magnetically stirred to obtain a homogeneous dispersion of the nanofibers.

Methanol was added as a non-solvent to the mixture to precipitate the PS composite powders. The composite was then dried in a vacuum oven at 80°C for 24 hours. Compression molding was used to make 1 mm thick samples of the composites for electrical property measurements. All the samples were preheated and pressed at 200°C under a pressure of 40 MPa for 20 minutes.

4.4.3 Morphological characterization

Transmission electron microscopy (TEM) was used to investigate the morphology of the nanofibers. The core-shell nanofiber samples for TEM were prepared by placing a drop of a suspension of core-shell nanofibers in methanol on copper grids. The composites samples were

ultra-microtomed to 70 nm in thickness using a glass knife at room temperature. TEM images were obtained at 60 kV using a Hitachi H-7650.

4.4.4 Electrical measurements

The electrical resistivity measurements were done on 1 mm thick rectangular samples. All the sample surfaces were cleaned with ethanol prior to measurement.

Two different resistivity measurement machines were used to cover the range of volume resistivity from insulating materials to conducting materials. Volume resistivity measurements were performed according to ASTM 257-75 standards, employing a Loresta GP resistivity meter (MCP-T610 model, Mitsubishi Chemical Co., Japan) for the samples with volume resistivity less than 10^4 Ω.cm. A four-pin probe was used, so that the effect of contact resistance did not distort the measurement. To measure the volume resistivity of materials with resistivities higher than 10^4 Ω.cm, a Keithley 6517A electrometer connected to a Keithley 8009 test fixture (Keithley Instruments, USA) was used at an applied voltage of 10V.

The EMI shielding measurements were carried out in the X band (8.2–12.4 GHz) using an Agilent vector network analyzer (model 8719 ES). The sample under test was sandwiched between two X-band waveguide sections, which were connected to separate ports of the vector network analyzer (VNA), and a signal was sent to the sample. The reflected and transmitted signals were measured by the VNA.

The EMI SE is expressed in dB and defined by the following equation:

$$SE = 10.\log\left(\frac{P_{in}}{P_{out}}\right) = 20.\log\left(\frac{E_{in}}{E_{out}}\right) = 20\log\left(\frac{H_{in}}{H_{out}}\right) \quad 3.1$$

where P_{in} is the incident energy field, P_{out} is the transmitted energy field, and E and H are the root mean squares of the electric and magnetic field strengths of the electromagnetic wave, respectively.

Dielectric spectroscopy was performed using a standard electrochemical interface (1287 Potentiostat + 1260 FRA, Solartron Analytical). The 1 mm thick samples were coated with silver paste to reduce the contact resistance. They were placed between the two keepers of the sample holder and locked and then sandwiched between the sample holders. The signal was applied to the sample through circular electrodes located in the middle of the sample holder (diameter of 1 mm). Real and imaginary resistances of samples were measured in the frequency range of 0.1-10^6 Hz. Real and imaginary permittivities were calculated using the complex resistance and frequency results.

4.5 Results and Discussions

The characterization of MWCNT-PANi core-shell nanofibers by TEM provided accurate information about the thickness of the PANi coating. Figures 4.1b to 1d shows MWCNTs coated with different amount of polyaniline. Figure 4.1d shows TEM images of MWCNT80-PANi20 nanofibers (MWCNT80-PANi20 denotes 80 wt% of MWCNT and 20 wt% of PANi in solution however, the final concentrations of PANi may be less than 20 wt%). A smooth PANi layer with an average thickness of 15 nm over the surface of MWCNT was observed.

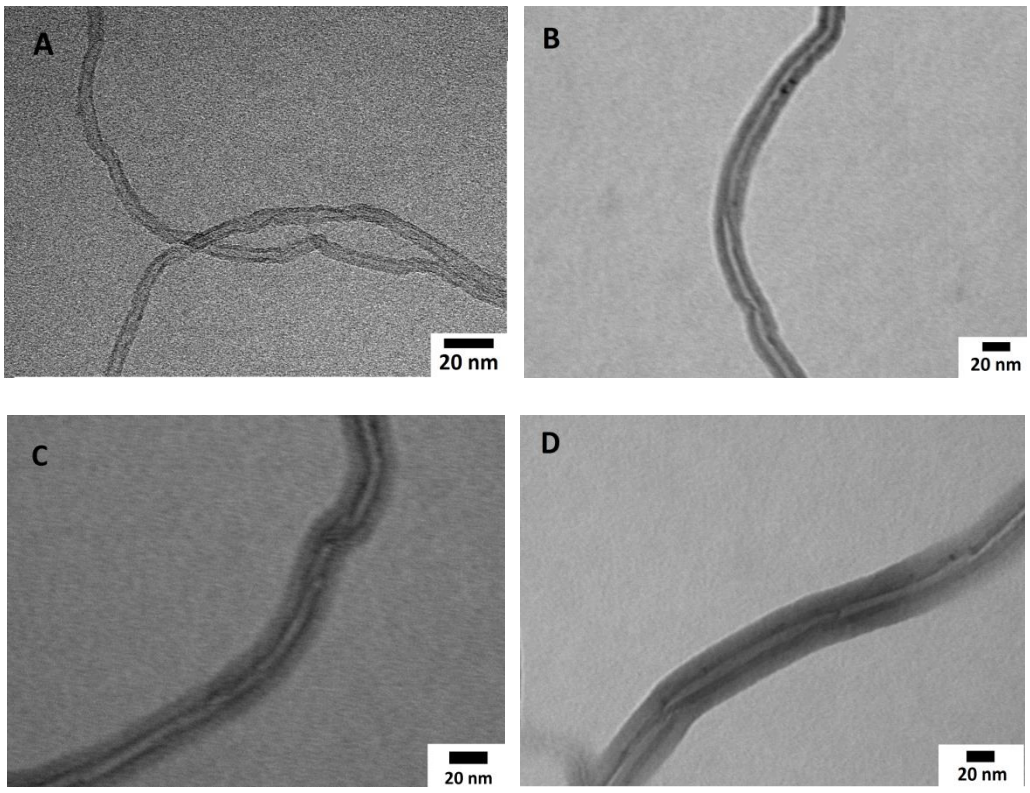

Figure 4.1 a) Uncoated MWCNT, b) MWCNT95-PANi5, c) MWCNT90-PANi10 and d) MWCNT80-PANi20

TEM image analyses of different concentrations of aniline and MWCNT show an increase in coating layer thickness of PANi with increase in the aniline/MWCNT ratio. Coating Thickness of PANi on the surface of MWCNTs at different PANi concentrations presented in Figure 4.2. Coating thickness reported for pure MWCNT is due to error in measurements. Subsequent increases in the coating layer resulted in decreases of the electrical conductivity of the core-shell nanofibers, due to the lower conductivity of PANi compared to MWCNT [21]. Even though PANi is conductive, it has a lower conductivity than MWCNTs; therefore, the conductivity of these core-shell nanofibers is tunable and can be adjusted according to each application.

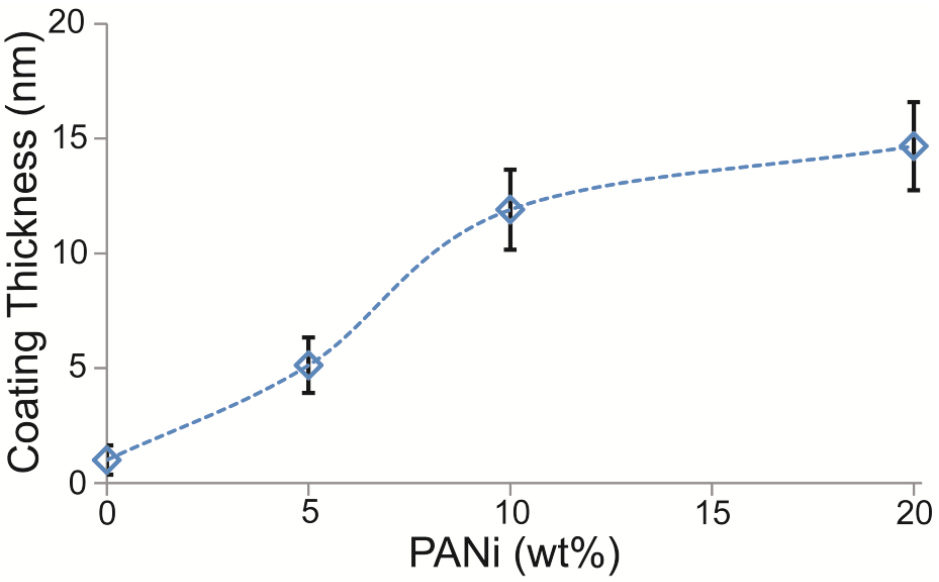

Figure 4.2 Coating thickness as a function of PANi concentrations.

The conductivity of nanofiller is a key parameter in determining the conductivity of polymer composites. MWCNTs are highly conductive materials with an electrical conductivity of 500 S/cm to 10^4 S/cm [36], while the conductivity of PANi can vary widely from 10^{-9} to 10^1 S/cm depending on its oxidation state (eg. Emeraldine base or Emeraldine salt).

The PANi as coating plays a dominant role in the conductivity of nanofiber. To determine the conductivity of the coating layer, we need to know the level of oxidation of the PANi backbone. The ultraviolet (UV) and visible (vis) spectra of the MWCNT-PANi core-shell nanofibers shown in Figure 4.3 are similar to those of the doped PANi backbone. Peaks at ~430 nm and ~590 nm are attributed to benzenoid (B) and quinoid (Q) rings, respectively. [37-40]. The Q/B ratio in coated sample was higher than 1. Q/B ratios close or higher than 1 indicate more doping and

greater conductivity of the PANi layer. Based on the UV-vis spectra, the PANi coating was partially doped and was conductive.

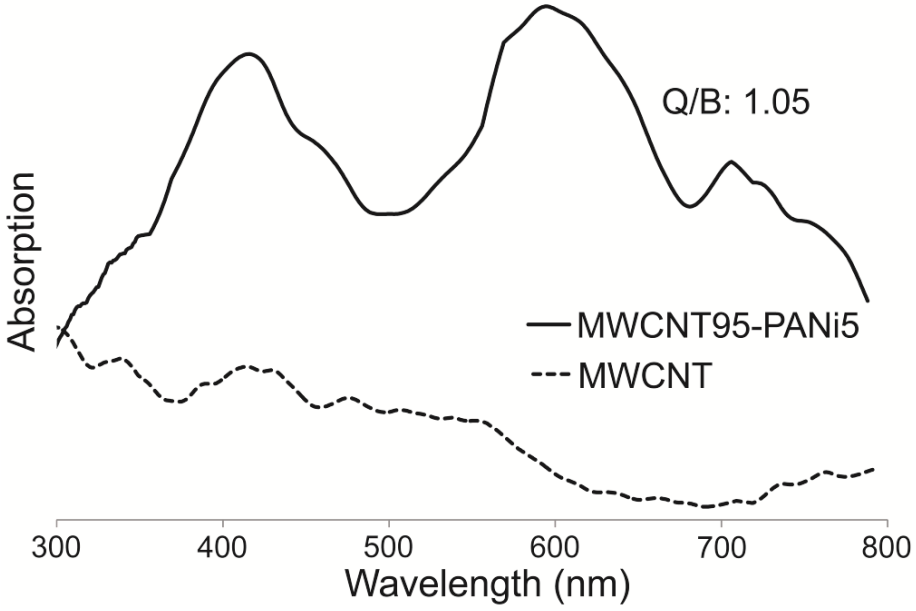

Figure 4.3 UV-visible spectra of core-shell nanofibers and pure MWCNT.

Figure 4.4 shows conductivity results of MWCNT-PANi composite with PS as a function of PANi concentrations. To study the effect of PANi in conductivity of these composites, two different MWCNT loadings were chosen: one close to electrical percolation threshold for pure MWCNT (0.5 wt%) and the other one far above the percolation threshold. For MWCNT loading below the percolation threshold, the conductivity increases three orders of magnitude by adding a coating made from 10 wt% PANi solution. Better dispersion is achieved if there is lower interfacial energy of PANi with PS (calculated as 4.72 dyne/cm and 2.44 dyne/cm using harmonic and geometric mean equation, respectively) compared to interfacial energy of MWCNTs with PS (calculated as 13.76 dyne/cm and 7.33 dyne/cm calculated using harmonic

and geometric mean equation, respectively)[41-43]. This better dispersion after coating results in a higher conductivity of polymer composites. However, polystyrene composites filled with 5 wt% of fillers much higher than percolation threshold show a slight decrease in conductivity when more PANi is added. When the mean gap width between MWCNTs is larger than 10 nm, conductivity is the result of transport processes within the polymer host matrix [44].When the mean particle–particle distance is below 10 nm, the dominant electron transfer mechanism is internal field emission [45]. Therefore, increasing PANi concentration, we reduces the gap between MWCNTs which led to a different mechanism of electron transmission. When PANi has higher coating thicknesses (see Figure 4.2) its role is more dominant; and the main mechanism of conductance is electron transport in PANi. Therefore, the conductivity of composite filled with 5 wt% of MWCNT80/PANi 20 (σ = 30 S/m) is about the same as the conductivity of PANi.

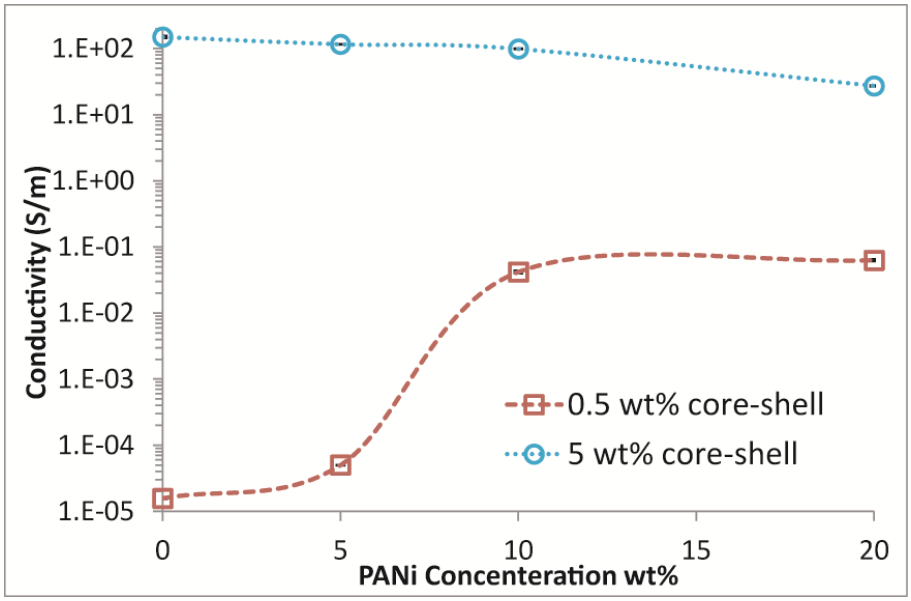

Figure 4.4 Conductivity of core-shell nanofibers composites with PS as a function of PANi concentrations at constant filler loadings (0.5 wt% and 5 wt% of nanofiller).

Figure 4.5 shows TEM images of the composites of pure MWCNTs (Fig 5a) and core-shell nanofibers (Fig 5b) at a nanofiller concentration of 1 wt% of MWCNT loading. MWCNT95-PANi5 core-shell nanofibers were used to make the composites. The TEM images show clusters of nanofillers in both samples; however, for the sample filled with core-shell nanofibers, the dispersion was much better than for the pure MWCNT sample. An intense agglomerate of MWCNTs can be observed in Figure 4.5a, while the nanofibers are much better dispersed in Figure 4.5b. Hence, the PANi layer increased the dispersion of nanofillers, as expected.

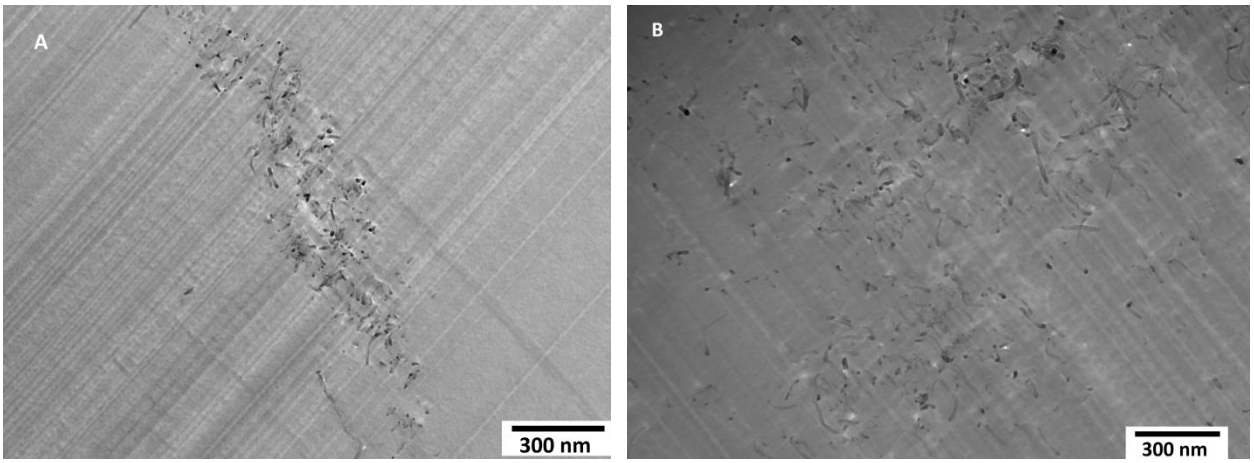

Figure 4.5 a) MWCNT/PS and b) MWCNT 95-PANi 5 in PS. Both samples are filled with 1 wt% of nanofillers.

The conductivity measurements of the PS matrix filled with different concentrations of core-shell nanofibers and pure MWCNTs are plotted in Figure 4.6a. There was a significant decrease in the electrical percolation concentration for MWCNT-PANi/PS composites (0.15 wt%) when compared to the MWCNT/PS composites (0.9 wt%), which is the result of the good dispersion attained by the coating of the nanofillers. Percolation thresholds for MWCNT80-PANi20/PS,

MWCNT90-PANi10/PS and MWCNT/PS were found to be 0.15 wt%, 0.18 wt% and 0.9 wt%, respectively. This large decrease in the percolation threshold is promising for industry, especially in terms of product weight and cost. Figure 4.6b shows the schematic of core-shell nanofibers and MWCNTs in polymer matrix. The coating layer of PANi led to better affinity between MWCNTs and polymer matrix when the MWCNT are coated with PANi. Therefore, the dispersion of nanofibers increases in polymer matrix, as shown in the TEM images of polymer composites in Figure 4.5. There is also a better distribution of the core-shell nanofibers throughout the entire polymer matrix for core-shell nanofibers when compared with composites made with pure MWCNTs.

The charge transfer mechanism between two nanofillers depends on the distance between them. When nanofillers get close enough to each other, electrons tunnel through the insulating gap between them. Better charge transition is obtained for the case of core-shell nanofibers where the insulating polymer in the gap is replaced by a conductive polymer with less electrical resistance.

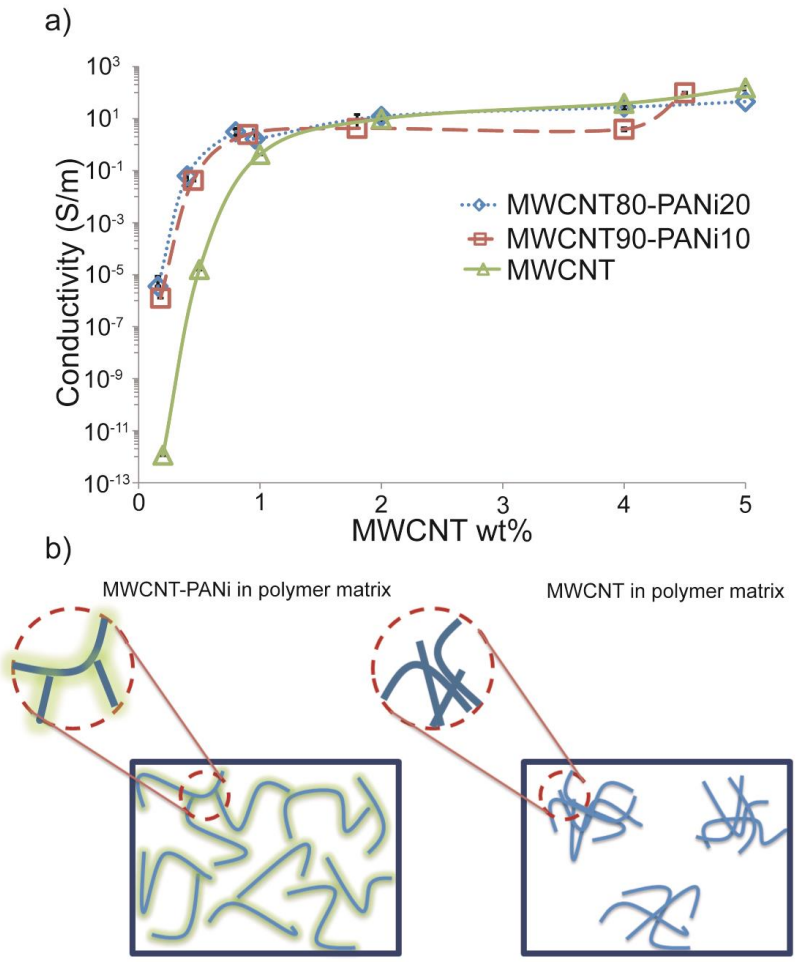

Figure 4.6 (a) Conductivity of core-shell nanofibers and MWCNT composites with PS (both reported as concentrations of MWCNT in the composite), (b) Schematic of nanofiber dispersion in polymer matrix.

The PANi coating also has some advantages in the EMI shielding properties of composites. The reflection and absorption of electromagnetic power were carried out in the X band, and are reported in Figure 4.7 for a sample of MWCNT80-PANi20/PS and a sample of pure MWCNT/PS. As the graph clearly shows, the PANi layer mostly increased the absorption part of the overall EMI SE. This increased in absorption was due to the PANi layer's capability for absorption of electromagnetic waves [46,47]. In both samples, the EMI SE increased as the filler

loading in composite increased. This improvement of the EMI SE is mainly attributed to the formation of conducting interconnected nanofiller networks in the insulating PS matrix.

Dielectric spectroscopy of composite samples filled with different concentrations of MWCNT90-PANi10 nanofibers and MWCNT was performed in the frequency range of 0.1 to 10^6 Hz. Materials with tan(δ) > 1 are considered as "lossy" materials. Thus, MWCNTs could be considered as the lossy core and PANi as the lossless coating layer. For core-shell particles with lossless coating, there is a relaxation that is associated with free charges in the core that are entrapped at the core-shell interface [48]. Generally, the curve of dielectric permittivity versus frequency is smooth, and no peak occurs.

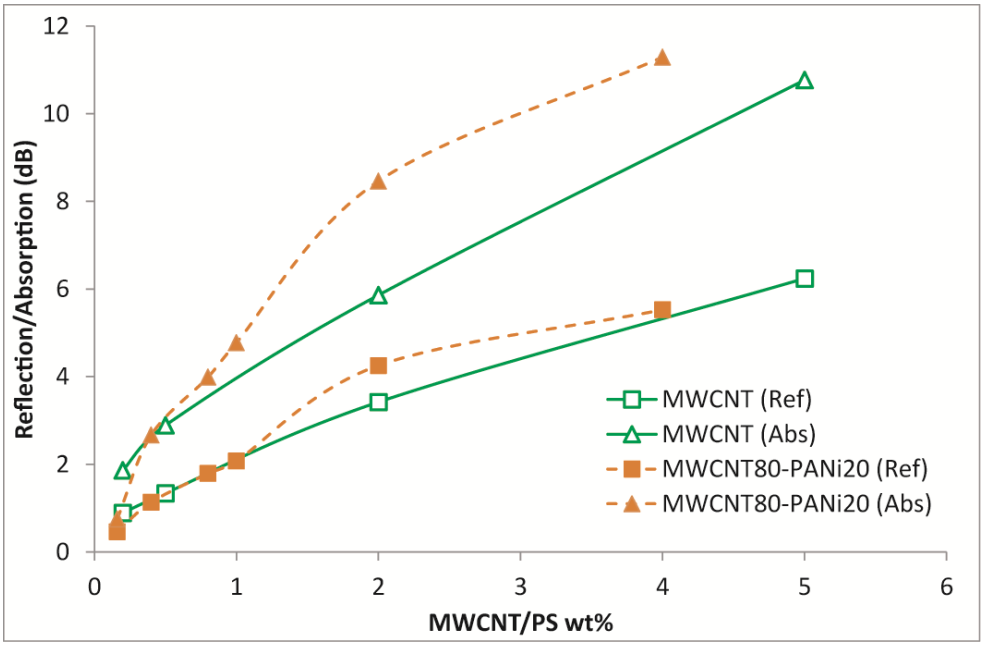

Figure 4.7 Absorption and reflection of core-shell nanofibers and MWCNT composites with PS (both reported as concentrations of MWCNT in the composite).

The dielectric results shown in Figure 4.8 show a sharp decrease in permittivity at low frequencies, which can be expressed as a power-law behavior known at low frequency dispersion (LFD) [49]. Dielectric loss at low frequencies is due to the composite resistance, and is independent of frequency. At higher frequencies, the dielectric permittivity is mainly dependent on the polarization of the core-shell nanofibers and on the remarkable polarization at the interface of the core and shell.

MWCNTs store electrical charge through double-layer charging [18-20]. PANi, as a conducting polymer with good conductivity and cycle stability, belongs to a group of materials that are able to store electrical charge through pseudocapacitance. MWCNT-PANi core-shell nanofibers utilize both pseudocapacitance and double-layer charging mechanisms and exhibit higher real permittivity than MWCNTs. Real permittivity, which is correlated with electrical charge storage within a medium, increased by an order of magnitude with the PANi coating of MWCNT at low frequencies for 0.5 wt% and 1 wt% MWCNT, as shown in Figure 4.8.

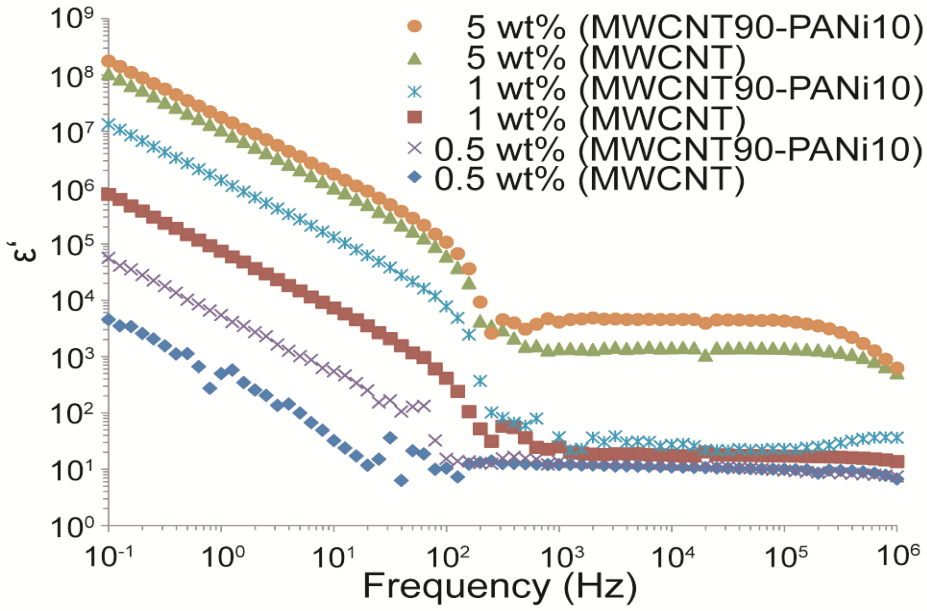

Figure 4.8 Real permittivity of MWCNT90-PANi10 nanofiber and pure MWCNT composites with PS.

The relaxation time was also lower for core-shell nanofibers, compared to that of pure MWCNTs, which means that there was greater interfacial charge polarization for the core-shell nanofiber composites. In addition to the charge polarization of neighboring nanofiller segments, the existence of interfacial charge polarization in the interface of MWCNT and PANi increased the real permittivity of composite.

According to Figure 4.8, the relaxation frequency generally increases with higher filler loading. Interfacial polarization occurred when localized charge carriers overcame certain potential barriers and jumped to another localized site. Increased filler content decreased the interfacial

potential energy, so that the localized charge carriers could jump more readily. An additional consideration with higher filler loading is that this increased the number of microcapacitors, which are composed of two nanofiller particles with insulating polymer inbetween. Forming more microcapacitors result in higher real permittivity [50, 51].

Imaginary permittivity, which is related to the dissipation of electrical energy within the composites, also increased as the amount of nanofiller increased. Higher amounts of nanofillers increase the likelihood of network formation and thus; for charge carriers to move and dissipate energy.

Figure 4.9 shows imaginary permittivity results for MWCNT and MWCNT90-PANi10/PS composites for different filler concentrations. Since MWCNT90-PANi10/PS composites are more conductive at low concentrations, they exhibited imaginary permittivity one order of magnitude higher than that of MWCNT/PS composites. This high imaginary permittivity of core-shell nanofibers was due to the coating layer, which ameliorates with dispersion and network formation. The higher conductivity resulted in greater energy dissipation in the system, which resulted in higher imaginary permittivity.

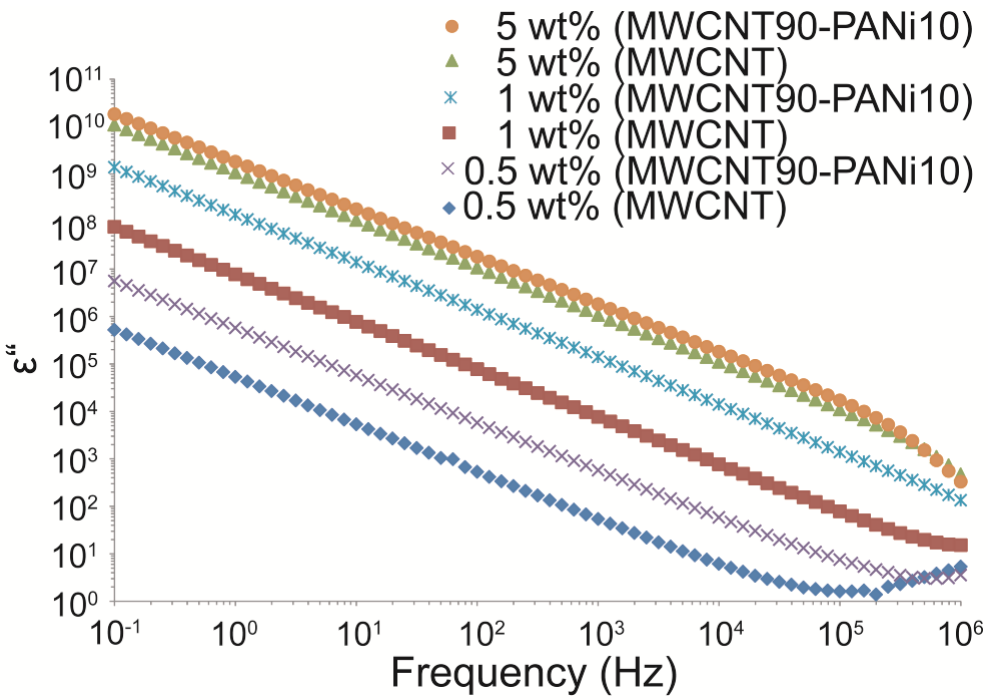

Figure 4.9 Imaginary permittivity of MWCNT90-PANi10 nanofiber and pure MWCNT composites with PS.

At low frequencies dielectric loss, which is the ratio of imaginary to real permittivity, was mainly controlled by the resistance of insulating polymer. At higher frequencies, as charge polarization occurred, the composites exhibited diverse dielectric losses. High real permittivity and relatively low dielectric loss makes MWCNT-PANi core-shell nanofibers an appropriate choice for supercapacitors and embedded capacitors in electronic circuit boards.

4.6 Conclusions

MWCNT-PANi core-shell nanofibers were fabricated via *in situ* polymerization. A uniform and smooth coating of PANi was achieved using sonication during the polymerization. The introduction of these core-shell nanofibers into a polystyrene matrix resulted in a lower electrical percolation threshold (0.15 wt%) than that achieved using pure MWCNT (0.9 wt%). The core-shell nanofibers utilize the contribution of both shell and core for electromagnetic interference shielding; however, each each contributes to EMI SE via different mechanism. For the shell incident EM waves are attenuated via absorption. The real and imaginary permittivities of composites made with the core-shell nanofibers were significantly higher than those made using the MWCNTs. Having a low dissipation factor and a high real permittivity makes these materials a good choice for use as supercapacitors or embedded capacitors.

4.7 References

[1] O. Breuer, U. Sundararaj, *Polymer Composites* **2004**, *25*, 630.

[2] Y. Yang, M. Gupta, *Nano Letters* **2005**, *5*, 2131.

[3] E. Konyushenko, J. Stejskal, M. Trchova, J. Hradil, J. Kovarova, J. Prokes, M. Cieslar, J. Hwang, K. Chen, I. Sapurina, *Polymer* **2006**, *47*, 5715.

[4] D. Makeiff, T. Huber, *Synthetic Metals* **2006**, *156*, 497.

[5] P. Saini, V. Choudhary, B. Singh, R. Mathur, S. Dhawan, *Materials Chemistry and Physics* **2009**, *113*, 919.

[6] S. Koul, R. Chandra, S. Dhawan, *Polymer* **2000**, *41*, 9305.

[7] Y. Zhou, Z. Qin, L. Li, Y. Zhang, Y. Wei, L. Wang, M. Zhu, *Electrochimica Acta* **2010**, *55*, 3904.

[8] E. Antolini, *Applied Catalysis B-Environmental* **2010**, *100*, 413.

[9] C. Peng, S. Zhang, D. Jewell, G. Chen, *Progress in Natural Science-Materials International* **2008**, *18*, 777.

[10] B. Dong, B. He, C. Xu, H. Li, *Materials Science and Engineering B-Solid State Materials For Advanced Technology* **2007**, *143*, 7.

[11] S. Srivastava, S. Sharma, S. Agrawal, S. Kumar, M. Singh, Y. Vijay, *Synthetic Metals* **2010**, *160*, 529.

[12] D. Cottevieille, A. Le Mehaute, C. Challioui, P. Mirebeau, J. Demay, *Synthetic Metals* **1999**, *101*, 703.

[13] J. Huang, S. Virji, B. Weiller, R. Kaner, *Abstracts of Papers of the American Chemical Society* **2004**, *228*, U445.

[14] Y. Liao, C. Zhang, Y. Zhang, V. Strong, J. Tang, X. Li, K. Kalantar-zadeh, E. Hoek, K. Wang, R. Kaner, *Nano Letters* **2011**, *11*, 954.

[15] M. Arjmand, M. Mahmoodi, G. Gelves, S. Park, U. Sundararaj, *Carbon* **2011**, *49*, 3430.

[16] M. Arjmand, T. Apperley, M. Okoniewski, U. Sundararaj, *Carbon* **2012**, *50*, 5126.

[17] N. Pinto, A. Acosta, G. Sinha, F. Aliev, *Synthetic Metals* **2000**, *113*, 77.

[18] P. Ramamurthy, A. Malshe, W. Harrell, R. Gregory, K. McGuire, A. Rao, *Solid-State Electronics* **2004**, *48*, 2019.

[19] F. Yakuphanoglu, I. Yahia, G. Barim, B. Senkal, *Synthetic Metals* **2010**, *160*, 1718.

[20] H. Lin, L. Li, J. Ren, Z. Cai, L. Qiu, Z. Yang, H. Peng, *Scientific Reports* **2013**, *3*.

[21] L. Li, Z. Qin, X. Liang, Q. Fan, Y. Lu, W. Wu, M. Zhu, *Journal of Physical Chemistry C* **2009**, *113*, 5502.

[22] S. Meuer, L. Braun, T. Schilling, R. Zentel, *Polymer* **2009**, *50*, 154.

[23] C. Hong, Y. You, C. Pan, *Polymer* **2006**, *47*, 4300.

[24] G. Cheng, J. Zhao, Y. Tu, P. He, Y. Fang, *Analytica Chimica Acta* **2005**, *533*, 11.

[25] K. An, S. Jeong, H. Hwang, Y. Lee, *Advanced Materials* **2004**, *16*, 1005.

[26] M. Lefenfeld, G. Blanchet, J. Rogers, *Advanced Materials* **2003**, *15*, 1188.

[27] H. Choi, S. Park, S. Kim, M. Jhon, *Diamond and Related Materials* **2005**, *14*, 766.

[28] C. Wang, Z. Wang, M. Li, H. Li, *Chemical Physics Letters* **2001**, *341*, 431.

[29] M. Wang, K. Pramoda, S. Goh, *Polymer* **2005**, *46*, 11510.

[30] H. Chae, T. Sreekumar, T. Uchida, S. Kumar, *Polymer* **2005**, *46*, 10925.

[31] H. Zeng, C. Gao, Y. Wang, P. Watts, H. Kong, X. Cui, D. Yan, *Polymer* **2006**, *47*, 113.

[32] T. Wu, Y. Lin, C. Liao, *Carbon* **2005**, *43*, 734.

[33] T. Makela, J. Sten, A. Hujanen, H. Isotalo, *Synthetic Metals* **1999**, *101*, 707.

[34] E. Konyushenko, N. Kazantseva, J. Stejskal, M. Trchova, J. Kovarova, I. Sapurina, M. Tomishko, O. Demicheva, J. Prokes, *Journal of Magnetism and Magnetic Materials* **2008**, *320*, 231.

[35] V. Mottaghitalab, B. Xi, G. Spinks, G. Wallace, *Synthetic Metals* **2006**, *156*, 796.

[36] G. Gelves, B. Lin, U. Sundararaj, J. Haber, *Advanced Functional Materials* **2006**, *16*, 2423.

[37] P. Dallas, D. Stamopoulos, N. Boukos, V. Tzitzios, D. Niarchos, D. Petridis, *Polymer* **2007**, *48*, 3162.

[38] S. Xing, Y. Chu, X. Sui, Z. Wu, *Journal of Materials Science* **2005**, *40*, 215.

[39] M. Jain, S. Annapoorni, *Synthetic Metals* **2010**, *160*, 1727.

[40] J. Kan, R. Lv, S. Zhang, *Synthetic Metals* **2004**, *145*, 37.

[41] M. Liu, K. Tzou, R. Gregory, *Synthetic Metals* **1994**, *63*, 67.

[42] S. Wu, *Journal of Physical Chemistry* **1970**, *74*, 632.

[43] S. Nuriel, L. Liu, A. Barber, H. Wagner, *Chemical Physics Letters* **2005**, *404*, 263.

[44] L. Jin, C. Bower, O. Zhou, *Applied Physics Letters* **1998**, *73*, 1197.

[45] V. Beek, V. Pul, *Carbon* **1964**, *2*, 121.

[46] P. Chandrasekhar, K. Naishadham, *Synthetic Metals* **1999**, *105*, 115.

[47] B. Wessling, *Synthetic Metals* **1998**, *93*, 143.

[48] N. Bowler, *Journal of Physics D-Applied Physics* **2004**, *37*, 326.

[49] M. Jiang, Z. Dang, M. Bozlar, F. Miomandre, J. Bai, *Journal of Applied Physics* **2009**, *106*.

[50] H. Jin, Y. Hou, X. Meng, F. Teng, *Solid State Communications* **2008**, *148*, 476.

[51] Z. Khattari, M. Maghrabi, T. McNally, S. Jawad, *Physica B-Condensed Matter* **2012**, *407*, 759.

Chapter 5

Rheological percolation in polystyrene composites filled with polyaniline-coated multiwall carbon nanotubes♣

5.1 Presentation of the Article

This article discusses a rheological method to investigate the percolation phenomenon in conductive polymer composites. Conductive polymer composites, which were synthesized, as discussed in Chapter 4, were investigated using rheometry. This work reveals the effect of nanofiller's coating on network formation using both rheological and electrical techniques.

In the first part of this article, the nanofiller dispersion in the PS matrix was investigated using optical microscopy, and change in glassy transition of polymer matrix using DSC. The Nanofiller dispersion showed a significant effect on the glass transition temperature of the polymer matrix in polymer composites. The following sections of this article revealed that the percolation phenomenon can be observed in a polymer matrix using different rheological parameters.

In this work, the major work has been done by Ali Sarvi and Dr. Sundararaj has supervised this work and helped with result and discussion section.

♣ Sarvi A, Sundararaj U "Rheological and electrical percolation in polystyrene composites filled with polyaniline-coated multiwall carbon nanotubes" *Synthetic Metals*, 2014, **194**, 109.

Rheological percolation in polystyrene composites filled with polyaniline-coated multiwall carbon nanotubes

Ali Sarvi and Uttandaraman Sundararaj*

Department of Chemical & Petroleum Engineering, University of Calgary, 2500 University Dr. NW, Calgary, AB Canada T2N 1N4

5.2 Abstract

Polyaniline (PANi)-coated multiwall carbon nanotubes (MWCNTs) and uncoated MWCNTs were added to a polystyrene (PS) matrix using solution and melt mixing. Electrical and rheological measurements were carried out on polymer composites to study the mechanism of conductive network formation. This work reveals the effect of nanofiller coating on network formation using both rheological and electrical techniques. PANi-coated MWCNTs exhibit a much lower electrical percolation threshold (0.4 wt%) than uncoated MWCNTs (0.7 wt%), due to better dispersion of PANi-coated MWCNTs in a PS matrix. Dispersion of nanofillers in a polymer matrix was studied using optical microscopy and differential scanning calorimetry (DSC). Rheological characterizations of composite samples revealed a percolation behavior at higher concentration than that found electrical percolation. The inverse of damping factor (G'/G'') was the best parameter to elucidate the percolation threshold in a polymeric composite

(i.e. PANi-coated MWCNT in PS had electrical percolation of 0.40 wt% and rheological percolation 0.52 wt%). A better affinity of PANi with PS led to better dispersion of nanofillers and lower rheological percolation for PS/MWCNT-PANi composites than those seen for PS/MWCNT composites.

5.3 Introduction

Electrically conducting polymer composites, due to their corrosion resistance, light weight, low cost and ease of processing, have received significant attention for the replacement of metals and inorganic materials for sensors, actuators, supercapacitors and electromagnetic interference (EMI) shields [1-5]. High electrical capacitance makes these composites suitable for use as embedded capacitors and supercapacitors [6-11]. Composites with tunable conductivity may be used as chemisensors, as well as different types of electronic pressure sensors and switches [11-14].

Multiwall carbon nanotubes (MWCNTs) are high aspect ratio nanofillers that demonstrate high conductivity, excellent mechanical properties and corrosion resistance. Different kinds of conductive nanofillers, such as MWCNTs, metal nanowires and graphene, can be used to make conductive composites. Among conductive nanofillers, MWCNTs have been most extensively investigated, since they provide high electrical conductivity in polymer composites at low filler loading and thus, are very relevant to industry [2, 15].

Polymer composites, through a gradual addition of MWCNTs, begin to form a long-range connectivity which is called percolation threshold. Below this threshold, no connected network

exists in any part of the composite, while above this threshold, a giant network on the order of the system size appears. Dispersion of nanofiller in a polymer matrix is an important parameter to decrease percolation concentration to its minimum value. Other parameters that affect percolation concentration are filler shape, density and aspect ratio. High aspect ratio MWCNT, with excellent electrical conductivity, is an outstanding candidate to achieve a conductive composite at a relatively low electrical percolation concentration. However, due to high van der Waals interactions between nanotubes, significant agglomeration occurs and good dispersion is hard to attain without surface functionalization and/or coating [16-18].

In this study, MWCNTs were coated with polyaniline, which is an intrinsically conductive polymer with conductivity of up to 10 S/cm (in emeraldine salt form). Coating helped create a better dispersion of MWCNTs in the PS matrix due to a lower interfacial energy of PANi with PS (calculated as 4.72 dyne/cm and 2.44 dyne/cm using harmonic and geometric mean equations, respectively) compared to interfacial energy of MWCNTs with PS (calculated as 13.76 dyne/cm and 7.33 dyne/cm calculated using harmonic and geometric mean equations, respectively) [19-21].

The effect of PANi coating on electrical conductivity was compared with uncoated MWCNTs mixed with PS, using both solution and melt mixing. One of the key objectives of this study was to use rheological techniques to monitor the rheological behavior of the polymer composite as we increased the filler loading. Rheological percolation thresholds were characterized by a gradual change in the material mechanical response from a liquid-like to a solid-like behavior, which is a consequence of the microstructural evolution of the system [22, 23]. One major feature of rheological measurements is their high sensitivity to microstructural changes. For

example, rheology can be used for the measurement of the early stage of network formation. One way to rheologically monitor crystallization is by means of a dynamic mechanical spectroscopy (DMS). In this case, small amplitude oscillatory shear (SAOS) flow is applied to the samples with different filler loading.

A more advanced use of SAOS experiments involves the determination of the so-called critical gel point. Winter and co-workers [23] were the first to recognize that polymer crystallization can be viewed as a physical gelation process, where the transition between liquid-like and solid-like behavior takes place at the critical gel point. Within this framework, we employed physical gelation theory to determine MWCNT network properties at its rheological percolation concentration.

5.4 Experimental Section

PANi polymer and CNT surfaces do not have a strong affinity for each other. Core-shell nanofibers, therefore, cannot be created by solution mixing. Rather, *in situ* polymerization of aniline monomers in the presence of MWCNTs was carried out to create core-shell nanofibers [24]. The MWCNTs were obtained from Nanocyl™, product no. NC7000, with an average diameter of 9.5 nm, average length of 1.5 μm and specific surface area of 250-300 m^2/g. Figure 5.1 shows the TEM micrographs of MWCNTs and PANi-coated MWCNTs.

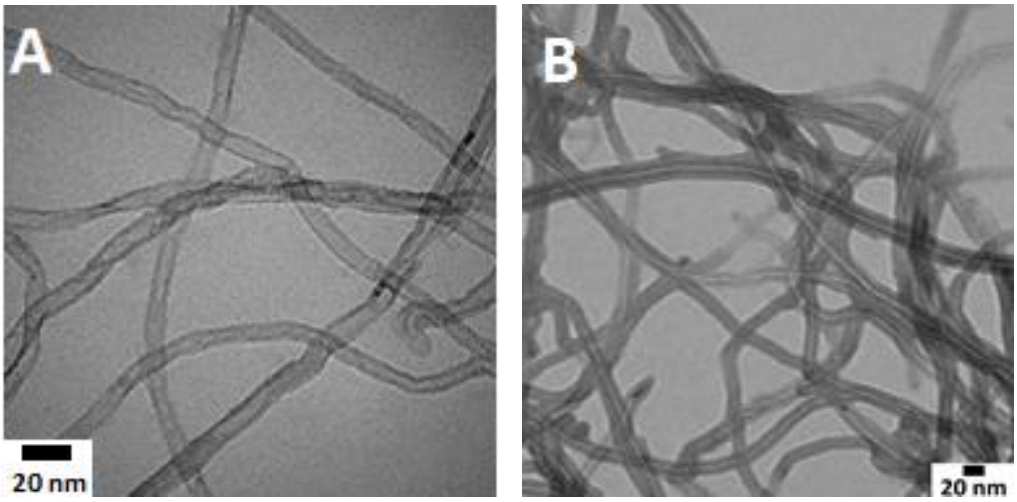

Figure 5.1 A) uncoated MWCNT B) PANi-coated MWCNT (TEM images were obtained at 60 kV using a Hitachi H-7650)

5.4.1 Solution Mixing Method

After making the MWCNT-PANi core-shell nanofibers, the next step was to disperse the core-shell nanofibers into polystyrene (PS) using a solution method [24, 25]. The same method was employed for making PS composites filled with uncoated MWCNTs. PS was used because of the excellent electrical and mechanical properties of its composites with conductive nanofillers. Core-shell nanofibers were dispersed in dimethylformamide (DMF) which was used as the medium for mixing with PS. Sonication was applied for an hour to ensure a good dispersion. PS (America Styrenics Styron 666D, *MI*=7.5, M_w=200,000 g mole^{-1} and T_g=100˚C) was also dissolved in DMF in a separate beaker. The nanofibers/DMF mixture was added to the PS/DMF solution, and the final mixture was magnetically stirred to obtain a homogeneous dispersion of the nanofibers.

Methanol was added as a non-solvent to the mixture and the PS composite powder precipitated out of solution. The composite was then dried in a vacuum oven at 80°C for 24 hours. Compression molding was used to make 1 mm thick samples of the composites for electrical property measurements. All the samples were preheated and pressed at 250°C, under a pressure of 40 MPa, for 20 minutes.

5.4.2 Melt Mixing Method

Samples were melt-mixed using a novel custom-built miniature mixer: the Alberta Polymer Asymmetric Mixer (APAM) [20]. This mixer has a capacity of about 2 ml and this is very valuable for materials made on a bench scale. PS granules were dry- mixed with MWCNTs, then melt-mixed in the APAM at 250 ºC for 15 min. The rotor speed was set at 80 rpm. Melt-mixed samples were compression-molded at the same condition of solution-mixed samples.

5.4.3 Characterizations and Measurements

The electrical resistivity measurements were done on 1 mm thick rectangular samples. All the sample surfaces were cleaned with ethanol prior to measurement.

Two different resistivity measurement machines were used to cover the range of volume resistivity from insulating materials to conducting materials. Volume resistivity measurements were performed according to ASTM 257-75 standards, employing a Loresta GP resistivity meter (MCP-T610 model, Mitsubishi Chemical Co., Japan) for the samples with volume resistivity less than 10^4 Ω.cm. A four-pin probe was used, so that the effect of contact resistance did not distort

the measurement. To measure the volume resistivity of materials with resistivities higher than 10^4 Ω.cm, a Hiresta UP resistivity meter and UR type probe were used at 100 V.

Rheological measurements were performed using a strain/stress controlled rheometer, MCR-302 Anton Paar. Disk-like samples, with 25 mm diameter and 1 mm thickness, were placed between the cone and plate of the rheometric fixture, with 25 mm diameter and angle of 1˚. Applied strain was set to be constant at 0.1%. Frequency sweeps from 0.1 to 300 Hz were performed to measure loss and storage modulus. The measurement temperature was set at 250 ºC.

The optical micrographs were obtained using an Olympus microscope fitted with a Mettler Toledo hot stage and connected to a Pulnix TMC-7 digital camera. The differential scanning calorimetry (DSC) tests were carried out on a TA Instruments Q100, using heating and cooling rates of 10°C/min.

5.5 Results and Discussion

The conductivity measurements of the PS matrix filled with different concentrations of PANi-coated MWCNTs and uncoated MWCNTs are plotted in Figure 5.2. A significant decrease in the electrical percolation concentration is obtained for MWCNT80-PANi20/PS composites (0.4 wt%), when compared to the solution-mixed MWCNT/PS composites (0.7 wt%) and melt-mixed MWCNT/PS composites (0.8 wt%). The lower percolation threshold of solution-mixed samples, compared with melt-mixed samples, is due to better dispersion of carbon nanotubes for composites made using solution mixing method. Surprisingly, the percolation threshold for polystyrene composites filled with PANi-coated MWCNTs is much lower than the two other samples. Our earlier investigations showed that the coating layer helped with better dispersion of

MWCNTs [24]. Since PANi is an intrinsically conductive polymer, the coating layer filled the insulative gap between MWCNTs at their contact spots, which significantly reduced the contact resistance and enhanced the conductivity of polymer composite.

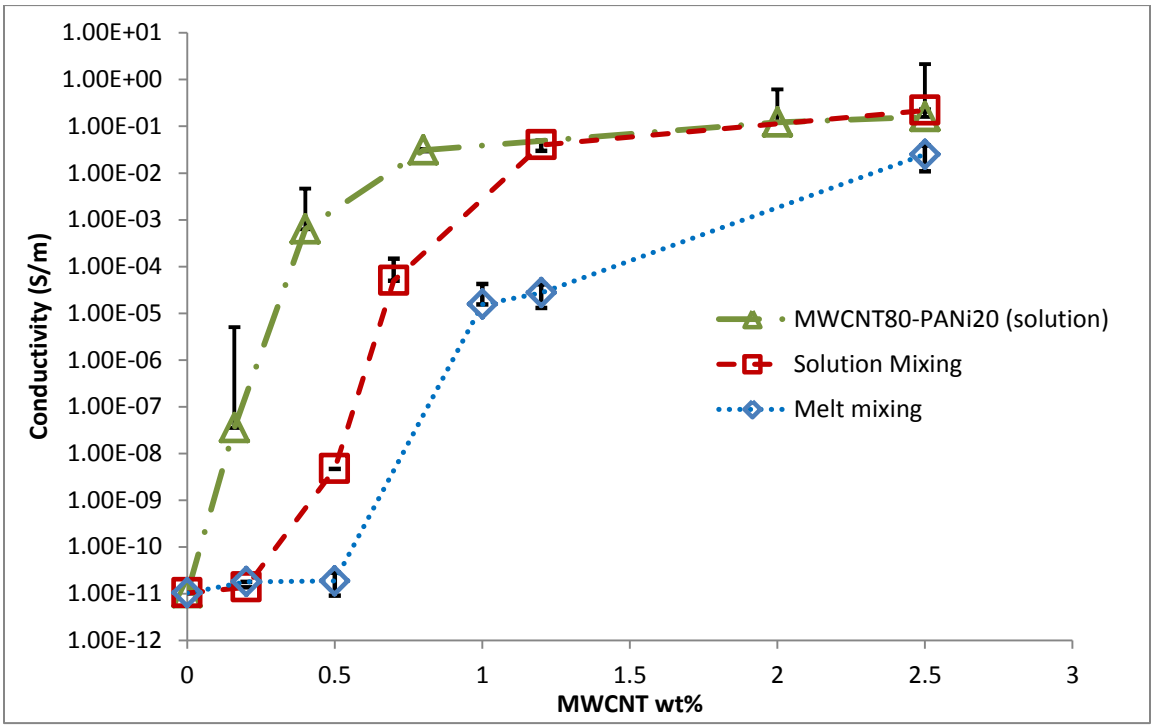

Figure 5.2 Conductivity of solution-mixed PS/CNT80-PANi20, solution mixed PS/CNT and melt mixed PS/CNT as a function of MWCNT

Optical micrographs of three different types of polymer composites support the electrical conductivity results. Figure 5.3A shows that PANi coated-MWCNTs are well-dispersed and well-distributed in polymer. Nanofiller clusters, with dimension size of one hundred nanometers, were able to form a conductive network ($\sigma=6.29\times10^{-4}$ S/m) at 0.4 wt% of nanofiller loading. Solution-mixed and melt-mixed samples without PANi were insulative at this filler level.

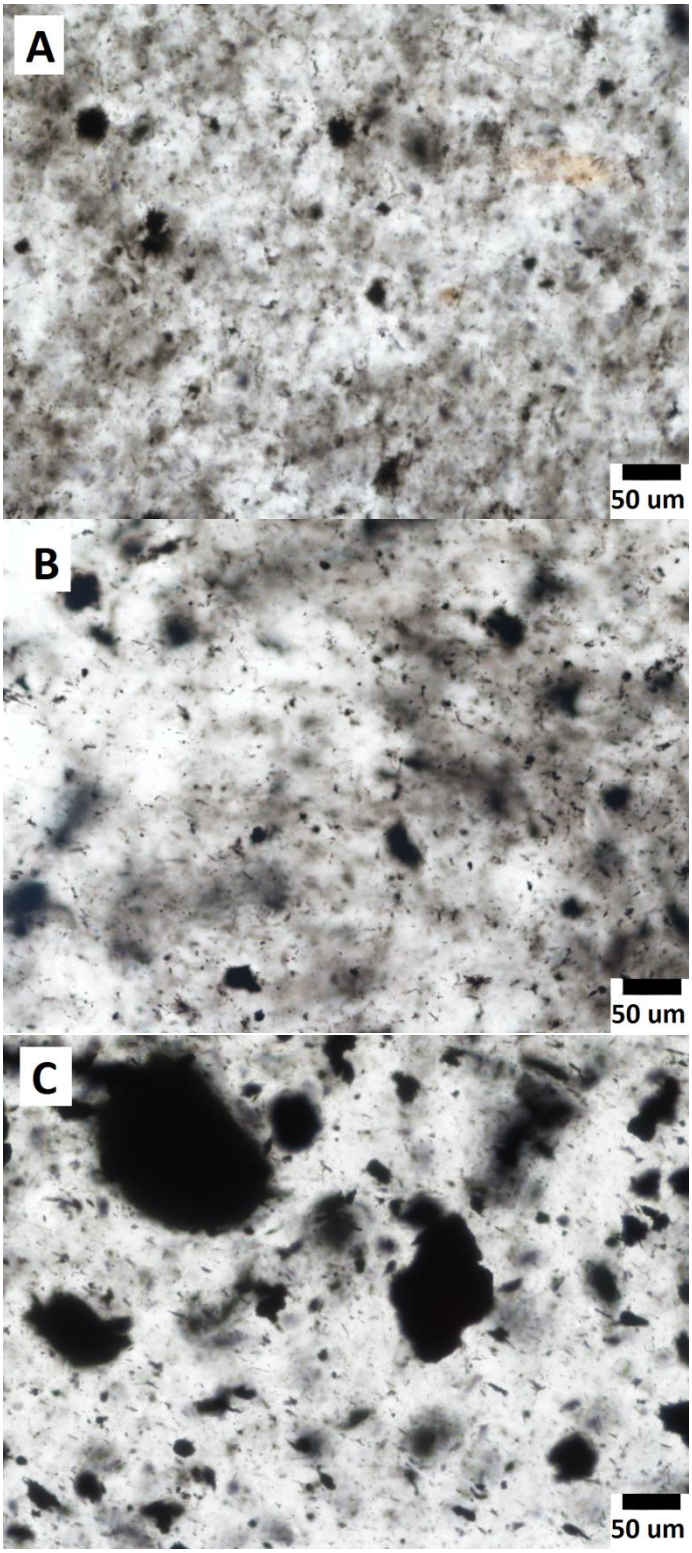

Figure 5.3 Optical Micrographs of A) Solution-mixed PS/CNT80-PANi20, B) solution mixed PS/CNT and C) melt mixed PS/CNT. In all cases, concentration is 0.5 wt% of nanofillers.

Figure 5.3B shows bigger clusters of MWCNTs in the range of a few microns to hundreds of micrometers. The ultrasonication technique, employed during the solution mixing process, resulted in a good distribution of MWCNTs. Figure 5.2C shows that there is a weak dispersion and also a weak distribution of MWCNTs in the polymer matrix. As a result, the percolation threshold for melt-mixed samples was significantly higher than that for the other samples. Decreasing percolation threshold of conductive polymer composites is important, due to the cost and weight of product, and processability of the compound. A low percolation threshold can be achieved by properly dispersing and distributing nanofillers. A perfect distribution, however, does not mean a minimized percolation threshold. In the case of conductive polymer composites, the formation of only a few paths is sufficient to transport charge carriers through the sample. A designed structure inside the polymer composite, with an optimum amount of nanofiller, can significantly decrease the electrical percolation concentration [26-28].

Figure 5.4 shows the glass transition temperature (T_g) for three different composites. As the graph indicates, the glass transition temperature decreased as more nanofiller was added to the polymer particularly in solution mixed samples. Once nanoparticles are dispersed, they can interfere with unperturbed radius of gyration or size of the polymer chain and increase the free volume and thus, act like a plasticizer [29]. The more nanoparticles that interact with the polymer chain, the more free volume that is created. The increase or decrease in T_g of polymer, however, is related to the type of interaction between the polymer and nanofiller. A "good" interaction (high affinity between filler and polymer) leads to increased T_g; a "bad" interaction, as in our sample results in a decreased T_g. Whether the interaction is good or bad, the more change in T_g, the more the interfacial interaction, as a result of higher surface areas provided by nanofillers. It is also noticeable, from Figure 5.4, that T_g for melt-mixed samples is higher than

for solution mixing and PANi-coated MWCNTs. The lower T_g for PS samples filled with the same nanofiller loading may be a result of nanofiller dispersion in the polymer. The better dispersion of nanofillers resulted in more interaction between nanofillers and polymer chains due to the increased area which, in turn, resulted in a lower T_g. Surface area in melt-mixed samples is very low, so there is little to no effect on T_g.

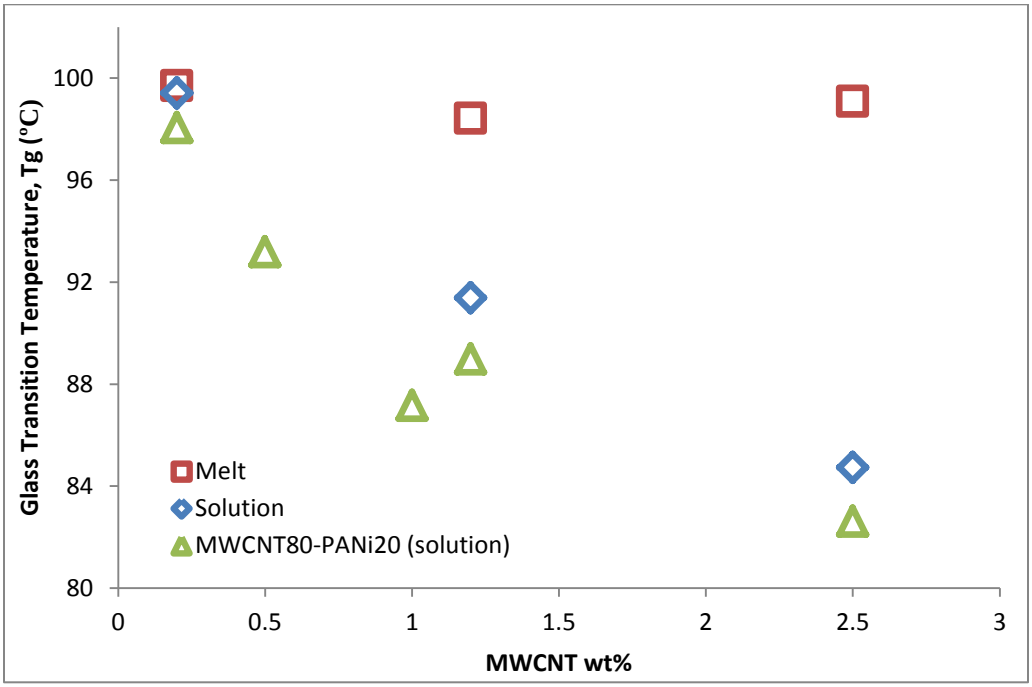

Figure 5.4 Glass transition temperature for three sample types as function of MWCNT loading.

Further investigations on solution-mixed and PS/MWCNT-PANi core-shell samples, which has been prepared using solution mixing, was performed to ensure that the change is glass transition of these samples is not due to residual solvent which might be entrapped in polymer/filler interface. Figure 5.5 shows a thermogravimetric analysis (TGA) of PS/MWCNT80-PANi20 filled with 2 wt% of nanofiller. As the figure shows, there is no significant decrease in weight of

polymer composites in temperatures below 200 ºC which may contribute to solvent residue. Derivate of weight also does not show any peak, except the peak for polymer degradation at around 400 ºC. Therefore, again it was confirmed that the change in glass transition of polymer composite is due to more filler/polymer interfacial interaction in solution-mixed samples compare to melt-mixed samples.

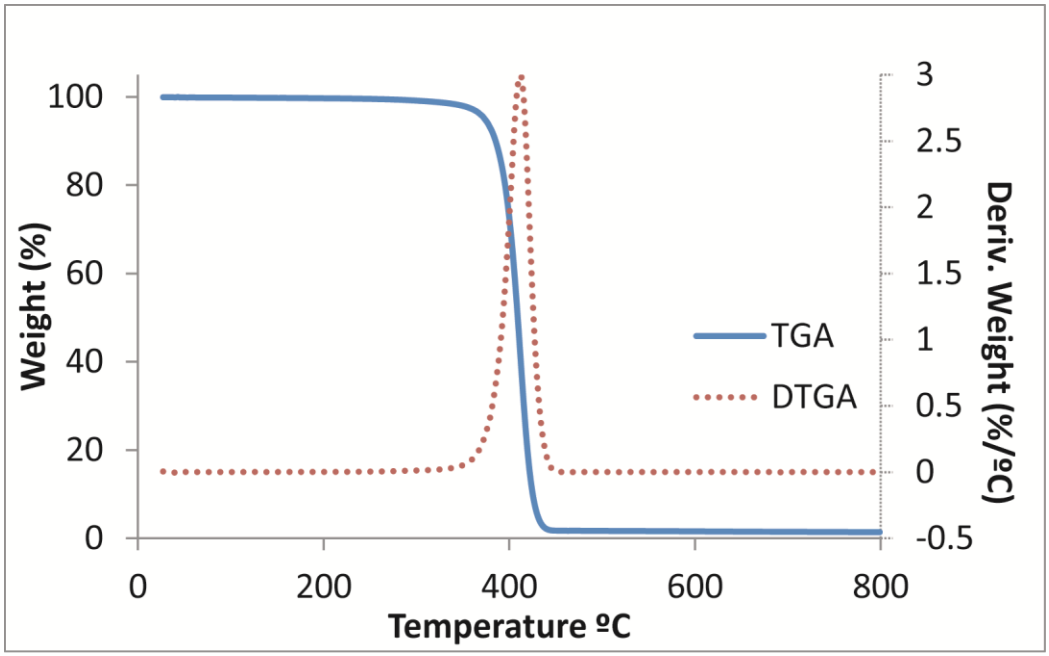

Figure 5.5 Thermogravimetric analysis of PS/MWCNT80-PANi20 filled with 2 wt% of nanofiller

Viscoelastic properties of PS/MWCNT80-PANi20 compositess are presented in Figure 5.6 for a range of nanofiller concentrations. Figure 5.6 provides evidence that nanofiller clusters have a dramatic effect on the rheological behavior, even at loading as low as 0.2 wt%. As the loading increases, storage modulus increases, although this increase is more evident at low frequencies. The damping factor, however, demonstrates a fundamental change in its behavior at low frequencies as loading is increased.

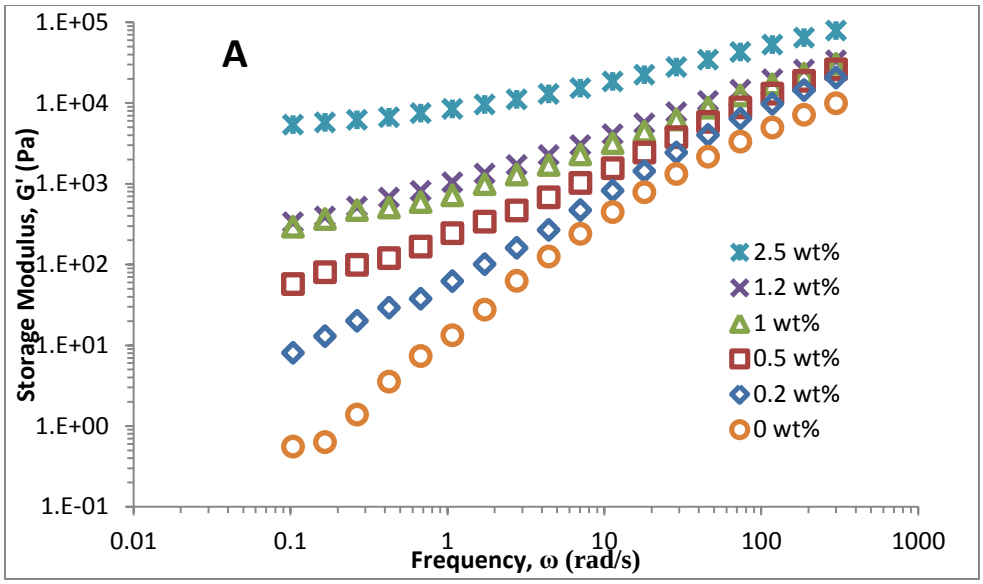

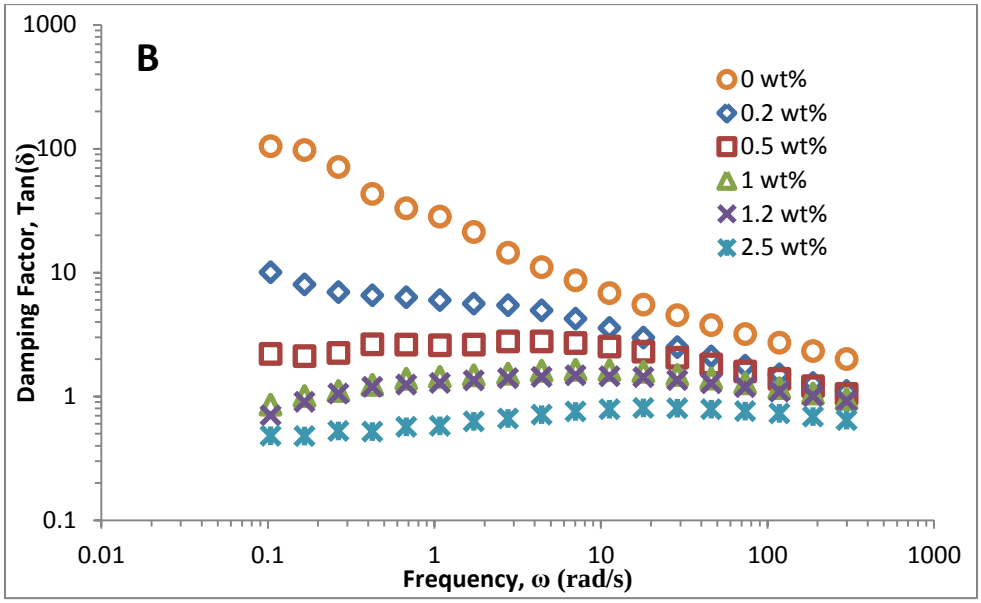

Figure 5.6 A) Storage modulus, B) Damping factor of PS/CNT80-PANi20 versus frequency at different filler concentrations; T=250 ºC and Strain 0.1%.

At 250 ºC, at low frequencies, PS chains are fully relaxed and exhibit typical homopolymer-like terminal behavior with the scaling property of approximately $G' \sim \omega^2$ [30]. At nanofiller loading

higher than 2 wt%, however, this terminal behavior disappeared, as the data in Figure 5.6A shows. As nanofiller loading increased, the polymer composites tend to deviate further from homopolymer-like behavior. Storage modulus due to network formation by adding nanofillers became more resistant to the shear at low frequencies (frequency-independent). Rheological parameters at low frequencies are very sensitive to any physical/chemical network in polymer. Rheological measurements have been carried out to study the early stage of crystallization in crystalline polymers, where relative crystallinity barely reaches 2% of the ultimate crystallinity [22, 23]. Rheological measurements, therefore, can be used as direct evidence to investigate the initial formation of the network of nanofillers. Figure 5.6B indicates a change in behavior of the sample from liquid-like to solid-like as the nanofiller increased. For PS/MWCNT80-PANI20 composites samples, it is observed that at filler loading near 0.5 wt%, a plateau in damping factor (tan(δ)) occurs at low frequencies. This plateau at low frequencies is an indication of network formation in polymer composites, which can be construed as the rheological percolation threshold.

Similar to the electrical percolation threshold, the rheological percolation threshold is correlated with power-law dependence of the rheological parameter with the filler loading [31]. To understand which rheological parameter describes the percolation better, storage modulus, loss modulus and inverse of damping factor (G'/G'') were plotted and are shown in Figure 5.7. The normalized log of conductivity shows an onset of percolation before rheological parameters. When conductive nanofiller approaches each other, at close distances (lower than 10 nm) electrical charges can jump from one conductive segment to the neighbor segment. While for an rheological percolation, at low viscosities, stronger interaction such as an chain entanglement is needed. Therefore, rheological percolation occurs slightly at higher concentration than the

electrical percolation. Among different rheological parameters, $\log(G'/G'')$ is closest to the electrical percolation of composites. It can be noted that G'/G'' is a derived parameter that holds some physical significance, as compared to G' and G'' that are directly measured [31]. Better prediction is also seen using complex viscosity values. The percolation values for the three sample types are tabulated in Table 5.1.

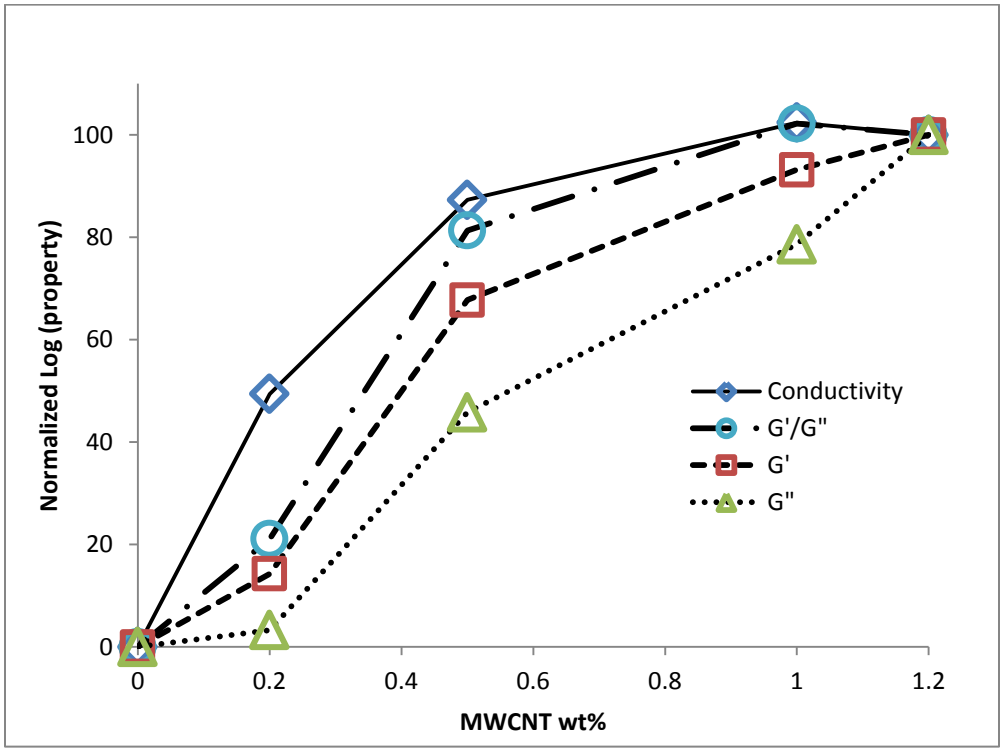

Figure 5.7 The log-normalized values of conductivity, inverse loss tangent, storage modulus and loss modulus of PS/MWCNT80-PANi20 composites as function of MWCNT concentration.

Table 5.1 shows electrical and rheological percolation values for the three different samples. As the results indicate, rheological percolation follows the same trend of electrical percolation through the samples. From Table 5.1 and Figure 5.7, it can be concluded that G' is good choice to report percolation among directly measured values, while the inverse of damping factor

(G'/G'') is the best choice to find the percolation threshold in a polymeric composite. Adding nanofiller to polymer causes an increase in both loss and storage moduli, however, at percolation threshold, the increase in storage modulus is more significant than the increase in loss modulus due to network elasticity. Therefore, the ratio of storage to loss modulus (G'/G'') is more sensitive to network formation. Electrical percolation happened when the first interconnected network formed. The initial conductive network was weak and brittle, which would be out of the sensitivity range of the rheometer. Thus, as previously mentioned rheological percolation happens at slightly higher concentration than the electrical percolation.

Table 5.1 Electrical and Rheological percolation threshold for melt-mixed PS/CNT, solution-mixed PS/CNT and PS/CNT80-PANi20.

Electrical or Rheological Parameter	***Percolation Threshold***		
σ	Melt Mixed PS/MWCNT	Solution Mixed PS/MWCNT	PS/MWCNT80-PANi20
G′/G″	0.8	0.7	0.4
G′	0.94	0.89	0.52
G″	0.96	0.92	0.57
η*	1.02	0.95	0.59
	0.99	0.94	0.51

Differences in rheological responses with the addition of nanofillers can be observed in the graphs of complex viscosity (η^*) versus complex modulus (G^*). As Figure 5.8a shows, a plot of

η^* vs G^* begins to diverge at concentrations higher than 1 wt%. Rheological percolation for melt-mixed PS/MWCNTs, therefore, occurs somewhere between 0.5 wt% and 1 wt% of nanofiller loading. At a filler loading below 0.5 wt%, a plateau in η^* at low G^* shows a Newtonian behavior at low frequencies. For solution-mixed PS/MWCNTs and PS/MWCNT80-PANi20 samples, in Figures 5.8b and 8c, complex viscosity deviates from Newtonian behavior at even lower filler concentrations. Since G^* increases with frequency, we can say that complex viscosity in concentrated samples sharply decreased as frequency increased (i.e. increase in G^* in Figure 5.8). High loading of nanofillers allowed a strong network to form, which then failed at high frequencies resulting in a sharp drop in viscosity. In other words, composites showed a shear-thinning type of behavior.

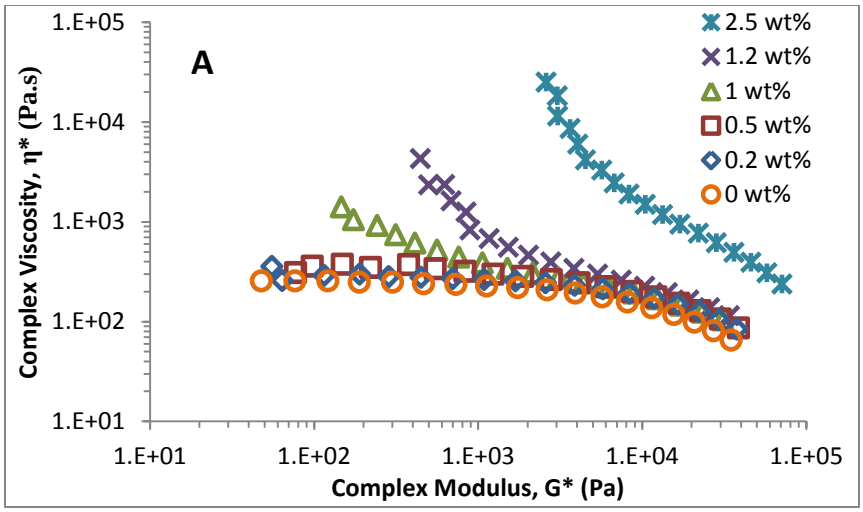

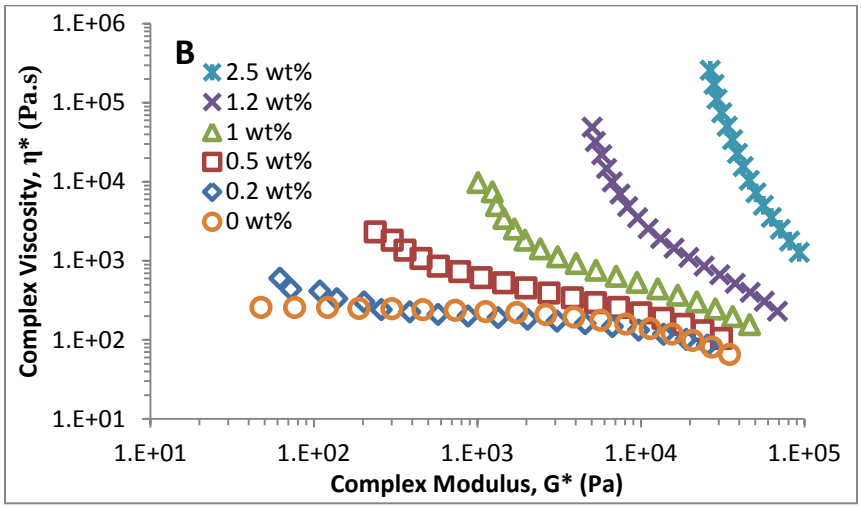

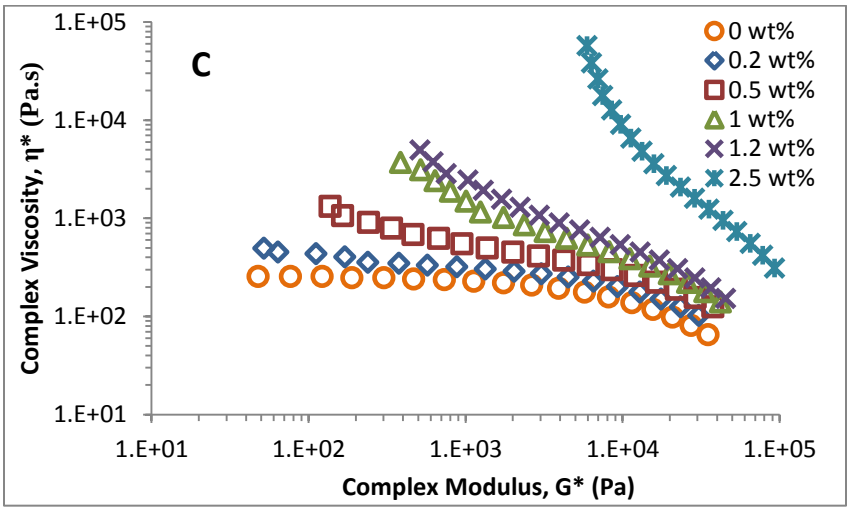

Figure 5.8 Complex viscosity of A) melt-mixed PS/CNT, B) solution-mixed PS/CNT, C) solution-mixed PS/CNT80-PANi20 versus storage modulus at different filler concentrations

To study the stiffness of the network, the MWCNT network can be considered as a physical gel. The infinite network at the gel point is revealed in a strong coupling of the relaxation modes over a wide range of size scales. A power-law relaxation modulus in the terminal zone is seen [22, 23]:

$$G'(\omega) = St^{-n} \quad 4.1$$

where *t* is time, *S* is the gel stiffness and *n* is the critical relaxation exponent. Figure 5.9 shows the gel parameters for three different composites in the range of nanofiller concentration. The decrease in the critical relaxation exponent and the increase in gel stiffness for higher nanofiller loading both indicate that the gel becomes harder and relaxes slower at higher loading. This is consistent with the sharp drop in viscosity for an increase in nanofiller concentration (Figure 5.8). Therefore, the critical gel is more resistant to the shear forces when filler loading increased. The relaxation exponent also shows a rheological percolation via a change in slope of the *n* versus MWCNT wt% which is an indication of a change in the gel formation mechanism. The gel parameters *S* and *n* for PS/MWCNT80-PANi20 fall between melt-mixed PS/MWCNT and solution-mixed PS/MWCNT composites.

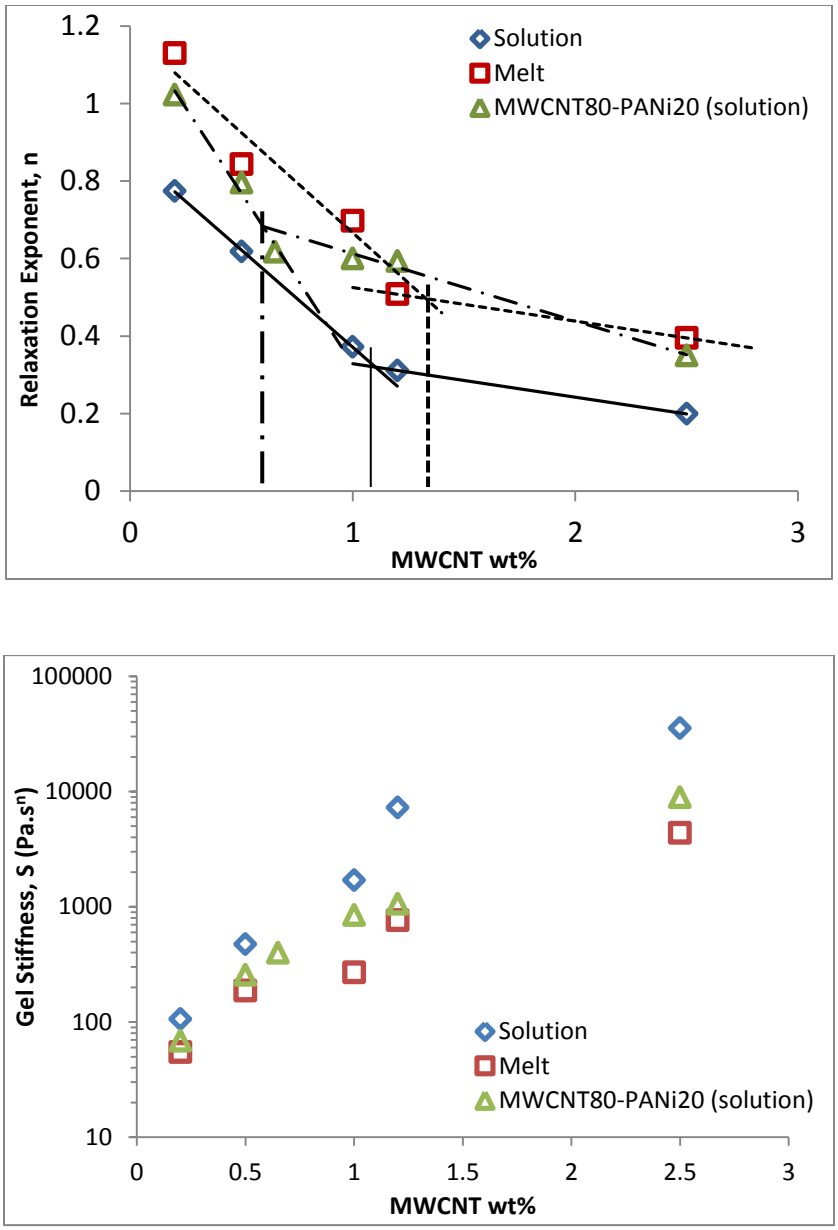

Figure 5.9 A) Relaxation Exponent and B) Gel Stiffness of melt mixed PS/CNT, solution mixed PS/CNT and PS/CNT80-PANi20 as a function of filler concentrations

Gel parameter results indicate that melt-mixed samples have low stiffness which shows a weak interaction among big clusters of MWCNTs. The gel network, therefore, has a lower resistance

to applied shear. Figure 5.9 also shows that critical gel in PS/MWCNT80-PANi20 is ~ 40 % lower in modulus than that in solution-mixed PS/MWCNT. Several possibilities for the difference between rheological behavior of uncoated and PANi-coated MWCNTs can be considered. One possibility is that the coating procedure reduced MWCNTs bending stiffness by creating defects [32]. Another possibility is that adding the coating layer decreased the aspect ratio of nanofillers (i.e. due to increased diameter, aspect ratio a=l/d decreased). That is the thickness of coating was measured to be about 15nm, which reduced the aspect ratio of MWCNTs fourfold from 160 to 40 (due to increase in diameter form 9.5 nm to ~40 nm). Nevertheless, the increase in steric hindrance also hindered the connection between MWCNT-MWCNT and MWCNT-floc (i.e. flocs are colloids which come out of suspension of MWCNTs in DMF) [32]. The overall elasticity of network decreased by using MWCNT coated with PANi.

5.6 Conclusion

In this study, the effect of PANi coating on dispersion and distribution of nanofillers was investigated. It was found that a lower percolation threshold was obtained for PANi-coated MWCNT as a result of better dispersion and also large-distance interaction of MWCNT-MWCNT and MWCNT-floc. Polystyrene samples filled with PANi-coated MWCNTs and bare MWCNTs, at different concentrations, were prepared using melt mixing and solution mixing techniques. It was found that the PANi-coated sample exhibited a good dispersion and low electrical percolation threshold. The good dispersion resulted in low rheological percolation concentration, as well. Rheological percolation was measured using different rheological parameters. The rheological percolation, defined by indirect rheological parameters such as the

ratio G'/G'', matches electrical percolation behavior. Critical gel parameters revealed that as the filler loading increased, the critical gel became harder and relaxed more slowly. It was found that due to the lower aspect ratio and weaker interaction between MWCNT-MWCNT and MWCNT-floc, the gel network for PANi-coated MWCNT is softer than that of uncoated MWCNT.

5.7 References

[1] Breuer O, Sundararaj U. Big returns from small fibers: A review of polymer/carbon nanotube composites. Polymer Composites. 2004;25(6):630-45.

[2] Yang Y, Gupta M. Novel carbon nanotube-polystyrene foam composites for electromagnetic interference shielding. Nano Letters. 2005;5(11):2131-4.

[3] Konyushenko E, Stejskal J, Trchova M, Hradil J, Kovarova J, Prokes J, et al. Multi-wall carbon nanotubes coated with polyaniline. Polymer. 2006;47(16):5715-23.

[4] Makeiff D, Huber T. Microwave absorption by polyaniline-carbon nanotube composites. Synthetic Metals. 2006;156(7-8):497-505.

[5] Saini P, Choudhary V, Singh B, Mathur R, Dhawan S. Polyaniline-MWCNT compositess for microwave absorption and EMI shielding. Materials Chemistry and Physics. 2009;113(2-3):919-26.

[6] Koul S, Chandra R, Dhawan S. Conducting polyaniline composite for ESD and EMI at 101 GHz. Polymer. 2000;41(26):9305-10.

[7] Zhou Y, Qin Z, Li L, Zhang Y, Wei Y, Wang L, et al. Polyaniline/multi-walled carbon nanotube composites with core-shell structures as supercapacitor electrode materials. Electrochimica Acta. 2010;55(12):3904-8.

[8] Antolini E. Composite materials An emerging class of fuel cell catalyst supports. Applied Catalysis B-Environmental. 2010;100(3-4):413-26.

[9] Peng C, Zhang S, Jewell D, Chen G. Carbon nanotube and conducting polymer composites for supercapacitors. Progress in Natural Science-Materials International. 2008;18(7):777-88.

[10] Dong B, He B, Xu C, Li H. Preparation and electrochemical characterization of polyaniline/multi-walled carbon nanotubes composites for supercapacitor. Materials Science and Engineering B-Solid State Materials For Advanced Technology. 2007;143(1-3):7-13.

[11] Srivastava S, Sharma S, Agrawal S, Kumar S, Singh M, Vijay Y. Study of chemiresistor type CNT doped polyaniline gas sensor. Synthetic Metals. 2010;160(5-6):529-34.

[12] Cottevieille D, Le Mehaute A, Challioui C, Mirebeau P, Demay J. Industrial applications of polyaniline. Synthetic Metals. 1999;101(1-3):703-4.

[13] Huang J, Virji S, Weiller B, Kaner R. Polyaniline nanofibers: Facile synthesis, chemical sensors and compositess. Abstracts of Papers of the American Chemical Society. 2004;228:U445-U.

[14] Liao Y, Zhang C, Zhang Y, Strong V, Tang J, Li X, et al. Carbon Nanotube/Polyaniline Composite Nanofibers: Facile Synthesis and Chemosensors. Nano Letters. 2011;11(3):954-9.

[15] Arjmand M, Mahmoodi M, Gelves G, Park S, Sundararaj U. Electrical and electromagnetic interference shielding properties of flow-induced oriented carbon nanotubes in polycarbonate. Carbon. 2011;49(11):3430-40.

[16] Li L, Qin Z, Liang X, Fan Q, Lu Y, Wu W, et al. Facile Fabrication of Uniform Core-Shell Structured Carbon Nanotube-Polyaniline Compositess. Journal of Physical Chemistry C. 2009;113(14):5502-7.

[17] Meuer S, Braun L, Schilling T, Zentel R. alpha-Pyrene polymer functionalized multiwalled carbon nanotubes: Solubility, stability and depletion phenomena. Polymer. 2009;50(1):154-60.

[18] Hong C, You Y, Pan C. A new approach to functionalize multi-walled carbon nanotubes by the use of functional polymers. Polymer. 2006;47(12):4300-9.

[19] Liu M, Tzou K, Gregory R. Influence of the doping conditions on the surface energies of conducting polymers. Synthetic Metals. 1994;63(1):67-71.

[20] Wu S. Surface and interfacial tensions of polymer melt. 2. Poly(methyl methacrylate), Poly(normal-butyl methacrylate), and Polystyrene. Journal of Physical Chemistry. 1970;74(3):632-&.

[21] Nuriel S, Liu L, Barber A, Wagner H. Direct measurement of multiwall nanotube surface tension. Chemical Physics Letters. 2005;404(4-6):263-6.

[22] Coppola S, Acierno S, Grizzuti N, Vlassopoulos D. Viscoelastic behavior of semicrystalline thermoplastic polymers during the early stages of crystallization. Macromolecules. 2006;39(4):1507-14.

[23] Pogodina N, Winter H. Polypropylene crystallization as a physical gelation process. Macromolecules. 1998;31(23):8164-72.

[24] Sarvi A, Sundararaj U. Electrical permittivity and electrical conductivity of multiwall carbon nanotube-polyaniline (MWCNT-PANi) core-shell nanofibers and MWCNT-PANi/polystyrene composites. Macromolecular Materials & Engineering. 2014; DOI: 10.1002/mame.201300406

[25] Sarvi A, Gelves G, Sundararaj U. Facile one step-synthesis and characterisation of high aspect ratio core-shell copper-polyaniline nanowires. Canadian Journal of Chemical Engineering. 2014; DOI: 10.1002/cjce.21973

[26] Sarvi A, Sundararaj U. Selective localization of MWCNTs in blends of poly(methyl methacrylate) and styrene-acrylonitrile copolymer. ANTEC 2013, Cincinnati, US.

[27] Gelves G, Al-Saleh M, Sundararaj U. Highly electrically conductive and high performance EMI shielding nanowire/polymer compositess by miscible mixing and precipitation. Journal of Materials Chemistry. 2011;21(3):829-36.

[28] Goldel A, Kasaliwal G, Potschke P. Selective Localization and Migration of Multiwalled Carbon Nanotubes in Blends of Polycarbonate and Poly(styrene-acrylonitrile). Macromolecular Rapid Communications. 2009;30(6):423-9.

[29] Tuteja A, Mackay M, Hawker C, Van Horn B. Effect of ideal, organic nanoparticles on the flow properties of linear polymers: Non-Einstein-like behavior. Macromolecules. 2005;38(19):8000-11.

[30] Du F, Scogna R, Zhou W, Brand S, Fischer J, Winey K. Nanotube networks in polymer compositess: Rheology and electrical conductivity. Macromolecules. 2004;37(24):9048-55.

[31] Kota A, Cipriano B, Duesterberg M, Gershon A, Powell D, Raghavan S, et al. Electrical and rheological percolation in polystyrene/MWCNT compositess. Macromolecules. 2007;40(20):7400-6.

[32] Urena-Benavides E, Kayatin M, Davis V. Dispersion and Rheology of Multiwalled Carbon Nanotubes in Unsaturated Polyester Resin. Macromolecules. 2013;46(4):1642-50.

Chapter 6

Electrospun conductive nanofibers of poly(vinylidene fluoride) filled with coated multi-wall carbon nanotubes♣

6.1 Presentation of the Article

This article provides new insight into how we can form a conductive network in electrospun mats where the orientation of conductive high aspect ratio fillers is a major problem. This orientation seems inevitable given the high spinning speeds and thus, viscoelastic stresses that align the fillers. Using thermodynamic manipulation - using the miscibility/immiscibility of a third phase (i.e. polyaniline) - we conceived a way to reconfigure and rearrange the structure of the conductive nanofiller (MWCNTs) in the polymer (PVDF). Essentially, we disrupted the orientation allowing for transverse connections. SEM and TEM images proved the formation of small strands, or segments, of nanofillers on the surface of nanofibers which resulted in the formation of a conductive network in the transverse direction of the electrospun mat. The effect of interfacial energies on the formation of this unique structure was discussed to reveal the driving force eliciting this phenomenon. Electrospinning is a successful method for piezoelectric properties of PVDF, which gives higher β -crystal than any processing method which significantly increases the piezoelectricity of PVDF. In this work, Dr. Silva helped with SEM images, and Dr. Bretas and Dr. Sundararaj have supervised this study and helped with result and discussion part. The major work has been done by Ali Sarvi.

♣ Submitted for publication

Electrospun conductive nanofibers of poly(vinylidene fluoride) filled with coated multiwall carbon nanotubes

A. Sarvi[1], A. B. Silva[2], R. E. S. Bretas[2] and U. Sundararaj[1*]

1. Department of Chemical & Petroleum Engineering, University of Calgary, 2500 University Dr, NW, Calgary, AB, T2N 1N4, Canada.

2. Department of Material Engineering, Federal University of Sao Carlos, Rodovia Washington Luís, km 235 - SP 310 - Jardim Guanabara, Sao Carlos, SP, 13565-905, Brazil.

6.2 Abstract

Conductive nanofibers of poly(vinylidene fluoride) (PVDF) filled with coated multiwall carbon nanotubes (MWCNTs) were fabricated using the electrospinning technique. MWCNTs were initially coated with polyaniline (PANi), which is intrinsically conductive. This addition of coated MWCNTs to PVDF created short conductive strands on the surface of the nanofibers, facilitating the formation of a conductive network in the transversal direction. Conductive nanofibers of PVDF are promising in terms of piezoelectricity and of sensitivity to chemicals for applications in electronic devices and sensors. Electrospun PVDF nanofibers mats demonstrate higher piezoelectricity than melt processed samples using traditional polymer processing techniques, such as compression molding. Spectroscopic imaging techniques were employed to

study the effects of the filler and processing conditions on the nanofiber structure. X-ray diffraction, Fourier transform infrared spectroscopy and differential scanning calorimetry results indicated a large increase in beta (β) phase crystals of PVDF using electrospinning. An increased content of β-phase crystals enhanced the piezoelectricity of the nanofibers.

6.3 Introduction

The physical properties of piezoelectric and pyroelectric electroactive polymers (EAPs) are different from those of conventional ceramic materials, indicating immense potential for these materials in electronic devices. These applications require EAPs in large-area, thin, flexible films and fabrics. Some advantages of EAPs that make them more suitable for additional applications include higher dielectric strength (30 V/μm) than piezoceramic materials (1.5 V/μm), outstanding elastic compliance, and good mechanical properties. Among all EAPs, poly(vinylidene fluoride) (PVDF) and its derivatives demonstrate the largest piezoelectric and pyroelectric coefficients [1-6].

The piezoelectric and pyroelectric properties of PVDF have been known for many years, with PVDF finding applications in nonlinear optics, transducers, and biomedical instruments [7]. PVDF has already been commercialized in transducers and actuator applications [6, 8, 9]. However, their use is still very limited, due to: low electromechanical coupling; high resistance against charge movements; and small force generation capability. In order to enhance the piezoelectric and pyroelectric properties of PVDF for a wider range of applications, a large amount of beta (β) phase crystals are required [1-10].

Furukawa et al. claimed that the piezoelectric activity comes from dipoles formed in the molecular arrangement of the Fluorine atoms in the structure [10]. A variety of methods, such as

the stretching of PVDF, the addition of different kinds of nanoclays and the use of a functionalized polymer, have been investigated in recent years to increase PVDF's piezoelectric properties [4-6, 10-11]. Stretched PVDF film has not shown a very strong piezoelectric property from an application point of view [7]. Moreover, the β crystalline phase obtained by film stretching was not stable with increasing temperature.

The melt processing of PVDF under high shear stress leads to a large β-phase crystals content, which significantly enhances the piezoelectricity of PVDF. A high orientation of PVDF in the flow direction results in the formation of a large amount of β-phase crystals, rather than alpha (α) phase crystals.

In this study, nanofibers of PVDF were fabricated using an electrospinning technique under an extreme electrical field. In this technique, a capillary (where the polymeric solution is placed) is connected to a high power supply; in the case of the PVDF solution, it accumulated electrostatic charges and when the electrical field was applied, the tip of the droplet outside the capillary was elongated. During the path between the capillary and the collector, the solvent evaporated; and nanofibers were produced by viscoelastic jet instabilities and deposited on the grounded collector [12-14].

The electrospinning technique has similarities with both electrospraying and conventional solution or melt spinning. A high orientation of the PVDF macromolecules in a high voltage field during the electrospinning process increases the crystalline β-phase, enhancing piezoelectricity. The piezoelectric effect is a reversible process. EAPs exhibit both a direct piezoelectric effect, which is the internal generation of electrical charge as a result of an applied mechanical force, and a reverse piezoelectric effect, which is the internal generation of a

mechanical strain due to applied electrical field [15]. Therefore, PVDF needs to be electrically conductive for some applications.

Since it is not intrinsically conductive, a conductive partner is needed to make PVDF conductive. One established method to obtain conductive thermoplastic is the addition of conductive nanofillers. Multiwall carbon nanotubes (MWCNTs) are high aspect ratio nanofillers that demonstrate high conductivity, excellent mechanical properties, and corrosion resistance. The main advantages of nanofibers filled with MWCNTs are their excellent properties, including structure scalability, greater flexibility, and a higher piezoelectric strain constant (d_{33}~−57.6pm/V) [16] than the commercially available PVDF thin films (d_{33}~−15pm/V) [17].

The dispersion of MWCNTs in the polymer is of paramount importance in the fabrication of a conductive polymer composite with a minimum filler loading (electrical percolation threshold) [12, 18, 19]. In this study, MWCNTs were coated with polyaniline (PANi) using in situ polymerization for better dispersion in the PVDF and a lower electrical percolation concentration [20, 21].

6.4 Experimental Section

The PVDF (Kynar 1000HD) was supplied by Arkema. A mixture of N,N-dimethylformamide (DMF, 99.5%, Merck) and acetone (Merck, 99.7%) was used as a solvent. The volume ratio of DMF to acetone was 3:1. The concentration of PVDF in the solution was kept at 12 wt% [12, 22], and different amounts of MWCNT-PANi core-shell nanofillers were added to the PVDF solution. The solutions were sonicated for 1 hour. The nanofibers were electrospun with a voltage of 20 kV and a work distance (i.e. distance between the syringe and the collector) of 5

cm. The nanofibers were collected on a high speed rotor rotating at 2,000 rpm. The injection speed of the solutions was adjusted by 0.03 ml/min based on the solution viscosity.

The *in situ* polymerization of aniline monomers in the presence of MWCNTs was carried out to create core-shell nanofibers. The MWCNTs were Nanocyl™, product no. NC7000, with an average diameter of 9.5 nm, an average length of 1.5 μm and a specific surface area of 250-300 m^2/g. Aniline (prepared by Sigma Aldrich Corporation) was distilled before being used; 2.1g of MWCNTs were treated in concentrated hydrochloride acid (HCl) under low-power sonication for ten hours at 70°C.

Four mmol of aniline were dissolved in 1 mole HCl. In another beaker, one mmol of ammonium persulfate (APS) was dissolved in 1 mole HCl. This APS solution was used as an initiator and was added dropwise into the aniline/MWCNT mixture. The polymerization setup was kept in an ice bath under low-power sonication during the reaction time (four hours). Acetone were used to terminate the reaction after 4 hours. Figure 6.1 shows transmission electron microscopy (TEM) imaging of MWCNTs. The conductivity of these core-shell nanofiller was ~1100 S/m.

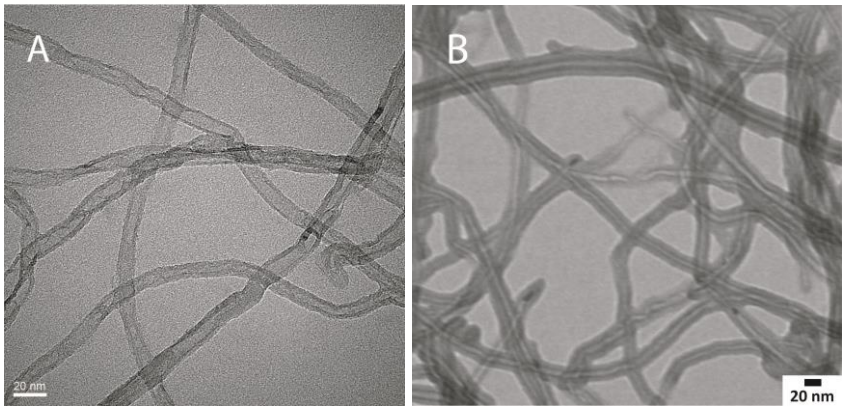

Figure 6.1 TEM images of: A) uncoated MWCNT, B) coated MWCNT with PANi

TEM and scanning electron microscopy (SEM) were used to investigate the morphology of the nanofibers. The core-shell nanofibers were deposited on copper grids, and the PANi phase was then stained using osmium tetroxide (OsO_4). TEM images were obtained at 60 kV using a Hitachi H-7650. For SEM imaging, samples were prepared by placing a piece of the nanofiber mat on aluminum (Al) stubs; the samples were gold-coated to enhance the resolution and prevent arcing of polymer by electron beam. SEM image were obtained at 20kV using a Philips scanning electron microscope (model XL 30 FEG).

The volume resistivity of samples with resistivities of less than10^4 Ω.cm was measured by placing a four-pin probe connected to a Loresta GP resistivity meter (MCP-T610 model, Mitsubishi Chemical Co., Japan). The volume resistivity measurements were performed according to ASTM 257-75 standards at 90 V. To measure the volume resistivity of samples with resistivities higher than 10^4 Ω.cm, a Hiresta UP resistivity meter and UR type probe were used at 100 V.

Infrared spectra were recorded on a Fourier transform infrared spectroscopy (FTIR) instrument from ThermoElectric Corporation, Chicago, IL (Nicolet Nexus 470 FTIR) with a resolution of 4 cm^{-1} and an accumulation of 128 scans. The differential scanning calorimetry (DSC) tests were carried out on a TA Instruments Q100, using a heating and cooling rate of 10°C/min. A Rigaku Geigerflex Powder Diffractometer was used for the X-ray diffraction experiments (λ = 1.79 Å). The device was equipped with a cobalt tube, graphite monochromator and scintillation detector.

6.5 Results and Discussions

The SEM images of electrospun nanofibers in Figure 6.2 show nanofibers in the range of 100-300 nm. Figure 6.2A shows smooth PVDF nanofibers with an average diameter of 250 nm. Blends of PVDF with 8 wt% of PANi (supplied by Sigma Aldrich, with a weight average molecular weight, M_w, of 65000 g/mol) were electrospun and PANi clusters were dispersed in nanofibers. However, PANi clusters on the surfaces of nanofibers bridged with clusters on neighboring nanofibers. Figure 6.2B shows PVDF/PANi nanofibers made by solution blending, with clusters of PANi located on the surface of nanofibers.

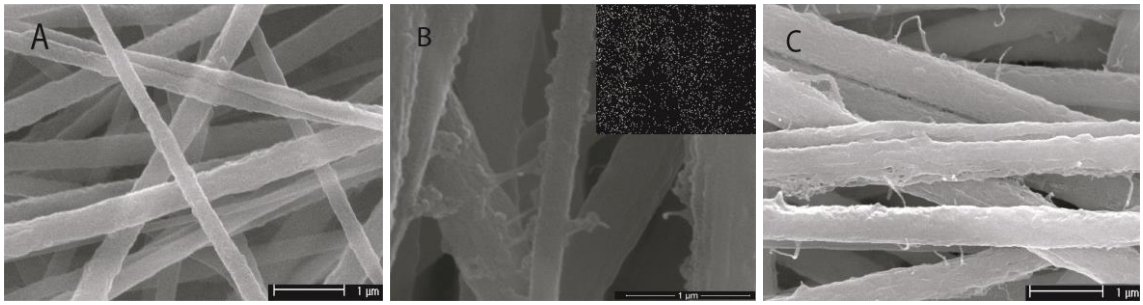

Figure 6.2 SEM images of nanofibers of: A) pure PVDF, B) blend of PVDF/PANi, C) PVDF/(MWCNT-PANi) 16 wt%

The pattern in the inset in Figure 6.2B comes from a nitrogen detector. Nitrogen, which results from the amine and imine groups in PANi, is an evidence of PANi clusters inside the nanofibers and bridges between the nanofibers. Considering the tendency of PANi to connect with neighboring clusters, it is expected that MWCNT-PANi core-shell nanofillers will participate in bridge development.

Figure 6.2C shows nanofibers of PVDF filled with 16 wt% of MWCNT-PANi core-shell nanofibers (synthesized with *in situ* polymerization of aniline in the presence of the MWCNTs).

Short strands of MWCNT-PANi nanofillers on the surface of the PVDF nanofibers increased the chance of a network formation in the transverse direction of the nanofibers. The interfacial energy of PANi with PVDF (~4.7 dyne/cm, calculated using the geometric mean equation [23-25]) was lower than that of MWCNTs with PVDF (~6.6 dyne/cm) [24-26], which allowed for better dispersion of the filler in the PVDF because of the lower interfacial energy for PVDF-PANi. However, clusters of MWCNT-PANi could still be seen in some nanofibers since the PANi coating can cause some agglomeration.

TEM images of PVDF/PANi nanofibers showed dark clusters of PANi distributed along the nanofibers, samples of which had been stained using OsO_4 to magnify the contrast between the PANi and PVDF phases. Figure 6.3A shows pure PVDF nanofibers, and Figure 6.3B shows the nanofibers made from PVDF/PANi blend. Clusters of PANi can be seen in Figure 6.3B, located at the surface of the nanofibers. These clusters resulted in bridging between nanofibers, which can be seen in Figure 6.2B.

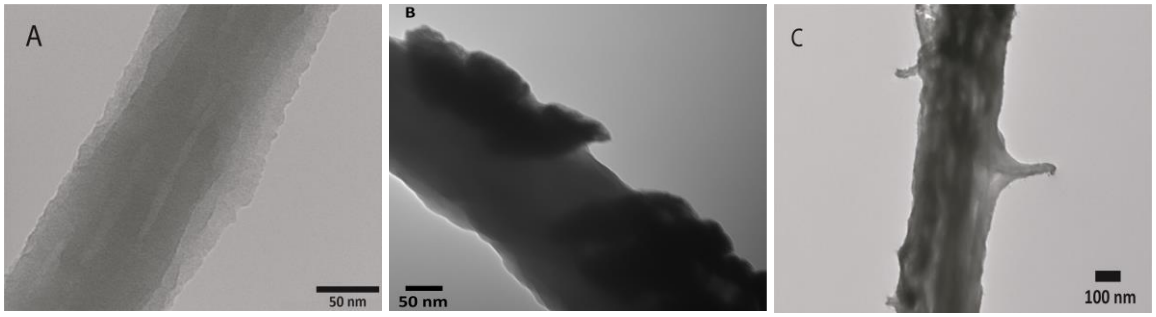

Figure 6.3 TEM images of nanofibers of: A) pure PVDF, B) blend of PVDF/PANi, C) PVDF/(MWCNT-PANi) 16 wt%

Introducing PANi-coated MWCNTs [Figure 6.3C] led to a better dispersion of MWCNTs and enhanced the probability of conductive network formation; whereas the use of uncoated

MWCNTs resulted in large clusters of MWCNTs in the nanofibers and produced an insulating material. Coating MWCNTs with PANi also resulted in nanofibers with large numbers of conductive strands, acting as conductive links between nanofibers.

Electrospun nanofibers were fabricated under extreme elongational condition and, as such, were highly oriented. This orientation of MWCNTs inside the nanofibers increased the electrical percolation concentration far beyond the processible filler concentration. Therefore, fabrication of electrically conductive nanofibers is difficult by just adding conductive nanofillers (Figure 6.4B). Moreover, the production of conductive nanofibers does not ensure a conductive nanofiber mat, due to air resistance between nanofibers.

Figure 6.3C shows that adding PANi-coated MWCNTs to PVDF resulted in short strands on the skin of the nanofibers instead of on the smooth surface of pure PVDF. The PANi tended to stay close to the surface of nanofibers and this allowed for MWCNTs to be located close to the surfaces of the nanofibers, where the MWCNT ends pulled out from the nanofibers and formed short strands (Figure 6.3C). As previously mentioned, it is very difficult to produce a conductive network in the direction of nanofibers when they are highly oriented; however, nanofibers with strands make it possible to obtain a conductive network in the transverse direction. Figure 6.4 illustrate the electrospun nanofibers for the four different case studied here. Figure 6.4D shows a schematic of PVDF nanofibers filled with PANi-coated MWCNTs versus uncoated MWCNTs (Figure 6.4B). The comparison shows how a conductive network forms in the transverse direction as shown in SEM images of nanofibers in Figure 6.2C.

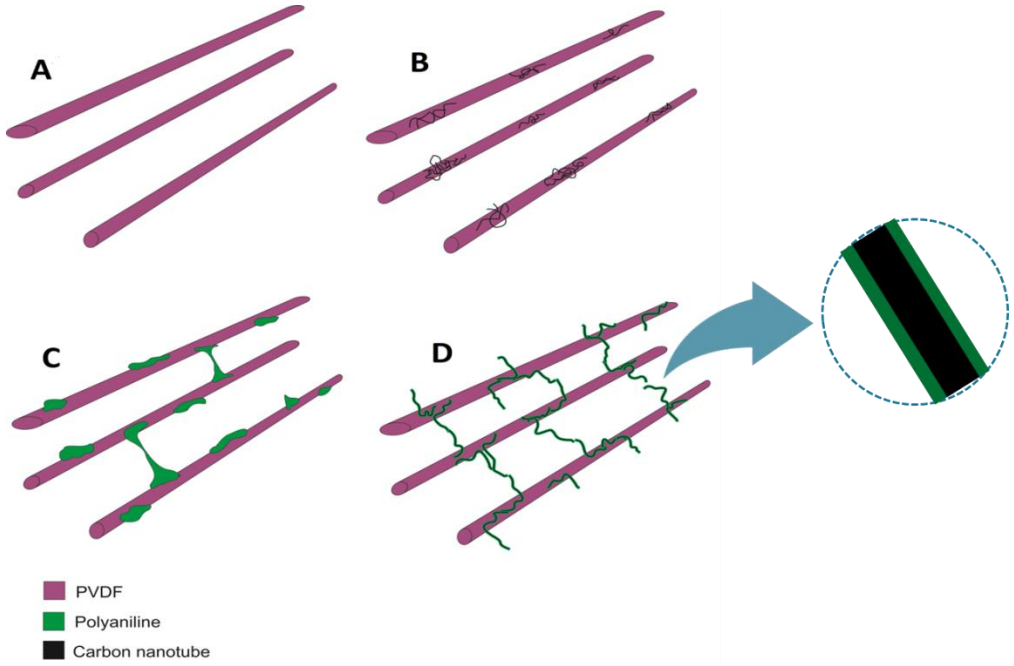

Figure 6.4 Nanofiber schematics of: A) pure PVDF, B) PVDF/MWCNT, C) blend of PVDF/PANi, D) PVDF/(MWCNT-PANi)

Conductivity measurements were performed on PVDF nanofibers filled with different loadings of coated and uncoated MWCNTs, and the results are presented in Figure 6.5. The conductivity results for PVDF/(MWCNT-PANi) confirm that a conductive nanofiber mat can be fabricated by covering nanofibers with conductive short strands. A highly conductive mat (1.7×10^{-1} S/m) was produced at a coated MWCNT loading of 24 wt%. The percolation threshold for PVDF/(MWCNT-PANi) was determined to be 13 wt% using percolation theory [18]. Producing nanofibers with filler concentrations of higher than 15 wt% was very difficult due to aggregation of uncoated MWCNTs. Nozzle blocked due to poor flow of solutions with large clusters of MWCNT. Therefore, no conductivity were reported for PVDF with more than 15 wt% uncoated MWCNT. Whereas, small clusters in the solution of PVDF filled with PANi-coated MWCNTs result in ample flow of solution in nozzle at 24 wt% of nanofiller loading.

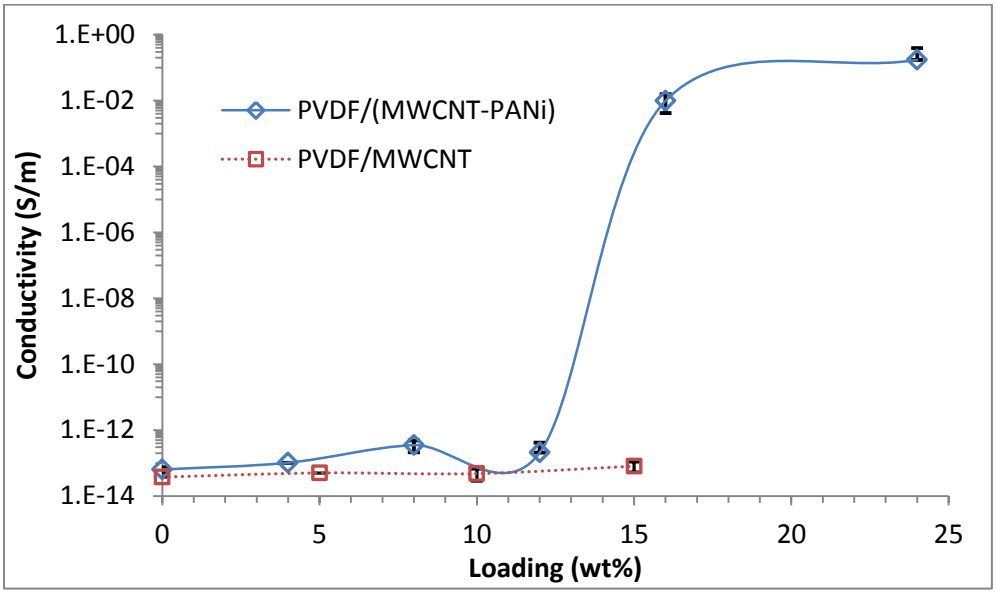

Figure 6.5 Conductivity results of nanofibers PVDF/MWCNT (square symbols) and PVDF/(MWCNT-PANi) (diamond symbols)

The high conductivity and piezoelectricity of the PVDF/(MWCNT-PANi) nanofibers make them suitable for many applications, such as nonlinear optics, transducers, and biomedical instruments [7]. As previously discussed, PVDF nanofibers demonstrate high piezoelectricity due to a high content of β-phase crystals [5-7], which were obtained with highly oriented PVDF nanofibers in a high voltage electric field.

Figure 6.6 shows wide-angle X-ray diffraction (WAXD) results for compression molded PVDF and electrospun PVDF nanofibers. The crystalline β phase of PVDF can be identified by the peak at 2θ = 24.1° (d = 0.43 nm), which contributes to both the 110 and 200 crystal planes; whereas the crystalline α phase shows two distinctive peaks at 21.4° and 30.8° and one at 20.3° [12, 27].

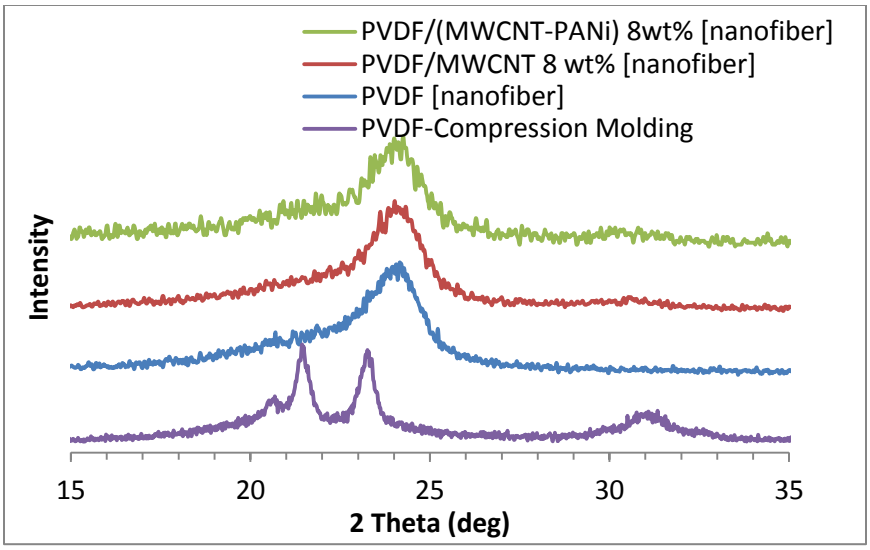

Figure 6.6 XRD spectra of nanofibers and compression molded PVDF

The WAXD results for the compression molded PVDF contained both α- and β-phase peaks, while the α-phase peaks disappeared and the characteristic β-phase peak was magnified for electrospun PVDF. The addition of MWCNT and MWCNT-PANi did not have a significant effect on the crystalline phase structure. However, the nucleation effect of nanofillers may have increased the crystalline content, or it may have reduced the crystalline content by hindering the crystal growth rate. The effect of nanofiller on crystal content is a function of its concentration in polymer [28, 29].

To investigate the effects of high elongation and nanofiller on the formation of β-phase crystals, FTIR experiments were performed on the samples. The FTIR spectrums for the samples are presented in Figures 6.7 and 8. Three absorbance peaks (all contributing to methylene rocking), are labeled: one at 840 cm^{-1}, which can be attributed to β-phase PVDF, and one each at 765 cm^{-1} and 795 cm^{-1}, which are associated with α-phase PVDF [12, 27].

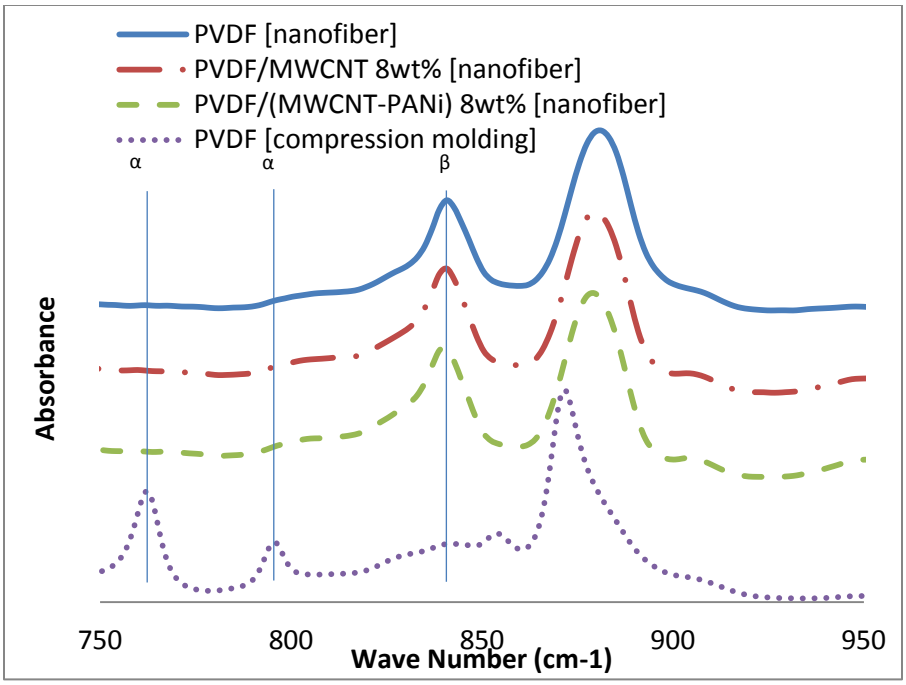

Figure 6.7 FTIR spectra of nanofibers and compression molded PVDF

The results confirm the WAXD findings on the effects of the electrospinning technique on the reduction of α-phase crystals and the formation of β-phase crystals for PVDF. The intensity of the β-phase crystal peak (at 840 cm^{-1}) for electrospun nanofibers was significantly higher than that of the compression molded PVDF. The addition of MWCNT and MWCNT-PANi did not have significant effects on the crystalline phase structure.

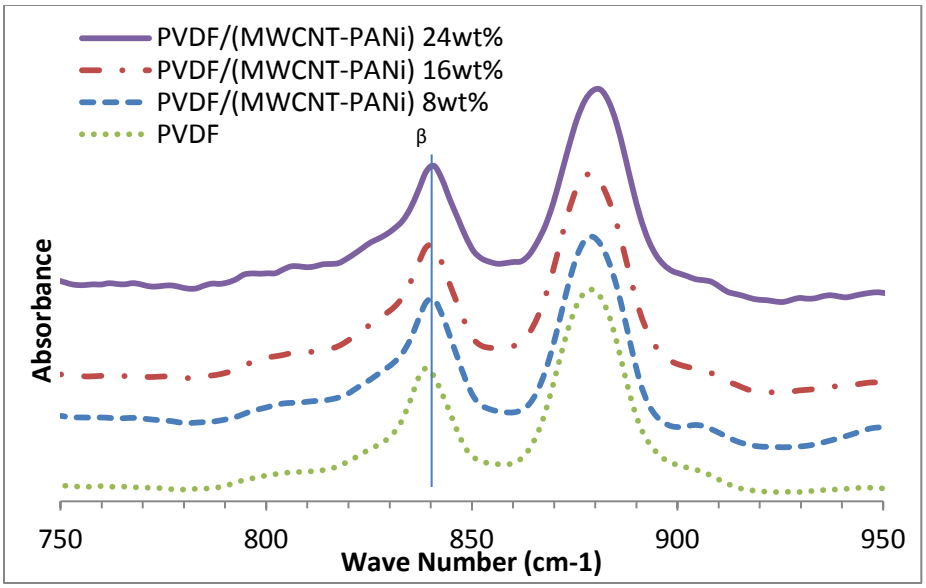

Figure 6.8 FTIR spectra of electrospun nanofibers

Figure 6.8 indicates that the MWCNT-PANi content in PVDF did not change the crystal structure; and, that there is no noticeable peak for a crystalline α phase for all electrospun nanofibers.

The filler concentration did have a minor effect on the amount of the crystalline phase. Kim et al. [30] have shown that CNTs play the role of nuclei in the formation of more β-phase crystals in a quiescent crystallization condition. However, it has been shown that, for samples under high elongation, the addition of nanofiller had a deleterious effect on the β-phase formation for PVDF samples [27]. In order to investigate the effect of the nanofiller concentration on the crystal content, DSC measurements were performed on the samples.

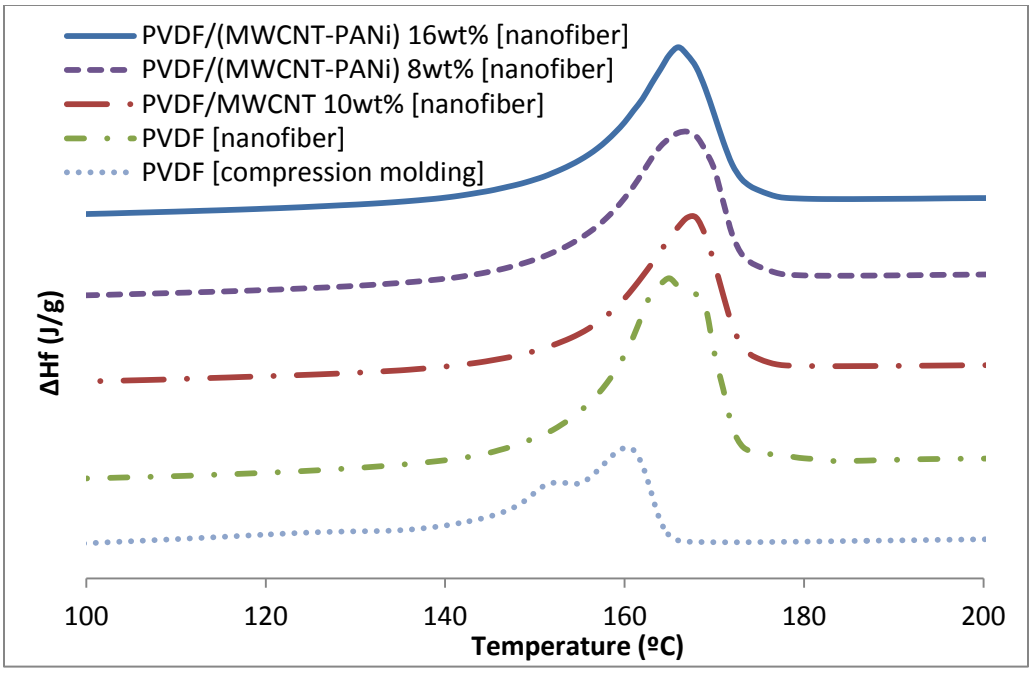

Figure 6.9 DSC thermograms of nanofibers and compression molded PVDF

DSC thermograms of the different samples are shown in Figure 6.9. The melting peak for electrospun nanofibers showed a shift to higher melting temperatures (~ 155°C) compared with that of compression molded PVDF samples (~ 144°C). This shift can be considered as evidence of the formation of β-phase crystals, which melt at higher melting points than α-phase crystals. The melting peak for compression molded samples had a shoulder that came from the melting of α-phase crystals. Nanofibers showed a narrow peak at higher melting temperatures, indicating the existence of β-phase crystals. The amount of α-phase crystals in electrospun samples was too small to be detected by DSC.

Using the DSC results and the following equation, the degree of crystallinity for samples were calculated [31].

$$X_C\ \% = [(\Delta H_m + \Delta H_c)/(\Delta H_f\,(1 - W_f))] \times 100\% \qquad 5.1$$

where X_C is the degree of crystallinity; W_f is the weight fraction of nanofillers; and, ΔH_m, ΔH_c and ΔH_f are: the heat of fusion for the sample; the heat of cold crystallization; and the heat of fusion for a 100% crystalline PVDF, respectively.

Table 6.1 DSC results of compression molding and electrospinning samples

Sample	*Processing Method*	*ΔH_m (J/g)*	*T_m (ºC)*	*X_C %***	*Conductivity (S/m)*
PVDF	Compression Molding*	33.23	144	29.2 ± 1.7	2.09×10^{-14}
PVDF/MWCNT 2wt%	Compression Molding*	22.42	142.4	21.8 ± 1.2	8.06×10^{-2}
PVDF/Closite30B 2wt%	Compression Molding*	30.24	155.7	29.5 ± 1.5	1.10×10^{-14}
PVDF	Electrospinning	57.2	155.6	51.9 ± 1.8	3.75×10^{-14}
PVDF/MWCNT 8wt%	Electrospinning	43.67	155.5	46.9 ± 1.2	4.76×10^{-14}
PVDF/(MWCNT-PANi) 8 wt%	Electrospinning	47.15	154.6	47.0 ± 1.3	3.49×10^{-13}
PVDF/(MWCNT-PANi)12 wt%	Electrospinning	47.5	154.4	49.2 ± 1.5	2.08×10^{-13}
PVDF/(MWCNT-PANi)16 wt%	Electrospinning	46.12	156	51.3 ± 1.1	9.77×10^{-3}
PVDF/(MWCNT-PANi)24 wt%	Electrospinning	45.74	154	56.1 ± 0.9	1.71×10^{-1}

* Compression molding was performed at 190 ºC

** Crystallinity results were presented with their standard deviation

The crystallinity results for electrospun and compression molded samples are given in Table 6.1. Comparing results for pure PVDF made by the two different processing methods provides insight into the effect of the processing method on the crystal structure and content. A higher melting temperature indicates that electrospun nanofibers contained more β-phase crystals than the compression molded samples. The high voltage also enhanced the amount of crystals in electrospun nanofibers to about twice that of compression molded PVDF, indicating the possibility of a higher piezoelectricity for the electrospun nanofibers.

The addition of Cloisite 30B to PVDF is an established method for increasing the amount of β-phase crystals [27]. A comparison of a PVDF sample with a Cloisite 30B loading of 2 wt% with a compression molded PVDF sample showed an increase in the melting temperature from 144°C to 155.7°C, which is evidence of a greater β-phase crystal formation. However, there was no increase in the degree of crystallization (29.5% versus 29.2%). One of the advantages of using the electrospinning technique instead of traditional melt processing methods is that we reach a high degree of crystallinity (51.9%) in PVDF without the addition of filler. Therefore, excellent mechanical properties of conductive PVDF nanofibers beside high piezoelectricity create an immense opportunity for electronic devices fabricated with these materials [32]. Degree of crystallinity results for PVDF/(MWCNT-PANi) nanofibers at different nanofiller concentration appears to have a deteriorating effect on crystal growth but further increase in filler loading enhances the degree of crystallinity probably due to nucleating effect of nanofillers.

6.6 Conclusions

Conductive PVDF nanofibers were produced by incorporating PANi-coated MWCNT nanofillers. Electrospinning PVDF and coated MWNCTs instead of uncoated MWCNTs resulted

in nanofibers covered with short strands. Short conductive strands consisting of coated MWCNTs facilitated the formation of a conductive network in the transverse direction of the nanofibers. Electrospun nanofibers exhibited higher amount of β crystalline phase compared to compression molded PVDF composites likely providing a higher piezoelectric effect. It was shown that the addition of nanofiller did not affect the crystal structure, but did influence the degree of crystallinity of the samples.

6.7 References

[1] Furukawa, T.; Date, M.; Fukada, E. Hysteresis phenomena in polyvinylidene fluoride under high electric-field. *Journal of Applied Physics* **1980**, *51*, 1135-1141.

[2] Baise, A.; Lee, H.; Oh, B.; Salomon, R.; Labes, M. Enhancement of pyroelectricity in a vinylidene fluoride-tetrafluoroethylene copolymer. *Applied Physics Letters* **1975**, *26*, 428-430.

[3] Koga, K.; Ohigashi, H. Piezoelectricity and related properties of vinylidene fluoride and trifluoroethylene copolymers. *Journal of Applied Physics* **1986**, *59*, 2142-2150.

[4] Kepler, R.; Anderson, R. Ferroelectricity in polyvinylidene flouride. Journal of Applied Physics **1978**, *49*, 1232-1235.

[5] Priya, L.; Jog, J. Intercalated poly(vinylidene fluoride)/clay nanocomposites: Structure and properties. *Journal of Polymer Science Part B-Polymer Physics* **2003**, *41*, 31-38.

[6] Levi, N.; Czerw, R.; Xing, S.; Iyer, P.; Carroll, D. Properties of polyvinylidene difluoride-carbon nanotube blends. *Nano Letters* **2004**, *4*, 1267-1271.

[7] Hattori, T.; Kanaoka, M.; Ohigashi, H. Improved piezoelectricity in thick lamellar beta-form crystals of poly(vinylidene fluoride) crystallized under high pressure. *Journal of Applied Physics* **1996**, *79*, 2016-2022.

[8] Kawai, H. Piezoelectricity of poly (vinylidene fluoride). *Japanese Journal of Applied Physics* **1969**, *8*, 975-&.

[9] Sessler, G. Piezoelectricity in polyvinylidene fluoride. *Journal of the Acoustical Society of America* **1981**, *70*, 1596-1608.

[10] Furukawa, T.; Date, M.; Fukada, E. Hysteresis phenomena in polyvinylidene fluoride under high electric-field. *Journal of Applied Physics* **1980**, *51*, 1135-1141.

[11] Dillon, D.; Tenneti, K.; Li, C.; Ko, F.; Sics, I.; Hsiao, B. On the structure and morphology of polyvinylidene fluoride-nanoclay nanocomposites. *Polymer* **2006**, *47*,1678-1688.

[12] Sarvi, A.; Chimello, V.; Silva, A. B.; Bretas, R. E. S.; Sundararaj, U. Coaxial Electrospun Nanofibers of Poly(vinylidene fluoride)/Polyaniline Filled With Multi-Walled Carbon Nanotubes. *Polymer Composites* **2014**, 35, 1198-1203.

[13] Ramakrishna, S.; Fujihara, K.; Teo, W-E.; Lim, T-C.; Ma, Z. *An Introduction to Electrospinning and Nanofibers*, World Scientific, London, 2005.

[14] Choi, S.; Jo, S.; Lee, W.; Kim, Y. An electrospun poly(vinylidene fluoride) nanofibrous membrane and its battery applications. *Advanced Materials* **2003**, *15*, 2027-2032.

[15] Gautschi, G. *Piezoelectric Sensorics: Force, Strain, Pressure, Acceleration and Acoustic Emission Sensors. Materials and Amplifiers*, Springer -Verlag Berlin Heidelberg, New York, 2002.

[16] Pu, J.; Yan, X.; Jiang, Y.; Chang, C.; Lin, L. Piezoelectric actuation of direct-write electrospun fibers. *Sensors and Actuators a-Physical* **2010**, *164*, 131-136.

[17] Celina, M,; Dargaville, T.; Chaplya, P.; Clough, R.; Chipara, M.; Edwards, D.; Benson, R.; Phillips, S. Piezoelectric PVDF materials performance and operation limits in space environments. *Materials For Space Applications* **2005**, *851*, 449-460.

[18] Weber, M.; Kamal, M. Estimation of the volume resistivity of electrically conductive composites. *Polymer Composites* **1997**,*18*, 711-725.

[19] Shrivastava, N.; Khatua, B. Development of electrical conductivity with minimum possible percolation threshold in multi-wall carbon nanotube/polystyrene composites. *Carbon* **2011**, *49*, 4571-4579.

[20] Konyushenko, E.; Stejskal, J.; Trchova, M.; Hradil, J.; Kovarova, J.; Prokes, J.; Cieslar, M.; Hwang, J.; Chen, K.; Sapurina, I. Multi-wall carbon nanotubes coated with polyaniline. *Polymer* **2006**, *47*, 5715-5723.

[21] Mottaghitalab, V.; Spinks, G.; Wallace, G. The development and characterisation of polyaniline-single walled carbon nanotube composite fibres using 2-acrylamido-2-methyl-1-propane sulfonic acid (AMPSA) through one step wet spinning process. *Polymer* **2006**, *47*, 4996-5002.

[22] Gasparini, T. M.; Bretas, R. E. S.; Silva, A. B.; Jr, R. G. Processing and characterization of oriented electrospun poly(vinylidene fluoride) mats. *J. Polymer Science B: Polymer Physics* **2012**, *50*, 1304–1311.

[23] Liu, M.; Tzou, K.; Gregory, R. Influence of the doping conditions on the surface energies of conducting polymers. *Synthetic Metals* **1994**, *63*, 67-71.

[24] Wu, S. Calculation of interfacial tension in polymer systems. *Journal of Polymer Science Part C-Polymer Symposium* **1971**, 19-&.

[25] Goldel, A.; Kasaliwal, G.; Potschke, P. Selective Localization and Migration of Multiwalled Carbon Nanotubes in Blends of Polycarbonate and Poly(styrene-acrylonitrile). *Macromolecular Rapid Communications* **2009**, *30*, 423-429.

[26] Nuriel, S.; Liu, L.; Barber, A.; Wagner, H. Direct measurement of multiwall nanotube surface tension. *Chemical Physics Letters* **2005**, *404*, 263-266.

[27] Sadeghi, F.; Sarvi, A.; Sundararaj, U. PVDF/Carbonnanotubes/Nanoclay Composites for Piezoelectric Applications. *Journal of International Polymer Processing* **2014**, *29*, 81-87.

[28] Grady, B.; Pompeo, F.; Shambaugh, R.; Resasco, D. Nucleation of polypropylene crystallization by single-walled carbon nanotubes. *Journal of Physical Chemistry B* **2002**, *106,* 5852-5858.

[29] Leelapornpisit, W.; Ton-That, M.; Perrin-Sarazin, F.; Cole, K.; Denault, J.; Simard, B. Effect of carbon nanotubes on the crystallization and properties of polypropylene. *Journal of Polymer Science Part B-Polymer Physics* **2005**, *43,* 2445-2453.

[30] Kim, Y.; White, J. Melt-intercalation nanocomposites with fluorinated polymers and a correlation for nanocomposite formation. *Journal of Applied Polymer Science* **2004**, *92*, 1061-1071.

[31] Lee, T.; Boey, F.; Khor, K. On the determination of polymer crystallinity for a thermoplastic PPS composite by thermal-analysis. *Composites Science and Technology* **1995**, *53*, 259-274.

[32] Choi, S.; Kim, J.; Ahn, Y.; Jo, S.; Cairns, E. Characterization of electrospun PVdF fiber-based polymer electrolytes. *Chemistry of Materials* **2007**, *19*, 104-115.

Chapter 7

Coaxial electrospun nanofibers of poly(vinylidene fluoride)/polyaniline filled with multi-walled carbon nanotubes♣

7.1 Presentation of the Article

This article demonstrates the fabrication of coaxial electrospun nanofibers of PVDF/PANi filled with carbon nanotubes. Our earlier studies in Chapter 6 showed that it is hard to attain conductive nanofibers using electrospinning due to the high orientation of carbon nanotubes in nanofibers, leading to discontinuity in conductive network and air gap resistance between nanofibers. This article, therefore, focused on coaxial electrospinning of PVDF nanofibers. Multi-layer nanofibers were produced and MWCNTs were introduced to the outer layer of core-shell nanofibers which enhanced the chance of network formation and reduced the electrical percolation threshold. Localizing MWCNT in the outer layer of coaxial electrospun nanofibers showed a significant decrease in the electrical percolation of the nanofibers' mat. Consequently, semi-conductive nanofibers were produced through the incorporation of MWCNTs in the outer layer of core-shell nanofibers. In this work, Dr. Silva helped with SEM images, Mr. Chimello designed the coaxial nozzle and Dr. Bretas and Dr. Sundararaj have supervised this study and helped with result and discussion part. The major work has been done by Ali Sarvi.

♣ Sarvi A, Chimello V, Silva AB, Bretas RES, Sundararaj U "Coaxial electrospun nanofibers of poly(vinylidene fluoride)/polyaniline filled with multi-walled carbon nanotubes" *Polymer Composites*, 2014, **35**, 1198.

Coaxial electrospun nanofibers of poly(vinylidene fluoride)/polyaniline filled with multiwall carbon nanotubes

A. Sarvi[1], V.Chimello[2], A. B. Silva[2], R. E. S. Bretas[2] and U. Sundararaj[1*]

1. Department of Chemical & Petroleum Engineering, University of Calgary, Canada

2. Programa de Pós-Graduação em Ciência e Engenharia de Materiais, Universidade Federal de São Carlos, Brazil

7.2 Abstract

Core-shell nanofibers of poly (vinylidene fluoride)/polyaniline/multiwall carbon nanotubes (PVDF/PANi/MWCNTs) have been produced using the coaxial electrospinning technique. The nanofibers were semi-conductive and had better piezoelectric properties than pure PVDF nanofibers. Piezoelectric PVDF nanofibers are capable of converting mechanical energy into electrical energy, which can be stored in charge storage devices. However, PVDF is not conductive and therefore, a conductive associate material is needed to transfer accumulated static charges into the capacitor. Fourier Transform Infrared (FTIR) spectroscopy and differential scanning calorimetry (DSC) were carried out to study the crystalline β-phase of PVDF. There was an increase in β-phase in the electrospun PVDF nanofibers filled with MWCNTs as compared with compression molded samples of neat PVDF. Incorporation of PANi as an intrinsically conductive polymer (ICP) and MWCNTs as conductive nanofiller helps the

movement of static charges. Core-shell nanofibers had conductivities of about seven orders of magnitude higher than simple electrospun nanofibers.

7.3 Introduction

Poly (vinylidene fluoride) has recently attracted a great deal of attention because of its potential applications as a piezoelectric/pyroelectric material [1]. PVDF has been known for many years for its piezoelectric and pyroelectric properties where it finds applications in nonlinear optics, microwave transducers and biomedical instruments [2]. High orientation of PVDF macromolecules in high voltage field during the electrospinning process enhances the crystalline β-phase which can increase piezoelectricity.

Nonwoven mats of PVDF containing nanofibers in the range of hundreds of nanometers in diameter are produced from polymeric solutions. The solution is contained in a capillary in which an electrode is immersed and attached to a high voltage supply; a high voltage field is thus applied between the capillary and the collector [3]. The liquid droplet at the tip of capillary accumulates electrostatic charges and it is elongated by the high voltage field; during the path between the capillary and the collector, the solvent evaporates and nanofibers are deposited on the grounded collector [4].

In this study, coaxial nanofibers of a blend of polyaniline (PANi) with PVDF were produced. PANi is an intrinsically conductive polymer with tunable conductivity over a wide range by protonation. Therefore, nanofibers of PVDF/PANi with high surface area and essential conductivity are good choices for applications such as actuators, sensors, transducers [5-7]. To further increase the conductivity, multi walled carbon nanotubes (MWCNTs) were also added to

the shell layer of core-shell nanofibers (where the core was PVDF and the shell was composed of a blend of PVDF/PANi). The main advantages of nanofibers filled with MWCNT are their excellent properties, including structure scalability, greater flexibility, and greater piezoelectric strain constant (d_{33}∼−57.6pm/V) [8] compared with commercially available PVDF thin films (d_{33}∼−15pm/V) [9]. Addition of MWCNTs into a polymer matrix commonly leads to conductive composites after a minimum essential MWCNT loading which is called the electrical percolation threshold [10, 11]. A conductive network is formed in the polymer matrix as the amount of MWCNTs increased in the composite. However, in the case of electrospun nanofibers, reaching the electrical percolation is difficult due to the high orientation of the nanotubes inside of the nanofibers, which causes disconnections along the nanofibers. Our earlier investigations on PVDF/PANi nanofibers showed that the PANi phase made bridges between the nanofibers and eliminated air resistance between them [12]. Therefore, conductive nanofibers of PVDF/PANi/MWCNTs with significantly low resistivity of 4.8×10^3 Ω.cm were produced with 24 wt% of MWCNTs loading [12].

A coaxial spinneret designed and built in house was used to produce core-shell nanofibers of PVDF(core)/PVDF-PANi-MWCNTs(shell). Low concentrations of PVDF were added to the PANi solution to increase the viscosity of relatively dilute PANi solutions to produce the shell layer. Thus, the blend of PVDF/PANi was electrospinnable while PANi by itself was not. The coaxial electrospinning method provides an alternative and effective way of fabricating semi-conductive PVDF fibers by locating MWCNT in the shell layer while decreasing the electrical percolation threshold. Selective localization of MWCNTs significantly reduces the electrical percolation concentration in polymer matrices [10, 13]. In the coaxial electrospinning, two different solutions were injected into a coaxial spinneret. PVDF solution was injected through

the inner capillary to form the core, and a blend of PVDF/PANi/MWCNTs was injected through the outer capillary to encapsulate the core PVDF nanofiber.

7.4 Experimental Section

PVDF (Kynar 1000HD) was supplied by Arkema. Polyaniline with weight average molecular weight M_w=65000 g/mol was supplied by Sigma Aldrich. A mixture of N, N-dimethylformamide (DMF, 99.5%, Merck), and acetone (Merck, 99.7%) was used as solvent. The volume ratio of DMF to acetone was 3:1. The MWCNTs were Nanocyl™, product no. NC7000, with average diameter of 9.5 nm, average length of 1.5 μm and specific surface area of 250-300 m^2/g. Concentration of PVDF in the solution was kept at 12 wt%. To produce the blend's nanofibers [14], PANi was dissolved in DMF and the solution was filtered to remove non-dissolved PANi. The concentration of PANi in the solution based on thermal gravimetric analysis (TGA) of nanofibers was found to be ~ 8 wt%. Different amount of MWCNTs were added to the PVDF solution; both, the PVDF/PANi mixture and the solution were sonicated for 1 hour.

The coaxial spinneret was designed using progeCAD 2009 Smart software. Assessing of the spinneret designs are reported in the literature [15-18]; the new coaxial spinneret was designed and made of brass. Figure 7.1 shows the spinneret scheme where sizes are in millimeter. This specific design facilitates cleaning, maintenance and also decreases polymer solution loss during the spinning process.

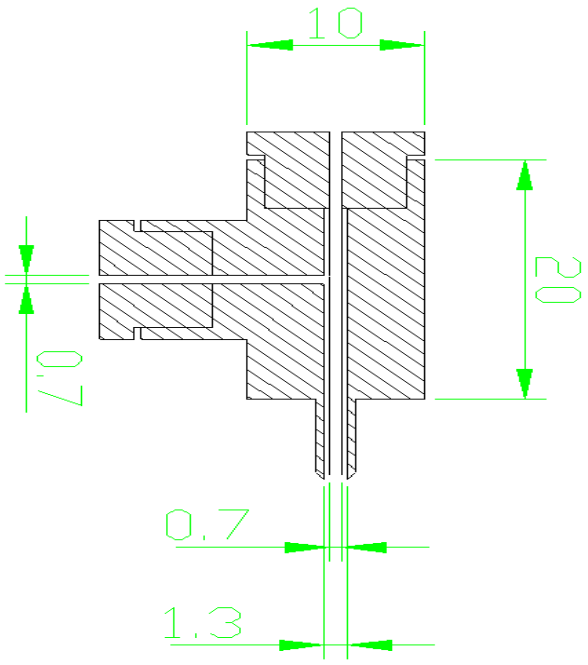

Figure 7.1 Scheme of coaxial spinneret

Nanofibers were electrospun using 20 kV of voltage, 5 cm of work distance (the distance between the syringe and the collector) and were collected on a high speed rotor rotating at 2,000 rpm. The injection speed of the solutions varied from 0.03 ml/min to 0.60 ml/min depending to the viscosity of the solution.

Transmission electron microscopy (TEM) and scanning electron microscopy (SEM) were used to investigate the morphology of the nanofibers. The core-shell nanofibers were deposited on copper grids and then the PANi phase was stained using OsO_4. TEM images were obtained at 60 kV using a Hitachi H-7650. For SEM imaging, samples were prepared by placing a piece of the

nanofibers mat on Al stubs; the samples were gold-coated to enhance the resolution. A Philips scanning electron microscope (model XL 30 FEG) was used at 20 kV.

Volume resistivity was measured by placing a UR type probe on the nanofibers mat surface. The applied voltage was 100V and the probe was connected to a Hiresta UP resistivity meter. Infrared spectra were recorded on a FTIR instrument from ThermoElectron Corporation, Chicago, IL Nicolet Nexus 470 FTIR with a resolution of 4 cm^{-1} and accumulation of 128 scans. The DSC tests were carried out on a TA Instruments Q100, using a heating and cooling rate of 10 °C/min. A Rigaku Geigerflex Powder Diffractometer was used for the X-ray diffraction experiments (λ = 1.79 Å). The device was equipped with a cobalt tube, graphite monochromator and scintillation detector.

7.5 Results and Discussions

Scanning electron microscopy images of coaxial electrospun nanofibers of PVDF/PVDF82-PANi8-MWCNT10 (82 wt% of PVDF, 8 wt% of PANi and 10 wt% of MWCNT in the shell layer) are shown in figure 7.2. SEM images show nanofibers with diameters between 100 and 300 nm with rough surface. Figure 7.2a shows the size distribution of nanofibers with average diameter of 150 nm. Figure 7.2b clearly shows a core fiber enveloped with a second layer of polymer where the core is pure PVDF and the shell is a blend of 82 wt% of PVDF and 8 wt% of PANi filled with 10 wt% of MWCNT. Incorporation of PANi in the PVDF nanofibers as Figure 7.2c shows, promoted the formation of conductive bridges between the nanofibers which eliminated air resistance between the fibers. In order to obtain a conductive nanofibers mat, besides increasing the conductivity of the nanofibers, making conductive connections between nanofibers and removing air resistance are necessary. Therefore, using doped PANi as a

conductive polymer increases the conductivity of nanofibers mat by bridging airgaps between nanofibers. X-ray spectroscopy of these bridges showed high content of nitrogen which comes from the amine groups of polyaniline.

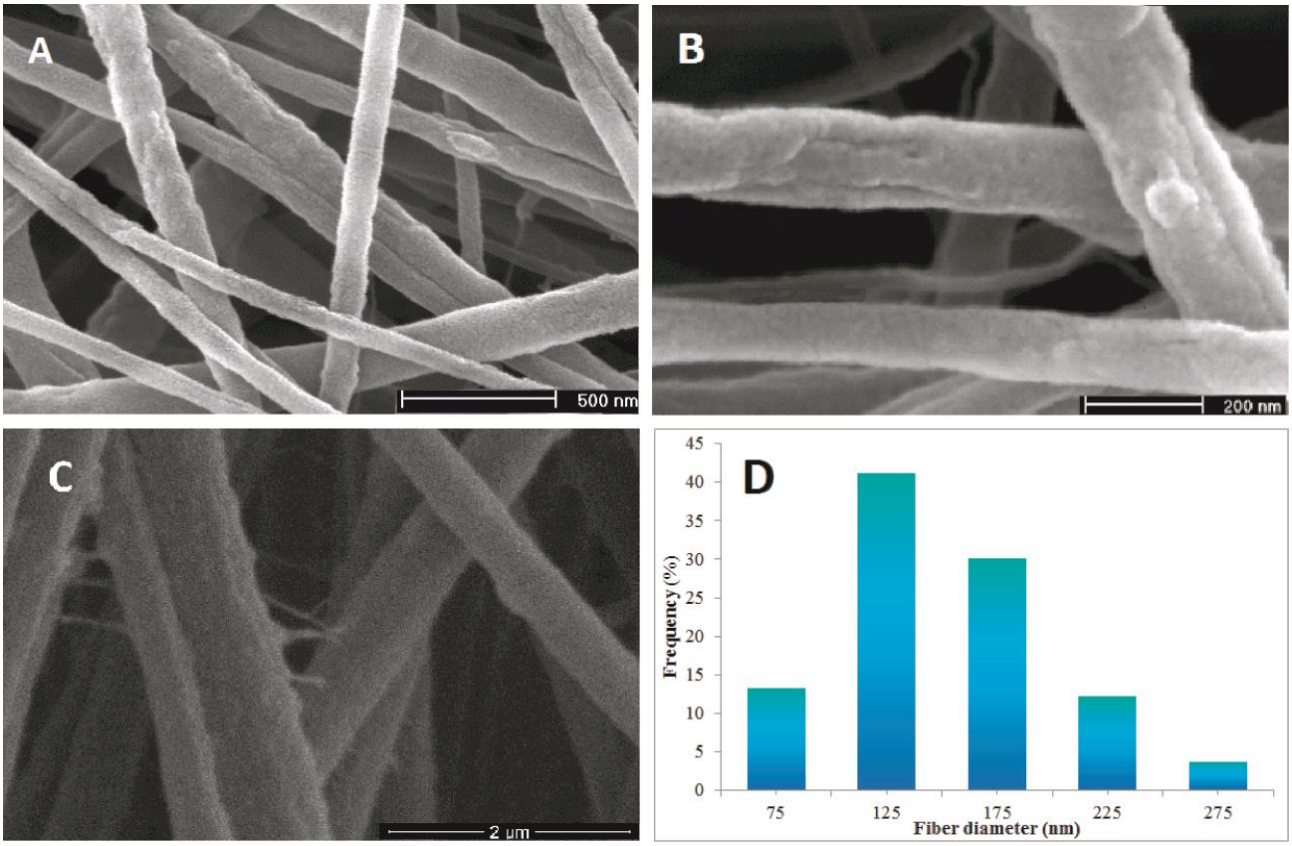

Figure 7.2 SEM images of: A) and B) PVDF/PVDF82-PANi8-MWCNT10 nanofibers and C) PVDF82/PANi8 nanofibers.

Figure 7.3a shows the blend of PVDF and PANi nanofibers fabricated by a simple electrospinning technique. The PANi phase was stained using OsO_4. The TEM image shows the dark PANi phase inside the PVDF nanofibers. A high tendency of PANi to aggregate results in agglomerates dispersed inside the PVDF matrix. Some elongated dark phases are also observed

in the nanofibers which were a mixture of both PVDF and PANi. The production of the core-shell nanofibers was also observed by transmission electron microscopy, as shown in Figure 7.3b. The coating thickness varied according to the diameter of the nanofibers. The average coating thickness for nanofibers was 49 nm and the average diameter of the core was about 100 nm.

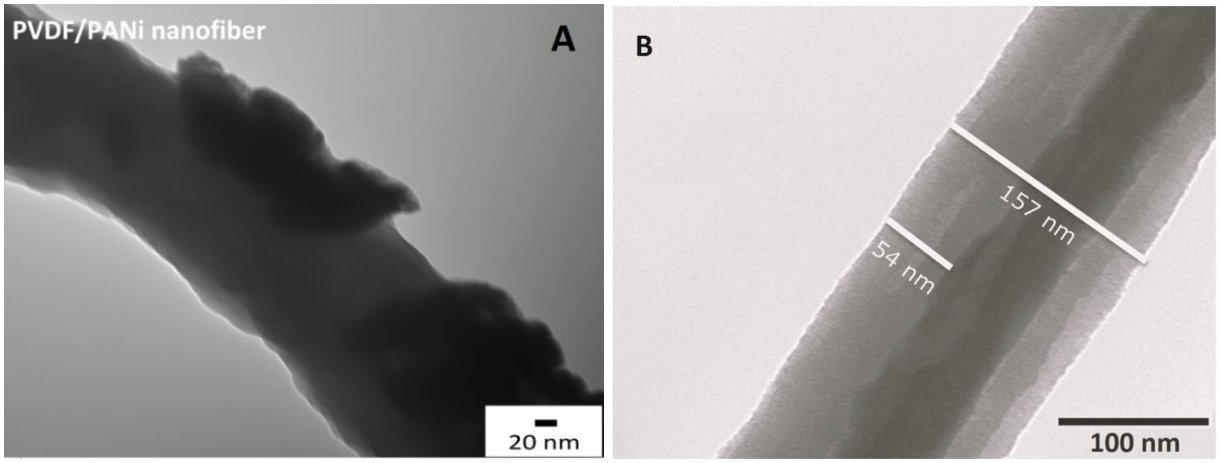

Figure 7.3 TEM images of: a) PVDF82/PANi8 nanofibers and b) PVDF/PVDF82-PANi8 core-shell nanofibers

Figure 7.4 shows wide-angle X-ray diffraction (WAXD) results for compression molded PVDF and electrospun PVDF nanofibers. The crystalline β phase of PVDF can be identified by the peak at 2θ = 24.1° (d = 0.43 nm), which contributes to both the 110 and 200 crystal planes; whereas the crystalline α phase shows two distinctive peaks at 21.4° and 30.8° and one at 20.3° [19].

The WAXD results for the compression molded PVDF contained both α- and β-phase peaks, while the α-phase peaks disappeared and the characteristic β-phase peak was magnified for electrospun PVDF. The addition of MWCNT and MWCNT-PANi did not have a significant effect on the crystalline phase structure. However, the nucleation effect of nanofillers may have

increased the crystalline content, or it may have reduced the crystalline content by hindering the crystal growth rate. The effect of nanofiller on crystal content is a function of its concentration in polymer [20, 21].

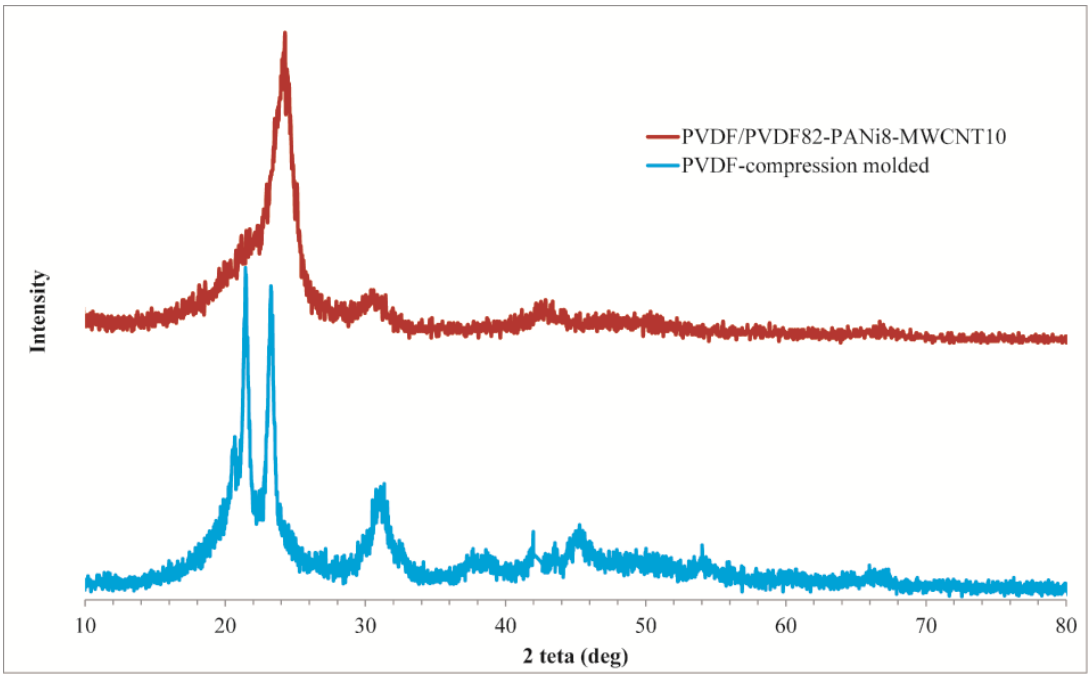

Figure 7.4 WAXD results of core-shell nanofibers and compression molded PVDF

To investigate the effect of MWCNT on the formation of the β phase PVDF crystals, FTIR experiments were performed on the samples. The FTIR spectra for the samples are presented in Figure 7.5. Three absorbance peaks contributing to CH_2 rocking, one at 840 cm^{-1} (attributed to β PVDF), and the other two at 764 cm^{-1} and 795 cm^{-1} (associated with α PVDF) [19] are labeled. The results clearly show the effect of CNT on the α-phase reduction. However the intensity of the peak of the β-phase crystal (at 840 cm^{-1}) with the addition of CNT. The effect of CNT addition in the formation of the β-crystal phase of PVDF has been previously studied [22]. Moreover, one of the established methods to produce β-PVDF is by stretching PVDF at temperatures of 50 to 100°C [2]. PVDF crystallizes mostly in the α-phase following either

quiescent crystallization or during cooling following cast extrusion. The most conventional method for production of β-PVDF is uniaxial stretching of PVDF samples with α-crystalline phase [2]. Electrospinning of nanofibers provides high orientation of polymer chains under high shear field. Therefore, it is expected that a higher amount of β-PVDF will be obtained using the electrospinning technique.

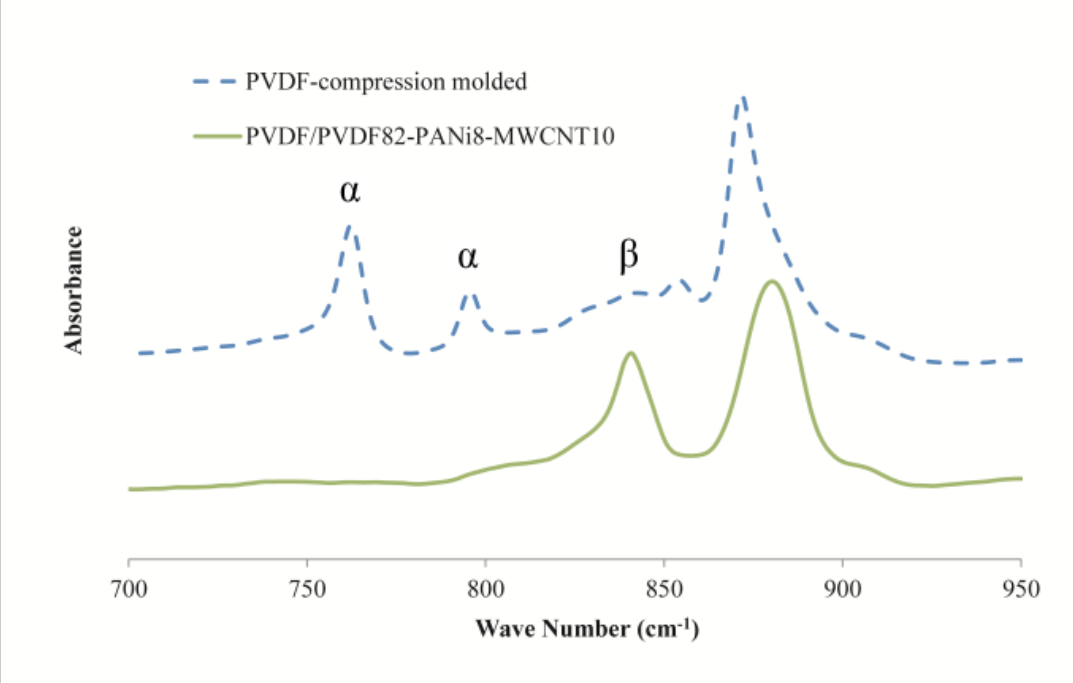

Figure 7.5 FTIR spectra of core-shell nanofibers and compression molded PVDF

DSC experiments can also be used to evaluate the crystalline structure of PVDF. The results for the first heating cycles that contain information about the thermal history of the samples are shown in Figure 7.6. Addition of CNT affects the crystal structure of the PVDF. The differences in unit cell and crystal type lead to changes in thermal behavior of the samples during melting. With addition of CNT and orientation by electrospinnig, the melting peak shifted to higher temperatures. This is attributed to the formation of more β-phase in the crystalline structure [23].

Although a double peak pattern is observed for neat PVDF, a single peak at higher melting point is observed for PVDF/PVDF82-PANi8-MWCNT10 nanofibers which is attributed to formation of a high amount of the β phase crystal [19, 23].

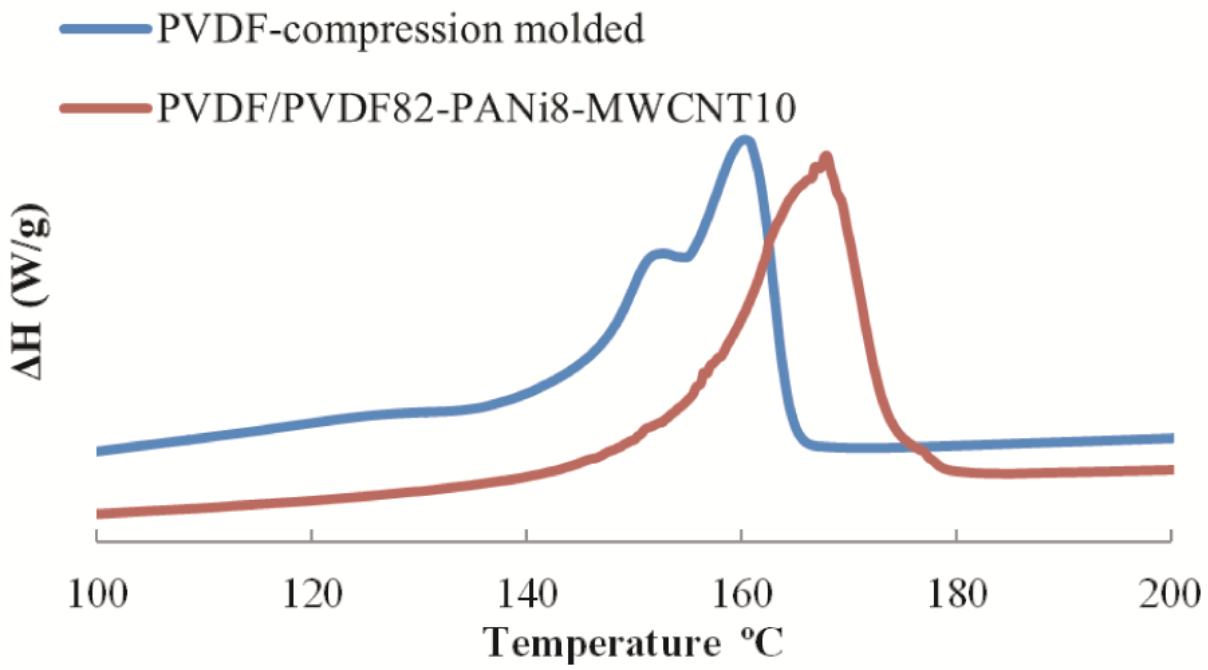

Figure 7.6 DSC thermogram of core-shell nanofibers and compression molded PVDF

SAXS (small angle x-ray scattering) conducted by Patro et al. [24] showed that the long period (L_w) and crystalline lamellar thickness (L_c) decreased with increasing MWCNT concentration (i.e. increasing concentration of nucleating agent) which is related to formation of the β phase [24]. However DSC and hot-stage optical microscopy revealed higher melting and crystallization temperatures, and formation of smaller spherulites with addition of MWCNTs [24]. The increase in melting point can be attributed to the type of crystal rather than to the spherulite size.

The conductivity of the nanofibers mat is very important because this enables us to use the generated electricity when PVDF is subjected to motion. Incorporation of carbon nanotubes into PVDF to increase its conductivity has been previously studied [25], and it is found that a good dispersion of CNT into PVDF is a crucial factor to acquire a lower percolation concentration of CNT. Arjmand et al. [26] studied the influence of CNTs orientation on conductivity and found that the electrical conductivity of high oriented samples decreased while the percolation threshold increased. Production of nanofibers using electrospinning causes a high level of orientation of the MWCNTs inside the nanofibers and the breakage of the MWCNTs network along nanofibers. Therefore, in order to reach the percolation threshold, high concentration of MWCNTs is needed. However, high loading of MWCNTs significantly increases the viscosity of the solution and thus nanofibers are difficult to produce. Placing MWCNTs in the shell layer of coaxial electrospun nanofibers can enhance the probability that a network forms at lower concentrations and has increased conductivity. Conductivity measurements of both simple and coaxial spun fibers are shown in Table 7.1. Introducing 10 wt% of MWCNTs into neat PVDF did not result in a significant change in conductivity of the nanofibers, because of the high percolation threshold of these fibers due to the air gaps between fibers. Incorporating conductive PANi increased conductivity by bridging the nanofibers and eliminating air resistance between them. Hence, selectively localizing MWCNTs in shell layers resulted in significant increase in conductivity of the nanofibers mat at the same filler loading. Insertion of MWCNTs in the shell layer enhanced their network formation and increased their conductivity. PANi´s role as a bridge and conductive partner in the thin shell layer was helpful to increase the conductivity of these nanofibers.

Table 7.1 Conductivity of nanofibers mats

Material	*MWCNT content (wt.%)*	*Spinneret type*	*Conductivity (S/m)*
PVDF	0	Needle	3.74×10^{-14}
PVDF/MWCNT	5	Needle	5.00×10^{-14}
PVDF/MWCNT	10	Needle	4.36×10^{-14}
PVDF/PANI/MWCNT	5	Needle	1.73×10^{-12}
PVDF/PANI/MWCNT	10	Needle	4.08×10^{-12}
PVDF/PVDF-PANi-MWCNT	10	Coaxial nozzle	2.75×10^{-7}

- PANi concentration in all samples was 8 wt.%

7.6 Conclusions

Core-shell nanofibers were successfully fabricated using the coaxial electrospinning technique. Placing CNTs and PANi in the shell layer resulted in a significant increase in conductivity of the nanofibers mat. Incorporation of PANi increased the conductivity of the nanofibers mat by bridging the nanofibers and eliminating air resistance. PVDF/PANi nanofibers had a higher amount of β-phase crystal when MWCNTs were added to the blend. Therefore, it is expected that nanofibers mat show higher piezoelectricity than compression molded PVDF.

7.7 References

[1] L. Priya, and J.P. Jog, *J. Polym. Sci. Part B: Polym. Phys.*, **41**, 31 (2003).

[2] T. Hattori, M. Kanaoka, and H. Ohigashi, *J. Appl. Phys.*, **79**, 2016 (1996).

[3] S. W. Choi, S. M. Jo, W. S. Lee, and Y-R. Kim, *Adv. Mater.*, **15**, 2027 (2003).

[4] S. Ramakrishna, K. Fujihara, W. E. Teo, T.C. Lim, and Z. Ma, *An Introduction to Electrospinning and Nanofibers*, World Scientific, London (2005).

[5] A. G. Holmes-Siedle, P. D. Wilson, and A. P. Verrall, *Materials & Design*, **4**, 910 (1984).

[6] T. Sato, H. Ishikawa, and O. Ikeda, *Applied Optics*, **21**, 3664 (1982).

[7] J. M. Ha, H. O. Lim, N. J. Jo, *Advanced Materials Research*, **29**, 363 (2007).

[8] J. Pu, X. Yan, Y. Jiang, C. Chang, and L. Lin, *Sensors and Actuators A: Physical*, **164**, 131 (2010).

[9] M. C. Celina, T. R. Dargaville, P. M. Chaplya, and R. L. Clough, *Materials Research Society Proceedings*, **851**, 449 (2005).

[10] G. A. Gelves, M. Al-Saleh, U. Sundararaj, *Journal of Materials Chemistry*, **21**, 829 (2011).

[11] N. K. Shrivastava, and B. B. Khatua, *Carbon*, **49**, 4571 (2011).

[12] A. Sarvi, A. B. Silva, V. Chimello, R. E. S. Bretas, and U. Sundararaj, *PPS 29*, Nuremberg, Germany (2013).

[13] A. Goldel, G. Kasaliwal, P. Potschke, *Macromo.Rapid.Commun.*, **30**, 423 (2009).

[14] L. M. M. Costa, R. E. S. Bretas, and R. Gregorio, *J. Mate r. Sci. Appl.*, **1**, 246 (2010).

[15] D. G. Yu, C. B. White, S. W. A. Bligh, K. White, N. P. Chatterton, and L. M. Zhu, *Macromo.Rapid.Commun.*, **32**, 744 (2011).

[16] D. G. Yu, K. White, J. H. Yang, X. Wang, W. Qian, Y. Li, *Mat.Lett.*, **67**, 78 (2012).

[17] B. S. Lee, S. B. Son, K. M. Park, J. H. Seo, S. H. Lee, I. S. Choi, K. H. Oh, and W. R. Yu, *Journal of Power Sources*, **206**, 267 (2012).

[18] D. Han, S. T. Boyce, and A. J. Steckl, *Mater.Res.Soc.Symp.Proc.*, 1094 (2008).

[19] F. Sadeghi, and A. Ajji, *Polym. Eng. Sci.*, **49**, 200 (2008).

[20] B. P. Grady, F. Pompeo, R. L. Shambaugh, and D. E. Resasco, *J. Phys. Chem. B*, **106**, 5852 (2002).

[21] W. Leelapornpisit, M. T. Ton-That, F. Perrin-Sarazin, K. C. Cole, J. Denault, B. Simard, *Journal of Polymer Science: Part B: Polymer Physics*, **43**, 2445 (2005).

[22] G. H. Kim, S. M. Hong, and Y. Seo, *Physical Chemistry Chemical Physics*, **11**, 10506 (2009).

[23] Y. Kim, and J. L. White, *J. Appl. Polym. Sci.*, **92**, 1061 (2004).

[24] T. U. Patro, M. V. Mhalgi, D. V. Khakhar, and A. Misra, *Polymer*, **49**, 3486 (2008).

[25] G-X. Chen, Y. Li, and H. Shimizu, *Carbon*, **45**, 2334 (2007).

[26] M. Arjmand, M. Mahmoodi, G. A. Gelves, S. Park, U. Sundararaj, *Carbon*, **49**, 3430 (2011).

Chapter 8

Enhancing Electrical Properties of MWCNTs in Miscible Blends of Poly(methyl methacrylate) and Styrene-Acrylonitrile copolymer by Selective Localization[♣]

8.1 Presentation of the Article

This article demonstrates a way to significantly decrease the electrical percolation threshold of conductive polymer composites. An interesting phase behavior of the immiscible polymer blends (i.e. PMMA/SAN) provided an opportunity to manipulate the morphology of the blend and structure of MWCNT network for tailoring the conductivity and electrical permittivity of the conductive composite. The electrical percolation threshold reported for these conductive blends (0.4 wt%) is uncompetitive with single phase polymers/MWCNT composites. In addition, varying the temperature resulted in a different morphology and change in the electrical properties of the composites (i.e. $\sigma=3.15\times10^{-14}$ S/cm, at 140 ˚C; $\sigma=2.21\times10^{-2}$ S/cm, at 260 ˚C), making them suitable for applications such sensors and switches. The dielectric properties of PMMA/SAN polymer blends filled with MWCNTs also shows an increase with temperature.

In this study, the major work has been done by Ali Sarvi. Dr. Sundararaj has supervised the work and helped with result and discussion part.

♣ Submitted for publication

Enhancing Electrical Properties of MWCNTs in Miscible Blends of Poly(methyl methacrylate) and Styrene-Acrylonitrile copolymer by Selective Localization

Ali Sarvi and Uttandaraman Sundararaj*

Department of Chemical and Petroleum Engineering, University of Calgary, 2500 University Dr, NW, Calgary, AB, Canada T2N 1N4

8.2 Abstract

Multiwall carbon nanotubes (MWCNTs) were introduced into poly(methyl methacrylate) (PMMA) and styrene-acrylonitrile copolymer (SAN) blends by melt mixing in an asymmetric miniature mixer. A composition of 70 wt% of PMMA and 30 wt% of SAN was mixed to create a co-continuous morphology. Transmission electron microscopy images of ultra-microtomed samples (70 nm in thickness) showed selective localization of MWCNTs inside the percolated SAN phase. The occurrence of the double percolation phenomenon resulted in lower electrical percolation thresholds of PMMA/SAN/MWCNT blends molded at high temperatures. Dielectric spectroscopy indicated a higher electrical permittivity for samples that were compression molded at 260°C. Due to the higher affinity of MWCNTs to SAN, there was a migration of MWCNTs into the SAN phase during the melt processing. Conductivity measurements revealed a

significant decrease in electrical percolation threshold (0.4 wt%) for PMMA70/SAN30 blends compared with MWCNT-filled SAN and PMMA (ca 0.8 wt%).

8.3 Introduction

Incorporation of conductive nanofillers into polymer matrices is attracting increased interest to create conductive polymer composites. These lightweight composites can be used as electromagnetic wave shields in the aerospace and electronics fields for devices such as laptops and cell phones [1]. High electrical permittivity makes these composites suitable for charge storage purposes, such as embedded capacitors in electronics circuit boards [2, 3]. They are a good alternative to metal in many applications, due to their enhanced mechanical properties.

Carbon nanotubes (CNTs) are high aspect ratio nanofillers that demonstrate high conductivity, excellent mechanical properties and corrosion resistance. CNTs have been extensively investigated in the last decade to increase the conductivity of composites and reduce the cost and weight compared to traditional composites [1-4].

The dispersion of CNTs is of paramount importance in reaching a low electrical percolation and maintaining good conductivity. Good dispersion without surface functionalization or coatings is difficult to achieve due to high Van der Waals interactions between the nanofillers [5-7].

Coating CNTs with a conducting polymer has been shown to result in a decrease in the percolation threshold of the composites. However, coated or functionalized CNTs exhibit lower conductivity than CNTs alone and it is important to maintain conductivity [1-3].

An ordered structure may decrease the electrical percolation threshold. Our group [8] reported a relatively low electrical percolation concentration for copper nanowires in polystyrene (PS). The

method of mixing and precipitation of miscible solvents that we used resulted in a honeycomb structure of nanowires in a polymer matrix. As a result, good dispersion is a necessity for a low percolation threshold, but not necessarily good distribution.

It has been reported that locating nanoparticles at the interface of immiscible or compatible polymer blends will decrease percolation threshold to the lowest possible filler loading. However, locating nanoparticles with high aspect ratio at the interface using melt processing was not feasible [4, 9]. Selective filling of only one phase of immiscible blend is another way to achieve lower percolation threshold [4, 10] and that is the approach used in this work.

Sumita et al. [11] first depicted this phenomenon by mixing carbon black with an immiscible blend to form a conductive filler network within a co-continues polymer phase which is called double percolation phenomenon. Conductive nanofillers are selectively dispersed into a percolated blend phase (first percolation) and form a conductive network (second percolation), which results in significantly reduced filler loading.

In this study, lower critical solution temperature (LCST) blends were used as the polymeric matrix for MWCNT. An LCST blend experiences phase separation when heating the blend up to and exceeding a critical temperature. Significant changes can be observed in the linear viscoelastic properties when polymer blends are heated above the critical temperature. The measured critical temperature varies with the materials used, blend composition and processing. Introducing conductive nanofillers into LCST blends with selective localization leads to double percolation.

poly(methyl methacrylate) (PMMA)/ styrene-acrylonitrile copolymer (SAN) blends show LCST behavior. PMMA (homopolymer) and SAN (copolymer) exhibit different critical

temperatures with different blend compositions. PMMA/SAN blends that show spinodal decomposition have been extensively studied in recent years [12, 13]. Furthermore, by varying the acrylonitrile (AN) content of the SAN copolymer, the miscibility of SAN with PMMA can be systematically adjusted [14, 15]. It is known that PMMA and SAN form a miscible blend when the AN content in SAN is in the range of 9 to 34 wt%. Outside of this range, PMMA and SAN are immiscible [16].

Huang et al. [17] claimed that introducing fillers into binary blends enhances phase stability. Incorporation of silica particles in PMMA/SAN blends increased the critical temperature. It has been reported by Du et al. [18] that the addition of SiO_2 causes the cloud point and binodal temperature to increase slightly for PMMA60/SAN40. The main stabilization mechanism proposed is the formation of a deformable barrier network providing a mechanical barrier against coalescence. Blends stabilized by solid anisotropic nanoparticles, like MWCNTs, phase separate at higher critical temperatures and therefore, have higher cloud points [19].

In this work, MWCNTs located preferentially in SAN phase. Due to the higher affinity of MWCNTs with SAN compared to PMMA, all the MWCNTs migrate into the SAN phase to form a network. Therefore, for melt-processed PMMA/SAN blends filled with MWCNTs, the electrical percolation threshold decreases significantly, due to double percolation. Potschke et al. [4] reported results for polycarbonate (PC) / SAN blends filled with MWCNTs where the volume resistivity results demonstrated a much lower percolation for the blend compared to that of SAN and PC alone.

8.4 Experimental Section

PMMA (Mw ~ 120,000) and SAN (Mw ~ 185,000, 30 wt% AN content) were supplied by Sigma Aldrich. MWCNTs (Nanocyl™, product no. NC7000) with an average diameter of 9.5 nm, average length of 1.5 μm and specific surface area of 250-300 m^2/g were used.

Samples were melt mixed using a novel miniature mixer (shown in Figure 8.1), called the Alberta Polymer Asymmetric Mixer (APAM) [20]. This mixer has a capacity of about 2 g of polymer and nanofiller. SAN and MWCNTs was first mixed at 260°C for an additional 10 min, and PMMA were then added and mixed for 10 min. The PMMA/SAN/MWCNT blends were molded using a hot press at 6,000 psi at different molding temperatures and then quenched, in order to freeze the blend structure.

Transmission electron microscopy (TEM) was used to investigate the morphology of the blends. The samples were ultra-microtomed (70 nm in thickness) using a glass knife at room temperature. TEM images were obtained at 80 kV using a TecnaiTM F20 transmission electron microscope.

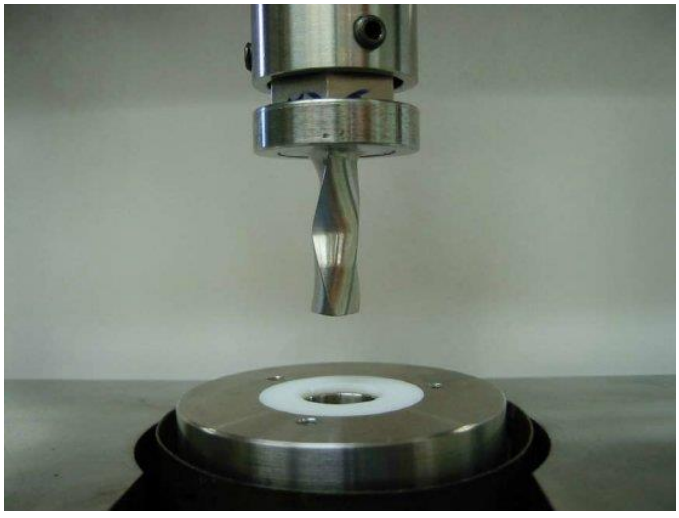

Figure 8.1 Alberta Polymer Asymmetric Mixer [20]

The cloud points were obtained using an Olympus hot stage microscope connected to a Mettler Toldeo light sensometer. The samples were placed at a pre-determined temperature (T_0=130°C) for 5 min and then heated up to 260°C at a rate of 2°C/min. [21, 22]. Light transmittance was plotted against temperature and the tangent line at high temperatures and the tangent line of the plateau at low temperatures were drawn. The intersection of two tangent lines corresponded to the cloud point of the blend.

Electrical resistivity measurements were done on 1 mm thick rectangular samples. All the sample surfaces were cleaned with ethanol prior to measurement. Two different resistivity measurement machines were used to cover the range of volume resistivity from insulating materials to conducting materials. Volume resistivity measurements were performed according to ASTM 257-75 standards at 90 V, employing a Loresta GP resistivity meter (MCP-T610 model, Mitsubishi Chemical Co., Japan) for samples with volume resistivities less than 10^4 Ω.cm. A four-pin probe was used, so that the effect of contact resistance did not distort the measurement. To measure the volume resistivity of materials with resistivities higher than 10^4 Ω.cm, a Hiresta UP resistivity meter and UR type probe were used at 100 V.

Dielectric spectroscopy was performed using a standard electrochemical interface (1287 Potentiostat + 1260 FRA, Solartron Analytical). The 1 mm thick samples were coated with silver paste to reduce the contact resistance. The real and imaginary resistances of samples were measured in the frequency range of 0.1 to 10^6 Hz. Real and imaginary permittivities were calculated using the complex resistance and frequency results.

8.5 Results and Discussions

The conductivity measurements of PMMA/MWCNT and SAN/MWCNT composites and PMMA70/SAN30 (70 wt% of PMMA and 30 wt% of SAN) composite blends filled with different concentrations of MWCNTs are plotted in Figure 8.2. According to the percolation theory [23], the electrical percolation concentrations for PMMA/MWCNT, SAN/MWCNT and PMMA70/SAN30/MWCNT are 0.7 wt%, 0.8 wt% and 1.2 wt%, respectively. All the composites were melt processed and molded at T=180°C where the PMMA/SAN blend begins to phase separate but it is not completely phase separated. Therefore, submicron SAN-rich phases are distributed all over the polymer matrix and there is no co-continuous morphology (Figure 8.3). Better affinity of MWCNT to the SAN phase leads to migration of MWCNTs into SAN-rich phases. The discontinuity of the dispersed phase resulted in higher electrical percolation for PMMA70/SAN30 blends molded at 180°C.

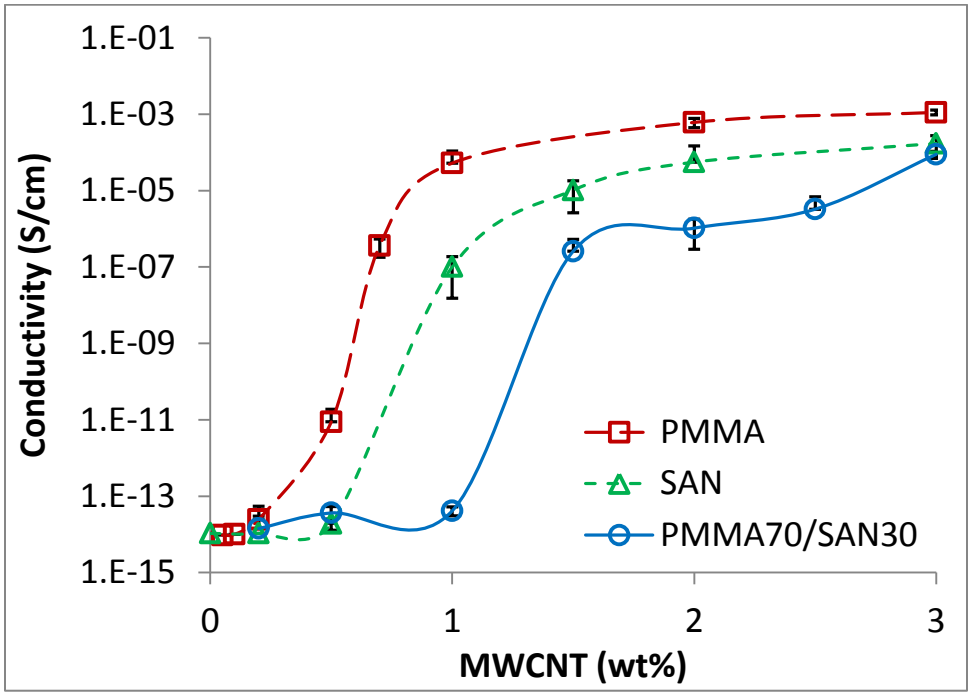

Figure 8.2 Conductivity of PMMA/MWCNT, SAN/MWCNT and PMMA70/SAN30/MWCNT blends molded at 180°C

The characterization of PMMA/SAN polymer blends filled with MWCNTs by TEM provided accurate information about the localization of MWCNTs in the polymer blends at different molding temperatures. Figure 8.3 shows TEM images of PMMA70/SAN30 blends filled with 2 wt% of MWCNTs. As the images show, the blends started to phase separate as the molding temperature was increased, as was expected. LCST blends go through a phase separation when heated up; the phase transition temperature is a function of blend composition.

In Figure 8.3a, the LCST blend was miscible at a molding temperature of 150°C, and the MWCNTs were homogeneously distributed over the sample. As the molding temperature increased to 160°C, the polymer mixtures started to phase separate and formed a co-continuous blend, which had a SAN-rich phase and a PMMA-rich phase. The dark regions in Figure 8.3b are mostly SAN polymer with MWCNTs.

Figure 8.3c shows a distinguishable phase separation at 200°C. The TEM image indicates that the blend at 200°C was above the critical temperature of phase separation for PMMA70/SAN30. The PMMA phase in Figure 8.3d was devoid of MWCNTs. The higher affinity of MWCNTs with SAN led to double percolation [4]: the SAN polymer first percolated in the PMMA matrix, and the network formation of MWCNTs inside the SAN phase is considered the second percolation.

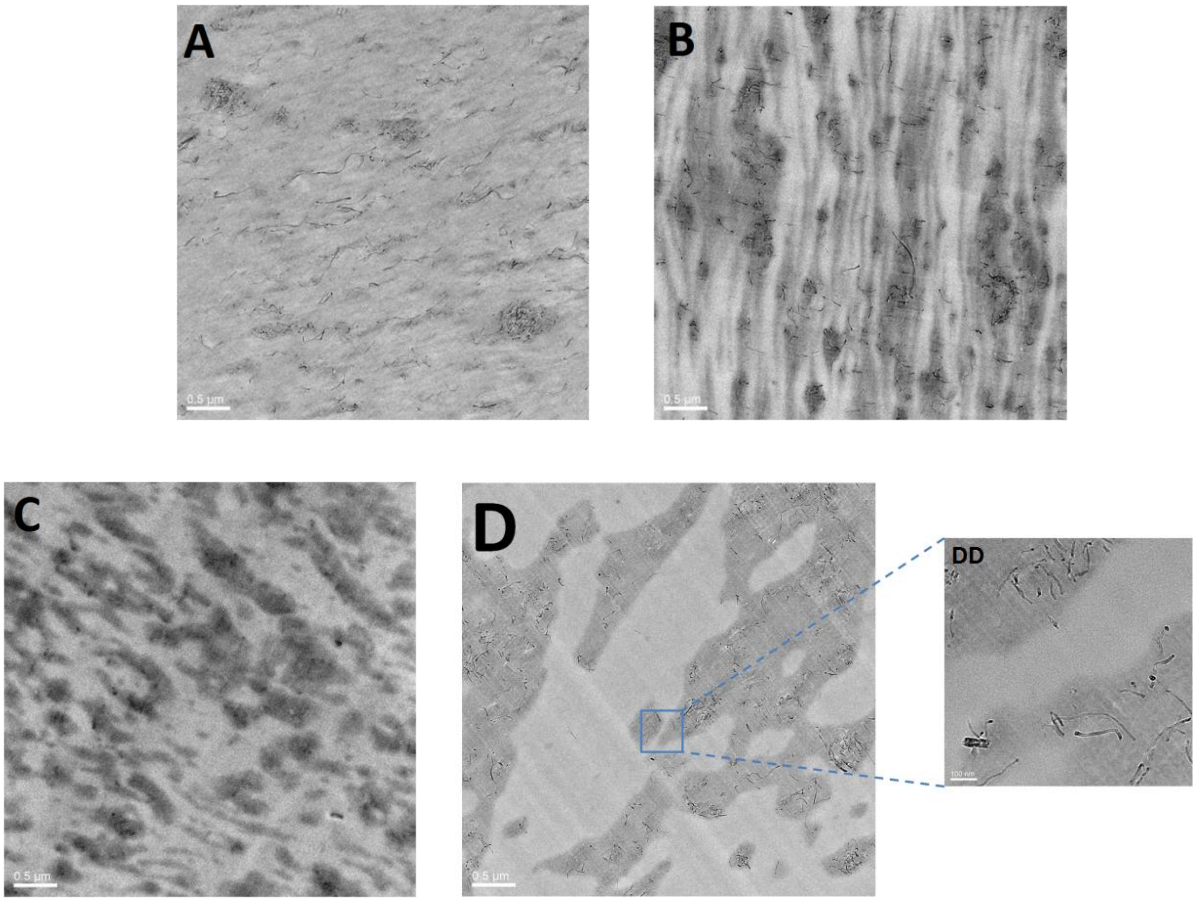

Figure 8.3 TEM images of PMMA70/SAN30 blends with 2wt% of MWCNTs at different molding temperatures; T_{mold}= (A) 140°C, (B) 160°C, (C) 200°C, (D) 260°C, (DD) 260°C at higher magnification

In the literature, localization of fillers in polymer blends is usually explained using arguments of minimization of interfacial energy. Filler tend to migrate to a polymer phase if this results in a lower interfacial energy. Surface energies of polymers and MWCNT reported in Table 8.1. Surface energy for PMMA was found by extrapolating results of Wu [24] to 260 °C, while the results for SAN surface energy are obtained from measurements by Pionteck and Kressler [25]. Interfacial energies for all polymers and the calculated filler interaction are reported in Table 8.2. These values were calculated using harmonic mean and geometric mean equations [4, 25]. In this

work, wetting coefficient ω_a is an indication of thermodynamic tendency of MWCNTs to migrate into PMMA or SAN phase [11].

$$\omega_a = (\gamma_{CNT\text{-}SAN} - \gamma_{CNT\text{-}PMMA})/(\gamma_{SAN\text{-}PMMA}) \quad 7.1$$

where γ is the different interfacial energy of the filler-polymer in the numerator and polymer-polymer in the denominator. The value of the wetting coefficient determines in which phase the filler will locate. For values higher than 1, the prediction is the filler will locate itself in PMMA; while for values lower than -1, there is a tendency of filler to locate in the SAN phase. For the values in between -1 and 1, it is expected that nanofillers would localize at the interface.

Table 8.1 Surface energy and polarities of polymers and MWCNTs

Materials	*Temperature °C*	*γ (dyne/cm)*	γ^d/γ	*Reference*
PMMA	260	22.52	0.7	[24]
SAN	260	29.5	0.76	[25]
MWCNT	__	45.3	0.41	[27]

However, calculations by Krasvitiaski et al. [26] and Potschke et al. [4] indicated that this interval for interfacial localization could be very narrow when the filler is high aspect ratio. Consequently, there is a low probability for MWCNTs which have high aspect ratio>100 to be located at the interface of two polymer phases. Negative wetting coefficient values of -0.31 and -4.8 were calculated from the harmonic and geometric mean equations, respectively. This predicts that MWCNTs should accumulate in the SAN phase. The experimental result is in

agreement with this prediction as shown by TEM images in Figure 8.3. MWCNTs are seen clearly to be located in dispersed phase of PMMA70/SAN30 blends.

Table 8.2 Interfacial energies calculated using harmonic and geometric mean equations

Materials & Wetting Coefficient	*Interfacial Energy * (dyne/cm)*	*Interfacial Energy ** (dyne/cm)*
PMMA/SAN	1.17	0.59
PMMA/MWCNT	12.14	6.72
SAN/MWCNT	11.78	3.89
ω_a	-0.31	-4.80

* According to harmonic mean equation

** According to geometric mean equation

Hot stage microscopy was employed for finding the cloud points of PMMA/SAN blend with different compositions. All the points are presented in Figure 8.4, and the binodal curve is shown. Figure 8.4 shows there is a miscibility window for the PMMA/SAN blends and this miscibility window is a function of blend composition and the processing temperature. The graph shows a good agreement with the phase diagram of PMMA/SAN blends previously has been reported in the literature [28].

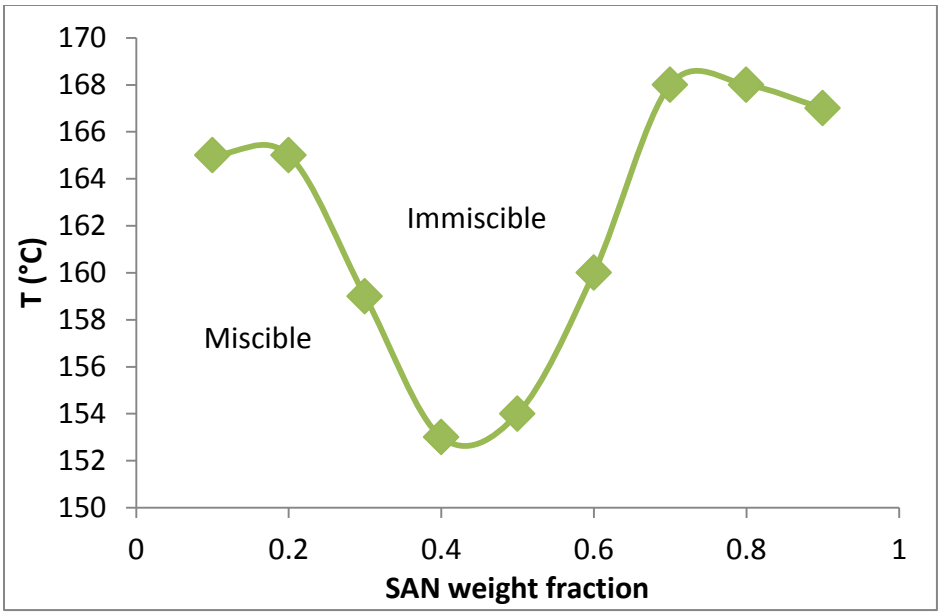

Figure 8.4 Phase diagram of PMMA/SAN

Miscible blends with SAN weight fraction higher than 0.25 develop an interpenetrating co-continue morphology if they are above critical temperature [29, 30]. Melt processing of these blends above the critical temperature leads to the double percolation phenomenon which reduces the MWCNT electrical percolation threshold concentration (see Figure 8.5 solid line) [4, 11].

Figure 8.5 shows conductivity results of PMMA70/SAN30 blends filled with 2wt% of MWCNTs at different molding temperatures. The polymer blends molded at low temperatures were insulating and became conductive as the molding temperature increased. Due to double percolation, the polymer blends processed at high temperatures had a low electrical percolation and was conductive with 2wt% of MWCNTs. Therefore, PMMA70/SAN30 blends filled with 2wt% molded at 260 ºC were conductive $\sigma=2\times10^{-2}$ S/cm (i.e. this concentration was above the electrical percolation concentration) whereas the same blend molded at 140 ºC was completely insulative ($\sigma=3\times10^{-14}$ S/cm). The percolation threshold for pure PMMA/MWCNT and pure SAN/MWCNT is much higher (Fig 7). The dotted line in Figure 8.5 represents light transmission

results for PMMA70/SAN30 blend as a function of temperature. Using light transmittance results, the cloud point was found at about 168°C for unfilled polymer blend. The conductivity results for 2 wt% of MWCNT indicated that electrical percolation happens at temperatures above 170°C.

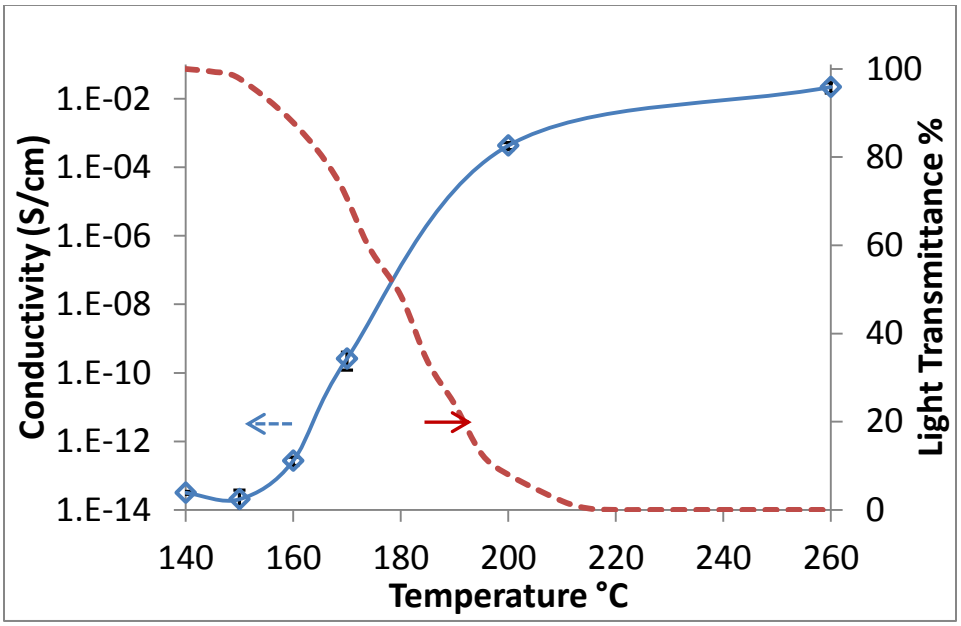

Figure 8.5 Conductivity of PMMA70/SAN30 blends with 2wt% of MWCNTs at different molding temperatures and light transmittance versus temperature for PMMA70/SAN30 blend.

For an LCST blend type, phase separation begins when the miscible mixture enters an unstable or metastable region as temperature is increased. The thermally induced phase separation can proceed by two different mechanisms: nucleation and growth (NG) or spinodal decomposition (SD). NG mechanism happens when the blend is brought to the metastable region and SD prevails when the blend is quenched to unstable region. For near-critical blend (PMMA composition ~ 60 wt%) blends experience SD to form a co-continuous morphology that resulted in double percolation phenomenon. Therefore, a higher conductivity can be achieved at filler

loading near 60 wt% PMMA. However, NG occurs for phase separation in *off-critical* blends (PMMA composition ≠ 60 wt%) resulting in droplet morphology [31-33]. Droplet morphology is expected to show lower conductivity than co-continuous morphology. Figure 8.6 shows conductivity results for different blend compositions filled with same content of MWCNT which were all compression molded at 260 ºC. *Near-critical* blends show three of orders of magnitude higher conductivity than *off-critical* blends. MWCNT prefer SAN phase and at higher SAN concentration, the ratio of MWCNT to SAN is lower. However, 2 wt% of MWCNT loading is far above the percolation threshold of SAN/MWCNT composites (electrical percolation concentration for SAN/MWCNT is 0.8 wt%) to ensure that increase in SAN content would still form a percolated network. Therefore, decrease in conductivity in *off-critical* blends is related to the droplet morphology in the blend that formed as a result of NG mechanism. Higher conductivity in *near-critical* blends is associated with co-continuous morphology that formed as a result of SD mechanism.

Introduction of MWCNTs changes the phase stability and affects the kinetics of phase separation of polymer blends due to interaction of the polymer components with MWCNTs [31]. The thermodynamic interaction parameter ($\chi_{SAN\text{-}PMMA}$) between SAN and PMMA may either increase or decrease by adding MWCNTs and it depends on blend composition [31,33]. Consequently, the cloud point of the blend can also change due to variation in $\chi_{SAN\text{-}PMMA}$. Huang et al. [32] found that adding functionalized silica nanoparticles with preferential selectivity of SAN phase, enhances phase separation temperature and this enhancement is more significant when PMMA is the major component. Nanoparticles have dimensions in nano-scale which are comparable to the gyration radius of the polymer chain. Therefore, adding these nano-sized particles will influence the configurational entropy of the polymer. For an LCST blend, $\chi_{SAN\text{-}PMMA}N$ (where N is the

degree of polymerization) decreases for blend of PMMA70/SAN30 after adding nanoparticles. As a result, the miscibility of blend is enhanced with decrease in $\chi_{SAN\text{-}PMMA}N$ and cloud point is shifted to higher temperatures. Higher cloud point means increased temperature at which electrical double percolation occurs.

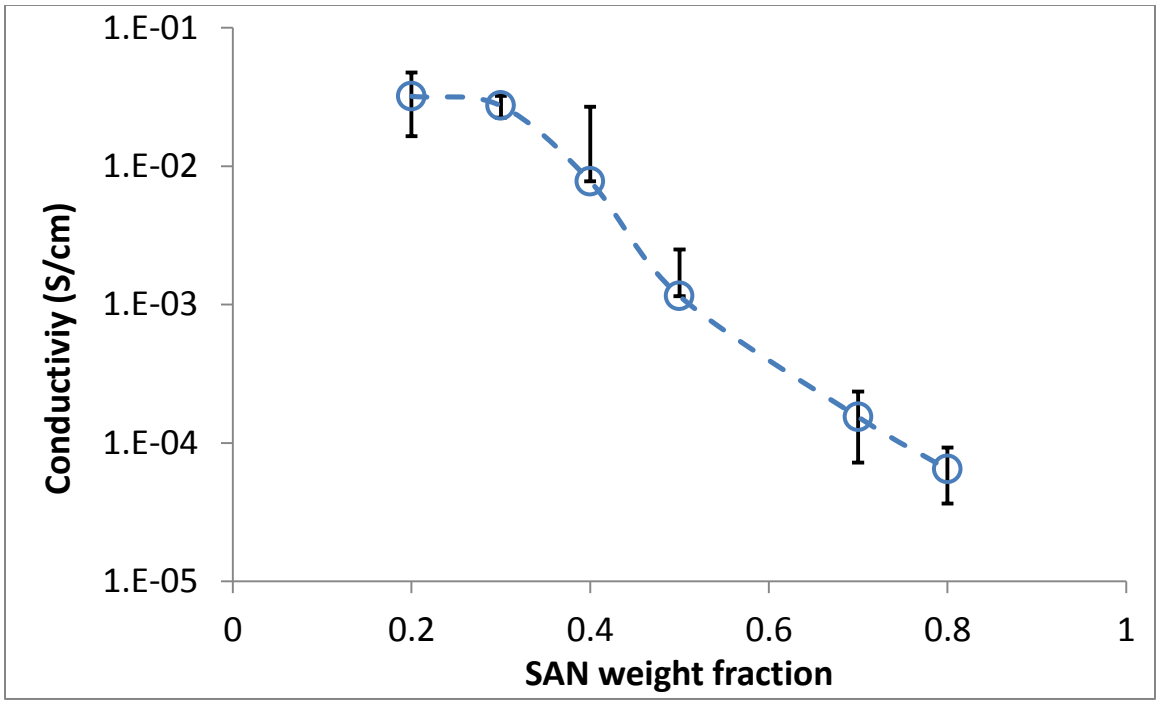

Figure 8.6 Conductivity results for different compositions of PMMA/SAN blend filled with 2 wt% MWCNT compression molded at 260 ºC.

Figure 8.7 shows electrical conductivity of PMMA70/SAN30 blend filled with three different concentrations of MWCNTs which were all compression molded at different temperatures. PMMA70/SAN30 filled with 1 wt% of MWCNTs shows the highest percolation temperature (176 ºC). Cloud temperature for unfilled PMMA70/SAN30 was found to be 159 ºC. This increase in cloud temperature is due to the influence of MWCNTs on phase stability in the PMMA/SAN mixture [31,32]. Kota et al [34] showed that the elastic modulus and electrical

conductivity are very sensitive to the onset of percolation. They also found that electrical percolation occurs slightly sooner than rheological percolation when we are increasing MWCNTs content [34]. Therefore, the conductivity graph in Figure 8.7 is indicative of phase separation of blend, and it is more precise as MWCNT loading nears percolation threshold (i.e. 1 wt% of MWCNTs).

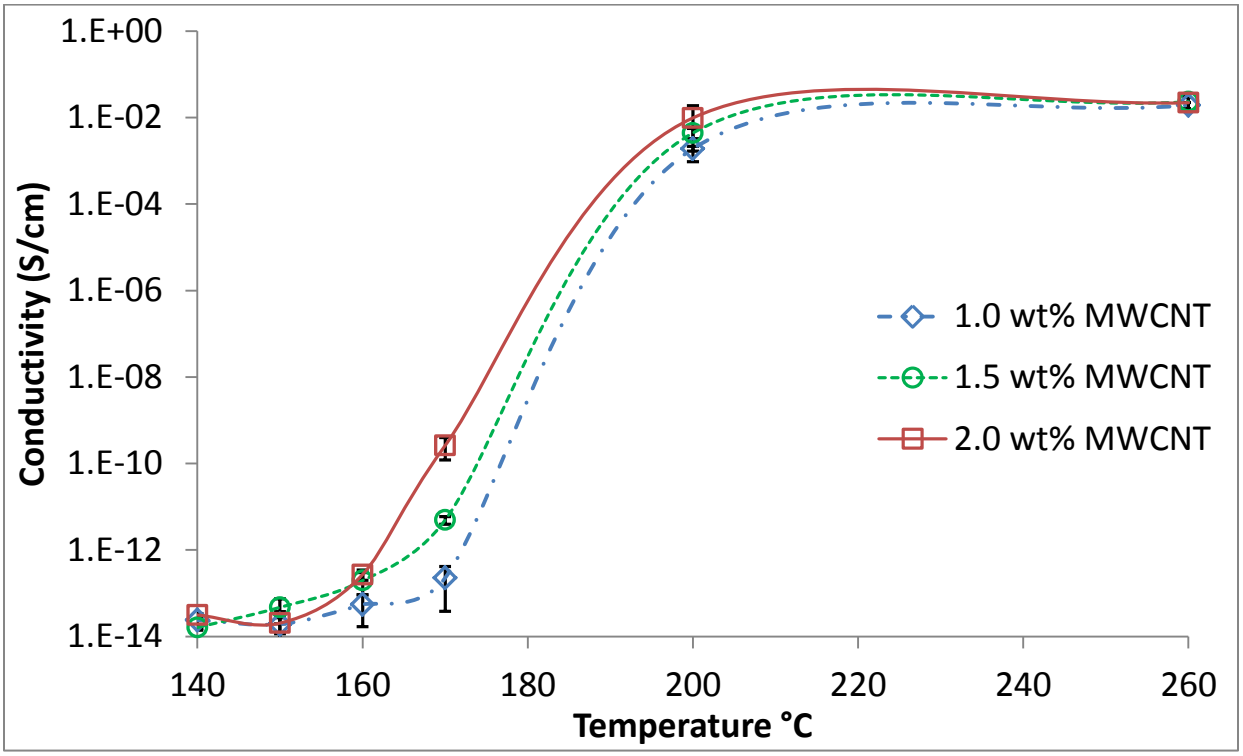

Figure 8.7 Conductivity of PMMA70/SAN30 filled with different concentrations of MWCNT at different temperatures

Dia et al [31] showed that increase in filler content enhances blend stability and increases the phase separation temperature. However, Figure 8.7 shows that electrical percolation shifts to lower temperatures as MWCNTs increases. This shift to lower temperatures is due to adding more conductive fillers which enhance the chance of formation of a conductive percolated

network. Therefore, change in conductivity for MWCNT loading near percolation threshold (i.e. 1 wt% of MWCNTs) is more indicative of phase separation temperature.

Dielectric spectroscopy of PMMA70/SAN30 composites filled with 2 wt% of MWCNTs molded at different temperatures was performed in the frequency range of 10 to 10^6 Hz. Figures 8.8a and 8.8b show the real and imaginary electrical permittivities, respectively, of the composites at different molding temperatures.

The real part of permittivity (ε′) is mainly associated with the amount of polarization occurring in the material and the imaginary part (ε″) is related with the dissipation of energy. The dielectric performance of the material depends on ionic, electronic, orientational, and space charge polarization [26]. In blends of PMMA/SAN filled with MWCNT, the dielectric properties mainly depend on the polarization of polymers, polarization of MWCNTs and on the remarkable polarization at the interface between MWCNTs and polymers. Using high molding temperature selectively localized MWCNTs in the SAN phase, which led to an increase in number of the microcapacitors in the composite since the selective localization brought MWCNTs near each other. Microcapacitors are composed of two nanofillers and the insulating polymer between them. Adding more microcapacitors results in the higher real permittivity [35, 36]. However, decreasing distance between MWCNTs reduces the interfacial potential energy, so that the localized charge carriers could jump more readily.

According to Figure 8.8, there was an order of magnitude increase in both the real and imaginary permittivities as the temperature increased. Dielectric loss (the ratio of ε" to ε') at very low frequencies was independent of frequency due to the composite resistance. At higher frequencies, the dielectric permittivity was mainly dependent on the polarization of the MWCNTs [35, 36].

The real permittivity for samples that are not completely phase separated, was low and frequency independent, indicating a high resistivity and low electrical polarization. Dielectric permittivity results demonstrate a large increase (two orders of magnitude) in real permittivity for the sample which is molded at 260 ºC due to the large difference between dielectric constant of SAN and MWCNTs and formation of more micorcapacitors. However, real permittivity began to decrease in higher frequencies due to high frequency relaxation, which decreases interfacial polarization.

Figure 8.8b shows the imaginary permittivity results at different molding temperatures for PMMA70/SAN30 blends filled with 2wt% of MWCNTs. The results are in agreement with conductivity results in Figure 8.5. The composite has higher imaginary permittivity and higher conductivity as the molding temperature increases. Higher conductivity resulted in greater energy dissipation in the composites, giving higher imaginary permittivity.

Dielectric loss is the ratio of imaginary to real permittivity. At low frequencies dielectric loss was mainly due to the resistance of insulating polymer. At higher frequencies, as charge polarization occurred, different samples exhibited different dielectric losses. High real permittivity ($\varepsilon'=3.4\times10^3$ at 10^5 Hz) and relatively low dielectric loss compared to ceramic-powder polymer composites ($\varepsilon'=1.5\times10^2$ at 10^5 Hz) [37-39], makes these PMMA/SAN LSCT blends filled with MWCNTs an appropriate choice for embedded capacitors in electronic circuit boards.

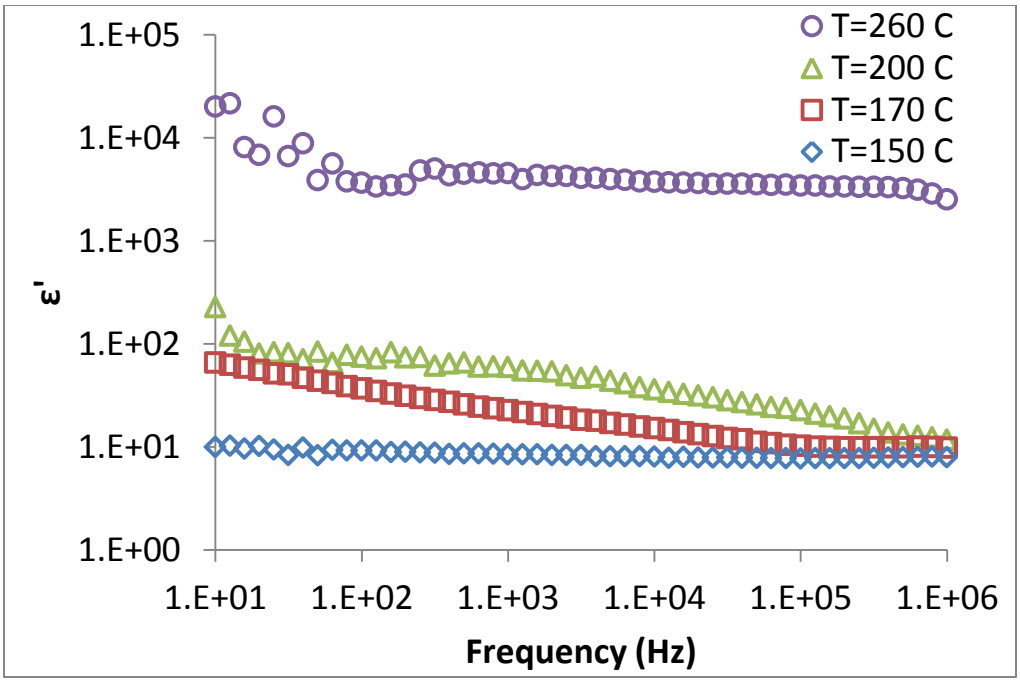

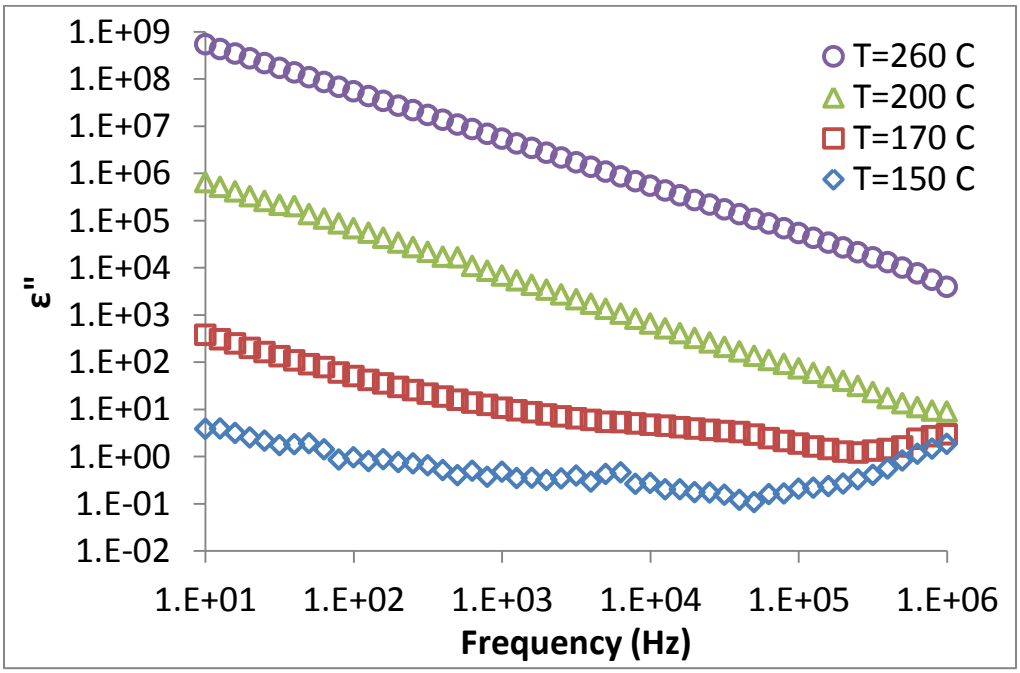

Figure 8.8 Real & imaginary permittivity results of PMMA70/SAN30 blends with 2wt% of MWCNTs by compression molding at different temperatures

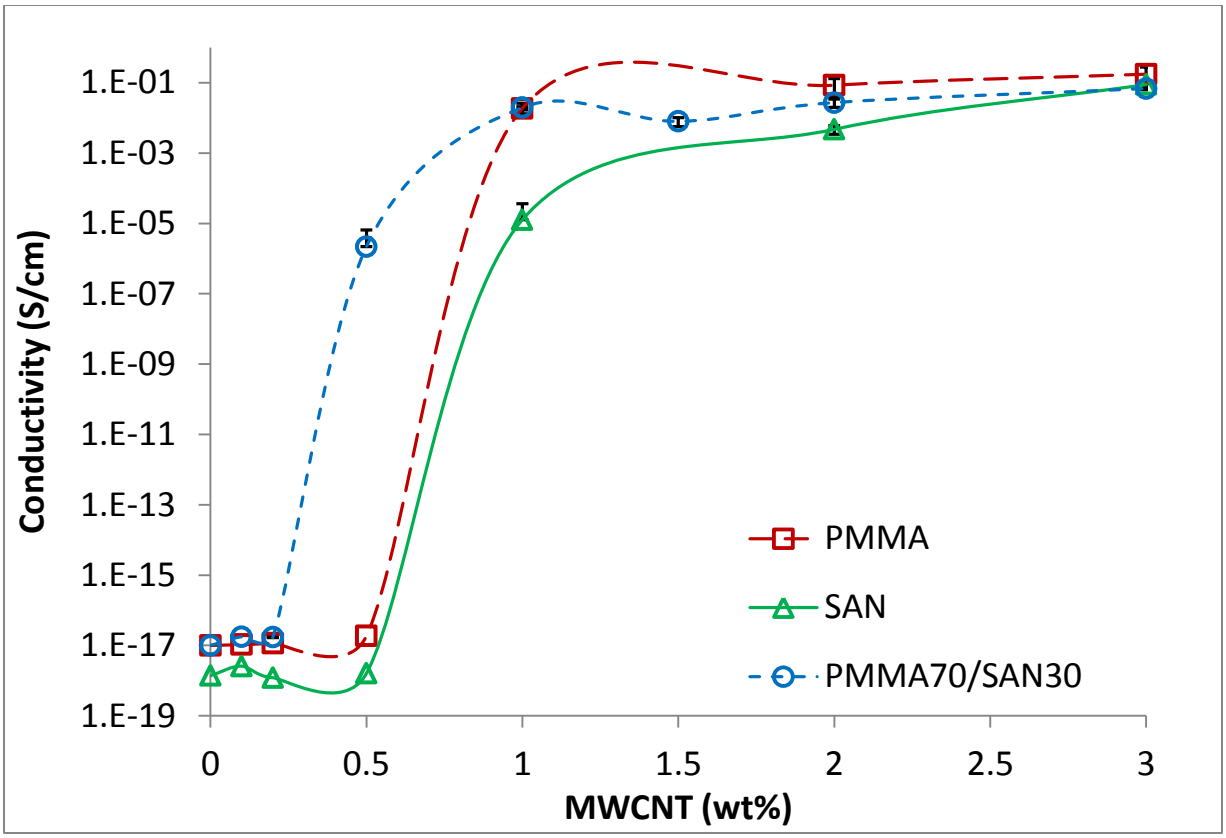

Figure 8.9 Conductivity of PMMA/MWCNT, SAN/MWCNT and PMMA70/SAN30/MWCNT blends molded at 260°C

The conductivity measurements of PMMA/MWCNT and SAN/MWCNT composites and PMMA70/SAN30 composite blends filled with different concentrations of MWCNTs are plotted in Figure 8.9. There was a significant decrease in the electrical percolation concentration for the PMMA/SAN blend composites compared to PMMA and SAN polymers filled with MWCNT. The electrical percolation concentration for the PMMA70/SAN30 blend was significantly lower than that obtained for SAN/MWCNT composites. According to the percolation theory [23], the percolation concentrations for PMMA/MWCNT, SAN/MWCNT and PMMA70/SAN30/MWCNT are 0.8 wt%, 0.8 wt% and 0.4 wt%, respectively. All the composites were melt processed and molded at T=260°C where the double percolation phenomenon played a

significant role in decreasing percolation threshold. This large decrease in the percolation threshold is extremely advantageous for industrial applications, in terms of product weight and cost. The conductivity values for SAN and PMMA alone filled with MWCNT compression molded at 260°C are slightly higher than that for samples molded at 180°C. Higher compression molding temperature led to lower viscosity and fewer polymer chains stayed in between contact spots of the MWCNT network which resulted in higher conductivity [40,41]. If we compare Figure 8.2 to Figure 8.9, increasing molding temperature has a profound impact on reducing the percolation threshold.

8.6 Conclusion

MWCNTs were incorporated into PMMA/SAN blends by melt mixing using the Alberta Polymer Asymmetric MiniMixer. TEM characterization of the blends indicated a selective localization of MWCNTs inside the percolated blend, which led to a significant decrease in the electrical percolation threshold. Higher affinity of MWCNTs with SAN (i.e. SAN wetting coefficient on MWCNT was calculated using interfacial energies and found to be most favorable) and the TEM images of blends prepared at high temperatures confirm this prediction. Conductivity measurements were employed as new way for investigating of phase separation mechanism in LCST blends. The effect of MWCNT on phase separation behavior studied in different compositions of blend. It was found that adding nanofiller enhanced the blend stability.

The conductivity measurements of blends at different molding temperatures demonstrated that, as the melt processing temperature increased, the electrical percolation concentration decreased. Insulative samples prepared at low temperatures became conductive when molded at higher temperatures. Processing temperature was a critical parameter to determine the blend

morphology and occurrence of double percolation effect; for example, changing molding temperature from 180°C to 260°C decreased the percolation threshold in the blend composites by three-fold. Electrical impedance results also showed higher electrical permittivity with increasing melt processing temperature. Enhancement of the electrical permittivity of these composites makes them suitable for charge storage applications, such as supercapacitors and embedded capacitors in electronic circuit boards. Double percolation phenomenon was observed in PMMA/SAN blends filled with MWCNTs, and resulted in significantly lower electrical percolation threshold concentration at about 0.4 wt% MWCNT at higher temperatures.

8.7 References

[1] Y. Yang, M. Gupta, *Nano Letters* **2005**, 5, 2131.

[2] Y. Zhou, Z. Qin, L. Li, Y. Zhang, Y. Wei, L. Wang, M. Zhu, *Electrochimica Acta* **2010**, 55, 3904.

[3] C. Peng, S. Zhang, D. Jewell, G. Chen, *Progress in Natural Science-Materials International* **2008**, 18, 777.

[4] A. Goldel, G. Kasaliwal, P. Potschke, *Macromolecular Rapid Communications* **2009**, 30, 423.

[5] L. Li, Z. Qin, X. Liang, Q. Fan, Y. Lu, W. Wu, M. Zhu, *Journal of Physical Chemistry C* **2009**, 113, 5502.

[6] S. Meuer, L. Braun, T. Schilling, R. Zentel, *Polymer* **2009**, 50, 154.

[7] C. Hong, Y. You, C. Pan, *Polymer* **2006**, 47, 4300.

[8] G. Gelves, M. Al-Saleh, U. Sundararaj, *Journal of Materials Chemistry* **2011**, 21, 829.

[9] S. Bose, A. Bhattacharyya, P. Kodgire, A. Misra, Polymer **2007**, 48, 356.

[10] M. Gultner, A. Goldel, P. Potschke, Composites Science and Technology **2011**, 72, 41.

[11] M. Sumita, K. Sakata, S. Asai, K. Miyasaka, H. Nakagawa, *Polymer Bulletin* **1991**, 25, 265.

[12] B. Keestra, J. Goossens, P. Anderson, *Chemical Engineering Science* **2011**, 66, 4960.

[13] J. You, Y. Liao, Y. Men, T. Shi, L. An, X. Li, *Macromolecules* **2011**, 44, 5318.

[14] M. Suess, J. Kressler, H. Kammer, *Polymer* **1987**, 28, 957.

[15] J. Cowie, D. Lath, *Makromolekulare Chemie-Macromolecular Symposia* **1988**, 16, 103.

[16] K. Chee, *European Polymer Journal* **1990**, 26, 423.

[17] Y. Huang, S. Jiang, G. Li, D. Chen, *Acta Materialia* **2005**, 53, 5117.

[18] D. Miao, W. Qiang, Z. Min, Z. Qiang, *European Polymer Journal* **2013**, 49, 2721.

[19] A. Baudouin, D. Auhl, F. Tao, J. Devaux, C. Bailly, *Polymer* **2011**, 52, 149.

[20] O. Breuer, U. Sundararaj, R. Toogood, *Polymer Engineering and Science* **2004**, 44, 868.

[21] J. Coutinho, J. Daridon, *Petroleum Science and Technology* **2005**, 23, 1113.

[22] J. Piglowski, M. Bryjak, *European Polymer Journal* **1998**, 34, 1669.

[23] M. Weber, M. Kamal, *Polymer Composites* **1997**, 18, 711.

[24] S. Wu, *Journal of Physical Chemistry* **1970**, 74, 632.

[25] J. Pionteck, J. Kressler, *Europhysics Conference Abstarcts, (Mulhouse. France): European Physical Society* **1995**, 31.

[26] A. Ohlan, K. Singh, A. Chandra, S. Dhawan, *Acs Applied Materials & Interfaces* **2010**, 2, 927.

[27] S. Nuriel, L. Liu, A. Barber, H. Wagner, *Chemical Physics Letters* **2005**, 404, 263.

[28] G. Wen, X. Li, Y. Liao, L. An, *Polymer* **2003**, 44, 4035.

[29] L. Mcmaster, *Advances in Chemistry Series* **1975**, 43.

[30] J. Lyngaaejorgensen, K. Sondergaard, *Polymer Engineering and Science* **1987**, 27, 351.

[31] D. Mia, Q. Wu, M. Zuo, Q. Zheng, *European Polymer Journal* **2013**, 49, 2721.

[32] C. Huang, J. Gao, W. Yu, C. Zhou, *Macromolecules* **2012**, 45, 8420.

[33] V. Ginzburg, *Macromolecules* **2005**, 38, 2362.

[34] K. Kota, B. Cipriano, M. Duesterberg, A. Gershon, D. Powell, S. Raghavan, H. Bruck, *Macromolecules* **2007**, 40, 7400.

[35]] H. Jin, Y. Hou, X. Meng, F. Teng, *Solid State Communications* **2008**, 148, 476.

[36] Z. Khattari, M. Maghrabi, T. McNally, S. Jawad, *Physica B-Condensed Matter* **2012**, 407, 759.

[37] Y. Rao, C. Wong, *Journal of Applied Polymer Science* **2004**, 92, 2228.

[38] P. Thomas, R. Ravindran, K. Varma, *Polymer Engineering & Science* **2013**, DOI: 10.1002/pen.23586

[39] T. Hu, J. Juuti, H. Jantunen, T. Vilkman, *Journal of the European Ceramic Society* **2007**, 27, 3997.

[40] C. Zhang, X. Yi, S. Asai, M. Sumita, *Composite Interfaces* **1999**, 6, 287.

[41] M. Sumita, H. Abe, H. Kayaki, K. Miyasaka, *Journal of Macromolecular Science-Physics* **1986**, B25, 171.

Chapter 9

Summary, Conclusions and Future Work

In this PhD thesis, knowledge in the field of CPCs and EAPs has been advanced for:

- Synthesis of CuNW-PANi core-shell nanofillers using solution mixing, which enhanced dispersion of CuNWs in a polymer matrix, resulting in a decrease in the percolation threshold.
- Synthesis of MWCNT-PANi core-shell nanofillers using the in-situ polymerization method was achieved and resulted in a significantly lower percolation threshold, higher electrical permittivity and higher EMI shielding.
- The relationship between rheological and electrical percolation in CPCs was investigated, and mechanisms of network formation using different mixing methods were studied. The effect of a coating layer on the network formation mechanism was also delineated.
- Immiscible polymer blends were used to decrease the percolation threshold via the "double percolation" concept.
- Temperature sensitive CPCs were developed, where conductivity changes with temperature via thermodynamic manipulation for LCST blends.
- Synthesis of multilayer electrospun conductive nanofibers using a co-axial nozzle was performed.

- ❖ New insight was gained into how to form a conductive network in electrospun mats, where the orientation of conductive high aspect ratio fillers is a major problem.
- ❖ Fabrication of conductive nanofibers mats with high piezoelectricity was done.

9.1 Effect of PANi-coating on nanofiller dispersion (CuNWs and MWCNTs)

High aspect ratio CuNW-PANi core-shell and MWCNT-PANi core-shell nanostructures were successfully synthesized by simple and reproducible techniques (Chapters 3 and 4) [1, 2]. A thin coating layer of PANi did not have a significant effect on the aspect ratio of the original nanofillers. A stable and uniform PANi coating over the surface of 25 nm diameter CuNW has been demonstrated, with PANi thickness ranging between 6 to 18 nm using different concentrations of PANi [1]. A uniform and smooth coating of PANi was achieved using sonication for MWCNT-PANi core-shell nanofibers during polymerization [2]. PANi coating thickness in MWCNT-PANi core-shell nanofibers is controlled with concentration of aniline in the solution. It was found that an increase in aniline concentration increases the PANi coating to up to 15 nm for MWCNT80-PANi20. In this PhD thesis, the effect of PANi coating on dispersion and distribution of nanofillers was investigated. It was found that a lower percolation threshold was obtained for PANi-coated nanofillers as a result of better dispersion and also large-distance interaction of nanofiller-nanofiller and nanofiller-aggregates. Good dispersion resulted in low rheological percolation concentration, as well as low electrical percolation threshold. The rheological percolation, defined by indirect rheological parameters such as the ratio G'/G'', better matches the electrical percolation behavior [3]. Optical micrographs and TEM images revealed that the dispersion of PANi-coated MWCNTs dispersed in PS improved in both microscopic and nano-scale levels. Better dispersion is achieved when there is lower interfacial

energy of PANi with PS (calculated as 4.72 dyne/cm and 2.44 dyne/cm using harmonic and geometric mean equation, respectively), compared to interfacial energy of MWCNTs with PS (calculated as 13.76 dyne/cm and 7.33 dyne/cm calculated using harmonic and geometric mean equation, respectively).

9.2 Effect of PANi-coating on electrical properties of CPCs

XPS characterization for PANi-coated CUNWs indicated a spontaneous chemisorption of the coating of polyaniline on the nanowires, which affects the oxidation level of PANi [1]. Oxidation states of PANi layers decreased after coating, which led to a decrease in electrical conductivity of the core-shell [1].

The introduction of core-shell nanofillers into the polystyrene matrix (Chapters 3, 4 and 5) resulted in a lower electrical percolation threshold than bare nanofillers (e.g. percolation threshold for MWCNT/PS after coating of MWCNT with PANi decreased from 0.9 wt% to 0.15 wt%).

PANi-coated MWCNTs demonstrated better electrical properties than bare MWCNTs. EMI shielding for PS composites filled with PANi-coated MWCNTs was higher than MWNCT/PS. The core-shell nanofibers utilized the contribution of both shell and core for electromagnetic interference shielding; however, each contributed to EMI SE via different mechanisms. For the shell incoming EM waves are attenuated via absorption. The real and imaginary permittivities of composites made with the core-shell nanofibers were significantly higher than those made using the MWCNTs [2]. Having a low dissipation factor and a high real permittivity makes these materials a good choice for use as supercapacitors or embedded capacitors.

9.3 PANi coating: A new insight into network formation in electrospun mats

Chapter 6 demonstrates new insight into how we can form a conductive network in electrospun mats, where the orientation of conductive high aspect ratio fillers is a major problem. Orientation seems inevitable given the high spinning speeds and thus, viscoelastic stresses that align the fillers. Using thermodynamic manipulation, i.e. using the miscibility/immiscibility of a third phase (i.e. polyaniline) we conceived a way to reconfigure and rearrange the structure of the conductive nanofiller (MWCNTs) in the polymer (PVDF). We disrupted the orientation allowing for transverse connections. SEM and TEM images proved the formation of small strands or segments of nanofillers on the surface of nanofibers, which resulted in formation of a conductive network in the transverse direction of the electrospun mat. The effect of interfacial energies on formation of this unique structure was discussed, to reveal the driving force eliciting this phenomenon. Thus, high conductivity of 1.71×10^{-1} S/m was reported for the first time in the literature for PVDF nanofiber mats.

Electrospinning is a successful method for piezoelectric properties of PVDF, which gives higher β-crystal than any processing method. Enhancing β-crystal content compared with an established method of producing piezoelectric films (i.e. introducing nanoclay Closite 30B) from 29.5% to 56.1 % for the electrospun mat significantly increases the piezoelectricity of PVDF. These novel products can find applications in the field of energy conversion and storage, where inorganic materials are not satisfactory due to their poor processability and mechanical properties. These applications require electroactive polymers in large-area, thin, flexible films and fabrics such as conductive nanofiber mats [4,5].

9.4 Fabrication of multilayer nanofibers (using electrospinning technique)

Multilayer nanofibers were successfully fabricated using a coaxial electrospinning technique (Chapter 7). The coaxial nozzle was designed and made in-house [4]. Different concentrations and compositions of solutions were injected into inner and outer cylinders to fabricate multilayer nanofibers. The flow rates, solution concentrations, applied voltage, collector rotation speed and work distance (distance between the nozzle and the collector) were optimized to obtain smooth and uniform nanofibers. The core of the fibers was pure PVDF and the shell consisted of 82 wt% of PVDF, 8 wt% of PANi and 10 wt% of MWCNT. Placing MWCNTs and PANi as conducting materials in the shell layer resulted in a significant increase in conductivity and a decrease in the electrical percolation of the nanofiber mat [4]. As mentioned in section 8.3, it is difficult to achieve conductive nanofiber mats due to the orientation of high aspect ratio fillers at high spinning speed. Incorporation of PANi increased the conductivity of the nanofiber mat by bridging the nanofibers and eliminating air resistance and making a network of nanofibers in the transverse direction.[4]. PVDF/PANi nanofibers had a higher amount of β-phase crystal when MWCNTs were added to the blend. Therefore, it is expected that nanofiber mats show higher piezoelectricity than compression molded PVDF.

9.5 Further decrease in the electrical percolation threshold: double percolation concept

In Chapter 8, immiscible polymer blends of PMMA/SAN were used to decrease the electrical percolation threshold in CPCs. MWCNTs were incorporated into the blend by melt mixing at 260ºC, where the blend is immiscible. Intensive mixing provided good dispersion of MWCNTs in the SAN phase. TEM characterization of the blends proved selective localization of MWCNTs inside the percolated phase, which led to a significant decrease in the electrical percolation

threshold. Higher affinity of MWCNTs with SAN (i.e. SAN wetting coefficient on MWCNT was calculated using interfacial energies and found to be most favorable) led to localizing of MWCNTs in the SAN phase. Double percolation phenomenon was observed in PMMA/SAN blends filled with MWCNTs and resulted in a significantly lower electrical percolation threshold concentration at about 0.4 wt% MWCNT for samples molded at high temperatures.

Immiscible polymer blends demonstrated different phase behavior with a change in temperature. Insulative samples prepared at low temperatures became conductive when brought to higher temperatures. Processing temperature was a critical parameter to determine the blend morphology and occurrence of the double percolation effect. For example, changing molding temperature from 180°C to 260°C decreased the percolation threshold in the blend composites by three-fold.

Electrical impedance results also showed higher electrical permittivity with an increasing melt processing temperature. Enhancement of the electrical permittivity of these composites makes them suitable for charge storage applications, such as supercapacitors and embedded capacitors in electronic circuit boards.

9.6 Recommendations

Coating of conductive nanofillers with ICPs, use of different nanofiller fabrication techniques, and incorporation of multiphase polymer blends opened up new ways to manipulate and optimize electrical and mechanical properties of CPCs. Considering these advances the following subjects are recommended for future work:

- ✓ Coating of CuNW and MWCNTs with PANi, as a member of the ICP family, were investigated in this work. There are some other ICPs, such as polypyrol and

polyacetylene, with higher electrical conductivity than PANi. Coating of conductive nanofillers with these ICPs is promising for fabricating CPCs with enhanced electrical properties.

- ✓ Placing MWCNTs in the shell layer of multilayer electrospun nanofibers resulted in a significant decrease in the percolation threshold and enhanced electrical conductivity of nanofiber mats. Using ICP-coated MWCNTs can further decrease the electrical percolation in nanofiber mats due to formation of short strands/segments on the nanofiber surface. These short strands led to a network formation in the transverse direction at low nanofiller loadings.
- ✓ Modeling of polymer composites filled with coated and uncoated nanofillers suing Monte Carlo simulation for predication of percolation threshold and electrical properties.
- ✓ PANi-coated MWCNTs are sensitive to acids and bases. Their conductivity largely changes with exposure to small concentrations of doping/dedoping agents (i.e. acids and bases). Investigation of gas sensitivity of these nanofillers reveals their capability for application as chemisensors.
- ✓ EMI shielding of PS composites filled with PANi-coated MWCNT is briefly discussed in Chapter 4 of this PhD thesis. Preliminary results of EMI SE for these novel materials demonstrates a huge potential for enhancing EMI SE of polymer composites with ICP-coated MWCNTs. The effect of coating layer thickness, sample thickness, different ICP types and different oxidation states of the coating layer on EMI SE should be investigated.
- ✓ PANi was revealed to be a superior material for charge storage applications. PANi is capable of storing electrical charges through the pseudocapacitance mechanism. To take

advantage of this material for charge storage applications, concentrated solutions of MWCNT-PANi cores-shells or CuNW-PANi core-shells can be prepared and tested for capacity measurements with “cyclic voltammetry” equipment.

- ✓ Conductive nanofiber mats of PVDF, due to high content of β-crystal and therefore high piezoelectricity, are very sensitive to mechanical forces. They can be used as highly sensitive force sensors. The piezoelectricity of this material needs to be measured directly and the sensitivity needs to be measured.
- ✓ Localizing conductive nanofiller in one phase of percolated binary blend led to a noteworthy decrease in the electrical percolation threshold. It is difficult to locate high aspect ratio nanofillers in the blend interface, If we consider this, even a lower percolation concentration can be obtained. Using ternary blends instead of binary blends can put the third phase at the interface the other two polymers in the blend. A co-continuous interphase can be obtained simply by adjusting blend compositions. Localizing MWCNTs, pure or functionalized, in a co-continuous interphase can lead to further decrease in the electrical percolation threshold of CPCs.
- ✓ Thermally sensitive conductive immiscible polymer blends (i.e. their conductivity changes with temperature) can find application in such areas as thermal switches or sensors. Investigation of the range of sensitivity and accuracy can be helpful for designing such sensors or switches.

9.7 References

[1] Sarvi A, Gelves G, Sundararaj U. Facile one step-synthesis and Characterisation of High Aspect Ratio Core-shell Copper-Polyaniline Nanowires. Canadian Journal of Chemical Engineering. 2014; DOI: 10.1002/cjce.21973.

[2] Sarvi A, Sundararaj U. Electrical permittivity and electrical conductivity of multiwall carbon nanotube-polyaniline (MWCNT-PANi) core-shell nanofibers and MWCNT-PANi/polystyrene composites. Macromolecular Materials & Engineering. 2014; DOI: 10.1002/mame.201300406.

[3] Sarvi A, Sundararaj U. Rheological percolation in polystyrene composites filled with polyaniline-coated multiwall carbon nanotubes. Synthetic Metals. 2014;194:109-117.

[4] Sarvi A, Chimello V, Silva AB, Bretas RES, Sundararaj U. Coaxial Electrospun Nanofibers of Poly(vinylidene fluoride)/Polyaniline Filled With Multi-Walled Carbon Nanotubes. Polymer Composites. 2014;35(6):1198-1203.

[5] Sadeghi F, Sarvi A, Sundararaj U. PVDF/ Carbonnanotubes /Nanoclay Composites for Piezoelectric Aapplications, International Polymer Processing. 2014;29(1):81-87.

Appendix

Coating Thickness Measurements, Interfacial Energy Measurements and Error Analysis

1. Measurement of coating thickness for CuNW-PANi and MWCNT-PANi core-shell

Coating thickness of PANi in CuNW/PANi and MWCNT/PANi nanofibers were measured using ImageJ software. Diameter of about 200 nanofibers for each PANi concentration was measured. The coating thickness was found by subtracting the original diameter of core form measured diameter of each nanofiber. For each point, the average and standard deviation was calculated from 200 nanofiber.

2. Interfacial energy calculation

Interfacial energies for polymer/polymer and polymer/filler which has been reported in Table 8.2 were calculated using harmonic mean and geometric mean equations.

Harmonic mean equation:

$$\gamma_{12} = \gamma_1 + \gamma_2 - 4\left[\frac{\gamma_1^d \gamma_2^d}{\gamma_1^d + \gamma_2^d} + \frac{\gamma_1^p \gamma_2^p}{\gamma_1^p + \gamma_2^p}\right]$$

Geometric mean equation:

$$\gamma_{12} = \gamma_1 + \gamma_2 - 2\left(\sqrt{\gamma_1^d \gamma_2^d} + \sqrt{\gamma_1^p \gamma_2^p}\right)$$

Here, there is a sample of interfacial energy calculation for PMMA/SAN blend.

Material	γ(dyne/cm)	γ^d/γ	γ^d	γ^p
PMMA	22.52	0.7	15.76	6.76
SAN	29.5	0.76	22.42	7.08

Harmonic mean equation:

$$\gamma_{PMMA-SAN} = 22.52 + 29.5 - 4\left[\frac{15.76 \times 22.42}{15.76 + 22.42} + \frac{6.76 \times 7.08}{6.76 + 7.08}\right] = 1.17$$

Geometric mean equation:

$$\gamma_{PMMA-SAN} = 22.52 + 29.5 - 2\left(\sqrt{15.76 \times 22.42} + \sqrt{6.76 \times 7.08}\right) = 0.59$$

3. Error analysis for conductivity measurements

Here are some examples of average conductivity and standard deviation calculation for conductivity Figures in this PhD dissertation:

Figure 5.2; melt-mixed samples of PS/MWCNT filled with 2.5 wt% of MWCNT.

Conductivities (S/m)	Average Conductivity (S/m)	Standard Deviation
$4.76\times10^{+1}$; 1.80×10^{-2}; 4.13×10^{-2}; 1.59×10^{-2}	2.51×10^{-2}	1.41×10^{-2}

Figure 6.5; electrospun nanofibers of PVDF/(MWCNT-PANi) filled with 16 wt% of MWCNT.

Conductivities (S/m)	Average Conductivity (S/m)	Standard Deviation
5.38×10^{-3}; 1.61×10^{-2}; 7.81×10^{-3}	9.77×10^{-3}	5.64×10^{-3}

Figure 8.2; samples of PMMA70/SAN30 filled with 2 wt% of MWCNT.

Conductivities (S/cm)	Average Conductivity (S/cm)	Standard Deviation
5.54×10^{-7}; 1.42×10^{-6}; 2.87×10^{-7}; 1.89×10^{-6}	1.04×10^{-6}	7.48×10^{-7}

Figure 8.6; melt-mixed samples of PMMA30/SAN70 filled with 2 wt% of MWCNT.

Conductivities (S/cm)	Average Conductivity (S/cm)	Standard Deviation
2.78×10^{-4}; 2.17×10^{-4}; 1.08×10^{-4}; 1.18×10^{-4}	1.54×10^{-4}	8.19×10^{-5}

Figure 8.7; melt-mixed samples of PMMA30/SAN70 filled with 1 wt% of MWCNT at 170.

Conductivities (S/cm)	Average Conductivity (S/cm)	Standard Deviation
1.14×10^{-13}; 4.42×10^{-13}; 1.22×10^{-13}	2.26×10^{-13}	1.88×10^{-13}

Figure 8.9; melt-mixed samples of PMMA30/SAN70 filled with 2 wt% of MWCNT.

Conductivities (S/cm)	Average Conductivity (S/cm)	Standard Deviation
3.57×10^{-2}; 1.96×10^{-2}; 2.33×10^{-2}; 3.03×10^{-2}	2.72×10^{-2}	7.20×10^{-3}